PLAXIS LE
Slope Stability
2D/3D LIMIT EQUILIBRIUM SLOPE STABILITY ANALYSIS

Verification Manual

Written by:
The Bentley Systems Team

Last Updated: Tuesday, September 14, 2021

Bentley Systems Incorporated

COPYRIGHT NOTICE

TRADEMARK NOTICE

1 INTRODUCTION

The word "Verification", when used in connection with computer software can be defined as "the ability of the computer code to provide a solution consistent with the physics of the problem. There are also other factors such as initial conditions, boundary conditions, and control variables that may affect the accuracy of the code to perform as stated.

"Verification" is generally achieved by solving a series of so-called "benchmark" problems. "Benchmark" problems are problems for which there is a closed-form solution or for which the solution has become "reasonably certain" as a result of longhand calculations that have been performed. Publication of the "benchmark" solutions in research journals or textbooks also lends credibility to the solution.

There are also example problems that have been solved and published in User Manual documentation associated with other comparable software packages. While these are valuables checks to perform, it must be realized that it is possible that errors can be transferred from one's software solution to another.

Consequently, care must be taken in performing the "verification" process on a particular software package. It must also be remembered there is never such a thing as complete software verification for "all" possible problems. Rather, it is an ongoing process that establishes credibility with time. Bentley Systems takes the process of "verification" most seriously and has undertaken a wide range of steps to ensure that the Slope Stability software will perform as intended by the theory of limit equilibrium slope stability.

The following models represent comparisons made to textbook solutions, hand calculations, and other software packages. We at Bentley Systems Ltd., are dedicated to providing our clients with reliable and tested software. While the following list of example models is comprehensive, it does not reflect the entirety of models, which may be posed to the Slope Stability software.

It is our recommendation that checks be performed on all model runs prior to presentation of results. It is also our recommendation that the modeling process move from simple to complex models with simpler models being verified through the use of hand calculations or simple spreadsheet calculations.

2 ACADS MODELS

The following group of models represents a series of models originally presented in the Australian ACADS study (Giam & Donald, 1989). The study presented a series of benchmark examples and allowed a variety of consultants using differing software packages to solve the models.

The results were then reviewed by an expert review panel and an answer was established. The Slope Stability software package was compared to these models in the following sections.

2.1 1(A) SIMPLE SLOPE

Project: Slopes_Group_1
Model: VS_1

This model contains a simple case of a total stress analysis without considering pore-water pressures. It is a simple analysis that represents a homogenous slope with given soil properties. This model is originally published by the ACADS study (Giam & Donald, 1989).

2.1.1 Geometry and Material Properties

The slope properties that are in use for this model are presented in Table 1. The requirements for this problem are the factor of safety and its corresponding critical circular failure surface.

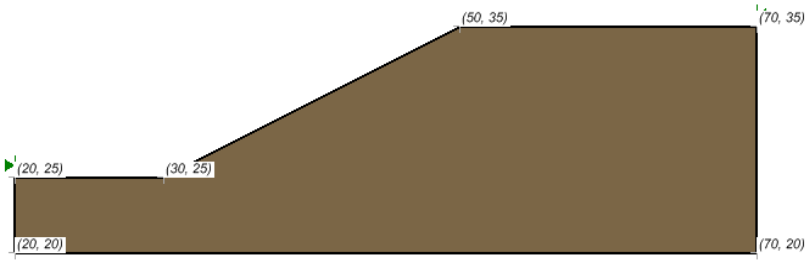

Figure 1 Geometry of the Simple Slope model

Table 1 Material Properties of the Simple Slope model

c (kN/m^2)	ϕ (degrees)	γ (kN/m^3)
3.0	19.6	20.0

2.1.2 Results and Discussions

The grid and radius method was used to identify a critical slip surface location. A grid of centers of 20 x 20 was used along with 11 tangent points.

This period of a total of 4851 circular slip surfaces. The results of the analysis for each different analysis method are presented in Table 2. The Factor of Safety published by the ACADS study was 1.00.

Table 2 Results of the Simple Slope model

Method	Factor of Safety		Difference (%)
	Slide	Slope Stability	
Ordinary	0.947	0.945	-0.211
Bishop Simplified	0.987	0.989	0.203
Janbu Simplified	0.939	0.939	0.000
Spencer	0.986	0.988	0.203
GLE	0.986	0.988	0.203

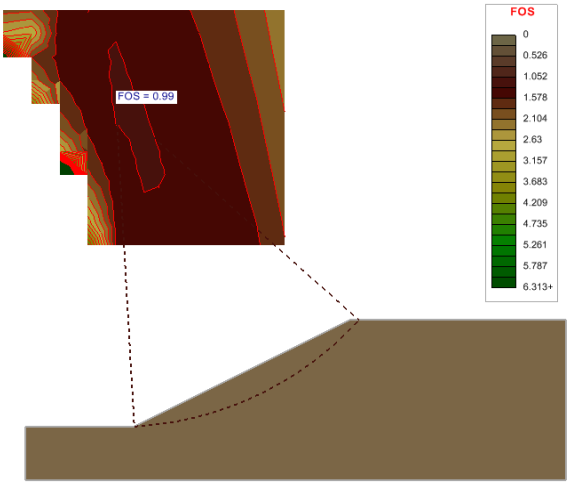

Figure 2 Solution of the Simple Slope model using the Spencer method

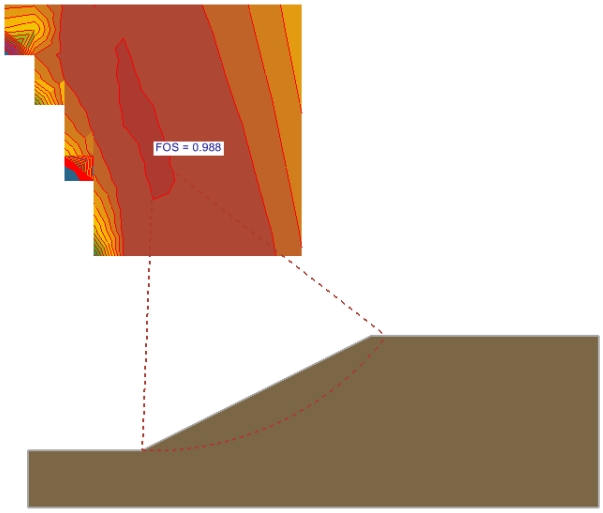

Figure 3 Solution of the Simple Slope model using the GLE method

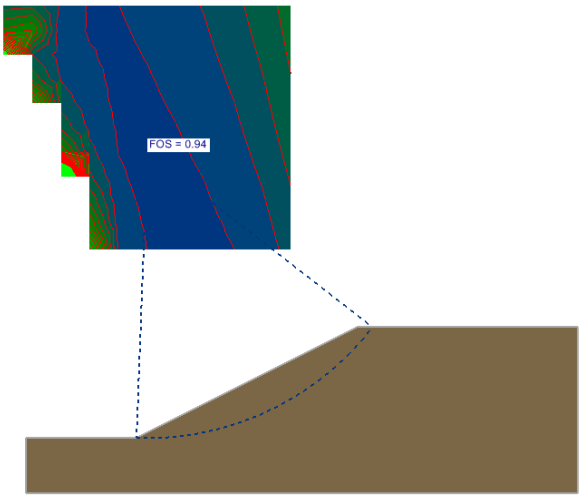

Figure 4 Solution of the Simple Slope model using the Janbu Simplified method

2.2 1(B) TENSION CRACK

Project: Slopes_Group_1
Model: VS_2

This model has the same slope geometry as verification problem #1, with the exception that a tension crack zone has been added as shown in Figure 5.

For this problem, a suitable tension crack depth is required. Water is assumed to fill the tension crack. The calculations the equation used to calculate the tension crack depth is shown below (Craig, 1997).

$$Depth = \frac{2c}{y\sqrt{k_a}}, k_a = \frac{1-\sin\phi}{1+\sin\phi}$$

2.2.1 Geometry and Material Properties

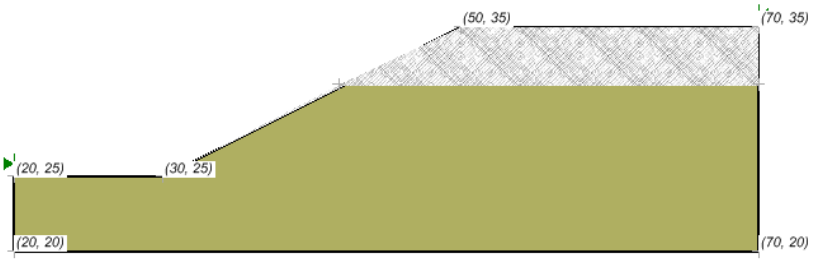

Figure 5 Geometry of the Tension Crack model

Table 3 Material Properties of the Tension Crack model

c (kN/m^2)	ϕ (degrees)	γ (kN/m3)
32.0	10.0	20.0

2.2.2 Results and Discussions

The grid and radius search technique was used to locate the most critical slip surface. A grid 20 x 20 grid of centers was used along with 11 tangents points.

A total of 4851 slip surface was generated. The values of the critical factor of safety are shown in Table 4. The Bishop, Spencer, GLE and Janbu's corrected, solutions are shown along with the location of the critical slip surface. The Factor of Safety published by the ACADS study is 1.65 to 1.70.

Table 4 Results of the Tension Crack model

Method	Factor of Safety					Difference (with Slide) (%)	Difference (with SLOPE/W) (%)
	Slide	Slope/W		Slope Stability			
		Moment	Force	Moment	Force		
Ordinary	1.521	1.52		1.521		0.00	0.07
Bishop Simplified	1.596	1.592		1.593		-0.19	0.06
Janbu Simplified	1.382		1.38		1.38	-0.15	0.29
Spencer	1.592	1.594	1.599	1.589	1.589	-0.19	0.31
M-P	1.592	1.588	1.594	1.59	1.59	-0.13	0.13
GLE	1.592	1.588	1.588	1.59	1.59	-0.13	0.13

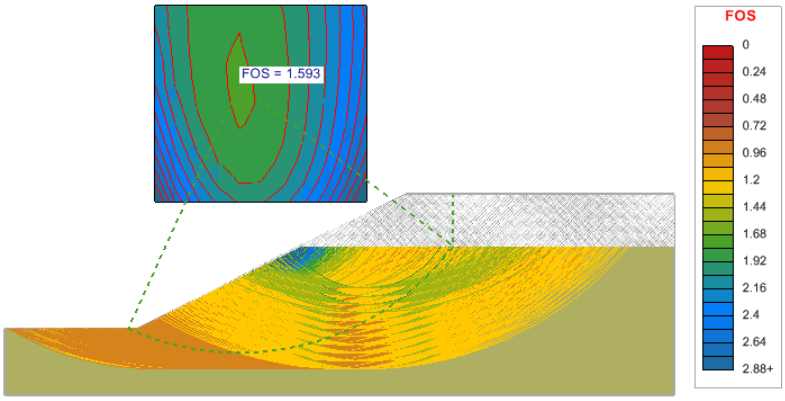

Figure 6 Solution of the Tension Crack model using the Bishop Simplified method

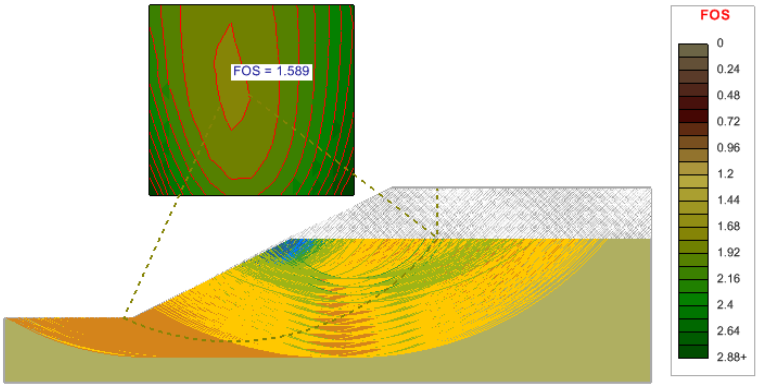

Figure 7 Solution of the Tension Crack model using the Spencer method

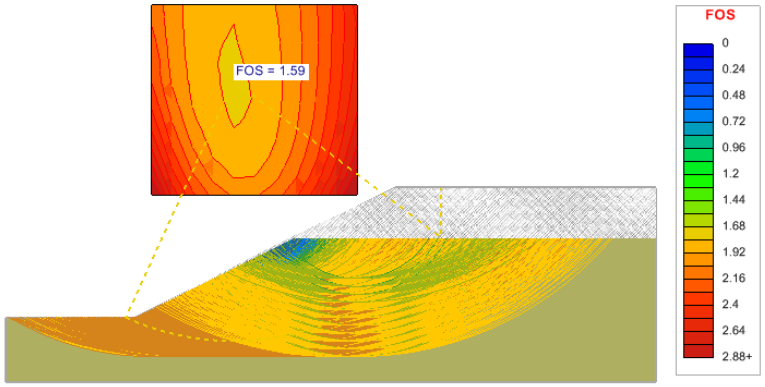

Figure 8 Solution of the Tension Crack model using the GLE Method

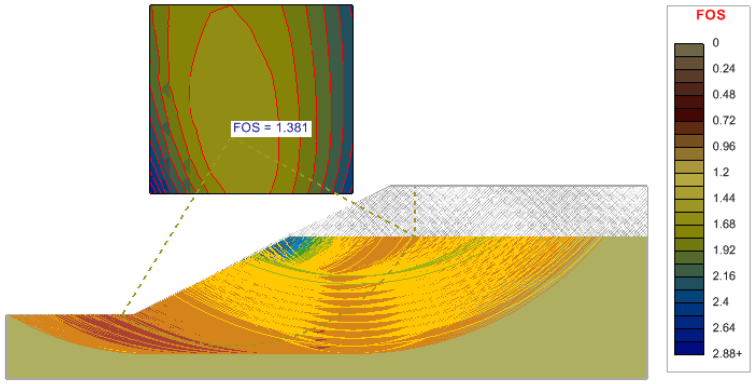

Figure 9 Solution of the Tension Crack model using the Janbu Simplified method

2.3 1(C) NON-HOMOGENEOUS

Project: Slopes_Group_1
Model: VS_3

This model is a non-homogenous three-layer slope with material properties shown in Table 5. The calculation of the factor of safety and its corresponding critical slip surface is shown.

2.3.1 Geometry and Material Properties

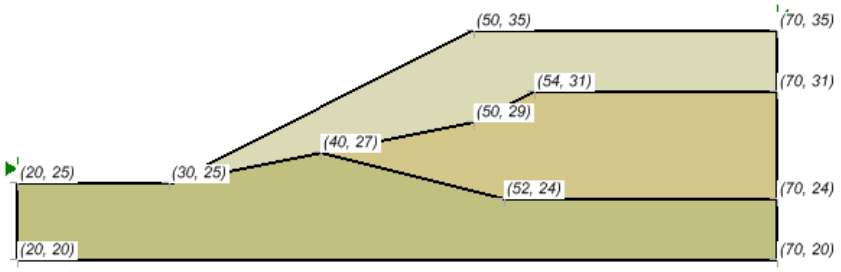

Figure 10 Geometry of the Non-Homogenous model

Table 5 Material Properties of the Non-Homogenous model

	c (kN/m^2)	ϕ (degrees)	γ (kN/m^3)
Soil #1	0.0	38.0	19.5
Soil #2	5.3	23.0	19.5
Soil #3	7.2	20.0	19.5

2.3.2 Results and Discussions

The grid and radius technique was used to determine the location of the critical slip surface. A slip surface centers search grid of 20 x 20 was used for the grid of centers and 11 tangents points were used at each grid center.

This resulted in total of 4851 trial slip surfaces. The results of the factor of safety calculations are shown in Table 6. The Factor of Safety published by the ACADS study was 1.39.

Table 6 Results of the Non-Homogenous model

Method	Factor of Safety			Difference (%)
	Slide	Slope Stability		
		Moment	Force	
Ordinary	1.232	1.231		-0.08
Bishop Simplified	1.405	1.405		0.00
Spencer	1.375	1.374	1.374	0.15
GLE	1.374	1.376	1.375	0.07

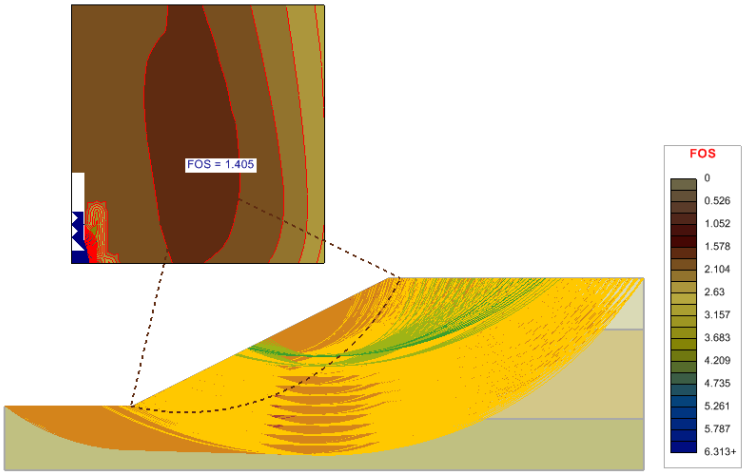

Figure 11 Solution of the non-homogenous model using the Bishop Simplified method

2.4 1(D) NON-HOMOGENOUS WITH SEISMIC LOAD

Project: Slopes_Group_1
Model: VS_4

This model is identical to the previous model with the exception that a horizontal seismically induced acceleration of 0.15g was included in the analysis. The intent of this model is to test the ability of the software to analyze seismic conditions.

2.4.1 Geometry and Material Properties

The model requires the calculations of the factor of safety and the corresponding location of the critical slip surface. No pore-water pressures are designated and therefore a total stress analysis is performed.

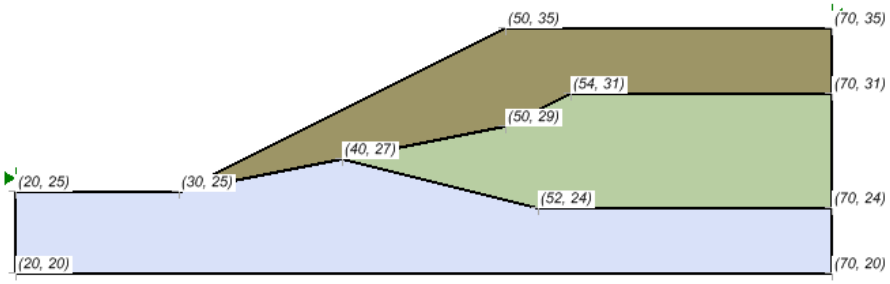

Figure 12 Geometry of the Non-Homogeneous with Seismic Load model

Table 7 Material Properties of the Non-Homogenous with Seismic Load

	c kN/m^2)	ϕ (degrees)	γ (kN/m^3)
Soil #1	0.0	38.0	19.5
Soil #2	5.3	23.0	19.5
Soil #3	7.2	20.00	19.5

2.4.2 Results and Discussions

The results of the analysis produce the following table of factors of safety for the Bishop, Spencer. GLE, Janbu Simplified methods. The Factor of Safety published by the ACADS study was 1.00.

Table 8 Results of the Non-Homogenous with Seismic Load model

Method	Factor of Safety			Difference (%)
	Slide	Slope Stability		
		Moment	Force	
Ordinary	0.884	0.884		0.00
Bishop Simplified	1.015	1.014	3	0.00
Janbu Simplified	0.897		0.897	0.00
Spencer	0.991	0.991	0.99	0.00
GLE	0.989	0.991	0.99	0.20

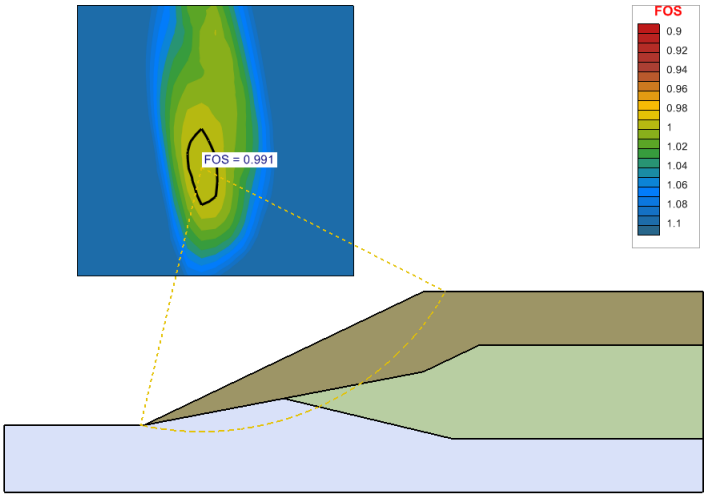

Figure 13 Results using the GLE method on VS_4 model

2.5 NON-HOMOGENOUS CRITICAL SEISMIC COEFFICIENT ANALYSIS

Project: Slopes_Group_3
Model: VS4_Critical_Ky

This model is identical to the previous model with the exception that an advanced seismic analysis was conducted to determine the critical seismic coefficient that results in a destabilized slope with FOS of 1.0. The intent of this model is to test the ability of the software to analyze seismic conditions.

2.5.1 Geometry and Material Properties

The model requires the calculations of the factor of safety and the corresponding location of the critical slip surface. No pore-water pressures are designated and therefore a total stress analysis is performed.

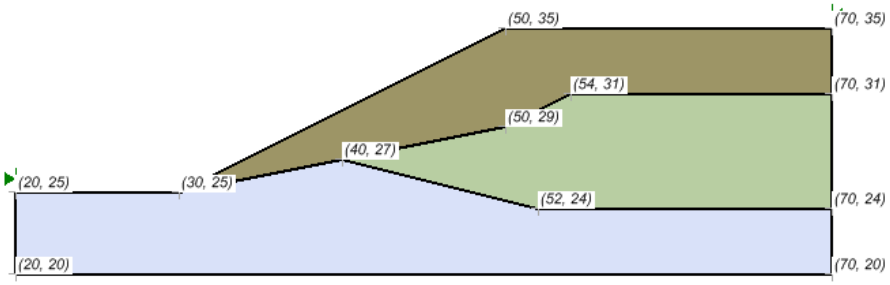

Figure 14 Geometry of the Non-Homogeneous Critical Seismic Coefficient Analysis model

Table 9 Material Properties of the Non-Homogenous Critical Seismic Coefficient Analysis

	c kN/m^2)	ϕ (degrees)	γ (kN/m^3)
Soil #1	0.0	38.0	19.5
Soil #2	5.3	23.0	19.5
Soil #3	7.2	20.00	19.5

2.5.2 Results and Discussions

The results of the analysis produce the following table of factors of safety for the Spencer, M-P and GLE.

Table 10 Results of the Non-Homogenous Critical Seismic Coefficient Analysis model

Method	Factor of Safety			Difference (%)
	Slide	Slope Stability		
		Moment	Force	
Spencer	0.146	0.145	0.145	0.00
M-P	0.146	0.145	0.146	0.00
GLE	0.146	0.145	0.145	0.00

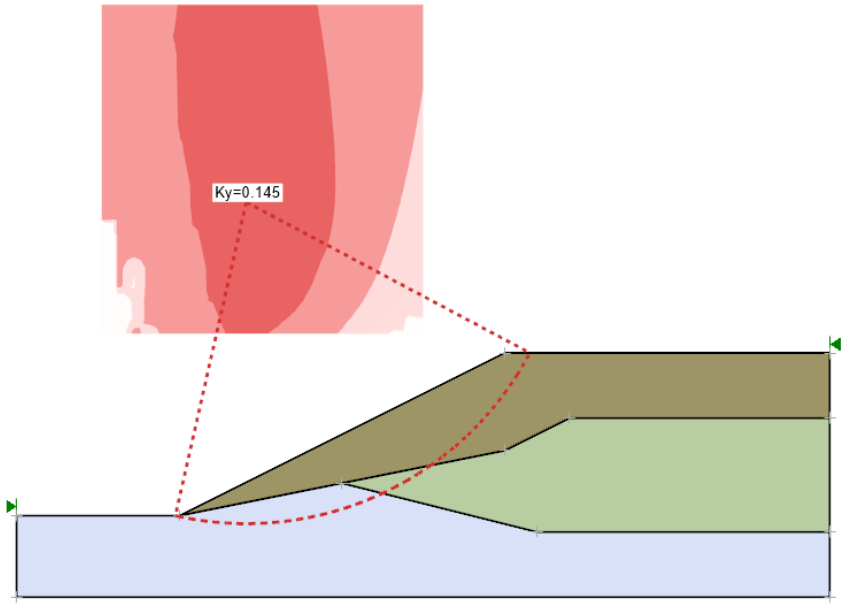

Figure 15 Results using the GLE method Critical Seismic Coefficient Analysis model

2.6 NON-HOMOGENOUS NEWMARK DISPLACEMENT ANALYSIS

Project: Slopes_Group_3
Model: VS4_Newmark_Disp

This model is identical to the previous model with the exception that a Newmark Displacement analysis was carried out on the slope. The intent of this model is to test the ability of the software to analyze seismic conditions.

2.6.1 Geometry and Material Properties

The model requires the calculations of the factor of safety and the corresponding location of the critical slip surface. No pore-water pressures are designated and therefore a total stress analysis is performed.

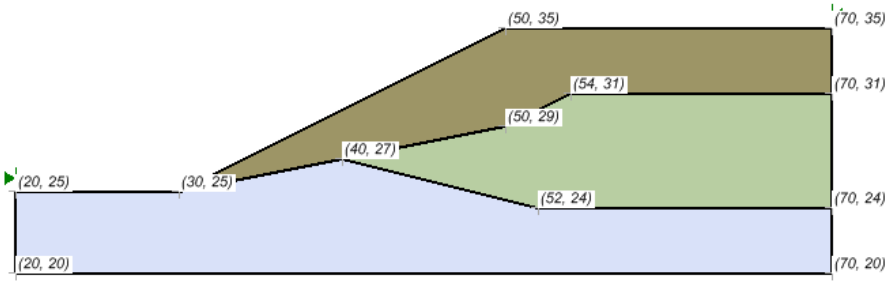

Figure 16 Geometry of the Non-Homogeneous Newmark Displacement Analysis model

Table 11 Material Properties of the Non-Homogenous Newmark Displacement Analysis

	c kN/m^2)	ϕ (degrees)	γ (kN/m^3)
Soil #1	0.0	38.0	19.5
Soil #2	5.3	23.0	19.5
Soil #3	7.2	20.00	19.5

2.6.2 Results and Discussions

The results of the analysis produce the following table of permanent displacements.

Table 12 Results of the Non-Homogenous Newmark Displacement Analysis

Method	Permanent Displacement			Difference (%)
	Slide (m)	Slope Stability		
		Moment (m)	Force (m)	
Bishop Simplified	0.02232	0.022		0.00
Janbu Simplified	0.10819		0.108	0.00
Corps #1	0.04233		0.042	0.00
Corps #2	0.03998		0.039	2.45
Lowe-Karafiath	0.05282		0.049	7.23
Spencer	0.0329	0.033	0.034	0.00
GLE	0.0349	0.033	0.034	5.44
M-P	0.0349	0.033	0.033	5.44
Sarma	0.0373	0.036	0.036	3.49

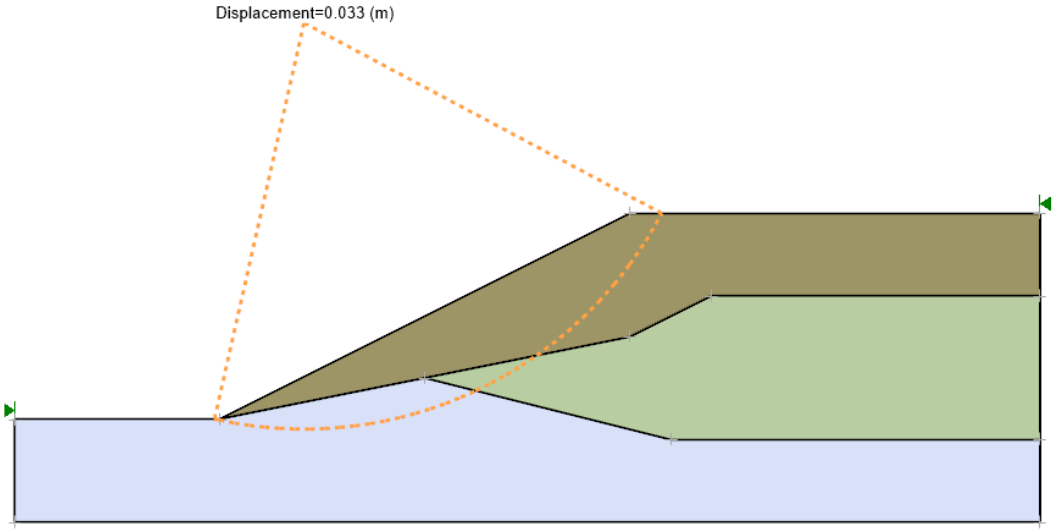

Figure 17 Results using the GLE method Newmark Displacement Analysis model

2.7 2(A) TALBINGO DAM, DRY

Project: Slopes_Group_1
Model: VS_5

This model is the Talbingo Dam (Giam & Donald, 1989) for the end-of-construction stage. Soil properties are given in Table 13 and the geometrical data is given in Table 14.

2.7.1 Geometry and Material Properties

The model requirements are that a factor of safety and a corresponding location of the critical failure surface must be calculated.

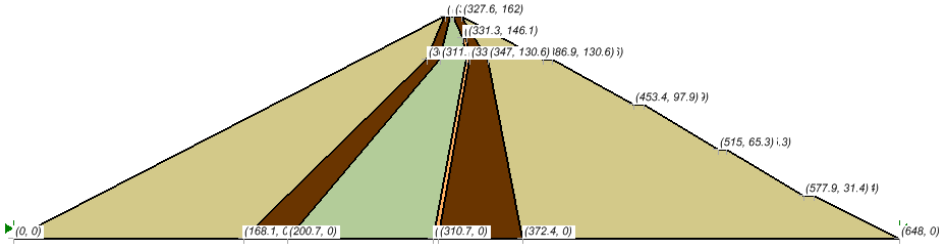

Figure 18 Geometry of the Talbingo Dam model

Table 13 Material Properties of the Talbingo Dam model

	c (kN/m^2)	ϕ (degrees)	γ (kN/m^3)
Rock fill	0	45	20.4
Transitions	0	45	20.4
Filter	0	45	20.4
Core	85	23	18.1

Table 14 Geometry Data of Talbingo Dam, with weak layer

Pt. #	Xc (m)	Yc (m)	Pt. #	Xc (m)	Yc (m)	Pt. #	Xc (m)	Yc (m)
1	0	0	10	515	65.3	19	307.1	0
2	315.5	162	11	521.1	65.3	20	331.3	130.6
3	319.5	162	12	577.9	31.4	21	328.8	146.1
4	321.6	162	13	585.1	31.4	22	310.7	0
5	327.6	162	14	648	0	23	333.7	130.6
6	386.9	130.6	15	168.1	0	24	331.3	146.1
7	394.1	130.6	16	302.2	130.6	25	372.4	0
8	453.4	97.9	17	200.7	0	26	347	130.6
9	460.6	97.9	18	311.9	130.6	-	-	-

2.7.2 Results and Discussions

Resulting Factor of Safety are calculated that are shown in Table 15. The Factor of Safety published by the ACADS study is (1.95)/1.90.

Table 15 Results of the Talbingo Dam model

Method	Factor of Safety (Neglect PWP, with no cracks)			Difference (%)
	Slide	Slope Stability		
		Moment	Force	
Ordinary	1.948	1.949		0.05
Bishop Simplified	1.948	1.95		0.10
Janbu Simplified	1.919		1.92	0.05
Spencer	1.948	1.95	1.95	0.10
GLE	1.948	1.95	1.949	0.10

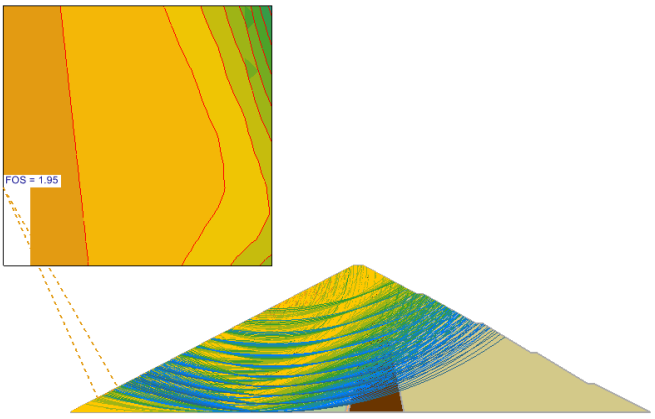

Figure 19 Solution of the Talbingo Dam model using the Bishop Simplified method

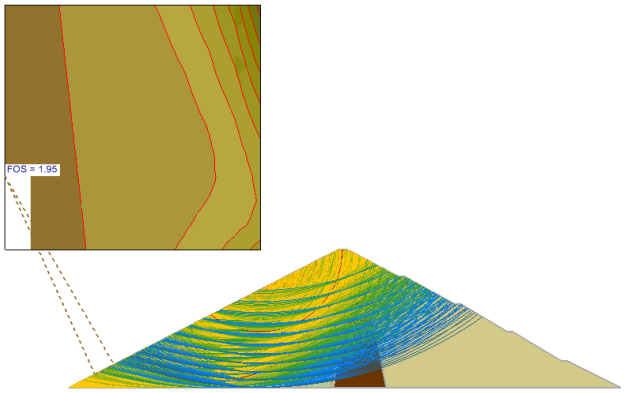

Figure 20 Solution of the Talbingo Dam model using the Spencer method

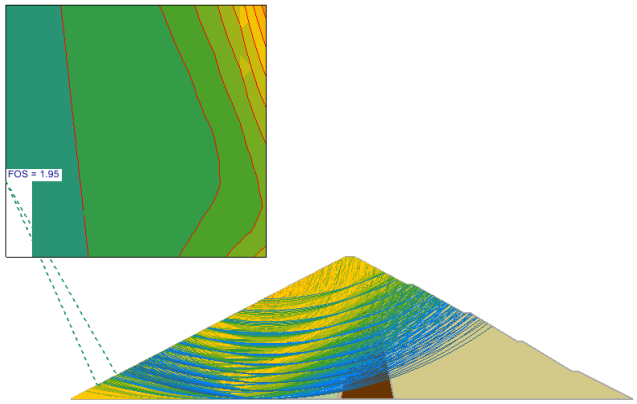

Figure 21 Solution of the Talbingo Dam model using the GLE Method

2.8 2(B) TALBINGO DAM, DRY PREDEFINED SLIP SURFACE

Project: Slopes_Group_1
Model: VS_6

The model #6 is identical to model #5 with the exception is that a singular slip surface of known center and radius is analyzed in this particular problem.

2.8.1 Geometry and Material Properties

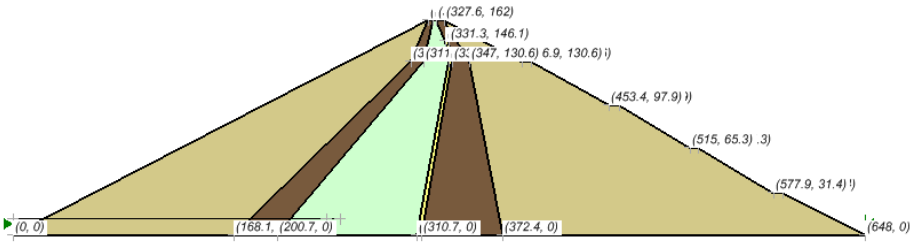

Figure 22 Geometry of the Talbingo Dam, Dry Predefined Slip Surface model

Table 16 - Data for slip circle

Xc	Yc (m)	Radium (m)
100.3	291	278.8

Table 17 - Material Properties of the Talbingo Dam

	c (kN/m^2)	ϕ (degrees)	γ (kN/m^3)
Rock fill	0	45	20.4
Transitions	0	45	20.4

Filter	0	45	20.4
Core	85	23	18.1

2.8.2 Results and Discussions

The following table illustrates the factor of safety and the methodology used for analyzing these conditions. The results are presented in Table 18. The Factor of Safety published by the ACADS study was 2.29.

Table 18 Results of the Talbingo Dam

Method	Factor of Safety (Neglect PWP, with no cracks)				Difference (%)
	Slide		Slope Stability		
	Moment	Force	Moment	Force	
Bishop Simplified	2.208		2.207		-0.05
Spencer	2.292		2.291	2.291	-0.04
GLE	2.301		2.298	2.298	-0.13

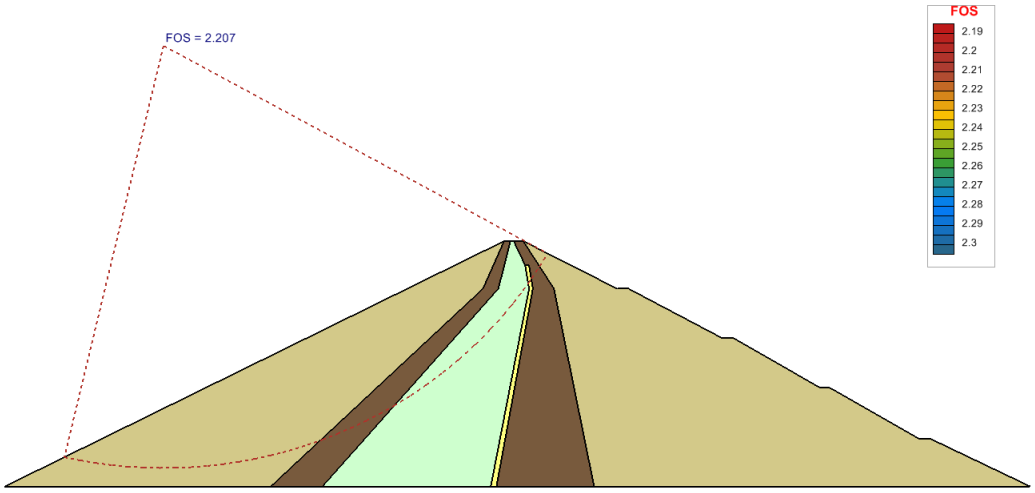

Figure 23 Solution using the Bishop Simplified method

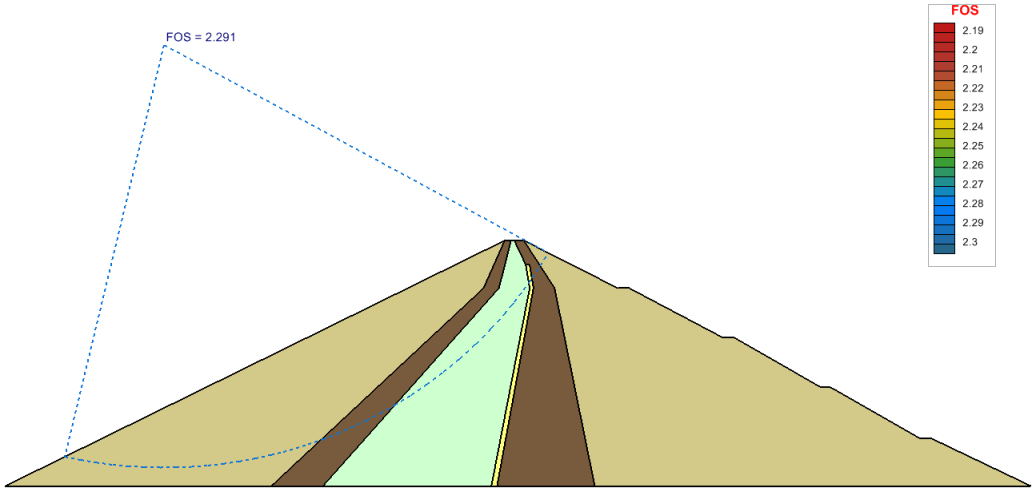

Figure 24 Solution using the Spencer method

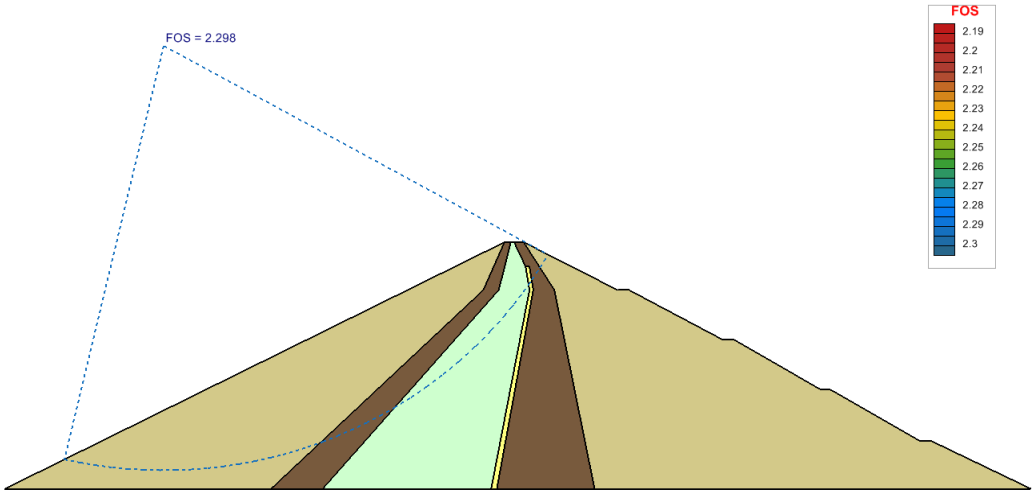

Figure 25 Solution using the GLE method

2.9 3(A) WATER TABLE MODELED WITH WEAK SEAM

Project: Slopes_Group_1
Model: VS_7

This particular model illustrates the analysis of a slope containing a both a water table and a weak layer. The water table is assumed to coincide with the base of the weak layer. In this case, the effects of negative pore-water pressure above the water tables were ignored.

2.9.1 Geometry and Material Properties

The tension crack zone is also ignored in this model. The requirement is to calculation of the Factor of Safety and the corresponding noncircular failure surface.

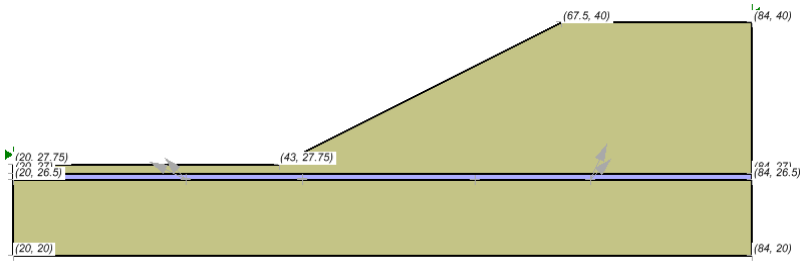

Figure 26 Geometry of the Water Table Modeled with the Weak Seam model

Table 19 - Material Properties of the Water Table

	c (kN/m^2)	ϕ (degrees)	γ (kN/m^3)
Soil #1	28.5	20.0	18.84
Soil #2	0	10.0	18.84

2.9.2 Results and Discussions

The results of the analysis can be seen in Table 20. The Factor of Safety published by the ACADS study was 1.26.

Table 20 – Results of the Water Table

Method	Factor of Safety			Difference (%)
	Slide	Slope Stability		
Spencer	1.258	1.269	1.268	0.87
GLE	1.246	1.264	1.264	1.45

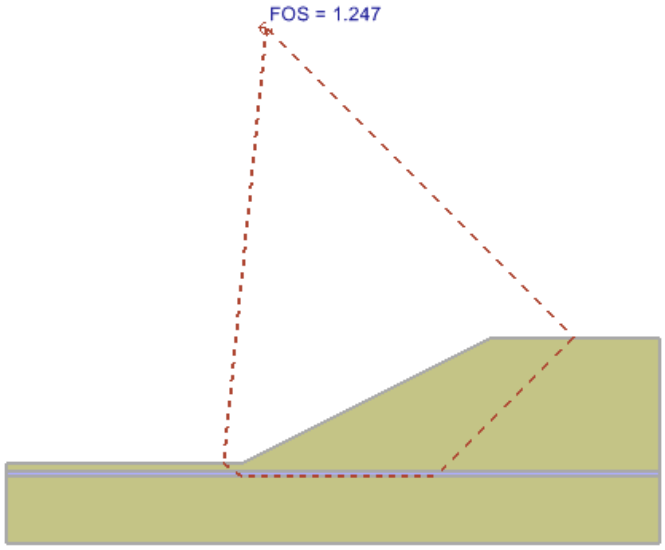

Figure 27 Solution using the GLE Method

2.10 3(B) WATER TABLE MODELED WITH WEAK SEAM WITH PREDEFINED SLIP SURFACE

Project: Slopes_Group_1
Model: VS_8

This problem #8 is identical to problem #7, except when a non-circular slip surface of known coordinates is analyzed.

NOTE:
The values for each model can be viewed in the ACADS document publication and presented alongside the Slope Stability solutions.

2.10.1 Geometry and Material Properties

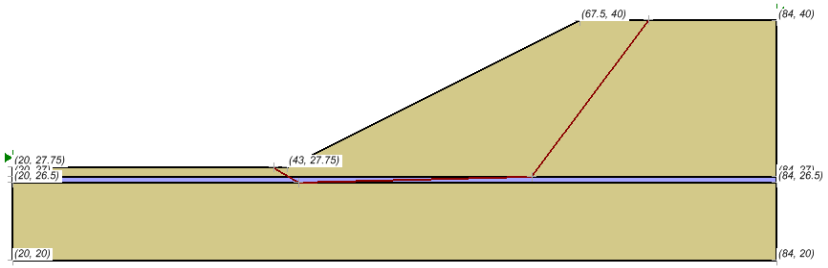

Figure 28 Geometry of the Water Table Modeled with Weak Seam with Predefined Slip Surface model

Table 21 Failure Surface Coordinates

X (m)	Y (m)
41.85	27.75
44.00	26.50
63.50	27.00
73.31	40.00

Table 22 Material Properties of the Water Table Modeled with Weak Seam

	c (kN/m^2)	ϕ (degrees)	γ (kN/m^3)
Soil #1	28.5	20.0	18.84
Soil #2	0	10.0	18.84

2.10.2 Results and Discussions

The Factor of Safety published by the ACADS study was 1.34.

Table 23 Results of pre-defined slip surface model

Method	Factor of Safety			Difference (%)
	Slide	Slope Stability		
		Moment	Force	
Spencer	1.277	1.277	1.277	0.00
GLE	1.262	1.258	1.258	-0.32

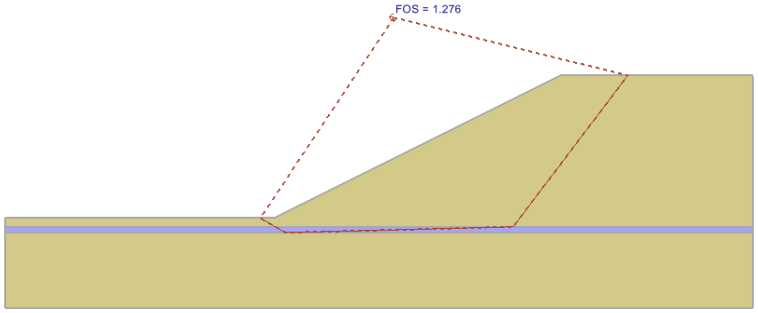

Figure 29 Solution using the Spencer method

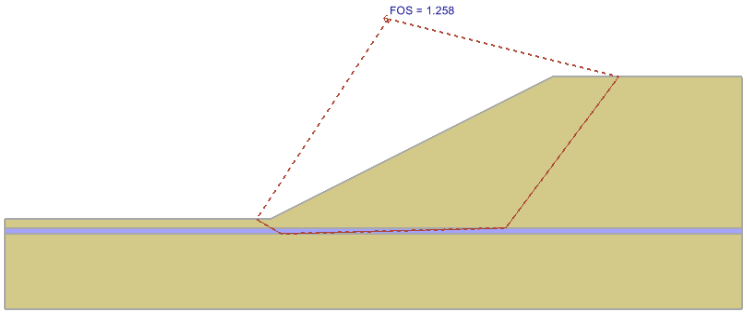

Figure 30 Solution using the GLE method

2.11 4 EXTERNAL LOADING, PORE-PRESSURE DEFINED BY WATER TABLE

Project: Slopes_Group_1
Model: VS_9, VS_9_Optimization, VS_9_Optimization_Greco

This is a more complex example involving a weak layer, pore-water pressures and surcharges. The ACADS verification program received a wide range of answers for this model and fully expected this during the program.

The soil parameters, external loadings and piezometric surface are shown in the following diagram. The tension cracks are ignored in this example. The model requirement is that the noncircular slip surface and the corresponding factor of safety are required.

2.11.1 Geometry and Material Properties

A block search for the critical noncircular failure surface is carried out by defining two line searches to block search squares within the weak layer. A number of different random surfaces were generated by the search and the results compared well with the actual results.

Table 24 External Loadings

X (m)	Y (m)	Normal Stress (kN/m^2)
23.00	27.75	20.00
43.00	27.75	20.00
70.00	40.00	20.00
80.00	40.00	40.00

Table 25 Data for Piezometric Surface

Pt. #	Xc (m)	Yc (m)
1	20.0	27.75
2	43.0	27.75
3	49.0	29.8
4	60.0	34.0
5	66.0	35.8
6	74.0	37.6
7	80.0	38.4
8	84.0	38.4

Pt#: Refer to Figure 31

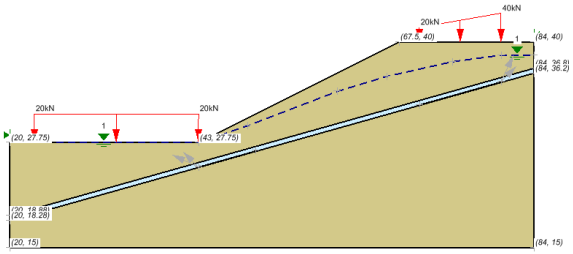

Figure 31 Geometry of the External Loading, Pore-Pressure defined by Water Table model

Table 26 Material Properties of the External Loading

	c (kN/m^2)	ϕ (degrees)	γ (kN/m^3)
Soil #1	28.5	20.0	18.84
Soil #2	0	10.0	18.84

2.11.2 Results and Discussions

The results of this model illustrate the difference between a model with no optimization and a model where optimization methods are used.

What is interesting in this case is that the optimized methods yield a lower Factory of Safety than the non-optimization techniques.

Table 27 – Optimization (Greco in Slope Stability)

Method	Factor of Safety (Optimization-Greco)			Difference (%)
	Slide	Slope Stability		
		Moment	Force	
Spencer	0.715	0.69	0.69	-2.82
GLE	0.685	0.676	0.675	-1.31

Table 28 – Optimization (Optimize Surfaces option in Slope Stability)

Method	Factor of Safety (Optimization-Greco)			Difference (%)
	Slide	Slope Stability		
		Moment	Force	
Spencer	0.715	0.697	0.696	-2.52
GLE	0.685	0.671	0.671	-2.19

Table 29 - No optimization

Method	Factor of Safety			Difference (%)
	Slide	Slope Stability		
		Moment	Force	
Spencer	0.760	0.722	0.722	-5.00
GLE	0.721	0.695	0.695	-3.61

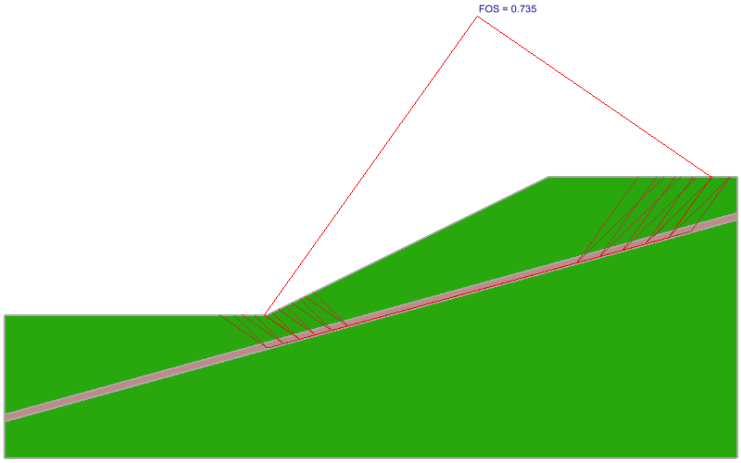

Figure 32 Solution using the Spencer Method

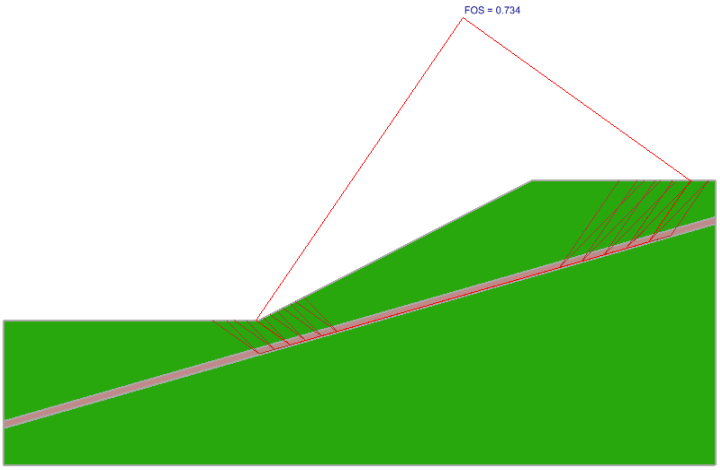

Figure 33 Solution using the GLE Method

3 SLOPE STABILITY GROUP 1

The following examples compare the results of Slope Stability against published solutions presented in textbooks or journal papers.

3.1 LANESTER EMBANKMENT VERIFICATION

Project: Slopes_Group_1
Model: VS_12

This problem is the Lanester embankment (in France) which was built with an induced failure for testing and research purposes in 1969 (Pilot et al, 1982). A dry tension crack zone is assumed to spread over the entire embankment for this model.

3.1.1 Geometry and Material Properties

The pore-water pressures are derived from Table data, from raw data presented for this model, and interpolated data across the model domain using the bilinear interpolation method. The location of the critical slip surface and the corresponding factor of safety are required for this model.

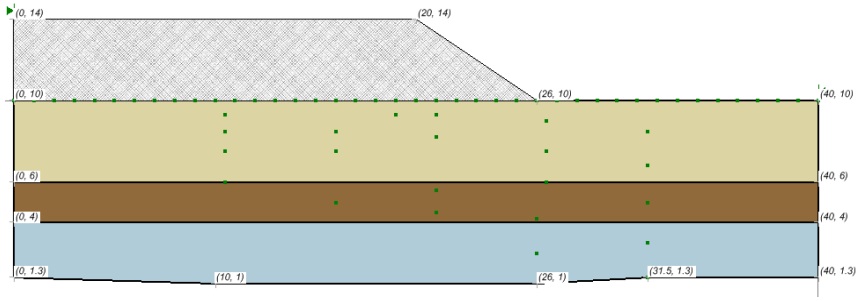

Figure 34 Geometry of the Lanester Embankment model

Table 30 Material Properties of the Lanester Embankment

	c (kN/m^2)	ϕ (degrees)	γ (kN/m^3)
Embankment	30	31.0	18.2
Soft Clay	4	37.0	14.0
Silty Clay	7.5	33.0	13.2
Sandy Clay	8.5	35.0	13.7

Table 31 Water Pressure Points

Pt. #	Xc (m)	Yc (m)	U kPa)	Pt.#	Xc (m)	Yc (m)	u (kPa)	Pt.#	Xc (m)	Yc (m)	u (kPa)
1	26.5	9	20	9	16	8.5	60	17	31.5	3	80
2	31.5	8.5	20	10	21	8.2	60	18	10.5	6	100
3	10.58	9.3	40	11	26.5	6	60	19	16	5	100
4	16	9.3	40	12	31.5	5	60	20	21	4.5	100
5	21	9.3	40	13	10.5	7.5	80	21	26	2.5	100
6	26.5	7.5	40	14	16	7.5	80	22	31.5	1.3	100
7	31.5	6.8	40	15	21	5.6	80	23	-	-	-
8	10.5	8.5	60	16	26	4.2	80	24	-	-	-

3.1.2 Results and Discussions

The results of the analysis are presented in Table 32.

Table 32 Results of the Lanester Embankment model

Method	Factor of Safety			Difference (%)
	Slide	Slope Stability		
		Moment	Force	
Spencer	1.079	1.072	1.071	-0.65
M-P	1.077	1.068	1.068	-0.84
GLE	1.077	1.068	1.068	-0.84
Note:No solution in **Slide** for the critical slip surface(Slope Stability) in Bishop				

Table 33 Results of the Lanester Embankment model

Method	Factor of Safety (Water Table)			Difference (%)
	Slide	Slope Stability		
		Moment	Force	
Spencer	2.645	2.647	2.647	0.08
M-P	2.644	2.647	2.647	0.11
GLE	2.644	2.647	2.647	0.11

3.2 CUBZAC-LES-PONTS EMBANKMENT

Project: Slopes_Group_1
Model: VS_13

In 1974, the Cubzac-les-Ponts embankment (in France) was built and a failure induced for testing and research purposes. This model represents an analysis of that particular problem.

3.2.1 Geometry and Material Properties

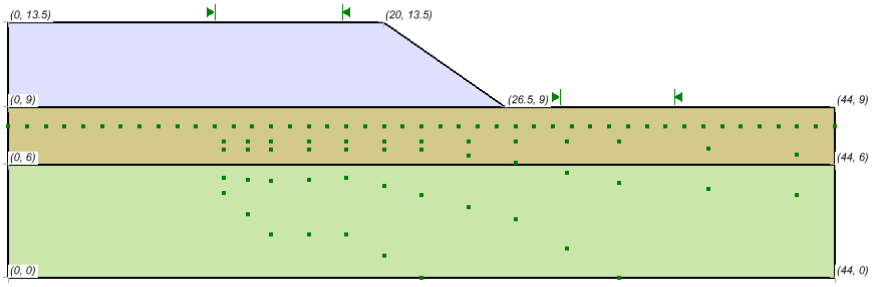

Figure 35 Geometry of the Cubzac-les-Ponts embankment model

Table 34 Water Pressure Points, u

Pt. #	Xc (m)	Yc (m)	u (kPa)	Pt.#	Xc (m)	Yc (m)	u (kPa)	Pt.#	Xc (m)	Yc (m)	u (kPa)
1	11.5	4.5	125	16	16	7.2	25	31	24.5	7.2	25
2	11.5	5.3	100	17	18	2.3	125	32	27	3.1	100
3	11.5	6.8	50	18	18	5.3	100	33	27	6.1	50
4	11.5	7.2	25	19	18	6.8	50	34	27	7.2	25
5	12.75	3.35	125	20	18	7.2	25	35	29.75	1.55	100
6	12.75	5.2	100	21	20	1.15	125	36	29.75	5.55	50
7	12.75	6.8	50	22	20	4.85	100	37	29.75	7.2	25
8	12.75	7.2	25	23	20	6.8	50	38	32.5	0	100
9	14	2.3	125	24	20	7.2	25	39	32.5	5	50
10	14	5.1	100	25	22	0	125	40	32.5	7.2	25
11	14	6.8	50	26	22	4.4	100	41	37.25	4.7	50
12	14	7.2	25	27	22	6.8	50	42	37.25	6.85	25
13	16	2.3	125	28	22	7.2	25	43	42	4.4	50
14	16	5.2	100	29	24.5	3.75	100	44	42	6.5	25
15	16	6.8	50	30	24.5	6.45	50	45	-	-	-

In Table 35 it presents the pore-water pressures at designated points. The pore-water pressures at the case of the slice were interpolation from the given data using a bio interpolation method. The location of the critical slip surface and the corresponding factor of safety are to be determined.

Table 35 Material Properties of the Cubzac-les-Ponts Embankment model

	c (kN/m^2)	ϕ (degrees)	γ (kN/m^3)
Embankment	0	35.0	21.2
Upper Clay	10	24.0	15.5
Lower Clay	10	28.4	15.5

3.2.2 Results and Discussions

The resulting factors of safety from the Slope Stability software are shown in Table 36.

Table 36 Results of the Cubzac-les-Ponts Embankment model

Method	Factor of Safety			Difference (%)
	Slide	Slope Stability		
		Moment	Force	
Bishop Simplified	1.314	1.317		0.23
Spencer	1.334	1.339	1.339	0.38
GLE	1.336	1.34	1.34	0.30

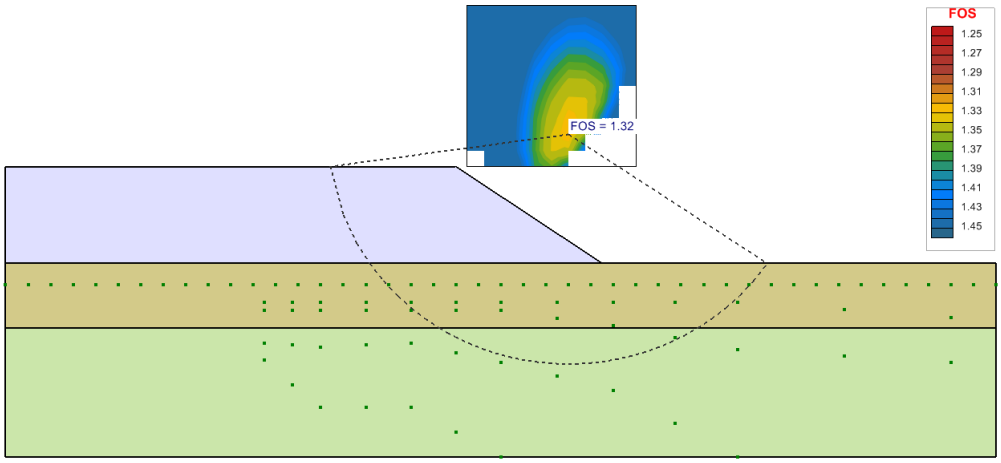

Figure 36 Results of the Cubzac-les-Ponts model using the Bishop Simplified method

3.3 ARAI AND TAGYO HOMOGENEOUS SLOPE

Project: Slopes_Group_1
Model: VS_14_Circular

Arai and Tagyo (1985) presented simple homogeneous soil slope with zero pore-water pressure. This model represents analysis of this particular problem and the results are provided in Table 38.

3.3.1 Geometry and Material Properties

There are no pore-water pressures input for this problem. The position of the critical slip surface, as well the calculated factor of safety is required in this analysis.

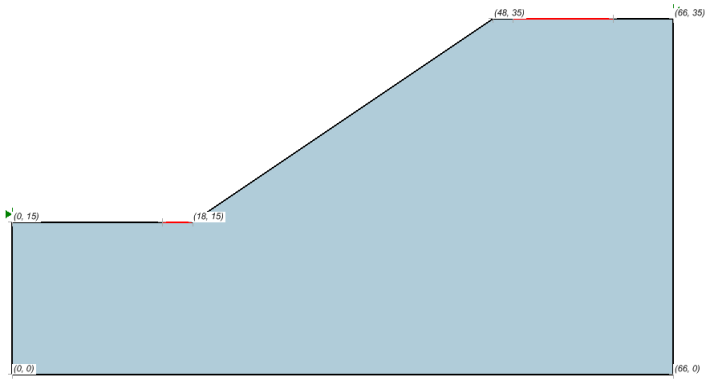

Figure 37 Geometry of the Arai and Tagyo Homogenous Slope Circular model

Table 37 Material Properties of the Arai and Tagyo Homogenous Slope Circular model

	c (kN/m^2)	ϕ (degrees)	γ (kN/m^3)
Soil	41.65	15.0	18.82

3.3.2 Results and Discussions

3.3.2.1 Part 1 Circular Slip Surface Results: using grid and radius method.

The following results were obtained using the grid and radius search technique.

Table 38 Circular Results – using auto refine search

Method	Factor of Safety		Difference (%)
	Slide	Slope Stability	
Bishop Simplified	1.409	1.406	-0.21
Janbu Simplified	1.319	1.323	0.30
GLE	1.406	1.404	-0.14

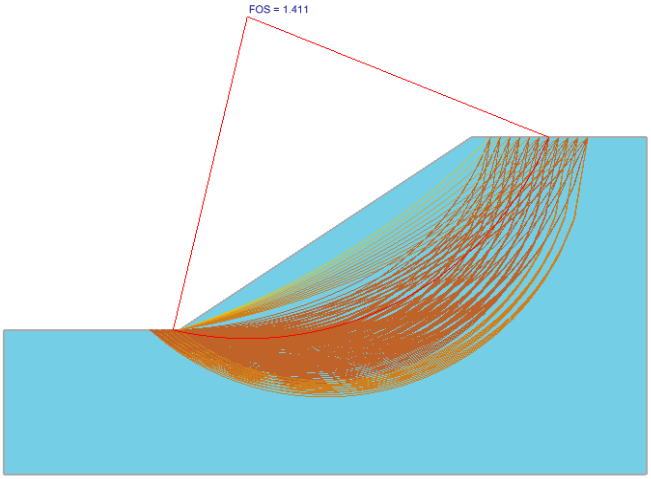

Figure 38 Circular Failure Surface using Bishop Simplified method

3.4 ARAI AND TAGYO LAYERED SLOPE

Project: Slopes_Group_1
Model: VS_15_Circular, VS_15_NonCircular

Arai and Tagyo (1985) present an example, which consists of a layered slope, where a layer of low shear strength is located between two high strength layers. The results of this analysis have also been presented by Kim, et al. (2002), Malkawi et al. (2001) and Greco (1996).

3.4.1 Geometry and Material Properties

There are no pore-water pressures in this example. The corresponding model and set up data are presented in the following section. The position of the most critical slip surface as well as the calculated factor of safety is required for this analysis.

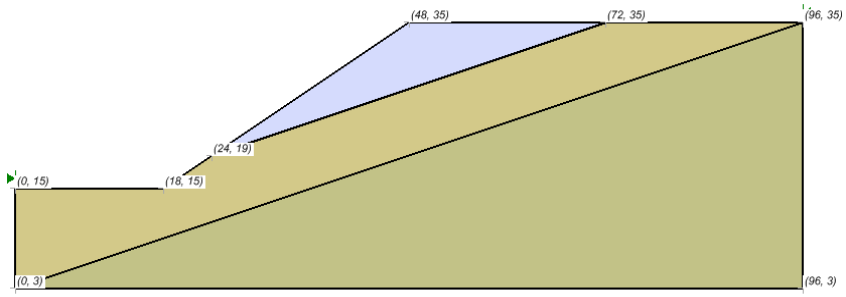

Figure 39 Geometry of the Arai and Tagyo Layered Slope model

Table 39 Material Properties of the Arai and Tagyo Layered Slope

	c (kN/m^2)	ϕ (degrees)	γ (kN/m^3)
Upper Layer	29.4	12.0	18.82
Middle Layer	9.8	5.0	18.82
Lower Layer	294	40.0	18.82

3.4.2 Results and Discussions

3.4.2.1 Circular results

The entry and exist point search method are used to determine the location of the critical slip surface. The results are shown in Table 40.

Table 40 Circular Results – using auto refine search

Method	Factor of Safety		Difference (%)
	Slide	Slope Stability	
Bishop Simplified	0.421	0.423	0.48
Janbu Simplified	0.410	0.415	1.22
Spencer	0.424	0.426	0.47

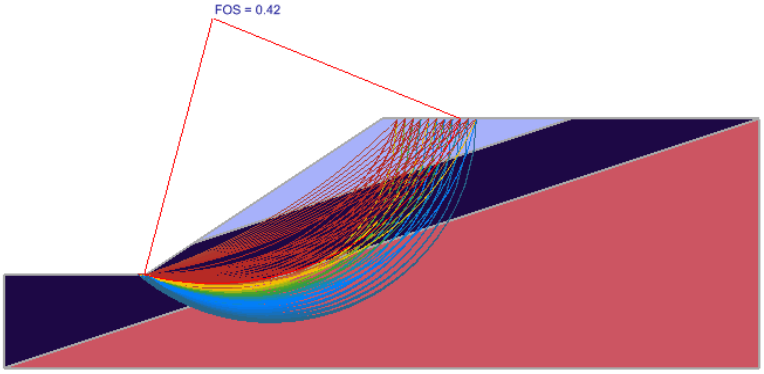

Figure 40 Circular Failure Surface using Bishop Simplified Method

3.4.2.2 Noncircular results

The noncircular slip surface analyses were performed using the Spencer method, and the Greco searching technique. The results of the Greco technique are presented in Table 41.

Table 41 Noncircular Results using Random search with Optimization (1000 surfaces)

Method	Factor of Safety				Difference (%)
	Slide		Slope Stability		
	Moment	Force	Moment	Force	
Janbu Simplified		0.394		0.397	0.76
Spencer	0.412	0.412	0.424	0.424	0.49

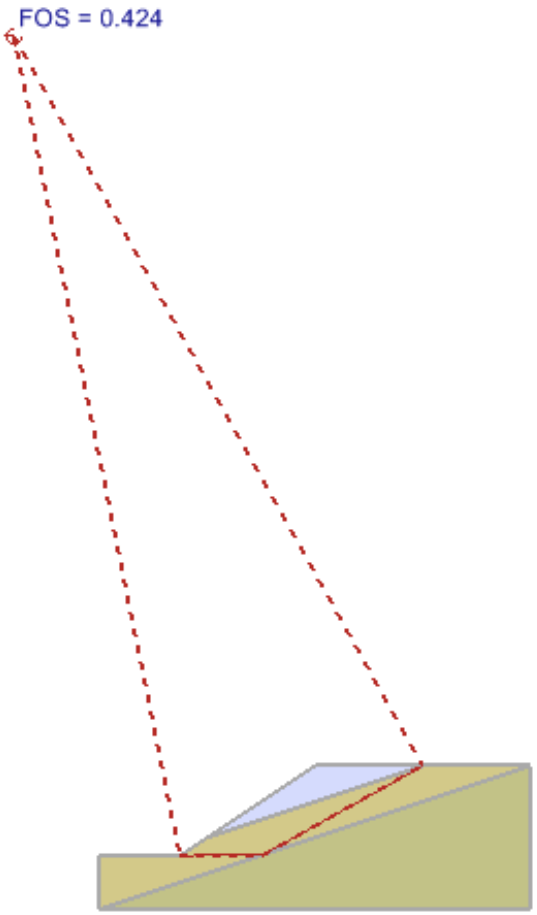

Figure 41 Noncircular Failure Surface using Spencer method and Random Search

3.5 ARAI AND TAGYO PORE-WATER PRESSURE SLOPE

Project: Slopes_Group_1
Model: VS_16_Circular, VS_16_NonCircular

This example 3 is from Arai and Tagyo, (1985). The model is a simple homogeneous soil slope with pore-water pressures.

3.5.1 Geometry and Material Properties

The model contains a high water table with a daylight facing water table existing along the slope. The location of the water table is shown in the below Figure 42.

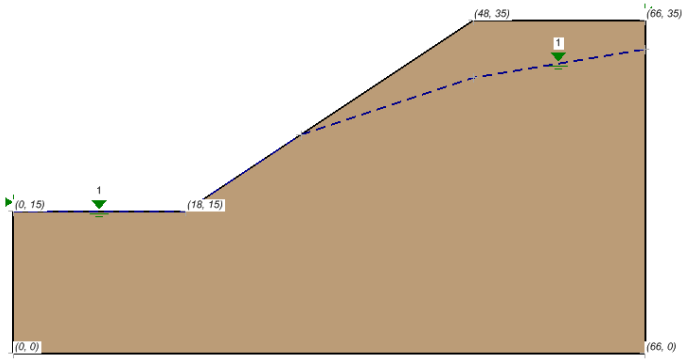

Figure 42 Geometry of the Arai and Tagyo Pore-Water Pressure Slope model

The pore-water pressures are calculated assuming hydrostatic conditions. Specific the pore-water pressures at point below the water table are calculated from the vertical distance to the water table and multiplying by the unit weight of water.

It is assumed that there is no effect of suction above the water table. The location of the vertical slip surface and the value of the factor of safety were required for this analysis.

Table 42 Material Properties of the Arai and Tagyo Pore-Water Pressure Slope model

	c (kN/m^2)	ϕ (degrees)	γ (kN/m^3)
Soil	41.65	15.0	18.82

3.5.2 Results and Discussions

3.5.2.1 Circular results

The grid and radius search technique was used to determine the location of the critical slip surface. The results are shown in Table 43.

Table 43 Circular Results using Auto Refine Search

Method	Factor of Safety		Difference (%)
	Slide	Slope Stability	
Bishop Simplified	1.117	1.124	0.63
Janbu Simplified	1.046	1.046	0.00
GLE	1.118	1.124	0.57

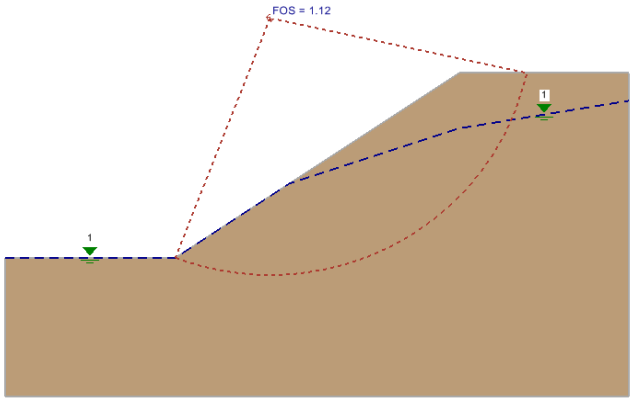

Figure 43 Failure Surface using Bishop Simplified method

3.5.2.2 Noncircular results

A noncircular analysis was also performed using the Greco search technique. The Greco search technique was applied with the Spencer and Janbu Simplified methods to yield the following Factor of Safety.

Table 44 Noncircular Results using Random Search with Monte Carlo Optimization

Method	Factor of Safety					Difference (%)
	Arai & Tagyo 1985	Slide		Slope Stability		
		Moment	Force	Moment	Force	
Janbu Simplified	0.995		0.968		0.967	-0.10
Spencer		1.094	1.094	1.097	1.096	-0.27

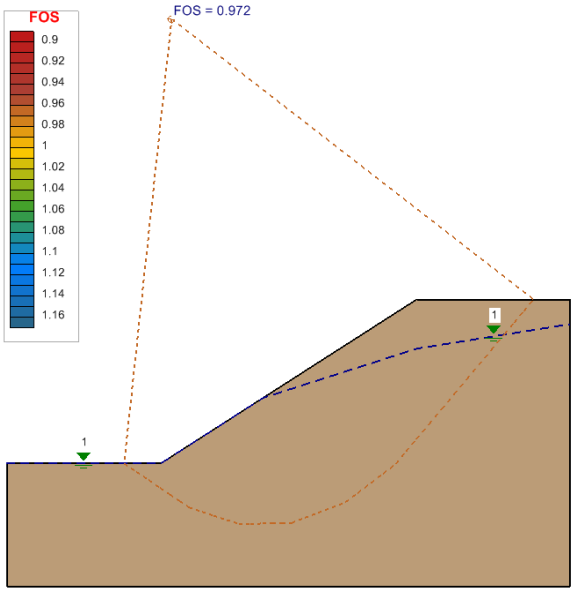

Figure 44 Noncircular Failure using Janbu Simplified Method

3.6 YAMAGAMI AND UETA SIMPLE SLOPE

Project: Slopes_Group_1
Model: VS_17_Circular, VS_17_NonCircular

This model was originally presented by Yamagami and Ueta (1988). The model consists of a simple homogeneous soil slope and zero pore-water pressures. The model was also analyzed by Greco in 1996.

3.6.1 Geometry and Material Properties

The location of the critical slip surface and the corresponding factor of safety are to be calculated.

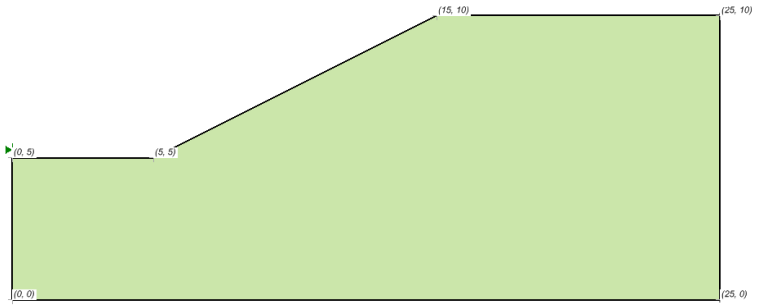

Figure 45 Geometry of the Yamagami and Ueta Simple Slope model

Table 45 Material Properties of the Yamagami and Ueta Simple Slope model

	c (kN/m^2)	ϕ (degrees)	γ (kN/m^3)
Soil	9.8	10.0	17.64

3.6.2 Results and Discussions

3.6.2.1 Circular results

The analysis was performed using a specified range of entry and exit points. The calculated factors of safety for the Bishop's Simplified and Ordinary method are tabulated in Table 46.

Table 46 Circular Results using auto refine search

Method	Factor of Safety		Difference (%)
	Slide	Slope Stability	
Ordinary	1.278	1.28	0.16
Bishop Simplified	1.344	1.346	0.15

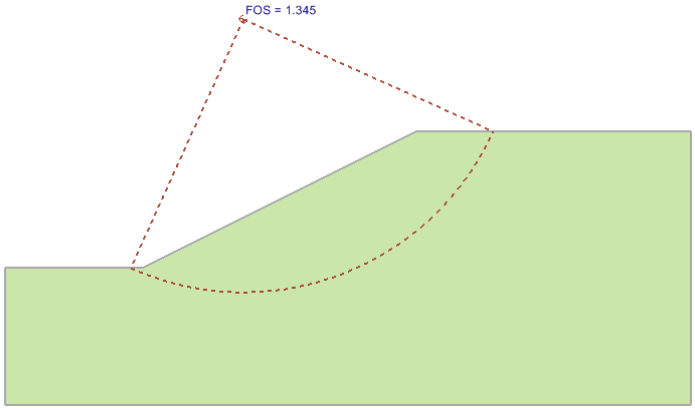

Figure 46 Failure surface using Bishop Simplified method

3.6.2.2 Noncircular results

The critical noncircular slip surface was obtained using the Greco search method. The Greco search method results as well as the Slope Stability results are presented in Table 47. In this particular case, the results of Slope Stability are believed to be more optimal.

Table 47 Noncircular Results using Random search with Monte Carlo optimization in SLIDE and using the GRECO search in Slope Stability

Method	Factor of Safety				Difference (%)
	Slide		Slope Stability		
	Moment	Force	Moment	Force	
Janbu Simplified		1.178		1.178	0.00
Spencer	1.324	1.324	1.324	1.319	0.00

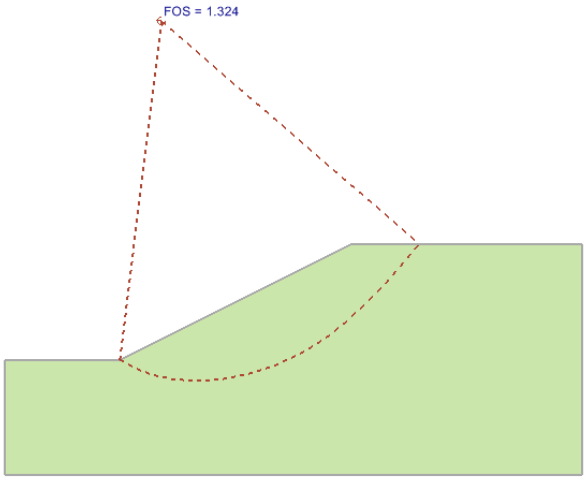

Figure 47 Noncircular failure using Spencer Method

3.7 BAKER SIMPLE SLOPE

Project: Slopes_Group_1
Model: VS_18_NonCircular

Baker (1980) published the results of this model, which was originally published by Spencer, (1969).

3.7.1 Geometry and Material Properties

It consists of a simple homogeneous soil slope with a pore-water pressure distribution defined by a pore pressure coefficient, r_u of 0.5.

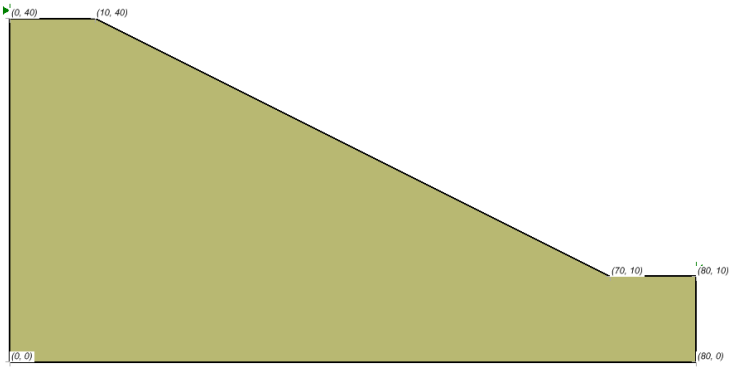

Figure 48 Geometry of the Baker Simple Slope model

Table 48 Material Properties of the Baker Simple Slope model

	c (kN/m^2)	ϕ (degrees)	γ (kN/m^3)	r_u
Soil	10.8	40.0	17.64	0.5

3.7.2 Results and Discussions

3.7.2.1 Noncircular results

This model is solved using the Greco search technique along with Spencer's method of calculating the factor of safety. The

results may for the critical slip surfaces are shown in Figure 49.

Table 49 Noncircular Results using Random Search with Monte Carlo optimization

Method	Factor of Safety						Difference (%)
	Baker (1980)	Spencer (1969)	Slide		Slope Stability		
			Moment	Force	Moment	Force	
Spencer	1.02	1.08	1.01	1.01	1.01	1.009	0.00

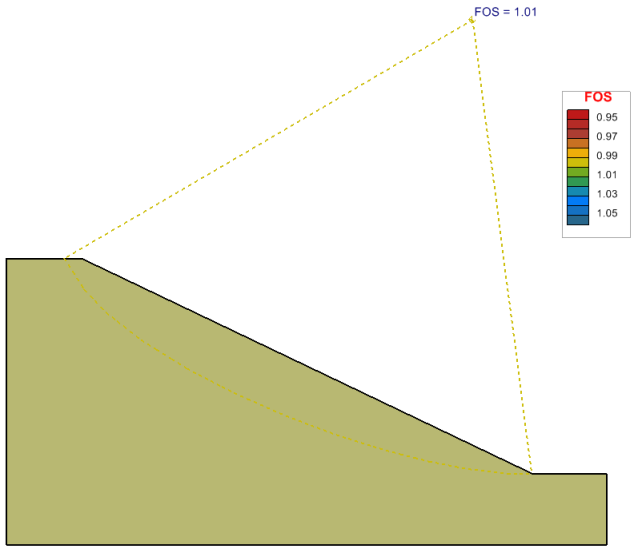

Figure 49 Noncircular Failure Surface using Spencer method along with the Greco search technique

3.8 GRECO LAYERED SLOPE

Project: Slopes_Group_1
Model: VS_19_NonCircular

This model was taken from Greco, 1996, Example # 4. It consists of a layered slope without pore-water pressures. It was originally published by Yamagami and Ueta (1988).

3.8.1 Geometry and Material Properties

The model consists of an earth dam type structure with three underlying soil layers.

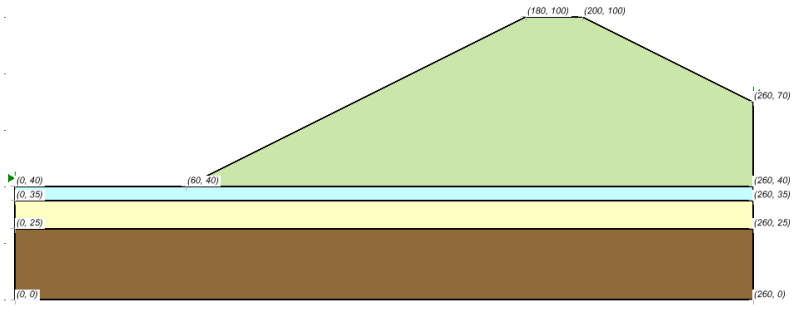

Figure 50 Geometry of the Greco Layered Structure model

Table 50 Material Properties of the Greco Layered Structure model

	c (kN/m^2)	ϕ (degrees)	γ (kN/m^3)

Upper Layer	49	29.0	20.38
Layer 2	0	30.0	17.64
Layer 3	7.84	20.0	20.38
Bottom Layer	0	30.0	17.64

3.8.2 Results and Discussions

3.8.2.1 Noncircular results

Using the Greco method, the following factors of safety were calculated for the Spencer method. The results are displayed in the Table 51 for the critical slip surface.

Table 51 Noncircular Results using random search with Monte Carlo technique with convex surfaces

Method	Factor of Safety						Difference (%)
	Greco 1996	Spencer 1969	Slide		Slope Stability		
			Moment	Force	Moment	Force	
Spencer	1.40-1.42	1.40-1.42	1.398	1.398	1.4	1.4	0.14
GLE			1.398	1.398	1.39	1.39	0.57

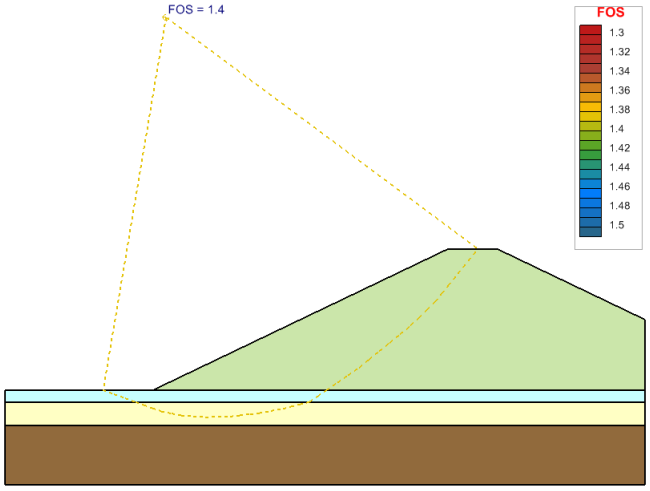

Figure 51 NonCircular failure surface using the Spencer method

3.9 GRECO WEAK LAYER SLOPE

Project: Slopes_Group_1
Model: VS_20_Circular, VS_20_NonCircular_Greco

This model is taken from Greco's paper (1986) (Example #5). The model was originally published by Chen and Shao (1988). It consists of a layered slope with pore-water pressures and designated by a phreatic line.

3.9.1 Geometry and Material Properties

The geometry also has a weak seam, and it is modeled as a 0.5m thick material layer at the base of the model. The critical slip surface and the corresponding factor of safety are to be calculated for a circular and noncircular slip surface.

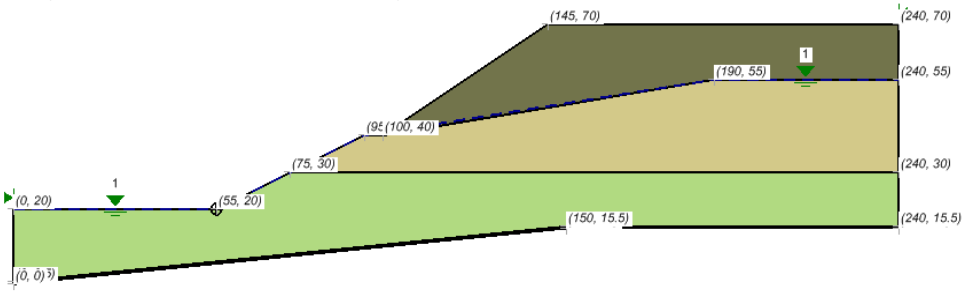

Figure 52 Geometry of the Greco Weak Layer Slope model

Table 52 Material Properties of the Greco Weak Layer Slope model

	c (kN/m^2)	ϕ (degrees)	γ (kN/m^3)
Layer 1	9.8	35.0	20.0
Layer 2	58.8	25.0	19.0
Layer 3	19.8	30.0	21.5
Layer 4	9.8	16.0	21.5

3.9.2 Results and Discussions

3.9.2.1 Circular Results

The results of the circular analysis are shown in Table 53.

Table 53 Circular Results using a grid search and a focus object at the toe (40x40 grid)

Method	Factor of Safety			Difference (%)
	Greco (1996)	Slide	Slope Stability	
Bishop Simplfied		1.087	1.074	-1.12
Janbu Simplified		0.995	0.984	-1.11
Spencer	1.08	1.093	1.081	-1.10

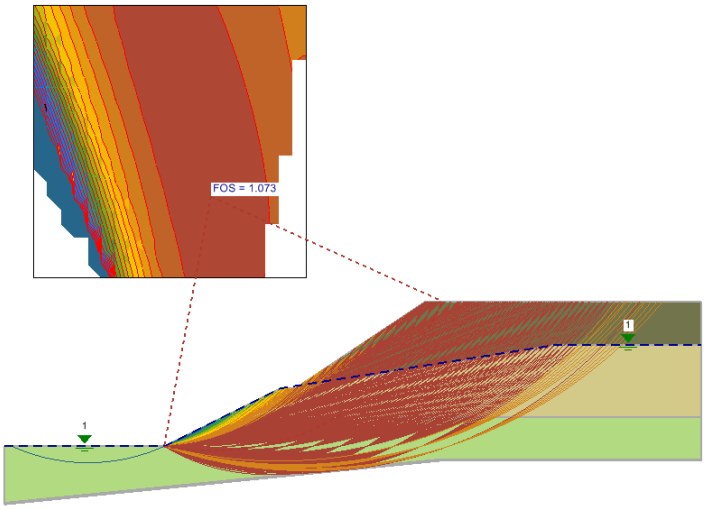

Figure 53 Circular Failure Surface using Bishop Simplified method

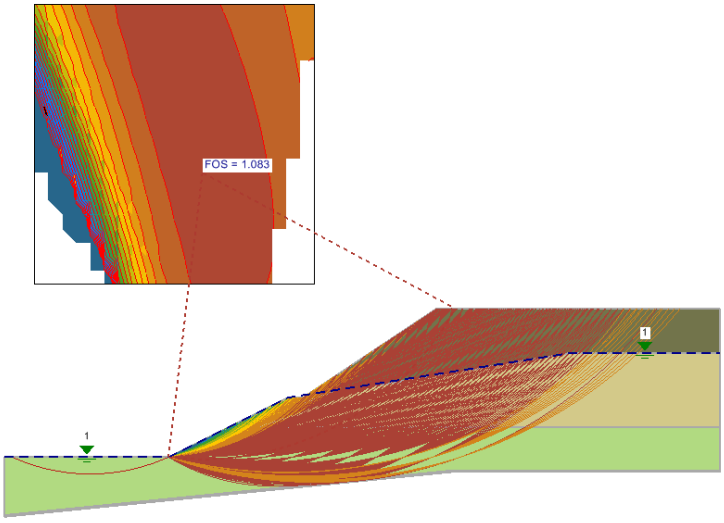

Figure 54 Circular Failure Surface using Spencer method

3.9.2.2 Noncircular results

The results were obtained using the block search method. The block search method produced the following Factor of Safety.

Table 54 Noncircular Results using block search polyline in the weak seam and Monte Carlo optimization

Method	Factor of Safety (Greco)		Difference (%)
	Slide	Slope Stability	
Spencer	1.007	0.987	-1.99

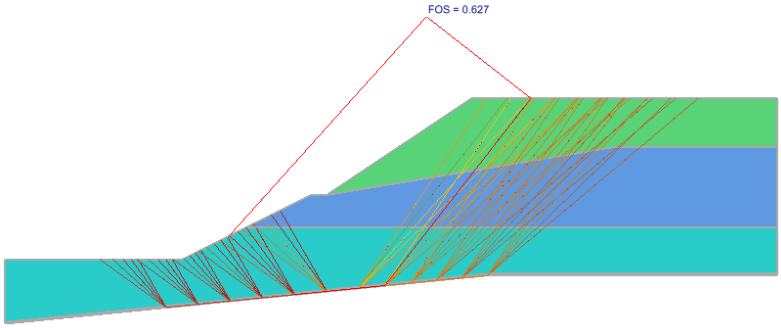

Figure 55 Noncircular Failure Surface using Spencer method and Block Search

3.10 FREDLUND AND KRAHN HOMOGENEOUS SLOPE

Project: Slopes_Group_1
Model: VS_21_Dry, VS_21_Ru, VS_21_WT

Fredlund and Krahn (1977) originally published this model. The intent of this model was to study the effect of various pore-water pressures and the resulting factor of safety.

3.10.1 Geometry and Material Properties

The model consists of a homogeneous slope consisting of three separate water conditions; namely:

1. Dry soil,
2. r_u defined pore-water pressures, and
3. Pore pressures defined using a water table, WT.

The calculations for this mode are performed in imperial units to be consistent with the original paper. Other authors such as Baker, (1980), Greco (1986) and Malkawi (2001) have also analyzed this slope.

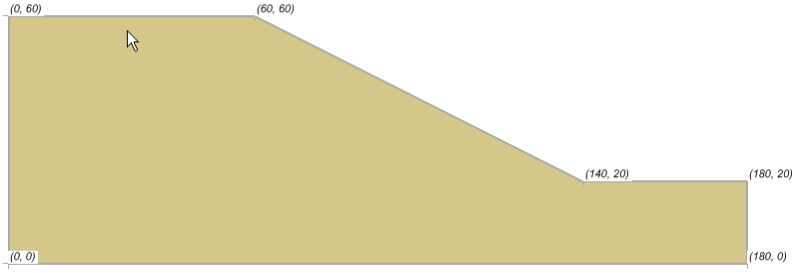

Figure 56 Geometry of the Fredlund and Krahn Homogenous Slope model

Table 55 Material Properties of the Fredlund and Krahn Homogenous Slope model

	c (psf)	ϕ (degrees)	γ (pcf)	r_u (case2)
Soil	10.8	40.0	17.64	0.5

3.10.2 Results and Discussions

The results of the defined circular analysis are presented in Table 56.

Table 56 Results of the Circular slip surface analysis

Case	Ordinary (F & K)	Ordinary	Bishop (F & K)	Bishop Simplified	Spencer (F & K)	Spencer	M-P (F & K)	M-P
1-Dry	1.928	1.930	2.080	2.079	2.073	2.075	2.076	2.075
2-Ru	1.607	1.609	1.766	1.762	1.761	1.760	1.764	1.760
3-WT	1.693	1.696	1.834	1.832	1.830	1.831	1.832	1.831

Table 57 Results–Dry

Method	Factor of Safety				Difference (%)
	Fredlund & Krahn (1977)	Slide	Slope Stability		
			Moment	Force	
Ordinary	1.928	1.931	1.931		0.00
Bishop Simplified	2.08	2.079	2.079		0.00
Spencer	2.073	2.075	2.075	2.075	0.00
M-P	2.076	2.075	2.075	2.075	0.00

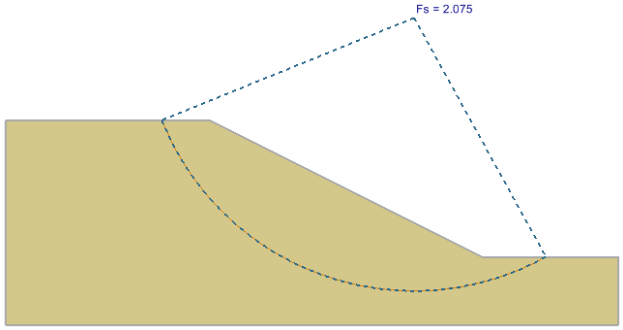

Figure 57 Location of the Circular slip surface for the Fredlund & Krahn (1977), Dry slope analysis with the Spencer method.

Table 58 Results of the analysis with ru pore-water pressures

Method	Factor of Safety				Difference (%)
	Fredlund & Krahn (1977)	Slide	Slope Stability		
			Moment	Force	
Ordinary	1.607	1.609	1.612		0.20
Bishop Simplified	1.766	1.763	1.762		-0.06
Spencer	1.761	1.76	1.76	1.76	0.00
M-P	1.764	1.76	1.76	1.76	0.00

Table 59 Results of the analysis with a designated water table, WT

Method	Factor of Safety				Difference (%)
	Fredlund & Krahn (1977)	Slide	Slope Stability		
			Moment	Force	
Ordinary	1.693	1.697	1.696		-0.06
Bishop Simplified	1.834	1.833	1.832		-0.06
Spencer	1.83	1.831	1.831	1.831	0.00
M-P	1.832	1.831	1.83	1.83	-0.06

3.11 FREDLUND AND KRAHN WEAK LAYER SLOPE

Project: Slopes_Group_1
Model: VS_22_Dry, VS_22_Ru, VS_22_WT

In 1977, Fredlund and Krahn published a paper, which contained a verification model consisting of a slope with a weak layer and three different designations of water pressure conditions. A number of different authors, such as Kim and Salgado (2002), Baker (1980), and Zhu, Lee and Jiang (2003), have also analyzed this slope.

3.11.1 Geometry and Material Properties

The model consists of a slope with a weak layer, which is sandwiched between soil strata. The water conditions are defined as follows:

1. Dry soil,
2. r_u defined pore-water pressures, and
3. Pore pressures defined using a water table, WT.

The model is set up in imperial units to be consistent with the original paper. The location of the weak layer appears to be slightly different in some of the mentioned references above. The results for this example model are sensitive to the location of the weak layer. Therefore, the results may vary in the second decimal place. The geometry is shown in Figure 58.

The location of the composite slip surface provided in the original paper was shown as having coordinates, xc = 120, yc = 90 and radius = 80. The GLE method was run with a half sign interslice force function for calculating the factor of safety.

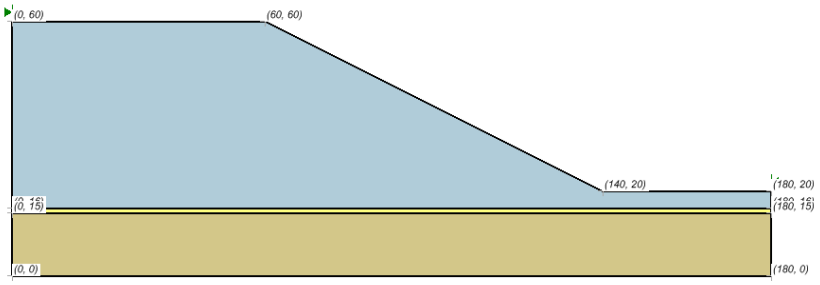

Figure 58 Geometry of the Fredlund and Krahn (1977) Weak Layer Slope model

Table 60 Material Properties of the Fredlund and Krahn (1977) Weak Layer Slope model

	c (psf)	ϕ (degrees)	γ (pcf)	Ru (case2)
Upper Soil	600	20	120	0.25
Weak Layer	0	10.0	120	0.25

3.11.2 Results and Discussions

The computer results for three cases are presented in Tables 56, 57 and 58 for Slope Stability, Fredlund and Krahn and Zhu et al, respectively.

Table 61 Composite Circular Results Slope Stability

Method	Case 1: Dry	Case 2: Ru	Case 3: WT
Ordinary	1.299	1.039	1.174
Bishop Simplified	1.382	1.123	1.242
Spencer	1.382	1.124	1.244
GLE/M-P	1.382	1.124	1.244

Table 62 Composite Circular Slip Surface Results Fredlund & Krahn (1977)

Method	Case 1: Dry	Case 2: Ru	Case 3: WT
Ordinary	1.288	1.029	1.171
Bishop Simplified	1.377	1.124	1.248
Spencer	1.373	1.118	1.245
GLE/M-P	1.370	1.118	1.245

Table 63 Composite Circular Slip Surface Results Zhu, Lee, and Jiang (2003)

Method	Case 1: Dry	Case 2: Ru	Case 3: WT
Ordinary	1.300	1.038	1.192
Bishop Simplified	1.380	1.118	1.260
Spencer	1.381	1.119	1.261
GLE/M-P	1.371	1.109	1.254

The computer results are also presented for each of the pore-water pressure conditions in Table 59 to 61. In this case, a comparison of 4 computer software package results is compared.

Table 64 Comparison of computed factors of safety for the Case of a Dry slope

Method	Factor of Safety					Difference (%)
	Fredlund & Krahn	Zhu, Lee & Jiang	Slide	Slope Stability		
				Moment	Force	
Ordinary	1.288	1.300	1.300	1.299		-0.08
Bishop Simplified	1.377	1.380	1.382	1.382		0.00
Spencer	1.373	1.381	1.382	1.382	1.382	0.00
M-P	1.370	1.371	1.372	1.372	1.372	0.00

Table 65 Comparison of computed factors of safety for the Case of a designated Ru value

Method	Factor of Safety					Difference (%)
	Fredlund & Krahn	Zhu, Lee & Jiang	Slide	Slope Stability		
				Moment	Force	
Ordinary	1.029	1.038	1.039	1.043		0.39
Bishop Simplified	1.124	1.118	1.124	1.123		-0.09
Spencer	1.118	1.119	1.118	1.124	1.124	0.54
M-P	1.118	1.109	1.118	1.114	1.114	-0.36

Table 66 Comparison of computed factors of safety for the Case of a designated water table, WT

Method	Factor of Safety					Difference (%)
	Fredlund & Krahn	Zhu, Lee & Jiang	Slide	Slope Stability		
				Moment	Force	
Ordinary	1.171	1.192	1.174	1.173		-0.09
Bishop Simplified	1.248	1.260	1.243	1.242		-0.08
Spencer	1.245	1.261	1.244	1.244	1.244	0.00
M-P	1.245	1.254	1.237	1.237	1.237	0.00

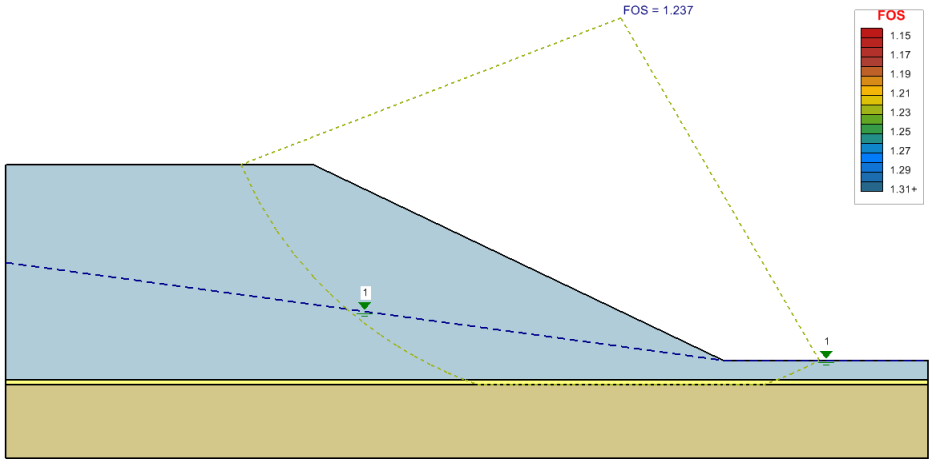

Figure 59 Solution when using Slope Stability and Ru value for the M-P method

3.12 LOW TWO LAYER SLOPE

Project: Slopes_Group_1
Model: VS_23

This model was originally published by Low (1989). The model consisted of a slope overlaying two soil layers. The soil properties defined are shown in Table 67. The middle and lower soils have constant and linear by varying undrained shear strengths.

3.12.1 Geometry and Material Properties

The position of the critical slip surface and the corresponding factor of safety were calculated for a critical slip surface using both the Bishop Simplified and Ordinary/Fellenius methods.

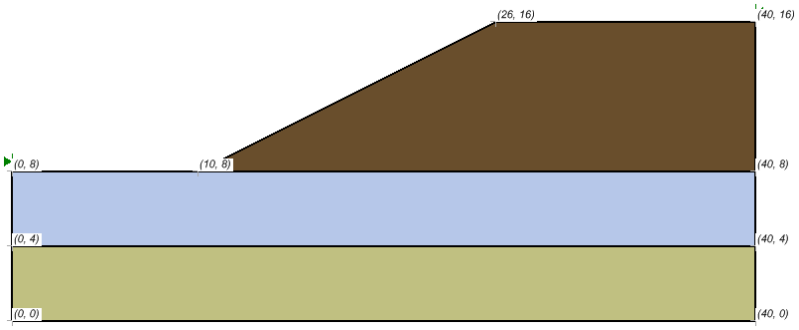

Figure 60 Geometry of the Low Two Layer Slope model

Table 67 - Material Properties of the Low Two Layer Slope model

	Cu_{top} (kN/m²)	Cu_{bottom} (kN/m²)	ϕ (degrees)	γ (kN/m³)
Upper Soil	95	95	15	20
Middle Soil	15	15	0	20
Lower Soil	15	30	0	20

3.12.2 Results and Discussions

The results of a circular slip surface analysis are presented in Table 63, showing a comparison with published results.

3.12.2.1 Circular Results

Table 68 Circular Results of the Low Two Layer Slope model

Method	Factor of Safety					Difference (%)
	Kim (2002)	Low (1989)	Slide	Slope Stability		
				Moment	Force	
Ordinary		1.36	1.37	1.365		-0.37
Bishop Simplified	1.17	1.14	1.192	1.175		-1.43

3.12.2.2 Grid and radius search method

The results of the grid and radius search method can be seen in the following figures.

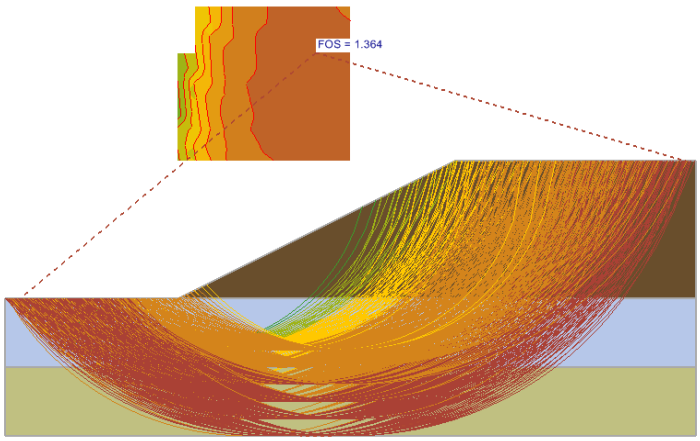

Figure 61 Circular Slip Surfaces using Ordinary/Fellenius Method

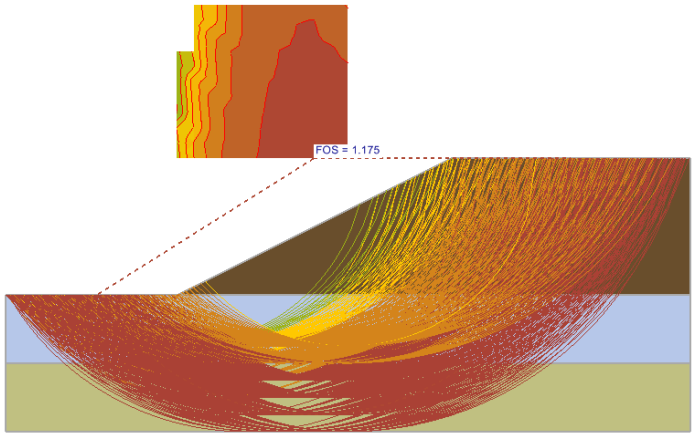

Figure 62 Circular Slip Surfaces using Bishop Simplified method

3.13 LOW THREE LAYER SLOPE

Project: Slopes_Group_1
Model: VS_24

This model is also taken from Low (1989) and it consists of a slope with three layers with three different undrained shear strength values.

3.13.1 Geometry and Material Properties

The geometry for a verification problem #24 is shown in Figure 63. The position of the critical slip surface and the corresponding factor of safety are calculated for a circular slip surface using both the Bishop Simplified and Ordinary/Fellenius methods. The material properties are shown in Table 69.

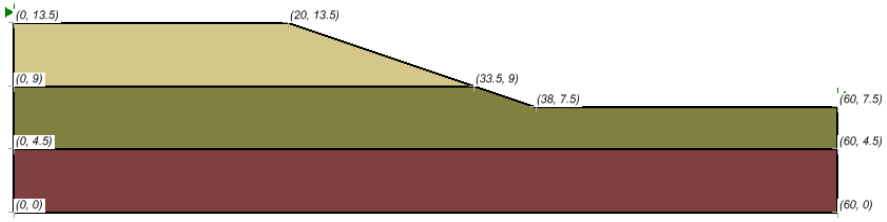

Figure 63 Geometry of the Low Three Layer Slope model

Table 69 Material Properties of the Low Three Layer Slope model

	Cu (kN/m^2)	(kN/m^3)
Upper Layer	30	18
Middle Layer	20	18
Bottom Layer	150	18

3.13.2 Results and Discussions

3.13.2.1 Circular Results

The following results were calculated using the auto refine search technique in Slope Stability.

Table 70 Circular Results–auto refine search technique

Method	Factor of Safety			Difference (%)
	Low (1989)	Slide	Slope Stability	
Ordinary	1.44	1.439	1.439	0.00
Bishop Simplified	1.44	1.439	1.439	0.00

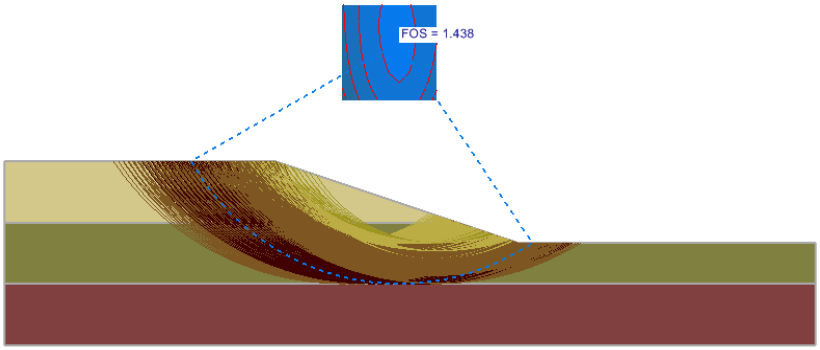

Figure 64 Circular Failure Surfaces using Bishop's Simplified method

3.14 CHEN AND SHAO FRICTIONLESS SLOPE

Project: Slopes_Group_1
Model: VS_25

Chen and Shao (1988) presented the problem to illustrate a plasticity solution for a weightless frictionless slope subjected to a vertical load. This problem was first solved by Prandtl (1921).

3.14.1 Geometry and Material Properties

The critical load position for the critical slip surface was defined by Prandtl and is shown in Figure 65. The critical failure surface has a theoretical factor of safety of 1.0.

The critical uniformly distributed load for failure is presented in the paper as 149.31 kN/m, with a length equal to the slope height of 10m.

NOTE:
A "custom" interslice shear force function was used with GLE and Morgenstern-Price methods as shown in Chen and Shao (1988).

x	F(x)
0	1
0.3	1
0.6	0
1	0

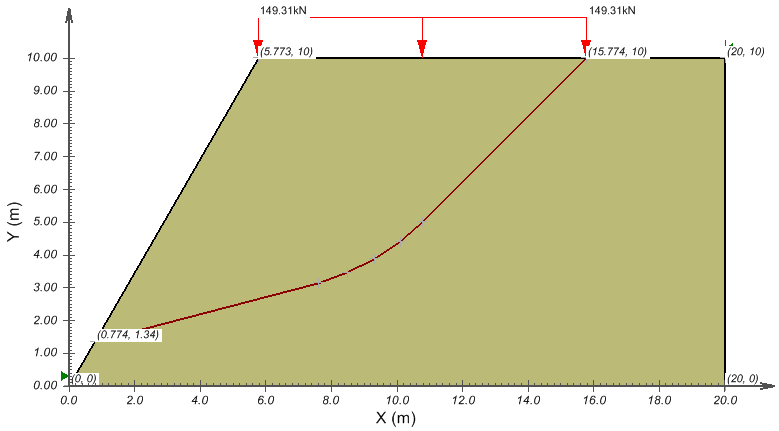

Figure 65 Geometry of the Chen and Shao Frictionless Slope model

Table 71 Material Properties of the Chen and Shao Frictionless Slope model

	c (kN/m^2)	ϕ' (degrees)	γ (kN/m^3)
Soil	49	0.0	1e-06

3.14.2 Results and Discussions

Table 72 Results of the Chen and Shao Frictionless Slope

Method	Factor of Safety				Difference (%)
	Theoretical F_s	Slide	Slope Stability		
			Moment	Force	
Spencer	1	1.051	1.049	1.049	-0.19
M-P	1	1.009	0.996	0.996	-1.29
GLE	1	1.009	1.000	1.000	-0.89

3.15 PRANDTL BEARING CAPACITY

Project: Slopes_Group_1
Model: VS_26

This verification test models the well-known Prandtl solution for bearing capacity; namely,

$$q_c = 2C(1+\pi/2)$$

3.15.1 Geometry and Material Properties

The material properties are given in Table 68. For an cohesion of 20kN/m^2, q_c is calculated to be 102.83 kN/m. A uniformly distributed load of 102.83kN/m was applied over a width of 10m as shown in Figure 68. The theoretical critical failure surface was used for the analysis.

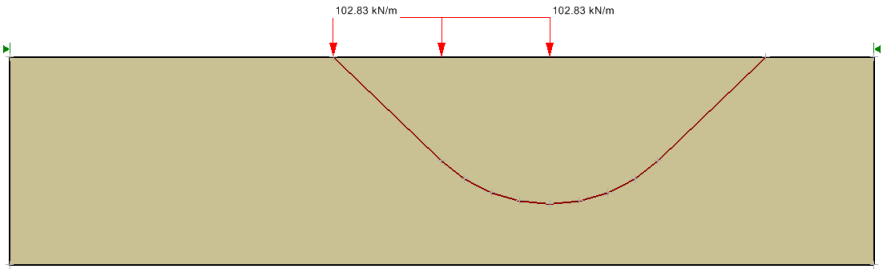

Figure 66 Geometry of the Bearing Failure model

Table 73 Material Properties of the Bearing Failure model

	c (kN/m^2)	ϕ' (degrees)	γ (kN/m^3)
Soil	20	0	1e-06

3.15.2 Results and Discussions

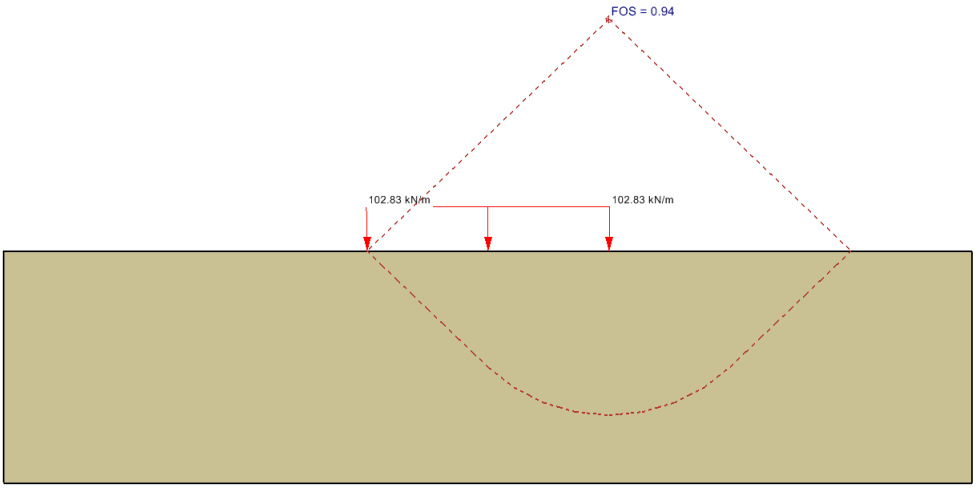

Figure 67 Presentation of the resulting factor of safety for the Prandtl bearing capacity problem

Table 74 Results of the Prandtl Bearing Capacity

Method	Factor of Safety				Difference (%)
	Theoretical F_s	Slide	Slope Stability		
			Moment	Force	
Spencer	1.000	0.941	0.940	0.939	-0.11

3.16 PRANDTL BEARING CAPACITY - NON-VERTICAL SLICES

Project: Slopes_ SarmaNonVerticalSlices
Model: VS_26_SarmaNonVerticalSlices

This verification test models the well-known Prandtl solution for bearing capacity; namely,

$$q_c = 2C(1+\pi/2)$$

3.16.1 Geometry and Material Properties

The material properties are given in Table 68. For an cohesion of 20kN/m^2, q_c is calculated to be 102.83 kN/m. A uniformly distributed load of 102.83kN/m was applied over a width of 10m as shown in Figure 68. The theoretical critical failure surface was used for the analysis.

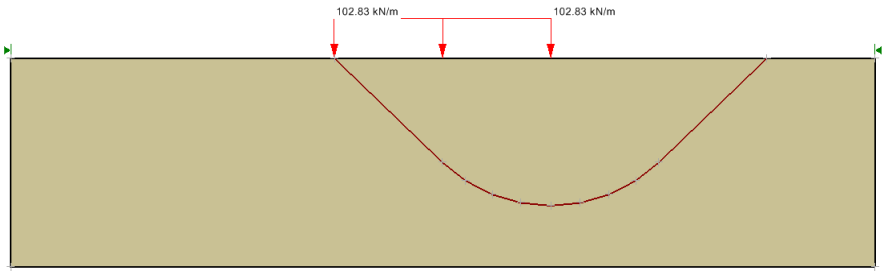

Figure 68 Geometry of the Bearing Failure model

Table 75 Material Properties of the Bearing Failure model

	c (kN/m^2)	ϕ' (degrees)	γ (kN/m^3)
Soil	20	0	1e-06

3.16.2 Results and Discussions

For this model, the vertical slices method gives a FOS of about 0.94, and the Sarma Non-Vertical Slices analysis can give the exact FOS from the theoretical solution.

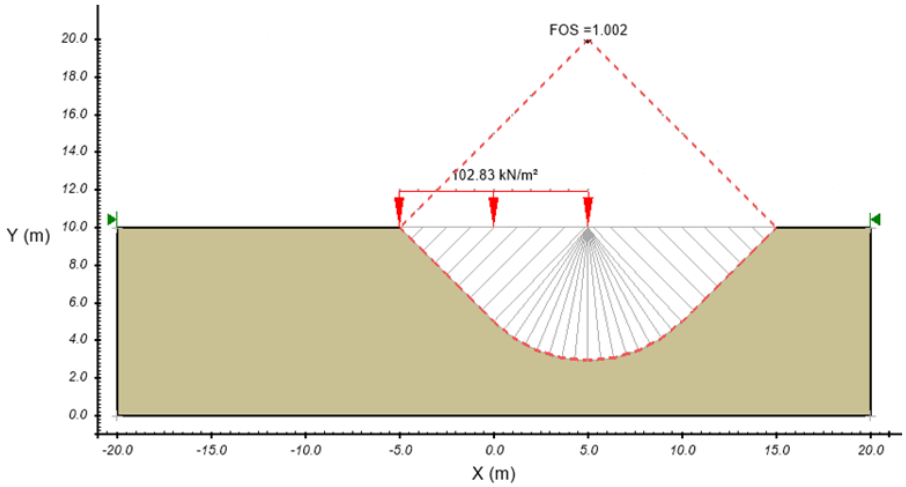

Figure 69 Resulting factor of safety for the Prandtl bearing capacity problem using Sarma Non-Vertical Slices analysis

Table 76 Results of the Prandtl Bearing Capacity

Method	Factor of Safety				Difference (%)
	Theoretical F_s	Slide	Slope Stability		
			Moment	Force	
Sarma Non-Vertical Slices	1.000	1.002	1.002		0.0

3.17 CHOWDHURY AND XU (1995)

Project: Slopes_Group_1
Model: VS_28

This set of verification problems were originally published by Chowdhury and Xu (1995). The Congress St. Cut model, which was first analyzed by Ireland (1954), contained the geometry for the first four examples.

3.17.1 Purpose

The purpose of these models is to perform a statistic analysis in which the probability of failure is calculated when the input parameters are represented in terms of means and standard deviations.

3.17.2 Geometry and Material Properties

In each of these examples 1 to 4, two sets of circular slip surfaces are considered. One set places the failure surface tangential to the lower boundary of Clay 2 layer and the second considers the slip surface tangential to the lower boundary of Clay 3. The soil models used for both clays are constant undrained shear strength.

NOTE:
Chowdhury and Xu do not consider the strength of the upper sand layer in the examples 1 to 4. As well, they use the Bishop Simplified method for all their analysis.

The unit weights for soil materials are not provided in the original paper by Chowdhury and Xu. Information also is not provided regarding the geometry of the critical slip surface.

In this particular example, material unit weights that enable Slope Stability to obtain factor of safety values, similar to those in addicted in the paper are used.

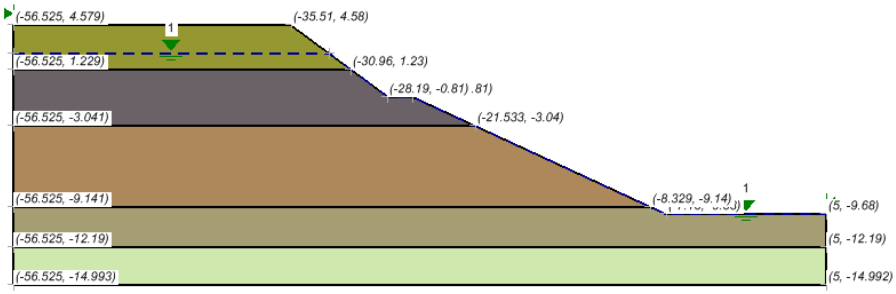

Figure 70 Geometry of the VS_28 Example 1

3.17.3 Example #1

Table 77 Example 1 Input Data

	Soil Layer		
	Clay 1	**Clay 2**	**Clay 3**
	c_1	c_2	c_3
Mean (kPa)	55	43	56
Stdv. (kPa)	20.4	8.2	13.2
γ (kN/m³)	21	22	22

Table 78 Results of Example 1 with Layer 2

Method	Factor of Safety							Difference (%)
	Chowdhury and Xu		Slide		Slope Stability			
					Moment	Force		
	Fs	PF(%)	Fs	PF(%)	Fs		PF(%)	
Bishop Simplified	1.128	26.592	1.128	24.61	1.128		24.35	0.00

Table 79 Results Example 1 with Layer 3

Method	Factor of Safety							Difference (%)
	Chowdhury and Xu		Slide		Slope Stability			
					Moment	Force		
	Fs	PF(%)	Fs	PF(%)	Fs		PF(%)	
Bishop Simplified	1.109	27.389	1.109	27.89	1.111		26.35	0.18

3.17.4 Example #2

Table 80 Example 2 Input Data

	Soil Layer		
	Clay 1	**Clay 2**	**Clay 3**
	c_1	c_2	c_3
Mean (kPa)	68.1	39.3	50.8
Standard Deviation (kPa)	6.6	1.4	1.5
γ (kN/m³)	21	22	22

Table 81 Results of Example 2 with Layer 2

Method	Factor of Safety							Difference (%)
	Chowdhury and Xu		Slide		Slope Stability			
					Moment	Force		
	F_S	PF(%)	F_S	PF(%)	F_S		PF(%)	
Bishop Simplified	1.1096	0.48	1.108	0.37	1.108		0.39	0.00

3.17.5 Example #3

Table 82 Example 3 Input Soil Data

	Soil Layer		
	Clay 1	Clay 2	Clay 3
	c_1	c_2	c_3
Mean (kPa)	136	80	102
Standard Deviation (kPa)	50	15	24
γ (kN/m^3)	21	22	22

	Chowdhury and Xu		Slope Stability	
Failure Mode (Layer)	Factor of Safety (Bishop Simplified)	Probability of Failure	Factor of Safety (Bishop Simplified)	Probability of Failure
Layer 2 (Clay 1)	2.2343	0.1151	2.244	0.0003
Layer 3 (Clay 2)	2.1396	0.00242	2.133	0.0008

3.17.6 Example #4

Table 83 Example 4 Input Data

	Soil Layer					
	Clay 1		Clay 2		Clay 3	
	c_1 (kPa)	ϕ_1 (°)	c_2 (kPa)	ϕ_2 (°)	c_3 (kPa)	ϕ_3 (°)
Mean (kPa)	55	5	43	7	56	8
Standard Deviation (kPa)	20.4	1	8.7	1.5	13.2	1.7
γ (kN/m^3)	17		22		22	

	Chowdhury and Xu		Slope Stability	
Failure Mode (Layer)	Factor of Safety (Bishop Simplified)	Probability of Failure	Factor of Safety (Bishop Simplified)	Probability of Failure
Layer 2 (Clay 1)	1.4239	0.01559	1.423	0.0217
Layer 3 (Clay 2)	1.5075	0.00468	1.506	0.005

3.17.7 Example #5

This example illustrates the stability of an embankment on a soft clay foundation. Two circular slip surface failure conditions are again considered. First slip surface one is tangent to the interface of the embankment and the foundation and second slip surface one is tangent to the lower boundary of the soft clay foundation.

Probabilities of failure are presented in the original paper by Chowdhury and Xu (1995), which are calculated using a commonly used definition of reliability index. As well, as assumption that all factor of safety distributed.

Slope Stability makes use of the Monte Carlo technique in calculating the probability of failure. It is assumed that all input variables used in Slope Stability are normally distributed.

Table 84 Example 5 Input Data

	Soil Layer			
	Layer 1		Layer 2	
	c_1 (kPa)	ϕ_1 (°)	c_2 (kPa)	ϕ_2 (°)
Mean (kPa)	10	12	40	0
Standard Deviation (kPa)	2	3	8	0
γ (kN/m3)	20		18	

	Chowdhury and Xu		Slope Stability	
Failure Mode (Layer)	**Factor of Safety (Bishop Simplified)**	**Probability of Failure**	**Factor of Safety (Bishop Simplified)**	**Probability of Failure**
Layer 1	1.1625	0.20225	1.159	0.1966
Layer 2	1.1479	0.19733		

Table 85 Material Properties

	c (kN/m^2)	ϕ (degrees)	γ (kN/m^3)
Sand	0	0	21

3.18 DUNCAN – LASH TERMINAL

Project: Slopes_Group_1
Model: VS_29

Duncan (2000) published a model that examines the failure of the 100ft high underwater slope at the lighter Abroad Ship (LASH) terminal at the Port of San Francisco, U.S.A.

The values that are used in this analysis were published by Duncan (2000). It was assumed that the cohesion was 100 psf an deviation of –20ft and increases linearly with depth at the rate of 9.8psf per ft.

The Latin-HyperCube simulation technique was performed using 10000 samples to compute both the probability of failure and the reliability index of the estimated failure surface, as defined with Duncan, (2000). Janbu, Spencer, and GLE methods were used to computer the factors of safety.

3.18.1 Geometry and Material Properties

The model geometry is illustrated in Figure 71.

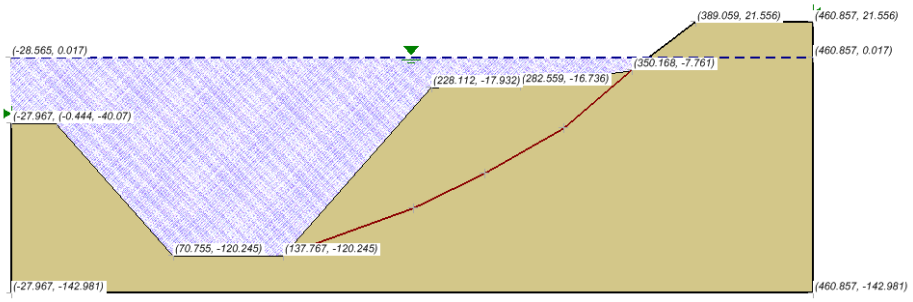

Figure 71 Geometry of the Duncan (2000) model

3.18.2 Results and Discussions

Table 86 Results of the Duncan (2000) model

Method	Factor of Safety		Difference (%)
	Slide	Slope Stability	
Janbu Simplified	1.127	1.138	0.98
Spencer	1.150	1.159	0.78
GLE	1.161	1.163	0.17

Note: Probability analysis cannot be performed at this time, because the cohesion change with depth is not included in Slope Stability.

3.19 BORGES AND CARDOSO - GEOSYNTHETIC EMBANKMENT

Project: Slopes_Group_1
Model: VS_30_case1, VS_30_case2

This example considers the stability of a geosynthetic-reinforced embankment on soft soil. The problem was originally published by Borges and Cardoso (2002).
The sand embankment region is represented by Mohr-Coulomb strength model and the foundation material is soft clay in which it contains varied undrained shear strength. The geosynthetic has a tensile strength of 200 KN/m, is not anchored, and has no adhesion.

3.19.1 Geometry and Material Properties

It also has a frictional resistance against slip of 33.7 degrees. The reinforcement force for this example is assumed to be parallel to the reinforcement.

This model is analyzed using the Bishop Simplified method. Since the original authors used the moment based limit equilibrium method for this model, the reinforcement is modeled as a passive force. This procedure is consistent with how the authors implemented reinforcement forces in the limit equilibrium methods in Slope Stability.

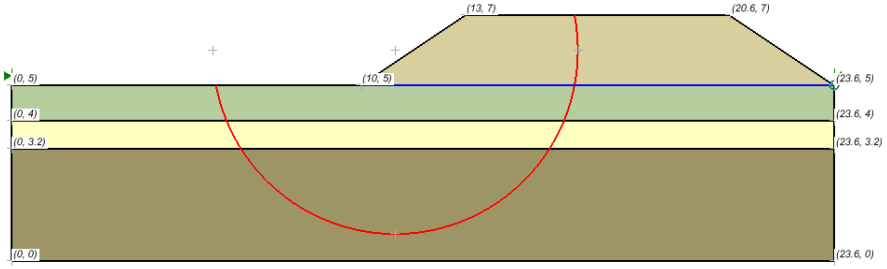

Figure 72 Geometry of the Borges and Cardoso Geosynthetic Embankment Case 1

Table 87 Material Properties of Borges and Cardoso-Embankment

	c (kN/m^2)	ϕ (degrees)	γ (kN/m^3)
Embankment	0	35	20

	c_u top (kN/m^2)	c_u bottom (kN/m^2)	γ (kN/m^3)
Upper Clay	8.490	8.490	17
Middle Clay	8.490	4.725	17
Lower Clay	4.725	13.125	17

3.19.2 Results and Discussion

Table 88 Results for Case 1

Method	Factor of Safety (Case 1-single circular)				Difference (%)
	Borges & Cardoso	Slide	Slope Stability		
			Moment	Force	
Bishop Simplified	1.74	1.659	1.664		0.30

Table 89 Results for Case 2

Method	Factor of Safety (Case 2-single circular)				Difference (%)
	Borges & Cardoso	Slide	Slope Stability		
			Moment	Force	
Bishop Simplified	1.77	1.692	1.696		0.24

3.20 BORGES AND CARDOSO - GEOSYNTHETIC EMBANKMENT #2

Project: Slopes_Group_1
Model: VS_31_Case1, VS_31_Case2

This model looks at the stability of a geosynthetic-reinforced embankment placed over a soft soil. This model was original published by Borges and Cardoso (2002). This is their Case 2 example.

The model is set up as a more compotent material overlaying soft clay with varying undrained shear strength. The geosynthetic has a tensile strength of 200 KN/m and a frictional resistance of 33.7 degrees. The geosynthetic is not anchored and has no adhesion.

In this case, the reinforcement force is parallel to the reinforcement. The Bishop Simplified method was used to analyze this model. The reinforcement is modeled as a passive force. This corresponds to the manner in which the authors implemented the reinforcement force in their original papers.

3.20.1 Geometry and Material Properties

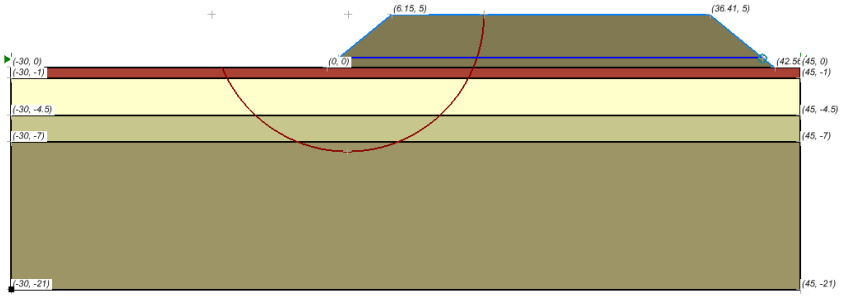

Figure 73 Geometry of the VS_31 Case 1 Example by Borges and Cardoso (2002)

Table 90 Material Properties of Borges and Cardoso – Embankment #2

	c (kN/m^2)	ϕ (degrees)	γ (kN/m^3)
Embankment	0	35	20
	c_u top (kN/m^2)	c_u bottom (kN/m^2)	γ (kN/m^3)
Clay 1	33	33	17
Clay 2	16	16	17
Clay 3	16	18.4	17
Clay 4	18.4	55.1	17

3.20.2 Results and Discussions

Table 91 Results for the VS_31 Case 1 example by Borges and Cardoso (2002)

Method	Factor of Safety (Case 1 - single circular slip surface)						Difference (%)
	Borges & Cardoso	Slide			Slope Stability (Slice = 30)		
		Slices = 25 (on Manual)	Slices = 30	Slices = 40	Moment	Force	
Ordinary		1.346	1.346	1.323	1.346		0
Bishop Simplified	1.19	1.176	1.176	1.166	1.176		0.00
Janbu Simplified		1.208	1.208	1.205		1.207	-0.08

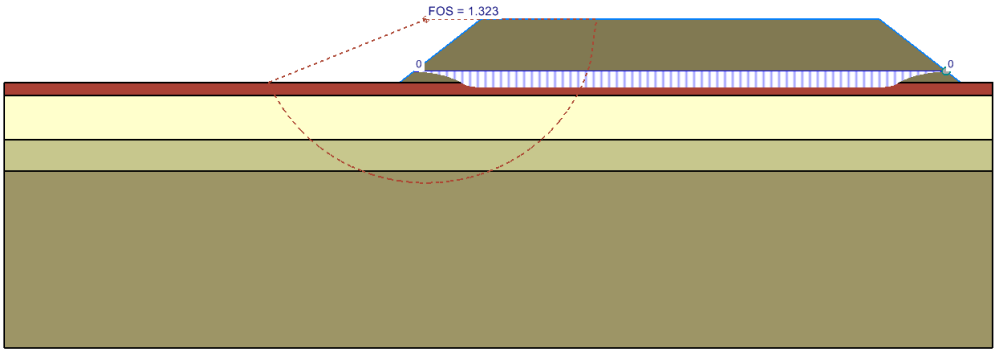

Figure 74 Results of the VS_31 Case 1 using the Ordinary method

Table 92 Results of Case 2 example by Borges and Cardoso (2002)

Method	Factor of Safety (Case 2 - single circular slip surface)						Difference (%)
	Borges & Cardoso	Slide			Slope Stability		
		Slices = 25 (on Manual)	Slices = 30	Slices = 40	Moment	Force	
Ordinary		1.282	1.282	1.277	1.282		0.00
Bishop Simplified	1.15	1.163	1.162	1.16	1.163		-0.06
Janbu Simplified		1.17	1.17	1.169		1.171	-0.09

3.21 BORGES AND CARDOSO - GEOSYNTHETIC EMBANKMENT #3

Project: Slopes_Group_1
Model: VS_32Case1, VS_32Case2, VS_32Case3

This is the case 3 example taken from Borges and Cardoso (2002). This particular model looks at the stability of a geosynthetic-reinforced embankment on soft soil.

3.21.1 Geometry and Material Properties

The material properties are the same as the previous two examples. The geosynthetic in this case has the tensile strength of 200 KN/m as well as a frictional resistance of 39.6 degrees. The Bishop Simplified analysis method is used for consistency with the method used by the authors.

The two embankment materials are implemented in the model. The lower embankment material is 0 to 1 m and the upper embankment material is from 1 to 7 m (Case 1) or 1 to 8.75m (Case 2). The geosynthetic is placed at the elevation 0.9 m, just inside on the lower embankment material.

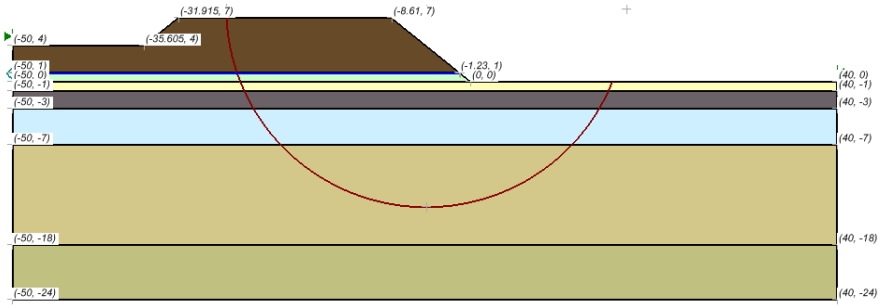

Figure 75 Geometry of the VS_32_Case 1 model

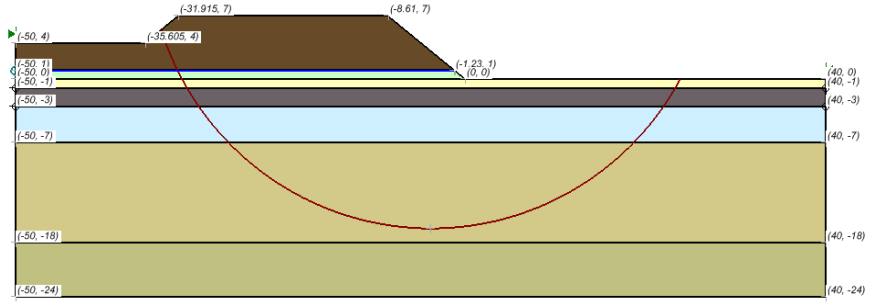

Figure 76 Geometry of the VS_32_Case 2 model

Table 93 Material Properties

	c (kN/m^2)	ϕ (degrees)	γ (kN/m^3)
Upper Embankment	0	35	21.9
Lower Embankment	0	33	17.2

	c_u (kN/m^2)	γ (kN/m^3)
Clay 1	43	18
Clay 2	31	16.6
Clay 3	30	13.5
Clay 4	32	17
Clay 5	32	17.5

3.21.2 Results and Discussions

Table 94 Results Case 1-Embankment Height = 7m

	Slope Stability Factor of Safety	Overturning Moment (kN/m/m)	Resisting Moment (kN/m/m)
Circle A (Slope Stability)			
Circle A (Borges & Cardoso)		34166	42695
Circle B (Slope Stability)			
Circle (Borges & Cardoso)		63870	75754

Table 95 Results Case 2-Embankment Height = 8.75m

	Slope Stability Factor of Safety	Overturning Moment (kN/m/m)	Resisting Moment (kN/m/m)
Circle C (Slope Stability)		64873	63846
Circle C (Borges & Cardoso)		65116	64784

Table 96 Results for Case 1

Method	Factor of Safety (Case 1)				Difference (%)
	Borges & Cardoso	Slide	Slope Stability		
			Moment	Force	
Bishop Simplified	1.25	1.225	1.227		0.16

Table 97 Results for Case 2

Method	Factor of Safety (Case 2)				Difference (%)
	Borges & Cardoso	Slide	Slope Stability		
			Moment	Force	
Bishop Simplified	1.19	1.219	1.220		0.08

Table 98 Results for Case 3

Method	Factor of Safety (Case 3)				Difference (%)
	Borges & Cardoso	Slide	Slope Stability		
			Moment	Force	
Bishop Simplified	0.99	0.984	0.984		0.00

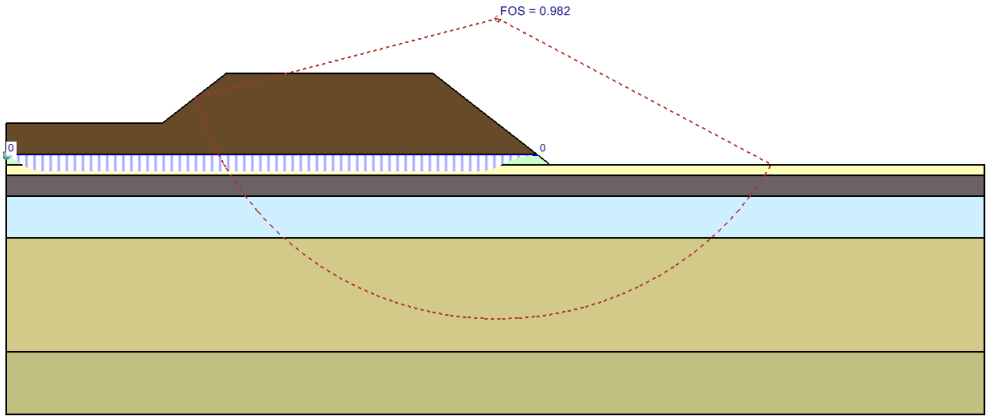

Figure 77 Results of the VS_32_Case 3 model using the Bishop Simplified method

3.22 SYNCRUDE PROBABILISTIC TAILINGS DYKE

Project: Slopes_Group_1
Model: VS_33

This example model was published by El-Ramly et al (2003). This model is designed for the calculation of the factor of safety for a Syncrude tailings dyke in Alberta, Canada. In this case, a probabilistic analysis is performed.

This paper does not consider spaciously variation of soil properties, and is therefore described as a simplified probabilistic analysis. The original geometry from the El-Ramly et al (2003) paper is shown in Figure 78.

The material parameters are input into Slope Stability as shown in Table 99. The soil parameters were considered probabilistic by El-Ramly et al. They varied the friction angle of the Kca clay-shale, the pore pressure ratio in the same layer, the friction angle of the Pgs sandy till layer and the pore pressure ratios in this layer in the middle and the toe of the dyke.

In the Slope Stability model we consider the variation of the friction angles of the Kca clay-shale and Pgs sandy till. The phreatic surface indicated in Figure 79 was used in place of the pore pressure ratios. In order in to be consistent the El-Ramly paper the Bishop Simplified analysis method was used.

A Monte Carlo analysis was used to calculate the probability of failure. It is worth noting that it is assumed that all probabilistic input parameters are normally distributed.

3.22.1 Geometry and Material Properties

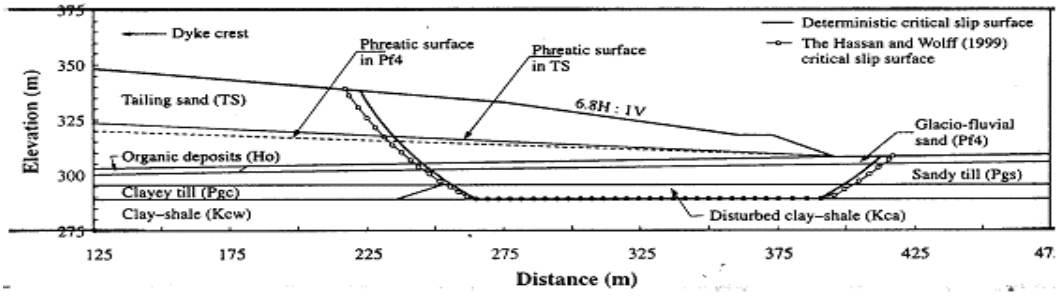

Figure 78 Original Geometry of the Syncrude Tailings Dyke model

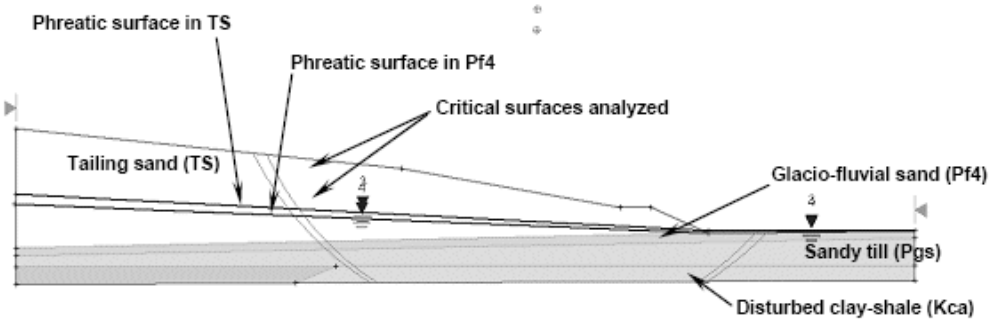

Figure 79 Phreatic Surface

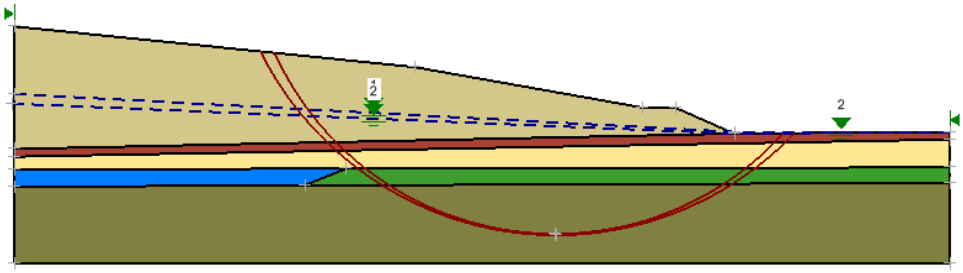

Figure 80 Geometry of the Syncrude Tailing Dyke model

Table 99 Material Properties of the Syncrude Tailing Dyke model

	c (kN/m^2)	ϕ (degrees)	Standard Deviation of ϕ (degrees)	γ (kN/m^3)
Tailings sand	0	34	-	20
Glacio-fluvial sand	0	34	-	17
Sandy till	0	34	-	17
Clayey Till	0	7.5	-	17
Distributed clay-shale	0	7.5	-	17

3.22.2 Results and Discussions

Table 100 Results of the Syncrude Tailing Dyke model

Method	Factor of Safety								Difference (%)
	El-Ramly		Slide			Slope Stability			
				Probabilistic			Probabilistic		
	Determ	PF(%)	Determ	Mean	PF(%)	Determ	Mean	PF(%)	
Bishop Simplified	1.31	0.16	1.305	1.327	0.154	1.303	1.304	3.65	-0.15

3.23 CANNON DAM

Project: Slopes_Group_1
Model: VS_34_Monte

The Cannon Dam model was published from Wolff and Harr (1987). The probabilistic analysis results from Slope Stability are compared to the results published in the paper by Wolff and Harr for a noncircular slip surfaces. Wolff and Harr (1987) used the point-estimate method for their probability analysis failure for the Cannon Dam.

The location of critical slip surface was taken from their paper. The input parameters; namely, friction angle for the Phase I and Phase II fills was calculated. The unit weights of the fills were back-calculated in order to match the factor of safety computed by Wolff and Harr. Wolff and Harr (1987) based on the stochastic properties provided in the paper originally published results that only satisfied force equilibrium.

3.23.1 Geometry and Material Properties

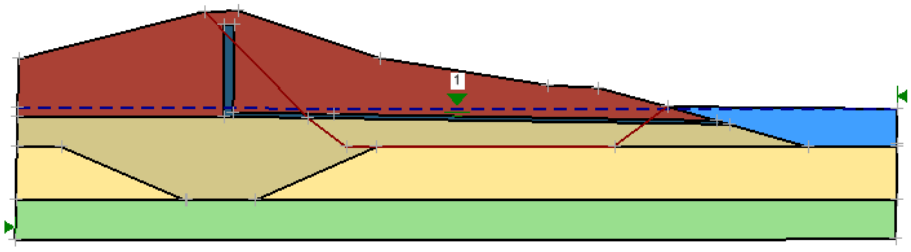

Figure 81 Geometry of the Cannon Dam model – VS_34

Table 101 Material Properties of the Cannon Dam

Material	c (lb/ft^2)	Standard Deviation of c (lb/ft^2)	ϕ (degrees)	Standard deviation of ϕ (degrees)	Correlation coefficient for c and ϕ	γ (lb/ft^3)

Phase I fill	2,230		6.33			150
Phase II fill	2,901.6		14.8			150
Material 3	1		50			150
Material 4	1		35			150
Spoil Fill	3,000		60			150
Filter	-		35			120

3.23.2 Results and Discussions

The results were compared to those obtained by GLE and the Spencer methods. It is assumed in the Slope Stability model that all the probabilistic input variables are normally distributed.

Table 102 Results of the Cannon Dam

Method	Factor of Safety								Difference (%)
	Wolff and Harr		Slide			Slope Stability			
				Probabilitistic			Probabilitistic		
	Deterministic	PF(%)	Deterministic	Mean	PF(%)	Deterministic	Mean	PF(%)	
Spencer	2.36	4.55	2.383	2.401	0.355	2.386	2.386		0.13
GLE			2.333	2.358	0.355	2.343	2.343		0.43

3.24 CANNON DAM #2

Project: Slopes_Group_1
Model: VS_35_1_Fig.7_SurfaceA, VS_35_1_Fig.7_SurfaceB, VS_35_1_Fig.7_SurfaceC, VS_35_1_Fig.7_SurfaceD, VS_35_1_Fig.7_SurfaceE, VS_35_1_Fig.8_SurfaceB, VS_35_1_Fig.8_SurfaceF, VS_35_1_Fig.8_SurfaceG, VS_35_1_Fig.8_SurfaceH

This model of the Cannon Dam in Missouri was presented by Hassan and Wolff (1999). The purpose of this verification model is to look at duplicating reliability index results for several circular failure surfaces as specified in the original paper. Hassan and Wolff (1999) presented a new reliability based approach in their paper. The cross-section of the Cannon Dam is shown below. The Bishop Simplified method of slices was used to analyze this verification problem. The present set of slip circles are those shown in Figure 82 of the Hassan and Wolff paper and Figure 83 shows the model input parameters.

The Hassan and Wolff (1999) paper does not provided all the required input parameters. Therefore we selected values for the missing parameters that allowed to us to match the factors of safety for some of the circles slip surfaces shown in Figure 82. The assumption is made in this analysis that all the probabilistic input variables are normally distributed for performing the Monte Carlo simulations.

The reliability indices calculated in Slope Stability are based on the mean and standard deviations of the factor of safety values calculated in the simulations. The reliability indices shown in the results section are calculated using the assumption that the factors of safety values are log-normally (Hassan and Wolff, 1999). The results obtained from Slope Stability and the results from Hassan and Wolff are shown in Table 104.

3.24.1 Geometry and Material Properties

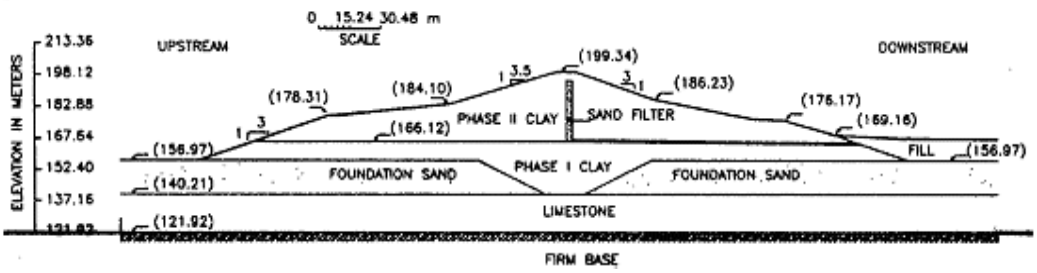

Figure 82 Hassan and Wolff's Geometry

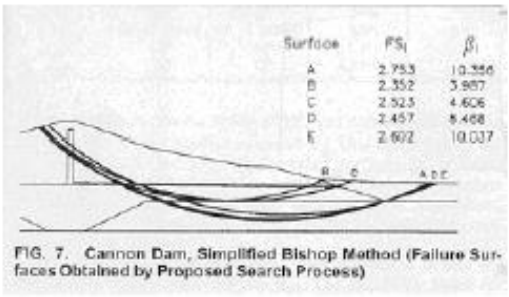

FIG. 7. Cannon Dam, Simplified Bishop Method (Failure Surfaces Obtained by Proposed Search Process)

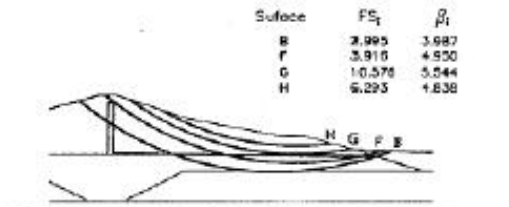

FIG. 8. Cannon Dam, Simplified Bishop Method (Search around Located Surface of Minimum Reliability Index)

Figure 83 Hassan and Wolff (1999) paper

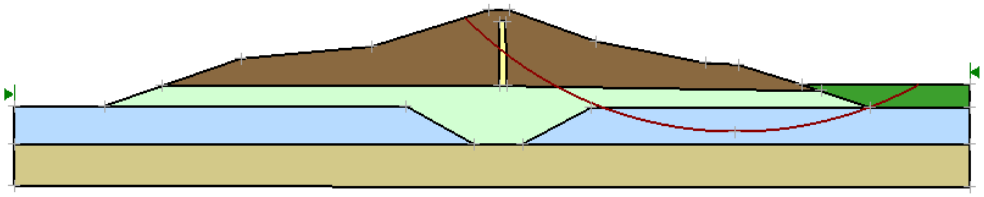

Figure 84 Geometry of VS_35_1_Fig7_Surface A - Cannon Dam #2

Table 103 Material Properties of the Cannon Dam #2

Material	c (lb/ft^2)	Standard Deviation of c (lb/ft^2)	ϕ (degrees)	Standard deviation of ϕ (degrees)	Correlation coefficient for c and ϕ	γ (lb/ft^3)
Phase I clay fill	117.79	58.89	8.5	8.5	0.1	22
Phase II clay fill	143.64	79	15	9	-0.55	22
Sand Filter	0	-	35	-	-	22
Foundation sand	5	-	18	-	-	22
Spoil fill	5	-	35	-	-	25

3.24.2 Results and Discussions

Table 104 Results of the Cannon Dam #2

		Factor of Safety										
		Hanssan and Wolff		Slide				Slope Stability				
					Probabilitistic				Probabilitistic			
Surfaces	Method	Determ	Reliability Index-lognormal	Determ	Mean	RI-Lognormal	PF(%)	Determ	Mean	RI	PF(%)	Difference (%)
Figure 7 Surface A	Bishop	2.8	4.55	2.551	2.6	10.95	0	2.55	2.664	9.00	0	-0.04
Figure 7 Surface B	Bishop	2.4	3.987	2.82	3.1	4.351	0.1	2.818	3.166	4.25	0.3	-0.071
Figure 7 Surface C	Bishop	2.5	4.606	2.777	3.1	4.263	1.2	2.782	3.117	4.21	0.3	0.18
Figure 7 Surface D	Bishop	2.5	8.468	2.583	2.6	11.09	0	2.582	2.697	9.07	0	-0.04
Figure 7 Surface E	Bishop	2.6	10.04	2.692	2.8	10.28	0	2.691	2.824	8.42	0	-0.04
Figure 8 Surface B	Bishop	3	3.987	2.676	2.9	4.858	0	2.676	3.141	4.21	0	0.00
Figure 8 Surface F	Bishop	3.9	4.95	3.598	3.8	5.485	0	3.596	3.984	5.03	0	-0.06
Figure 8 Surface G	Bishop	11	5.544	6.074	6.1	5.563	0	6.071	6.670	4.84	0.3	-0.05
Figure 8	Bishop	6.3	4.838	11.23	11	6.394	0	11.224	12.26	5.95	0	-0.05

3.25 LI AND LUMB - RELIABILITY INDEX

Project: Slopes_Group_1
Model: VS_36

This model is original presented in Li and Lumb (1987) and Hassan and Wolff (1999). The purpose of this model is to analyze the reliability indices of a simple homogenous slope. The verification compares of the reliability index of the deterministic global circular surface and the minimum reliability index value obtained from an analysis of multiple slip surfaces.

3.25.1 Geometry and Material Properties

The geometry is presented in Figure 85 and the material properties are presented in Table 105. In this analysis the Bishop Simplified method of analysis was used. A Monte Carlo analysis was used which assumes that all input probability variables are normally distributed.

The reliability indices are calculated on the assumption that the factors of safety values are distributed log normal. This interpretation is consisted with the original analysis presented by Hassan and Wolff (1999). Separate reliability indices are calculated for the minimum deterministic critical slip surface, as well as the critical probabilistic slip surface.

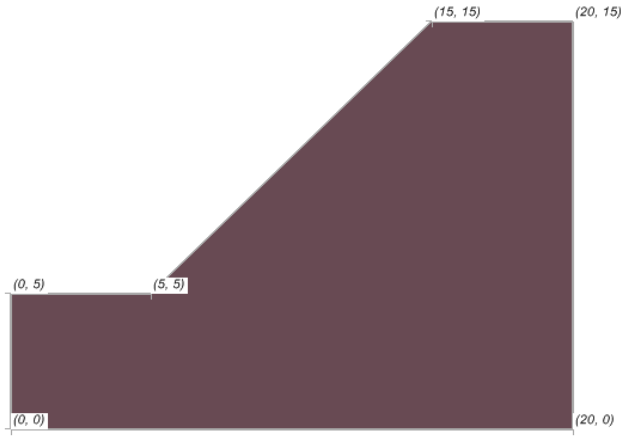

Figure 85 Geometry of the Li and Lumb – Reliability Index model

Table 105 Material Properties of the Li and Lumb (1987) reliability index

Property	Mean Value	Standard deviation
c (kN/m^2)	18	3.6
ϕ (degrees)	30	3
γ (kN/m^3)	18	0.9
R_u	0.2	0.02

3.25.2 Results and Discussions

The overall reliability indices of the slope are compared with reliability calculated by Hassan and Wolff (1999). The results are shown in the Table 106:

Table 106 Results of the Li and Lumb (1987) reliability index

	Factor of Safety								
	Hassan and Wolf (1999)		Slide			Slope Stability			
Method		Reliability Index Log normal	F_S	Reliability Index Log normal	Probability of Failure (%)	F_S	Reliability Index Log normal	Probability of Failure (%)	Difference (%)
Bishop Simplified			1.339			1.338			-0.08
Janbu Simplified			1.261			1.257			-0.32

3.26 REINFORCEMENT BACK ANALYSIS

Project: Slopes_Group_1
Model: VS_37_NoReinforcement, VS_37_ReinZone

This model is originally presented in the reference manual of slope stability program XSTABL (1999). A back analysis is used to determine the amount of reinforcement required to stabilize a slope.

Relatively simple geometry and slope conditions are used along with one non-cohesive soil material. The analysis proceeds in two steps:

- Determining the reinforcement needed to stabilize a slope to predetermine a factor of safety value of 1.5, and
- Establishing the minimum required length of reinforcement.

In Figure 86 it describes the slope model and the solution. In XSTABL the slip surfaces past only through the toe of the slope. This type of restriction has been duplicated in Slope Stability by placing an exist point near the toe of the slope.

3.26.1 Geometry and Material Properties

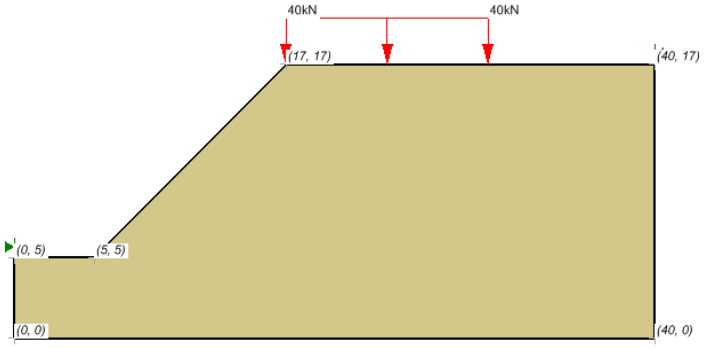

Figure 86 Geometry of the NoReinforcement Back Analysis model

It should also be noted that when there is no cohesive, the slip surface would tend to rise to the ground surface. Therefore, a minimum depth was imposed on considered slip surfaces. The next step involved changing the slope and including a reinforced zone with a higher friction angle calculated from the formula presented in the XSTABL Reference Manual, (1999).

$$\phi_{reinf} = \tan^{-1}\left[F_r \tan(\phi)\right]$$

$$where F_r = \frac{F_{\min}}{F_{crit}}$$

The length of the reinforced zone was varied manually until the factor of safety value very close to 1.5 was obtained. The results can be seen in Table 107.

3.26.2 Results and Discussions

Table 107 Results Back Analysis – Reinforcement

Method	Factor of Safety		Difference (%)
	Slide	Slope Stability	
Ordinary		0.756	
Bishop Simplified	0.765	0.76	0.71
Janbu Simplified	0.739	0.756	2.30

Table 108 NoReinforcement

Method	Factor of Safety		Difference (%)
	Slide	Slope Stability	
Bishop Simplified	0.765	0.771	0.78
Janbu Simplified	0.739	0.743	0.54

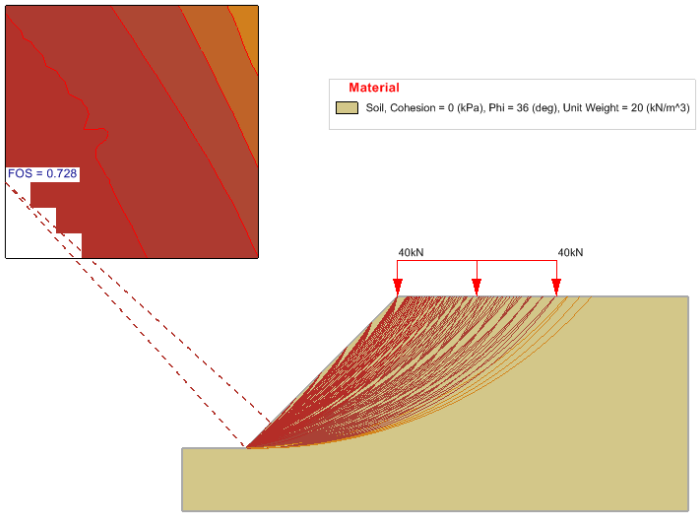

Figure 87 Results of the NoReinforcement Back Analysis model

Table 109 Reinforced Zone, neglect pore-water pressures and no cracks

Method	Factor of Safety				Difference (%)
	Slope/W		Slope Stability		
	Moment	Force	Moment	Force	
Ordinary					
Bishop Simplified	1.504		1.533		1.93
Janbu Simplified		1.247		1.279	2.57

3.27 TANDJIRIA – GEOSYNTHETIC REINFORCED EMBANKMENT

Project: Slopes_Group_1
Model: VS_39_Clay_NoRein_Circular, VS_39_Clay_NoRein_NonCircular, VS_39_Clay_Rein_Circular, VS_39_Clay_Rein_NonCircular,
VS_39_Sand_NoRein_Circular, VS_39_Sand_NoRein_NonCircular,
VS_39_Sand_Rein_Circular, VS_39_Sand_Rein_NonCircular

This model was originally presented by Tandjiria (2002) as their example #1 problem. The stability of a geosynthetic-reinforced embankment on soft soil was examined. This problem examines the stability of the embankment when it consists of sand or an undrained clay fill. The objective of this example is to compute the required reinforcement force to yield a factor of safety of 1.35.

Circular and noncircular critical slip surfaces were examined. In each case presented, the embankment was first modeled without reinforcement and the critical slip surfaces determined. Then the determined critical slip surface was used in the reinforcement model to determine the reinforcement force to achieve a factor of safety of 1.35.

The above approach was used for both the clay embankment with a circular and noncircular slip surface. All cases incorporate a tension crack in the embankment. Water is allowed to fill the tension cracks in the case of the clay embankment.

In this case the reinforcement was located at the base of the embankment. Both Spencer and GLE methods were used to analyze the slope. The GLE method used a half sine interslice function.

NOTE:
The reinforcement is modeled as an active force since Tandjiria (2002) modeled the force in this manner.

3.27.1 Geometry and Material Properties

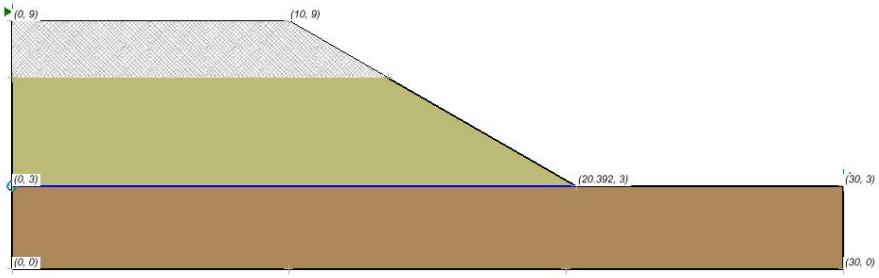

Figure 88 Clay Fill Embankment (circular) Reinforcement

Table 110 Material Properties of the clay fill embankment

	c_u/c (kN/m^2)	ϕ (degrees)	γ (kN/m^3)
Clay Fill Embankment	20	0	19.4
Sand Fill Embankment	0	37	17.0
Soft Clay Foundation	20	0	19.4

3.27.2 Results and Discussions

Table 111 Circular Results clay embankment with no reinforcement

Method	Factor of Safety					Difference (%)
	Tandjiria (2002)	Slide		Slope Stability		
		Moment	Force	Moment	Force	
Spencer	0.981	0.975	0.975	0.975	0.975	0.00
GLE		0.975	0.975	0.975	0.975	0.00

Table 112 Noncircular Results-clay embankment with no reinforcement

Method	Factor of Safety				Difference (%)
	Slide		Slope Stability		
	Moment	Force	Moment	Force	
Spencer	0.932	0.932	0.825	0.826	-11.95
GLE	0.937	0.937	0.934	0.934	0.22

Table 113 Circular Results-sand embankment with no reinforcement

Method	Factor of Safety				Difference (%)
	Slide		Slope Stability		
	Moment	Force	Moment	Force	
Spencer	1.209	1.209	1.211	1.211	0.17
GLE	1.218	1.218	1.22	1.22	0.16

Table 114 Noncircular Results sand embankment with no reinforcement

Method	Factor of Safety				Difference (%)
	Slide		Slope Stability		
	Moment	Force	Moment	Force	
Spencer	1.188	1.188	1.182	1.181	-0.51
GLE	1.196	1.196	1.184	1.184	-1.00

Table 115 Circular Results clay embankment with reinforcement

Method	Factor of Safety							Difference (%)
	Tandjiria (2002)	Slide			Slope Stability			
	Rein Force kN/m	Moment	Force	Rein Force kN/m	Moment	Force	Rein Force kN/m	
Spencer	170	1.35	1.35	169	1.349	1.349	169	-0.07
GLE	170	1.35	1.35	169	1.349	1.349	169	-0.07

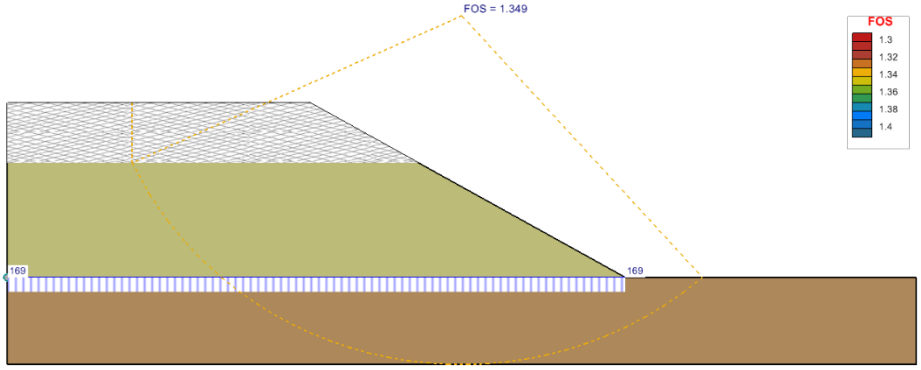

Figure 89 Results of the Clay embankment reinforcement circular

Table 116 Noncircular Results clay embankment with reinforcement

Method	Factor of Safety							Difference (%)
	Tandjiria (2002)	Slide			Slope Stability			
	Rein Force kN/m	Moment	Force	Rein Force kN/m	Moment	Force	Rein Force kN/m	
Spencer	190	1.351	1.351	184	1.353	1.352	184	0.15
GLE	190	1.366	1.366	184	1.367	1.367	184	0.07

Table 117 Circular Results sand embankment with reinforcement

Method	Factor of Safety							Difference (%)
	Tandjiria (2002)	Slide			Slope Stability			
	Rein Force kN/m	Moment	Force	Rein Force kN/m	Moment	Force	Rein Force kN/m	
Spencer	45	1.35	1.35	44	1.347	1.347	44	-0.22
GLE	45	1.357	1.357	44	1.354	1.354	44	-0.29

Table 118 Noncircular Results sand embankment with reinforcement

Method	Factor of Safety							Difference (%)
	Tandjiria (2002)	Slide			Slope Stability			
	Rein Force kN/m	Moment	Force	Rein Force kN/m	Moment	Force	Rein Force kN/m	
Spencer	56	1.35	1.35	56	1.358	1.357	53	0.59
GLE	56	1.359	1.359	56	1.362	1.362	53	0.22

3.28 BAKER AND LESCHINSKY - EARTH DAM

Project: Slopes_Group_1
Model: VS_42_circular, VS_42_noncircular

This model was original published by Baker and Leshchinsky (2001). It was presented to illustrate the use of safety maps as practical tools for slope stability analysis.

3.28.1 Geometry and Material Properties

The geometry of the model can be seen in Figure 90. The model consists of a clay core with granular fill surrounding the core. The model has a solid base.

A dry tension crack is placed at the top of the model to stimulate a 5m thick crack layer. All trial slip surfaces must be plotted on the dam to obtain a safety map of regional safety factors of safety. Noncircular slip surfaces and corresponding factor of

safety are also required in this analysis.

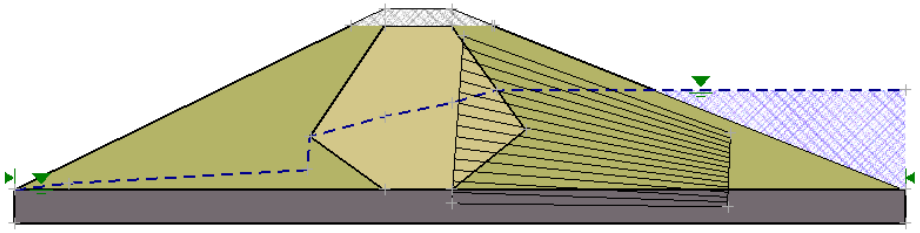

Figure 90 Geometry of the Baker and Leshchinsky Earth Dam Circular model

Table 119 Material Properties of the Earth Dam Circular model

	c (kN/m^2)	ϕ (degrees)	γ (kN/m^3)
Clay core	0	20	20
Granular Fill	0	40	21.5
Hard Base	200	45	24

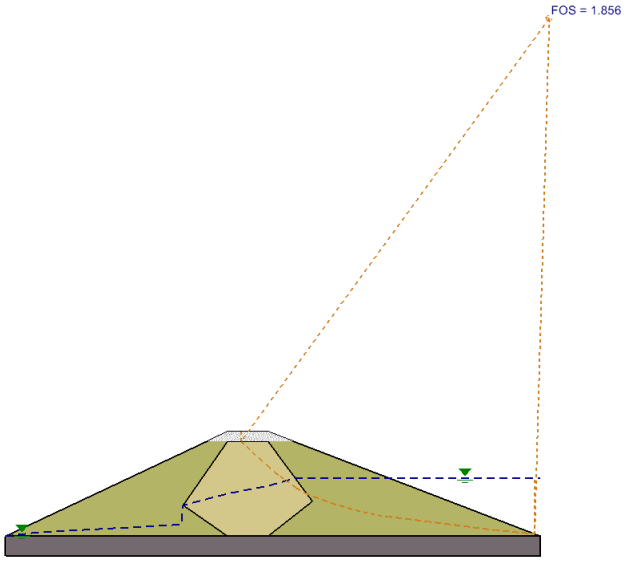

Figure 91 Geometry of the VS_42_noncircular model

3.28.2 Results and Discussions

Table 120 Results - Circular failure surface, 80 x 80 grid

Method	Factor of Safety (VS_42_Circular Slip Surfaces)				Difference (%)
	Baker & Leshchinsky	Slide	Slope Stability		
			Moment	Force	
Spencer	1.91	1.923	1.923	1.923	0.00

Table 121 Results Noncircular using Random Search with Optimization (zero faces)

Method	Factor of Safety (VS_42_Non-Circular Slip Surfaces)				Difference (%)
	Baker & Leshchinsky	Slide	Slope Stability		
			Moment	Force	
Spencer	1.91	1.857	1.857	1.856	0.00

3.29 BAKER - PLANAR HOMOGENEOUS

Project: Slopes_Group_1
Model: VS_43_BlockSearch, VS_43_Circular

This model is original published by Baker (2001), and looks at the factor of safety of planar slip surfaces. The results are compared at various failure plane angles. The slope presented is homogenous and dry.

3.29.1 Geometry and Material Properties

The geometry can be seen in Figure 92. In this case, there are two tests that must be run on this slope. The first test is that the plot of factors of safety versus *x*-coordinate are required for all critical failure planes passing through the toe of the slope.

Subsequently, the critical circular slip surfaces in Zone A must determined at which point the safety factors versus *x*-coordinate for Zone A must be plotted. A method of locating the factor of safety as a function of the failure plane angle is presented.

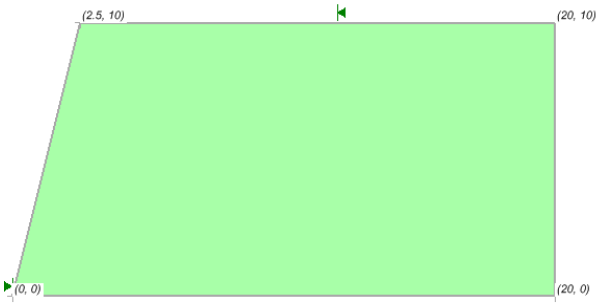

Figure 92 Geometry of the Baker (2001) - Planar Homogeneous Slope

Table 122 Material Properties of the Baker (2001) - Planar Homogenous Slope

	c (kN/m^2)	ϕ (degrees)	γ (kN/m^3)
Material	30	30	20

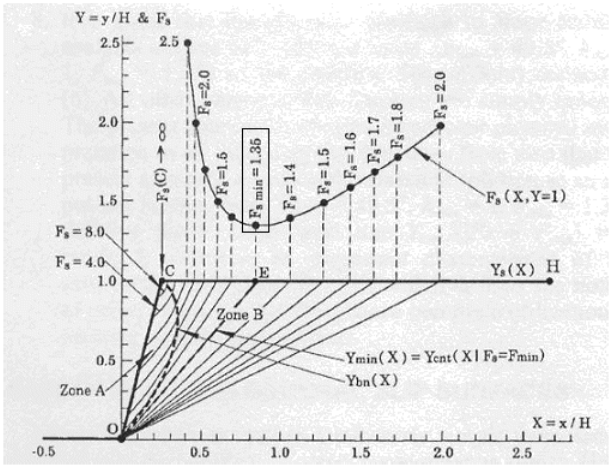

Figure 93 Baker's (2001) Distribution

3.29.2 Results and Discussions

Table 123 Results non-circular Baker (2001)

Method	Factory of Safety							Difference (%)
	Baker (2001)	RocPlane 2.0		Slide		Slope Stability		
		Fs	Angle	Fs	Angle	Fs	Angle	
Janbu Simplified	1.35	1.351	49.5	1.352	49.5	1.352	49.5	0

3.30 SHEAHAN - AMHEARST SOIL NAILS

Project: Slopes_Group_1
Model: VS_47

This problem was published by Sheahan (2003). It examines the Amhearst test wall, which was a soil nailed wall in clay that failed due to over excavation.

3.30.1 Purpose

The purpose of the analysis is to determine the location of the critical planar slip surface and associated factor of safety.

3.30.2 Geometry and Material Properties

This particular analysis involves a planar failure through a soil nailed wall. The factor of safety is calculated for the undrained, homogeneous slope. In this case the slope is reinforced by two rows of nails.

The shotcrete plate on the soil nails has a weight of 14.6 kN/m. This weight is modeled as a point load at the top of the wall face.

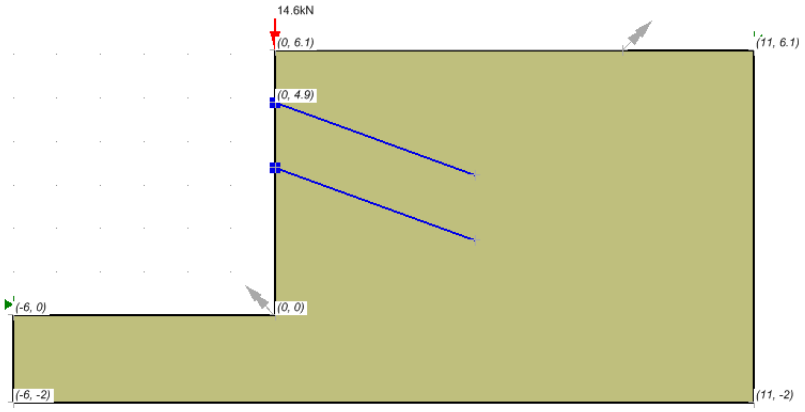

Figure 94 Geometry of the Sheahan Amhearst Soil Nails Model

Table 124 Material Properties of the Sheaham Amhearst Soil Nails model

Material	c (kN/m^2)	γ (kN/m^3)
Amherst Clay	25	18.9

Table 125 Soil Nail Properties

Type	Out-of-plane Spacing (m)	Tensile Strength (kN)	Plate Strength (kN)	Bond Strength (kN)	Length (m)	Number of rows
Passive	1.5	118	86	15	4.9	2

3.30.3 Results and Discussions

Table 126 Results – Sheahan-Amhearst Soil Nails

Method	Factor of Safety				Difference (%)
	Sheahan (2003)	Slide	Slope Stability		
			Moment	Force	
Janbu Simplified	0.887	0.888		0.89	0.23

3.31 SHEAHAN - CLOUTERRE TEST WALL

Project: Slopes_Group_1
Model: VS_48, VS_48_45Deg, VS_48_50Deg, VS_48_55Deg, VS_48_60Deg, VS_48_65Deg, VS_48_70Deg

This problem was presented by Sheahan (2003) and it examines the Clouterre Test Wall. The test wall was constructed using Fontainebleu sand and failed by backfill saturation. The test was carried out as part of the French national project on soil nailing.

3.31.1 Purpose

The purpose of this analysis is to determine the factor of safety for six different plane angles ranging from 45 to 70 degrees.

3.31.2 Geometry and Material Properties

The relationship between the failure slope angle and the factor of safety of a homogeneous slope is examined in this case.

The primary resistance against failure is friction generated by the soil weight. The test wall was reinforced using seven rows of soil nails and a shotcrete plate weighting 13.2 kN/m. The shotcrete plate weighting was modeled as point load acting on the wall face.

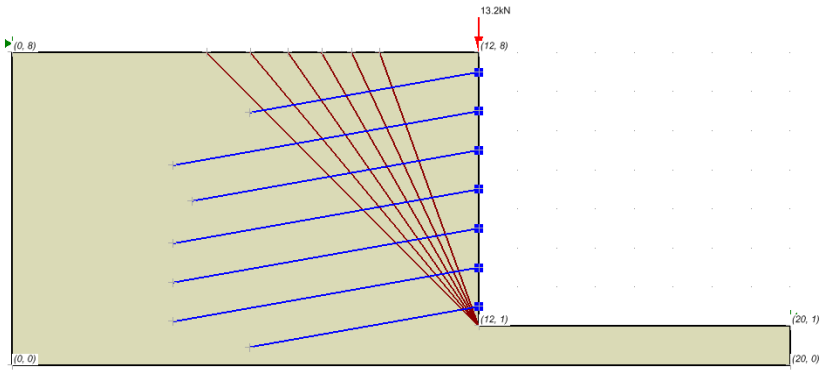

Figure 95 Geometry of the Sheahan Clouterre Test Wall model

Table 127 Material Properties of the Sheahan Clouterre Test Wall model

Material	c (kN/m^2)	ϕ (degrees)	γ (kN/m^3)
Fontainebleau Sand	3	38	20

Table 128 Soil Nail Properties

Type	Out-of-plane Spacing (m)	Tensile Strength (kN)	Plate Strength (kN)	Bond Strength (kN)
Passive	1.5	15	59	7.5

3.31.3 Results and Discussions

Table 129 Results Janbu Simplified (Sheahan, 2003)

Method	Factory of Safety			Difference (%)
	Slide	Slope Stability		
		Moment	Force	
Janbu Simplified	0.921		0.922	0.11

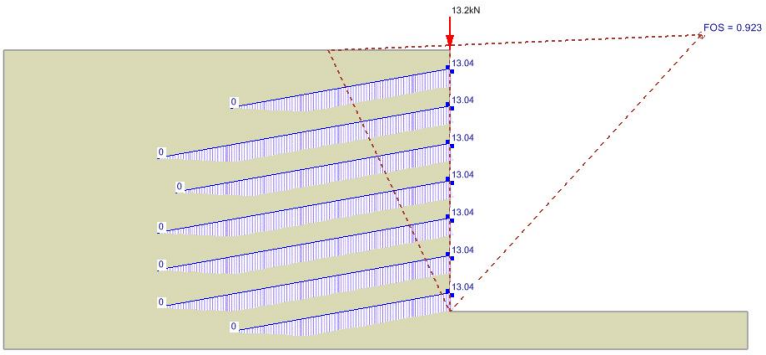

Figure 96 Results of theVS_48 model using the Janbu Simplied method

Table 130 Results for different slope angles of the failure surface

Slope Angle	Factor of Safety			Difference (%)
	Sheahan	Slide Janbu Simplified	Slope Stability Janbu Simplified	
45	1.176	1.124	1.123	-0.09
50	1.070	1.043	1.043	0.00
55	0.989	0.989	0.989	0.00
60	0.929	0.946	0.945	-0.11
65	0.893	0.921	0.922	0.11
70	0.887	0.922	0.924	0.22

3.32 SNAILZ - REINFORCED SLOPE

Project: Slopes_Group_1
Model: VS_49

This model was taken from the SNAILZ reference manual (http://www.dot.ca.gov/hq/esc/geotech). The model has two materials and is a slope reinforced with a soldier pile tieback wall. Imperial units are used for this particular model.

3.32.1 Purpose

The purpose of this model is to determine the factor of safety for a given slip surface.

3.32.2 Geometry and Material Properties

There are two different types of reinforcements in this model. Each of the two rows of soil nails has different bar diameters, which results in different tension capabilities. The soldier piles are modeled using a micro-pile in Slope Stability.

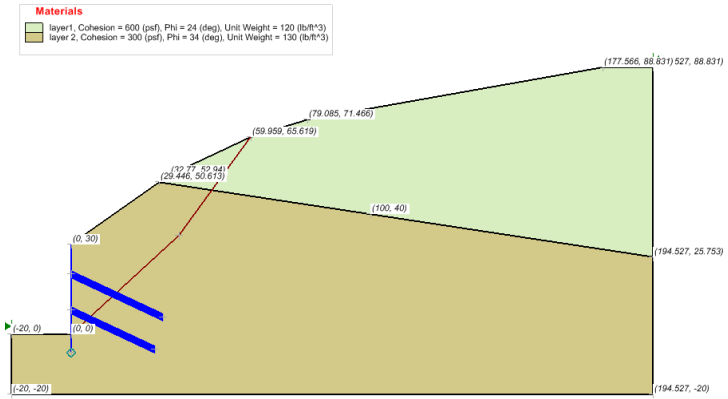

Figure 97 Geometry of the Snailz Reinforced Slope model

Table 131 Material Properties of the Snailz Reinforced Slope

Material	c (psf)	ϕ (degrees)	γ (pcf)
Layer 1	600	24	120
Layer 2	300	34	130

Table 132 Soil Nail Properties (Active)

	Out-of-plane Spacing (m)	Tensile Strength (lb)	Plate Strength (kN)	Bond Strength (kN)
Soil Nail: top now	8	120344.9	120344.9	13571.68
Soil Nail: bottom row	8	164217.3	164217.3	13571.68
Micro-pile (active)	1	Pile shear strength: 5900 lb.		

3.32.3 Results and Discussions

Table 133 Results of the Snailz Reinforced Slope

Method	Factor of Safety				Difference (%)
	SNAILZ	Slide	Slope Stability		
			Moment	Force	
Janbu Simplified	1.52	1.446		1.446	0.00

3.33 SNAILZ - GEOTEXTILE LAYERS

Project: Slopes_Group_1
Model: VS_50

This problem is taken from the SNAILZ reference manual. It examines a slope, which has been reinforced with geotextile layers extending to different depths into the slope. It should be noted that SNAILZ models the geotechnical characteristics with soil nails as having the same parameters as it would have if it were not equipped with geotextile reinforcement.

The problem at hand involves two layers with multiple reinforcement parameters. In this model, each horizontal reinforcement consists of parallel rows varying in length, tensile capacity and bond strength. The rows are all evenly spaced at 1.8 ft, except for row 14, which is spaced 1.8 ft. The problem at hand considers rows that are evenly spaced. The rows are numbered starting at the crest. The factor of safety is required for the two failure surfaces given in Figure 98.

3.33.1 Geometry and Material Properties

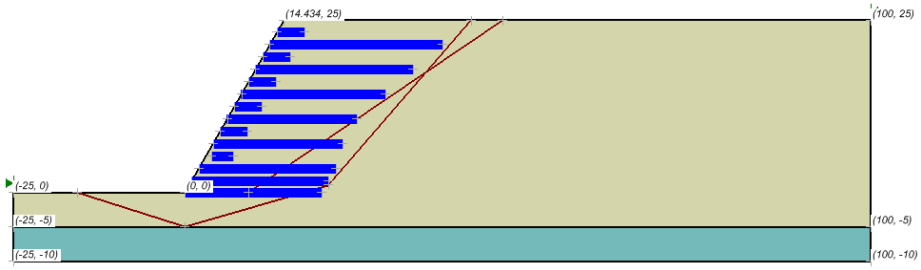

Figure 98 Geometry of the Snailz Geotextile Layers model

Table 134 Material Properties of the Snailz Geotextile Layers

Material	c (psf)	ϕ (degrees)	γ (pcf)
Layer 1	600	24	120
Layer 2	300	34	130

	Out-of-plane Spacing (ft)	Tensile Strength (lb)	Plate Strength (lb)	Bond Strength (lb/ft)	Length (ft)
Rows: 1,3,4,7, 9,11	1	1103	1103	1206.37	4
Rows: 12, 13, 14	1	2212	2212	1206.37	20
Rows: 8	1	1103	1103	965.096	19
Rows: 6	1	1103	1103	732.822	21
Rows: 4	1	1103	1103	482.548	23
Rows: 2	1	1103	1103	241.274	25
Rows: 10	1	1103	1103	1206.31	19

3.33.2 Results and Discussions

Table 135 Results for Case 1

Method	Factor of Safety			Difference (%)
	Slide	Slope Stability		
		Moment	Force	
Janbu Simplified	1.354		1.354	0.00
Spencer	1.618	1.617	1.617	-0.06
GLE	1.621	1.617	1.616	-0.25

Note: “Corrected” Janbu method is not available in Slope Stability, so the results were compared to the Janbu Simplified method

3.34 ZHU - FOUR LAYER SLOPE

Project: Slopes_Group_1
Model: VS_51

This model was presented by Zhu (2003). The problem consists of four soil layers with a designated slip surface, using a number of different methods. The multiple layers slope is analyzed using circular slip surfaces.

Tension cracks are placed through the top layer and the slope is assumed to be subjected to earthquake conditions with a seismic coefficient of 0.1. In this case, the factor of safety for the surface with 100 slices is required using all methods of analysis. The tolerance level is set at 0.001.

3.34.1 Geometry and Material Properties

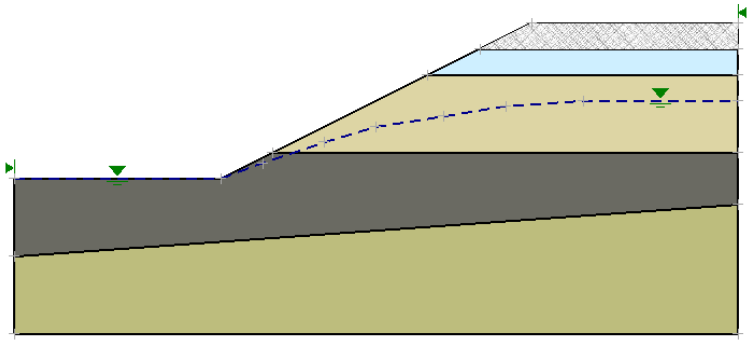

Figure 99 Geometry of the Zhu Four Layer Slope model

Table 136 Material Properties of the Zhu Four Layer Slope

Material	c (kN/m^2)	ϕ (degrees)	γ (kN/m^3)
Layer 1 (top)	20	32	18.2
Layer 2	25	30	18.0
Layer 3	40	18	18.5
Layer 4 (bottom)	40	28	18.8

3.34.2 Results and Discussions

Table 137 Results for Case 1

Method	Factor of Safety				Difference (%)
	Zhu	Slide	Slope Stability		
			Moment	Force	
Ordinary	1.066	1.075	1.072		-0.28
Bishop Simplified	1.278	1.288	1.285		-0.23
Janbu Simplified	1.112	1.121		1.115	-0.54
Corps of Engineers #2	1.377	1.420		1.41	-0.70
Lowe-Karafiath	1.290	1.288		1.295	0.54

Spencer	1.293	1.302	1.300	1.299	-0.15
M-P	1.313	1.313	1.309	1.309	-0.31
GLE	1.313	1.313	1.309	1.309	-0.31

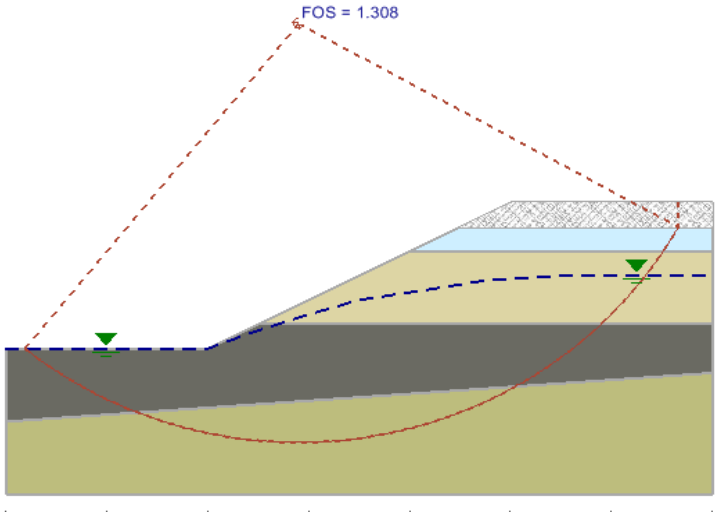

Figure 100 Results of using the GLE method VS_51

3.35 ZHU AND LEE - HETEROGENEOUS SLOPE

Project: Slopes_Group_1
Model: VS_52

Zhu and Lee (2002) presented this model to analyze a heterogeneous slope under wet and dry conditions. Four different slip surfaces were analyzed for each of these conditions.

A dry tension crack was placed at the top of the slope and the factor of safety was required for eight separate cases, four distinct slip surfaces under dry conditions, and four distinct slip surfaces when a water table was included (Table 2).

In this case surfaces 1 and 3 were circular, while surfaces 2 and 4 are noncircular. Critical slip surfaces 1 and 2 are shallow, and critical slip surfaces 3 and 4 are deep.

3.35.1 Geometry and Material Properties

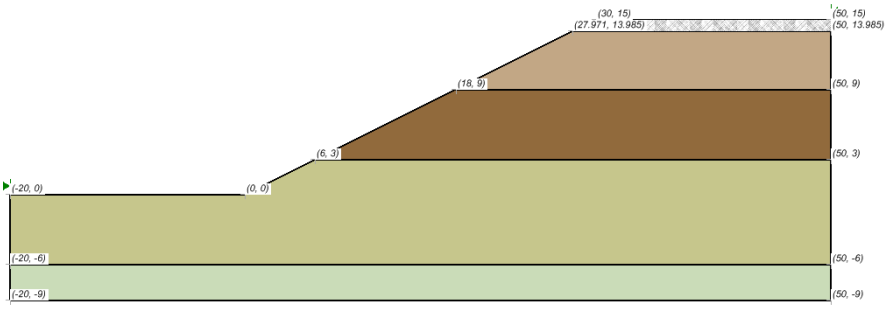

Figure 101 Geometry of the Zhu and Lee Heterogenous Slope model (VS_52_1_dry)

Table 138 Material Properties of the Zhu and Lee Heterogenous Slope model

Material	c (kN/m^2)	ϕ (degrees)	γ (kN/m^3)
Layer 1 (top)	20	18	18.8
Layer 2	40	22	18.5
Layer 3	25	26	18.4
Layer 4 (bottom)	10	12	18.0

Table 139 Water Table Geometry wet condition

Coordinates	Arc
(0, -20)	
(0,0)	
(6,3)	
	(100568, 5.284)
	(25.314, 9.002)
	(39.149, 10.269)
(50,10.269)	

3.35.2 Results and Discussions

Table 140 Surface 1 Circular, shallow

Method	Factor of Safety (1-dry-single circular)				Difference (%)
	Zhu & Lee	Slide	Slope Stability		
			Moment	Force	
Ordinary	1.935	1.934	1.934		0.00
Bishop Simplified	2.011	2.010	2.010		0.00
Spencer	2.035	2.017	2.017	2.017	0.00
M-P	2.035	2.017	2.017	2.017	0.00

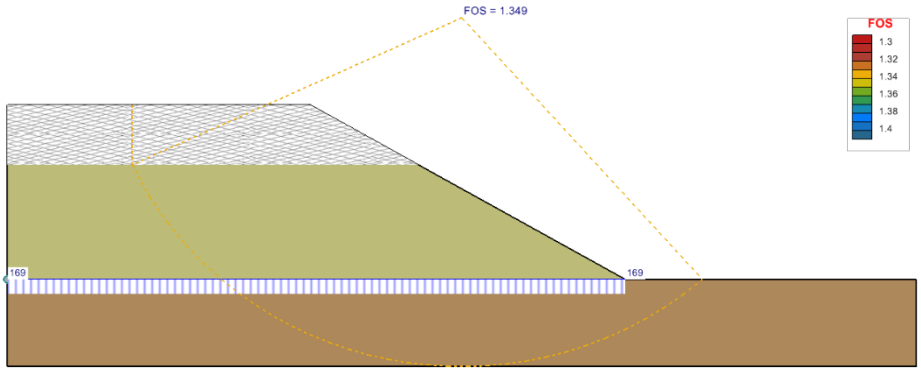

Figure 102 Results using the M-P method VS_52_1_dry

Table 141 Results - Surface 2 Circular, deep Grid search

Method	Factor of Safety (1-wet single circular)				Difference (%)
	Zhu & Lee	Slide	Slope Stability		
			Moment	Force	
Ordinary	1.496	1.460	1.460		0.00
Bishop Simplified	1.534	1.526	1.526		0.00
Spencer	1.559	1.533	1.533	1.533	0.00
M-P	1.559	1.533	1.533	1.533	0.00

Table 142 Results Surface 3 Circular, deep Grid search

Method	Factor of Safety (3-dry Grid tangent)				Difference (%)
	Zhu & Lee	Slide	Slope Stability		
			Moment	Force	
Ordinary	1.229	1.495	1.490		-0.33
Bishop Simplified	1.429	1.804	1.799		-0.28
Spencer	1.836	1.804	1.801	1.801	-0.17
M-P	1.823	1.790	1.790	1.790	0.00

Table 143 Results Surface 3 Wet Grid Tangent

Method	Factor of Safety (3-wet Grid Tangent)				Difference (%)
	Zhu & Lee	Slide	Slope Stability		
			Moment	Force	
Ordinary	0.922	0.812	0.854		5.17
Bishop Simplified	1.079	1.176	1.162		-1.19
Spencer	1.211	1.189	1.175	1.174	-1.18
M-P	1.197	1.174	1.167	1.167	-0.60

Table 144 Results Surface 4 Noncircular, deep dry Path search

Method	Factor of Safety (4-dry Path Search)				Difference (%)
	Zhu & Lee	Slide	Slope Stability		
			Moment	Force	
Spencer	1.772	1.797	1.743	1.743	-3.01
M-P	1.765	1.776	1.746	1.746	-1.69

Table 145 Results Surface 5 Non-circular wet path search

Method	Factor of Safety (4-wet-Path Search)				Difference (%)
	Zhu & Lee	Slide	Slope Stability		
			Moment	Force	
Spencer	1.150	1.176	1.146	1.145	-2.55
M-P	1.141	1.162	1.139	1.139	-1.98

3.36 PRIEST - RIGID BLOCKS

Project: Slopes_Group_1
Model: VS_53, VS_53_Dry

This model was presented by Priest (1993) for the analysis of rigid blocks. It also contains a sensitivity analysis on various parameters. The model presents a homogeneous slope undergoing failure along a specified noncircular surface. In this case the slope has a tension crack, which is 15m deep at the crest.

3.36.1 Purpose

The purpose of this analysis is to determine a factor of safety for the block.

3.36.2 Geometry and Material Properties

A water table is also present in this analysis. Water fills the tension crack 25% at the line of failure.

The water table is also assumed to be horizontal until it passes the intersection between the tension crack and the failure plane. The water table then dips steeply and linearly approaches the toe.

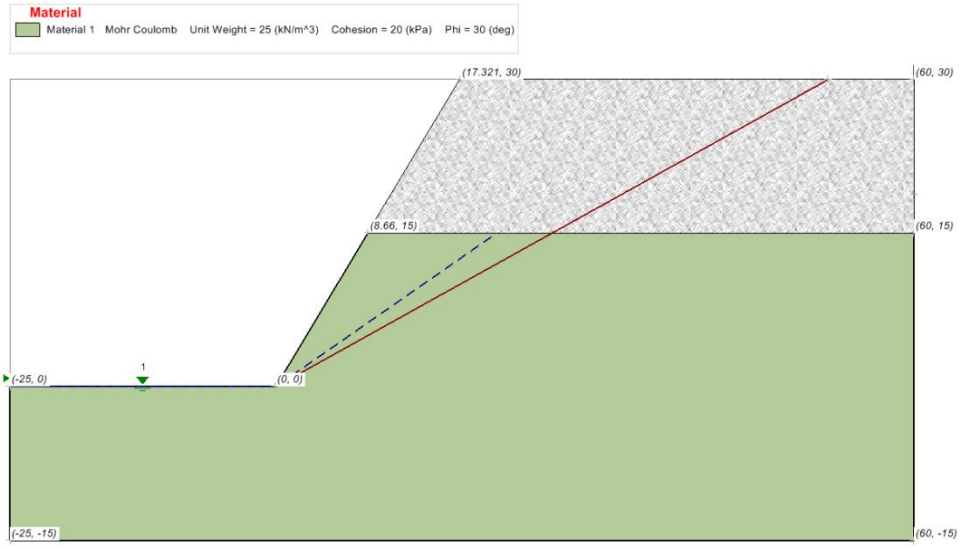

Figure 103 Geometry of the Priest Rigid Block Model (VS_53)

Table 146 Material Properties of the Priest Rigid Block model

Material	c (kN/m^2)	ϕ (degrees)	γ (kN/m^3)
Material 1	20	30	25

3.36.3 Results and Discussions

Table 147 Results of the Priest Rigid Block model

Method	Factor of Safety					Difference (%)
	Priest	Rocplane	Slide	Slope Stability		
				Moment	Force	
Janbu Simplified	1.049	1.049	1.049		1.049	0

3.37 YAMAGAMI – STABILIZING PILES

Project: Slopes_Group_1
Model: VS_54_nopile, VS_54_withpile

This model was taken from Yamagami (2000) and it examines the reinforcement of an unstable slope. The slope is reinforced using stabilizing piles. The homogeneous slope can be seen in Figure 104.

The model is analyzed using a circular slip surface. The single row of micro-piles, act as passive reinforcement. The piles are spaced 1m apart horizontally and have shear strength of 10.7 kN.

3.37.1 Purpose

The purpose of this analysis is to determine factor of safety for the slope with or without reinforcement.

3.37.2 Geometry and Material Properties

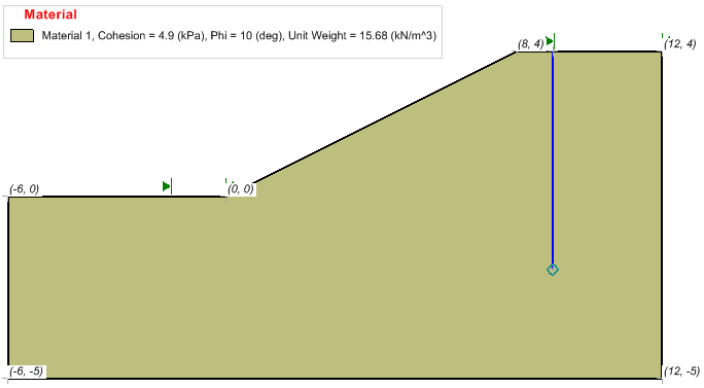

Figure 104 Geometry of the Yamagami example with Pile (VS_54)

Table 148 Material Properties of the Yamagami example

Material	c (kN/m^2)	ϕ (degrees)	γ (kN/m^3)
Material 1	4.9	10	15.68

3.37.3 Results and Discussions

Table 149 No Pile Results

Method	Factor of Safety (no pile)				Difference (%)
	Yamagami (2000)	Slide	Slope Stability		
			Moment	Force	
Bishop Simplified	1.1	1.102	1.102		0.00

Table 150 With Pile Results

Method	Factor of Safety (with pile)				Difference (%)
	Yamagami (2000)	Slide	Slope Stability		
			Moment	Force	
Bishop Simplified	1.2	1.193	1.194		0.08

3.38 POCKOSKI AND DUNCAN - SIMPLE SLOPE

Project: Slopes_Group_1
Model: VS_55

Pockoski and Duncan (2000) presented this model. The analysis of a homogeneous, un-reinforced slope is first presented. A water table is present and the slip surfaces are circular.

3.38.1 Purpose

The purpose of this model is to confirm the ability of Slope Stability to analyze a simple slope using seven different software packages. Also it is to calculate critical slip surface and the factor of safety.

3.38.2 Geometry and Material Properties

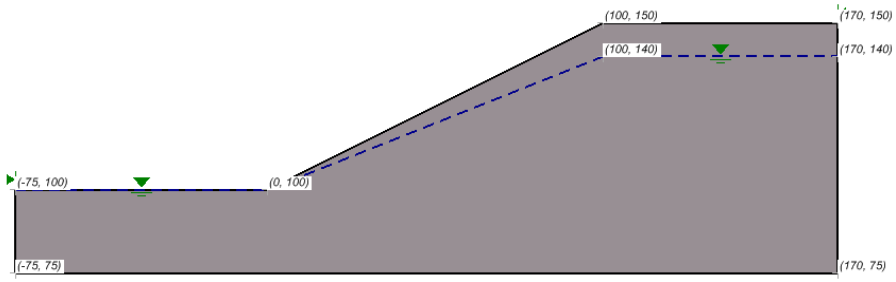

Figure 105 Geometry of the Pockoski and Duncan Simple Slope model

Table 151 Material Properties of the Pockoski and Duncan Simple Slope

Material	c (psf)	ϕ (degrees)	γ (pcf)
Sandy Clay	300	30	120

3.38.3 Results and Discussions

Table 152 Results of the Pockoski and Duncan Simple Slope model

Method	Factor of Safety								Difference (%)
	UTEXAS4	Slope/W	WINSTABL	XSTABL	RSS	Slide	Slope Stability		
							Moment	Force	
Ordinary	-	1.04	-	-	-	1.052	1.076		2.28
Bishop Simplified	1.29	1.29	1.29	1.29	1.29	1.293	1.292		-0.08
Janbu Simplified	1.15	1.15	1.2	1.24	1.15	1.151		1.151	0.00

Lowe-Karafiath	1.32	-	-	-	-	1.318		1.324	0.46
Spencer	1.3	1.3	1.34	-	-	1.3	1.298	1.298	-0.15

3.39 POCKOSKI AND DUNCAN - TENSION CRACKS

Project: Slopes_Group_1
Model: VS_56

This is second test slope presented by Pockoski and Duncan (2000). This model is similar to the previous model with the exception that a dry tension crack is included.

3.39.1 Geometry and Material Properties

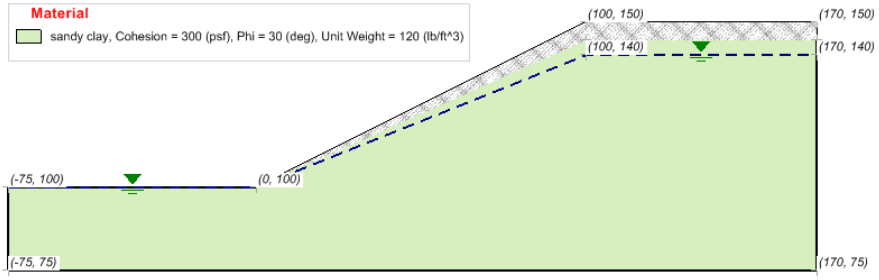

Figure 106 Geometry of the Pockoski and Duncan model

Table 153 Material Properties of the Pockoski and Duncan model

Material	c (psf)	ϕ (degrees)	γ (pcf)
Sandy Clay	300	30	120

3.39.2 Results and Discussions

Table 154 Results of the Pockoski and Duncan model

Method	Factor of Safety								Difference (%)
	UTEXAS4	Slope/W	WINSTABL	XSTABL	RSS	Slide	Slope Stability		
							Moment	Force	
Ordinary	-	1.02	-	-	-	1.03	1.058		2.72
Bishop Simplified	1.28	1.28	1.31	1.28	1.28	1.285	1.284		-0.08
Janbu Simplified	1.14	1.14	1.18	1.23	1.13	1.142		1.139	-0.26
Lowe-Karafiath	1.31	-	-	-	-	1.305		1.314	0.69
Spencer	1.29	1.29	1.32	-	-	1.289	1.29	1.29	0.08

SNAIL F_s = 1.18 (Wedge method)

GOLD-NAIL F_s = 1.30 (Circular method)

3.40 POCKOSKI AND DUNCAN - REINFORCED SLOPE

Project: Slopes_Group_1
Model: VS_57_composite, VS_57_No composite

This is a continuation of the Pockoski and Duncan (2000), comparison of eight different computer programs for the analysis of reinforced slopes. This is the third test slope.

In this case, a water table is also included. The slope is analyzed with and without composite slip surfaces in order to compare results with programs that have this option as well as those that do not have this option.

3.40.1 Geometry and Material Properties

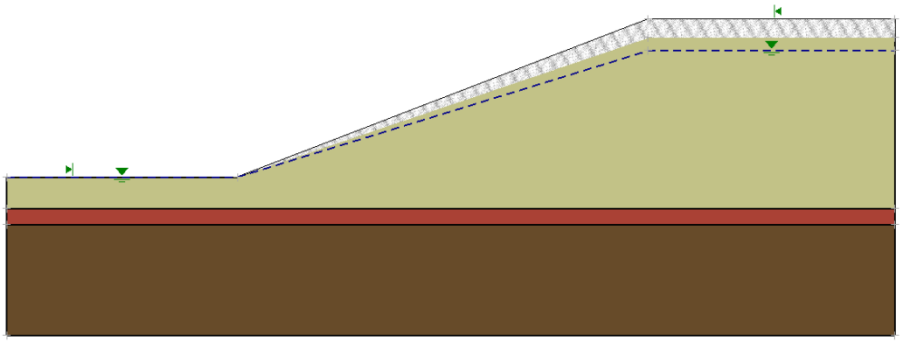

Figure 107 Geometry of the VS_57_composite/non circular

Table 155 Material Properties

Material	c (psf)	ϕ (degrees)	γ (pcf)
Sandy Clay	300	35	130
Highly Plastic Clay	0	25	130

3.40.2 Results and Discussions

Table 156 Composite Surface Non Circular

Method	Factor of Safety Composite surfaces/NonCircular					Difference (%)
	Slope/W	XSTABL	Slide	Slope Stability		
				Moment	Force	
Ordinary	0.85		0.944	1.014		7.42
Bishop Simplified	1.39	1.41	1.392	1.391		-0.07
Janbu Simplified	1.21	1.34	1.222		1.22	-0.16
Lowe-Karafiath			1.385		1.41	1.81
Spencer	1.4		1.4	1.399	1.398	-0.07

SNAIL F_s = 1.39 (Wedge method)

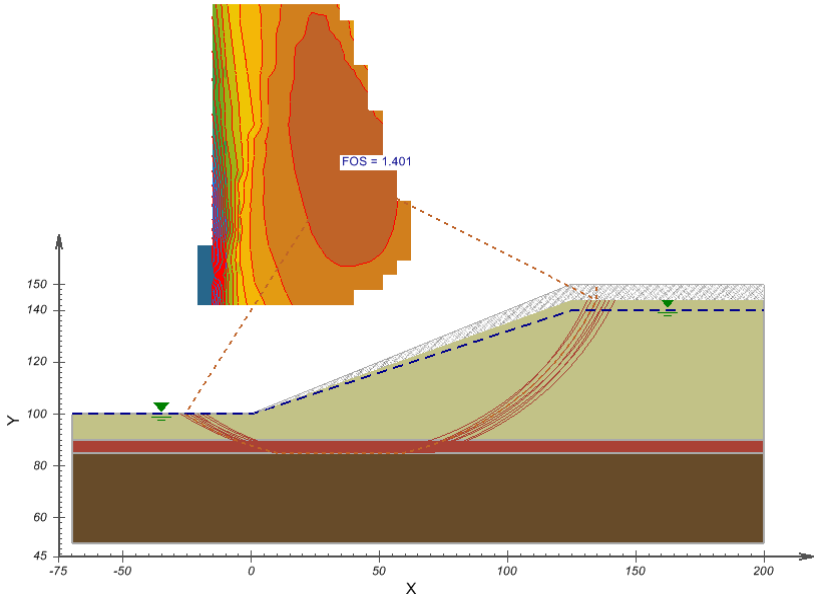

Figure 108 Results VS_57 composite using Spencer method

Table 157 No Composite Surfaces Circular

Method	Factor of Safety –No composite surfaces/Circular						Difference (%)
	UTEXES4	WINSTABL	RSS	Slide	Slope Stability		
					Moment	Force	
Ordinary				1.11	1.102		-0.72
Bishop Simplified	1.41	1.39	1.41	1.417	1.413		-0.28
Janbu Simplified	1.2	1.23	1.24	1.263		1.258	-0.40
Lowe-Karafiath	1.12			1.414		1.428	0.99
Spencer	1.42	1.45		1.422	1.418	1.418	-0.28

GOLD-NAIL F_s = 1.40 (Circular method)

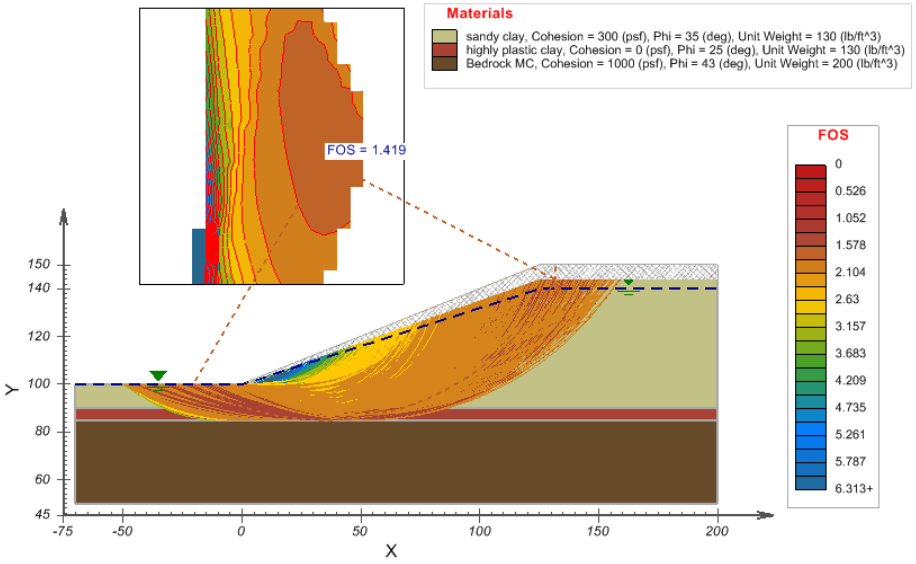

Figure 109 Results VS_57 no composite using the Spencer method

3.41 POCKOSKI AND DUNCAN - TIE-BACK WALL

Project: Slopes_Group_1
Model: VS_58

This is the fourth test slope analysis provided by Pockoski and Duncan (2000). This model analyzes a tie-back wall in a layered soil.

3.41.1 Purpose

The purpose of the model is to determine the location of critical failure surface and the factor of safety.

3.41.2 Geometry and Material Properties

A water table is presented and each layer is horizontal. Three identical rows of active grouted tie back reinforcement are modeled in this tie back wall.

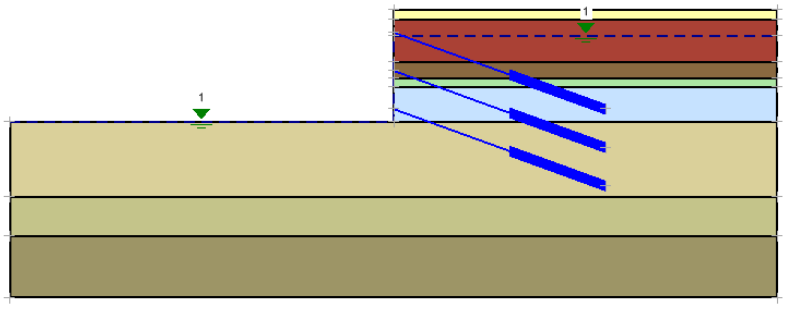

Figure 110 Geometry of the Pockoski and Duncan Tie Back Wall model

Table 158 Material Properties of the Pockoski and Duncan Tie Back Wall model

Layer	c (psf)	ϕ (degrees)	γ (pcf)
Granular Fill (GF)	0	30	120.4
Cohesive Fill (CF)	0	30	114.7
Organic Silt (OS)	900	0	110.2
OC Crust (OC)	2485	0	117.8
Upper Marine Clay (UM)	1670	0	117.8
Middle Marine Clay (MM)	960	0	117.8
Lower Marine Clay (LM)	1085	0	117.8
Glaciomarine Deposits (GD)	1500	0	147.1

Table 159 Grouted Tieback Properties all rows

Tensile Cap. (lbs)	Plate Cap. (lbs)	Bond Strength (lb/ft)	Bond Length (ft)	Out-of-Plane Spacing (ft)
247343	247343	4000	40	4

3.41.3 Results and Discussions

Table 160 Results

Method	Factor of Safety						Difference (%)
	UTEXAS4	Slope/W	WINSTABL	Slide	Slope Stability		
					Moment	Force	
Ordinary		1.12		1.125	1.125		0.00
Bishop Simplified	1.14	1.14	1.16	1.147	1.149		0.17
Janbu Simplified	1.13	1.05	1.12	1.061		1.061	0.00
Lowe-Karafiath	1.20			1.175		1.311	11.57
Spencer	1.14	1.14	1.20	1.145	1.146	1.146	0.09

GOLD-NAIL F_s = 1.19 (Circular)
SNAIL F_s = 1.03 (Wedge method-noncircular)

3.42 POCKOSKI AND DUNCAN - REINFORCEMENT

Project: Slopes_Group_1
Model: VS_59

This is the fifth test slope provided by Pockoski and Duncan, (2000). This scenario varies the effect of the reinforcement. The analysis represents a tie back wall and homogeneous sand.

3.42.1 Geometry and Material Properties

A single row of active grouted tieback support is installed for this problem. A water table is present, circular critical slip surfaces are considered and the resulting factor of safety is required.

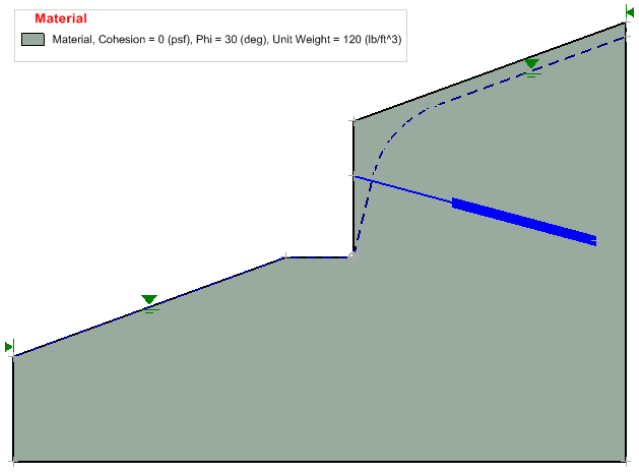

Figure 111 Geometry of the Reinforcement model VS_59

Table 161 Material Properties of the Pockoski and Duncan Reinforcement model

Material	c (psf)	ϕ (degrees)	γ (pcf)
Sand	0	30	120

Table 162 Soil Nail Properties

Tensile Cap. (lbs)	Plate Cap. (lbs)	Bond Strength (lb/ft)	Bond Length (ft)	Out-of-Plane Spacing (ft)
184077	184077	5000	22	8

3.42.2 Results and Discussions

Table 163 Results Circular

Method	Factor of Safety						Difference (%)
	UTEXAS4	Slope/W	WINSTABL	Slide	Slope Stability		
					Moment	Force	
Ordinary	-	0.62	-	0.626	0.702	-	12.14
Bishop Simplified	0.56	0.60	0.74	0.583	0.583	-	0.00
Janbu Simplified	0.64	0.61	0.76	0.583	-	0.584	0.17
Lowe-Karafiath	0.76			0.588	-	0.59	0.34
Spencer	0.65	0.60	0.59	0.594	0.592	0.592	-0.33

GOLD-NAIL F_s = 0.62 Circular

SNAIL F_s = 0.62 Wedge method noncircular

3.43 POCKOSKI AND DUNCAN - SOIL NAILS

Project: Slopes_Group_1
Model: VS_60

This is the seventh test slope providing by Pockoski and Duncan (2000). This model analyzes a soil nailed wall in homogenous clay. There is a dry tension crack down to the first nail. Two uniformly distributed loads of 500 lb/ft and 250 lb/ft are applied on the high bench.

3.43.1 Purpose

The purpose of the model is to calculate the critical slip surface (through the toe) as well as the factor of the safety.

3.43.2 Geometry and Material Properties

There are also five parallel rows passive soil nails that reinforce the wall. In this case, each row has identical strength characteristics.

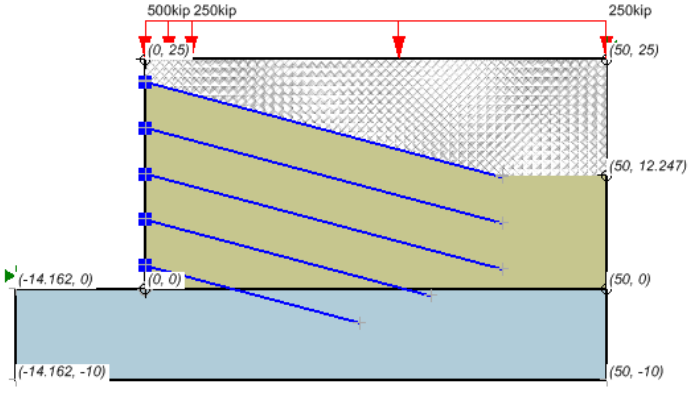

Figure 112 Geometry of the Pockoski and Duncan Soil Nails model (VS_60)

Table 164 Material Properties of the Pockoski and Duncan Soil Nails model

Material	c (psf)	ϕ (degrees)	γ (pcf)
Sand	800	0	120

Table 165 Soil Nail Properties

Tensile Cap. (lbs)	Plate Cap. (lbs)	Bond Strength (lb/ft)	Out-of-Plane Spacing (ft)
25918	25918	1508	5

3.43.3 Results and Discussions

Table 166 Results Dry Circular

Method	Factor of Safety (Dry Circular)						Difference (%)
	UTEXAS4	SLOPE/W	WINSTABL	Slide	Slope Stability		
					Moment	Force	
Ordinary	-	1.00	-	0.99	0.994		0.40
Bishop Simplified	1.00	1.01	1.06	0.997	0.994		-0.30
Janbu Simplified	1.08	1.07	1.10	1.041		1.041	0.00
Lowe-Karafiath	1.00			1.021		1.02	-0.10
GLE	1.02	1.02	0.99	1.01	1.026	1.027	1.58

GOLD-NAIL F_s = 0.91 Circular Method
SNAIL F_s = 0.84 Wedge Method

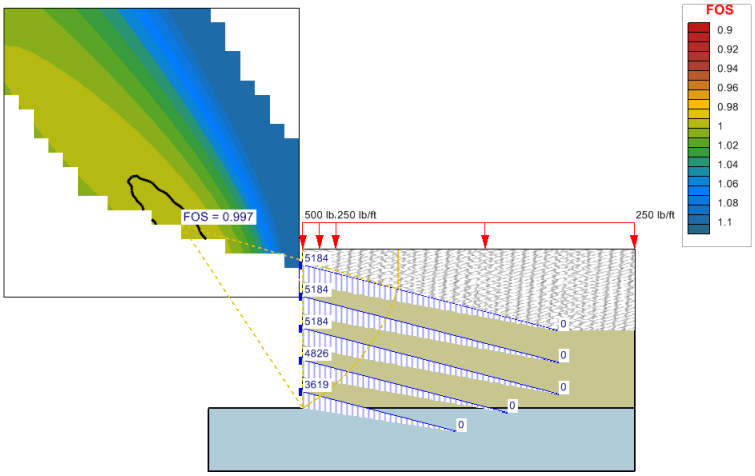

Figure 113 Results using the GLE method VS_60

3.44 LOUKIDIS - SEISMIC COEFFICIENT

Project: Slopes_Group_1
Model: VS_62

This model was published by Loukidis et al. (2003) and provides a method for determining the critical seismic coefficient k_c. The seismic coefficient determined corresponds a factor of safety of 1.0. This is their first example.

3.44.1 Purpose

The purpose of this verification problem is to reproduce a safety factor of 1 using Spencer's method and the seismic coefficients presented in the Loukidis et al. paper (2003).

3.44.2 Geometry and Material Properties

A simple homogenous earth slope is subjected to seismic loading. Both circular and noncircular slip surfaces are considered in the analysis and all slip surfaces must pass through the toe of the slope. Two independent pore-water pressures conditions are given consideration:

- Dry slope, and
- R_u of 0.05.

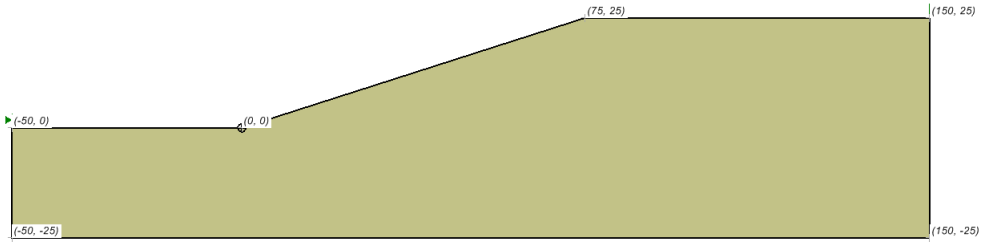

Figure 114 Geometry of the Loukidis Seismic Coefficient model (VS_62_Dry)

Table 167 Seismic Coefficients

Dry Slope	0.432
R_u = 0.5	0.132

3.44.3 Results and Discussions

Table 168 Results Dry Slope (k_c = 0.432)

Type	Spencer	Bishop Simplified
Circular (Grid Search)	1.001	0.991
Noncircular (Path search with optimization)	0.999	0.989

Table 169 Results R_u = 0.5 (k_c = 0.132)

Type	Spencer	Bishop Simplified
Circular (Grid Search)	1.001	0.987
Noncircular (Path search with optimization)	0.998	0.966

Table 170 Results Wet Circular

Method	Factor of Safety (Wet Circular)			Difference (%)
		Slope Stability		
	Slide	Moment	Force	
Bishop Simplified	0.987	0.991		0.41
Janbu Simplified	0.899		0.901	0.22
Corp Engineers#1	0.984		0.988	0.41
Corp Engineers#2	0.994		1.002	0.81
Lowe-Karafiath	0.976		0.982	0.61
Spencer	1.001	1.009	1.008	0.80
M-P	1.00	1.008	1.008	0.80
GLE	1.00	1.008	1.008	0.80

Loukidis F_s = 1.00 (Spencer)

Table 171 Results Wet No-Circular

Method	Factor of Safety (Wet Non-Circular)			Difference (%)
	Slide	Slope Stability		
		Moment	Force	
Bishop Simplified	**0.966**	**0.967**		**-0.41**
GLE	1.012	1.006	1.006	0.60

Loukidis F_s = 1.00 (Spencer)

3.45 LOUKIDIS - SEISMIC COEFFICIENT #2

Project: Slopes_Group_1
Model: VS_63

This is the second example problem presented by Loukidis et al., 2003. The effect of the critical seismic coefficient is examined in this example. This model analyzes a layered dry slope under seismic loading conditions.

3.45.1 Purpose

The purpose of the model is to bring the Spencer's factor of safety to 1.0 using the author's presented seismic coefficient of 0.115. The Loukidis analysis was for the case of a log-spiral surface.

3.45.2 Geometry and Material Properties

This problem is analyzed in Slope Stability by using a Greco search technique with a Monte Carlo optimization. The critical slip surface in this case passes through the material boundary on the slope between the middle and lower layers.

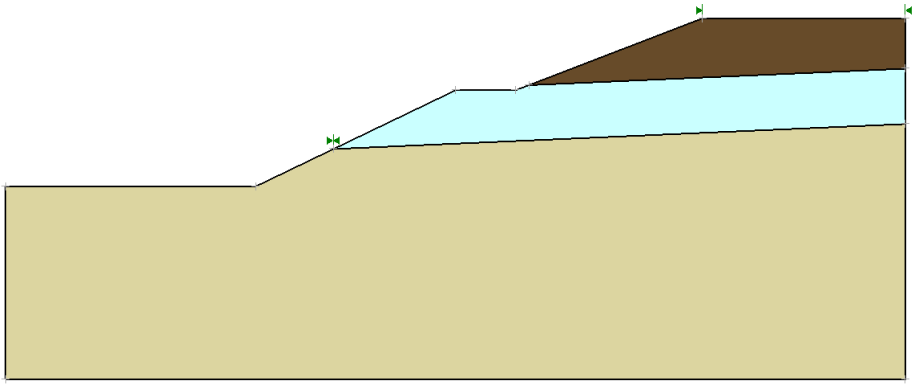

Figure 115 Geometry of the Loukidis Seismic Coefficient model

Table 172 - Material Properties of the Loukidis Seismic Coefficient model

Layer	c (kN/m^2)	ϕ (degrees)	γ (kN/m^3)
Top	4	30	17
Middle	25	15	19
Bottom	15	45	19

3.45.3 Results and Discussions

Table 173 Results of the Dry Circular

Method	Factor of Safety (Dry Circular)				Difference (%)
	Loukidis et al (2003)	Slide	Slope Stability		
			Moment	Force	
Spencer	1.00	0.991	0.992	0.992	0.10

4 SLOPE STABILITY GROUP 2

This chapter represents the second set of examples problems used to verify the Slope Stability software.

It also represents a collection of classic examples, which verify the calculation of the factor of safety in various cases. Including variations in material properties, water table locations, circular and non-circular slip surfaces and anchors.

4.1 SIMPLE MULTI - LAYER SLOPE

Project: Slopes_Group_2
Model: VW_1

This example creates a simple multi-layer slope in which the potential slip surfaces crosses three or four different material and there is a water table in the example.

4.1.1 Purpose

The primary purpose of this model is to analyze a typical case with circular slip surfaces. The Bishop Simplified method was used to calculate the factor of safety.

4.1.2 Geometry and Material Properties

In this model approximately 20 points were used in the grid and radius search method. The pore-water pressures were specified using a piezometric line. The model consists of silty clay over layering sandy clay tills.

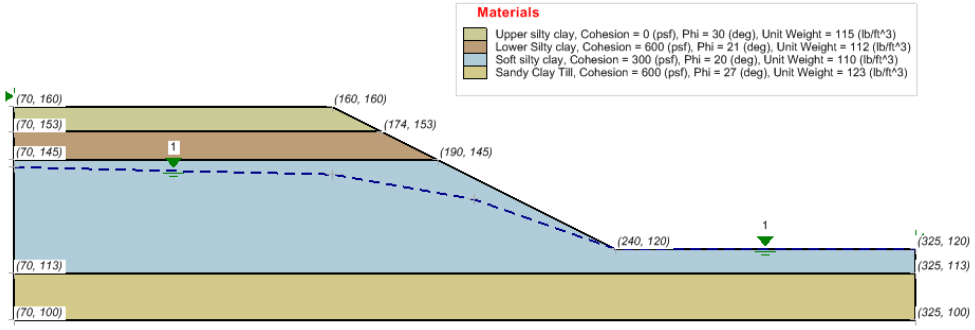

Figure 116 Geometry of the Simple Multi-Layer Slope Model

4.1.3 Results and Discussions

In Table 174, it illustrates the location of the critical slip surface. The analysis resulted in a factor of safety of approximately 1.2.

Table 174 Results of the Simple Multi-Layer Slope model

Method	Factor of Safety				Difference (%)
	Slope/W		Slope Stability		
	Moment	Force	Moment	Force	
Ordinary	1.101		1.104		0.27
Bishop Simplified	1.211		1.214		0.25
Janbu Simplied		1.090		1.113	0.36
Corps. of Engineers #1		1.255		1.257	0.16
Corps. of Engineers #2		1.290		1.294	0.31
Lowe-Karafiath		1.249		1.248	-0.08
Spencer	1.210	1.210	1.213	1.213	0.25
M-P	1.211	1.214	1.213	1.213	0.17
GLE	1.211	1.211	1.213	1.213	0.17

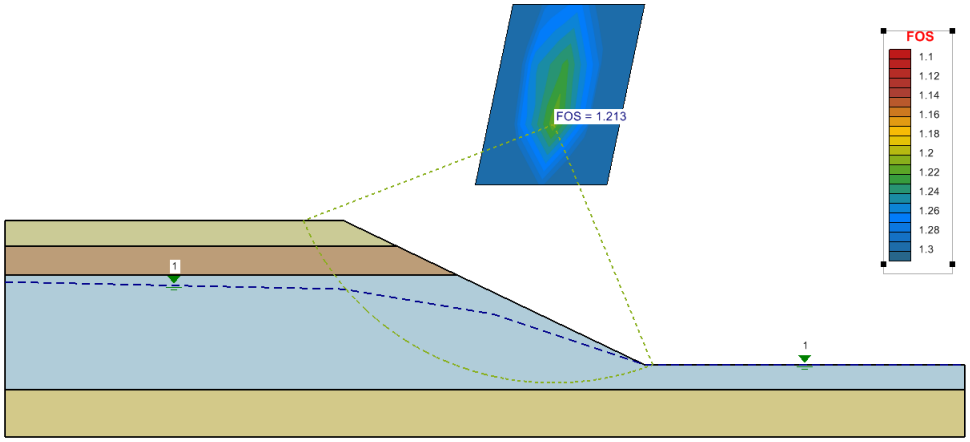

Figure 117 Results using the GLE method VW_1

4.2 BLOCK SEARCH MODEL

Project: Slopes_Group_2
Model: VW_3

The Morgenstern-Price method of calculations is used in this case. Tension cracks are also applied in the upper zone as well as downstream water bonded.

4.2.1 Purpose

The purpose of this example is to illustrate the use of the block search technique to generate a series of potential slip surfaces.

4.2.2 Geometry and Material Properties

The minimum block slip surface is selected given the contribution of a number of trial slip surfaces and the influence of the associated tension crack zone.

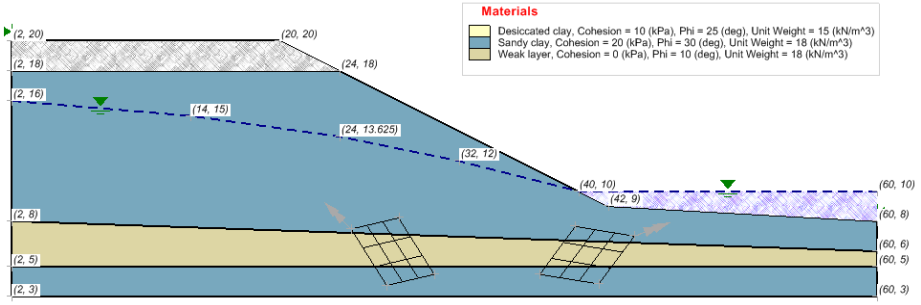

Figure 118 Geometry of the Block Search Model

4.2.3 Results and Discussions

In the following table it illustrates the identification of the most critical slip surfaces with the calculated Factor of Safety approximately equal to 1.0.

Table 175 Results of the Block Search model

Method	Factor of Safety				Difference (%)
	Slope/W		Slope Stability		
	Moment	Force	Moment	Force	
Ordinary	0.974		0.974		0.00
Bishop Simplified	1.065		1.065		0.00
Janbu Simplified		1.035		1.033	0.19
Corps of Engineers #1		1.218		1.223	0.41
Corps of Engineers #2		1.268		1.267	-0.08
Lowe-Karafiath		1.303		1.276	-2.07
Spencer	1.078	1.071	1.079	1.079	0.09

M-P	1.076	1.072	1.077	1.077	0.09
GLE	1.074	1.074	1.077	1.076	0.28

Note: The difference between Slope/W and Slope Stability for the Lowe-Karafiath and the Corps of Engineers #2 method is due to different assumptions made regarding the interslice force functions in Slope/W. Slope/W uses positive values when the base angle is negative. This difference has been extensively studied and we believe the Slope Stability implementation to be reasonable.

4.3 COMPOSITE SLIP SURFACES

Project: Slopes_Group_2
Model: VW_4

This model is characterized by tension crack zones, pore-water pressures specified by piezometric lines and downstream water ponding.

4.3.1 Purpose

The purpose of this model is to illustrate the use of composite slip surfaces. The analysis method in this case is the Morgenstern-Price method of analysis.

4.3.2 Geometry and Material Properties

The following figure indicates the identified location of the critical slip surface.

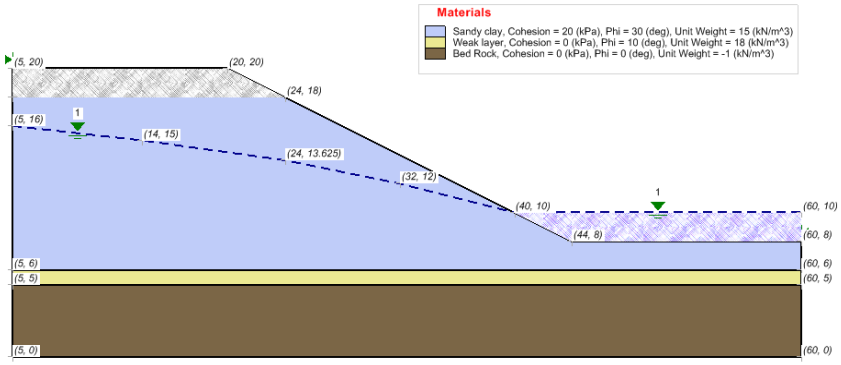

Figure 119 Geometry of the Composite Slip Surfaces model

4.3.3 Results and Discussions

The resulting Factor of Safety is approximately equal to 1.14. The base of the slip surfaces is truncated at the bedrock layer as necessary. Also, the upper portion of the slip surface goes vertical once it encounters the tension crack zone.

Table 176 Results of the Composite Slip Surfaces model

Method	Factor of Safety				Difference (%)
	Slope/W		Slope Stability		
	Moment	Force	Moment	Force	
Ordinary	0.855		0.882		3.16
Bishop Simplified	1.125		1.121		-0.36
Janbu Simplified		1.062		1.043	-1.79
Corps of Engineers #1		1.333		1.333	0.00
Corps of Engineers #2		1.221		1.2	-1.72
Lowe-Karafiath		1.299		1.141	-12.16
Spencer	1.140	1.139	1.14	1.14	0.00
M-P	1.113	1.11	1.107	1.107	0.54
GLE	1.112	1.112	1.107	1.107	-0.45

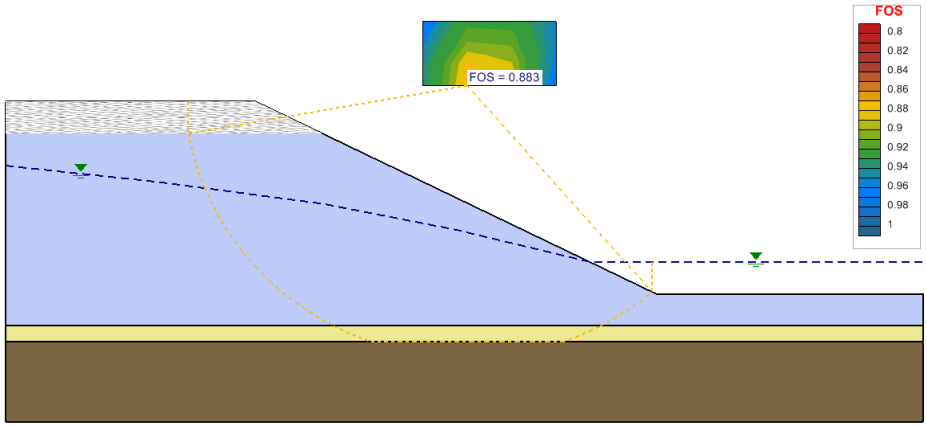

4.4 RETAINING WALL

Project: Slopes_Group_2
Model: VW_5

This model illustrates the use of fully specified slip surfaces, a single search center and a retaining wall in order to calculate the location of the critical slip surface.

4.4.1 Purpose

The primary purpose of this model is to illustrate the analysis of the stability of a gravity retaining wall using a fully specified slip surface.

4.4.2 Geometry and Material Properties

The Spencer Method is used to calculate the factor of safety. In the following figure it shows the calculations for the Factor of Safety on specified slip surfaces.

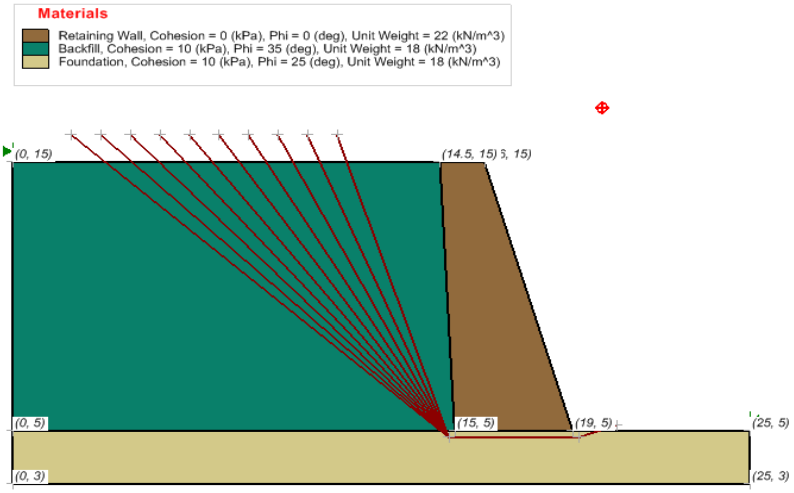

Figure 120 Geometry of the Retaining Wall model

4.4.3 Results and Discussions

A final factor of safety of 1.677 was calculated.

Table 177 Results of the Retaining Wall model

Method	Factor of Safety				Difference (%)
	Slope/W		Slope Stability		
	Moment	Force	Moment	Force	
Ordinary	1.368		1.369		0.07
Bishop Simplified	1.479		1.481		0.14
Janbu Simplified		1.320		1.323	0.23
Corps of Engineers #1		1.697		1.700	0.18
Spencer	1.677	1.669	1.685	1.685	0.48
M-P	1.678	1.672	1.682	1.681	0.24
GLE	1.680	1.680	1.682	1.682	0.12

4.5 FABRIC MODEL

Project: Slopes_Group_2
Model: VW_6_Fabric

This model has contained no pore-water pressures and represents a single specified circular slip surface. A single applied line load is applied to the crest of the slope. The geo-fabric reinforcements are entered as anchor loads with full bond length and variable applied loads.

4.5.1 Purpose

The purpose of this example is to show how geo-fabric reinforcement can be represented in a slope stability analysis. In this case, the GLE method is used to calculate the factor of safety.

4.5.2 Geometry and Material Properties

The calculation of the Factor of Safety is shown in the following figure. A factor of safety of 1.502 was calculated using Slope Stability. Of particular interest is the free bond diagram for slices 5 and 10, which are shown in the Figure 121.

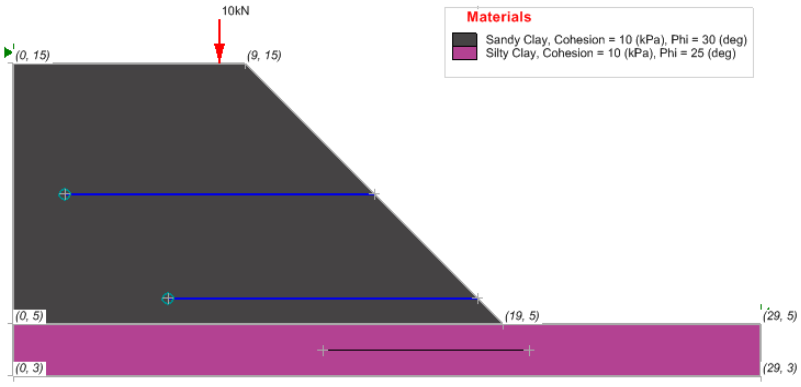

Figure 121 Geometry of the Fabric Model (VW_6)

4.5.3 Results and Discussions

In this case, the line load applied at crest of the slope is specified as 10KN/m and is shown in the free body diagram of Slice no. 5. A force mobilize load of 21.165 KN/m was calculated as the force in the anchor. The calculation of this force can be seen in free body diagram for Slice 10.

4.5.4 Table 178 Fabric model Results

Method	Factor of Safety				Difference (%)
	Slope/W		Slope Stability		
	Moment	Force	Moment	Force	
Ordinary	1.518		1.525		0.46
Bishop Simplified	1.663		1.668		0.30
Janbu Simplified		1.496		1.508	0.80
Corps of Engineers #1		1.703		1.705	0.12
Corps of Engineers #2		1.783		1.808	1.40
Spencer	1.643	1.646	1.650	1.634	0.73
M-P	1.641	1.637	1.646	1.646	0.31
GLE	1.640	1.640	1.646	1.646	0.37

Note: Reinforcement constant = 50 KN

Table 179 Fabric No rein/no line load

Method	Factor of Safety (No reinforcement / no line load)				Difference (%)
	Slope/W		Slope Stability		
	Moment	Force	Moment	Force	
Ordinary	1.291		1.297		0.46
Bishop Simplified	1.444		1.447		0.21
Janbu Simplified		1.292		1.300	0.62
Corps of Engineers #1				1.484	
Corps of Engineers #2				1.572	
Lowe-Karafiath				NA	
Spencer	1.426	1.429	1.43	1.430	0.07
M-P			1.427	1.427	
GLE	1.423	1.423	1.427	1.427	0.28

Table 180 Fabric no reinforcement/with line load

Method	Factor of Safety (No reinforcement with line load)				Difference (%)
	Slope/W		Slope Stability		
	Moment	Force	Moment	Force	
Ordinary	1.281		1.287		0.47
Bishop Simplified	1.434		1.436		0.14
Janbu Simplified		1.283		1.291	0.62
Spencer	1.416	1.418	1.421	1.407	0.78
GLE	1.413	1.413	1.417	1.417	0.28

Table 181 Fabric with rein and no line load

Method	Factor of Safety (with rein but no line load)				Difference (%)
	Slope/W		Slope Stability		
	Moment	Force	Moment	Force	
Ordinary	1.386		1.392		0.43
Bishop Simplified	1.535		1.538		0.20
Janbu Simplified		1.397		1.387	0.72
Spencer	1.517	1.512	1.523	1.508	0.26
GLE	1.514	1.514	1.518	1.518	0.26

4.6 BISHOP AND MORGENSTERN - HOMOGENEOUS

Project: Slopes_Group_2
Model: VW_7

This example problem is based on an example problem original published by Bishop and Morgenstern, (1960). The solutions presented in the original work developed a series of stability charts that could then be used to estimate the factor of safety for simple, homogenous earth slopes.

4.6.1 Purpose

The purpose of this model is to illustrate agreement between the Slope Stability software and the original slope stability charts.

4.6.2 Geometry and Material Properties

The slope of this particular model is at a ratio to 4 horizontal to 1 vertical. The grid and radius search technique was used to identify the location of the critical slip surface.

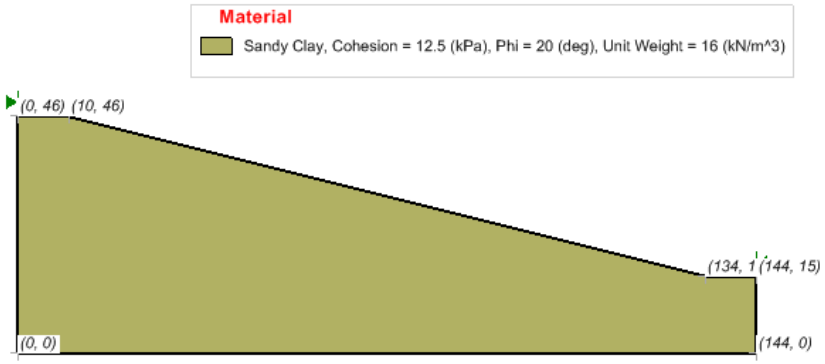

Figure 122 Geometry of the Bishop and Morgenstern Homogenous Model

4.6.3 Results and Discussions

The location of the critical slip surface and the calculation of the factor of safety can be seen in the following table. A factor of safety of 1.35 was calculated which agrees well with stability chart calculations. In this case, the Bishop Simplified method and the Morgenstern-Price method yields similar results.

Table 182 Chart results Bishop and Morgenstern Homogenous model

Method	Factor of Safety				Difference (%)
	Slope/W		Slope Stability		
	Moment	Force	Moment	Force	
Ordinary	1.231		1.232		0.08
Bishop Simplified	1.337		1.338		0.08
Janbu Simplified		1.261	1.262		0.08
Corps of Engineers #1		1.344		1.345	0.07
Corps of Engineers #2		1.351		1.352	0.07
Lowe-Karafiath		1.347		1.346	-0.08
Spencer	1.338	1.339	1.339	1.339	0.08
M-P	1.338	1.34	1.339	1.338	0.08
GLE	1.338	1.338	1.339	1.338	0.08

4.7 FREDLUND AND KRAHN (1977)

Project: Slopes_Group_2
Model: VW_8

This example model was originally presented by Fredlund and Krahn (1977). It represented a comparison study of various slope stability methods.

4.7.1 Purpose

In this example, the slope is comprised of three layers. The upper layer contains a weak layer at its base. The weak layer

subsequently overlays a bedrock layer.

4.7.2 Geometry and Material Properties

The critical slip surface will potentially come down and follow along the weak layer, but will not extend into the strong bedrock.

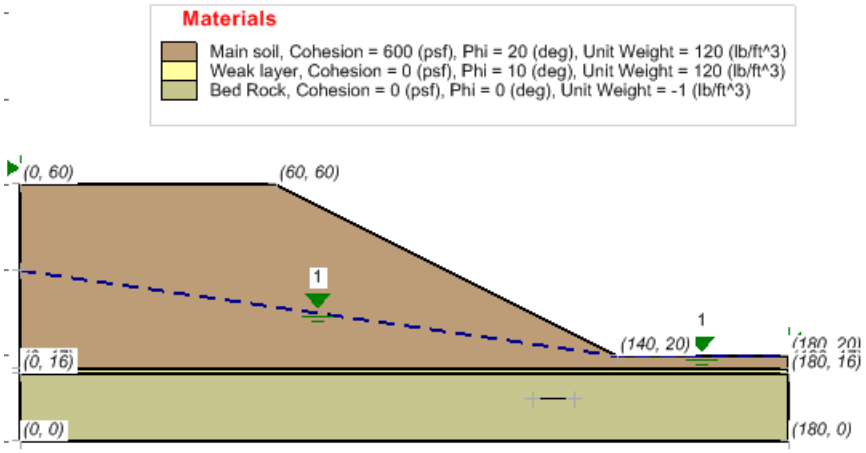

Figure 123 Geometry of the Fredlund and Krahn (1977) Model

4.7.3 Results and Discussions

The following table shows the results of the calculations for this model. The results compare reasonably to the results calculated by Fredlund and Krahn (1977).

Table 183 Results of the Fredlund and Krahn (1977)

Method	Factor of Safety				Difference (%)
	Slope/W		Slope Stability		
	Moment	Force	Moment	Force	
Ordinary	1.147		1.151		0.35
Bishop Simplified	1.210		1.213		0.25
Janbu Simplified		1.186		1.191	0.42
Corps of Engineers #1		1.272		1.273	0.08
Corps of Engineers #2		1.259		1.263	0.32
Spencer	1.212	1.212	1.215	1.214	0.25
M-P	1.205	1.205	1.209	1.208	0.33
GLE	1.205	1.205	1.209	1.208	0.33

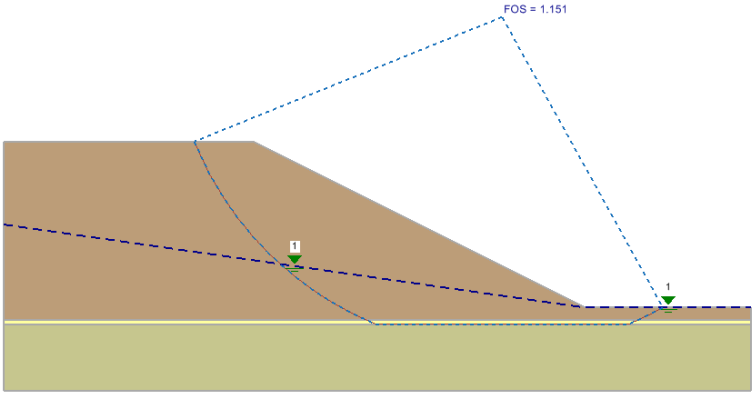

Figure 124 Critical slip surface calculated for the Fredlund and Krahn model (Ordinary method)

4.8 SIMPLE TWO MATERIAL MODEL

Project: Slopes_Group_2
Model: VW_9

This example consists of a simple two layers slope with a water table. The problem is analyzed using the Bishop Simplified method as well as the Morgenstern Price method.

4.8.1 Purpose

The purpose of this example is to illustrate the calculation of the Factor of Safety for a simple slope example.

4.8.2 Geometry and Material Properties

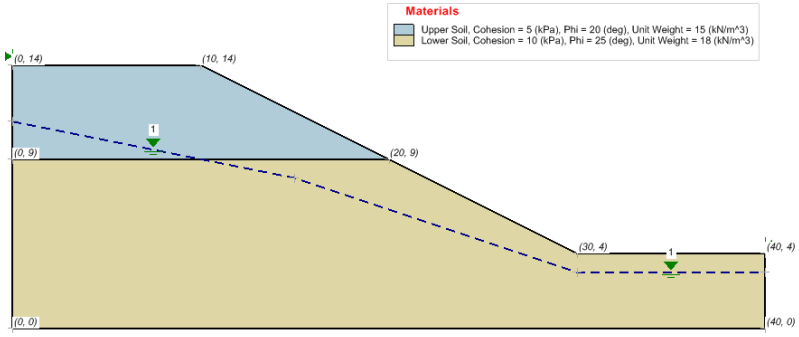

Figure 125 Geometry of the Simple Two Material slope model

	c (kN/m^2)	ϕ (degrees)	γ (kN/m^3)
Upper Soil	5.0	20.0	15.00
Lower Soil	10.0	25.0	18.00

4.8.3 Results and Discussions

The factors of safety calculated for this example are shown in Table 184. The results agree well with those calculated using the Slope/W software.

Table 184 Results of the Simple Two Material model

Method	Factor of Safety				Difference (%)
	Slope/W		Slope Stability		
	Moment	Force	Moment	Force	
Ordinary	1.279		1.283		
Bishop Simplified	1.464		1.466		0.14
Janbu Simplified		1.286		1.290	
Corps of Engineers #1		1.502		1.505	0.20
Corps of Engineers #2		1.534		1.536	0.13
Lowe-Karafiath		1.498		1.505	0.47
Spencer	1.467	1.469	1.469	1.469	0.14
M-P	1.466	1.471	1.468	1.467	0.14
GLE	1.466	1.466	1.468	1.468	0.14

4.9 INFINITE SLOPE MODEL

Project: Slopes_Group_2
Model: VW_11

This example illustrates the use of the software to calculate the stability of a semi-infinite slope. In this case the Morgenstern-price method was used to calculate the Factor of Safety.

4.9.1 Geometry and Material Properties

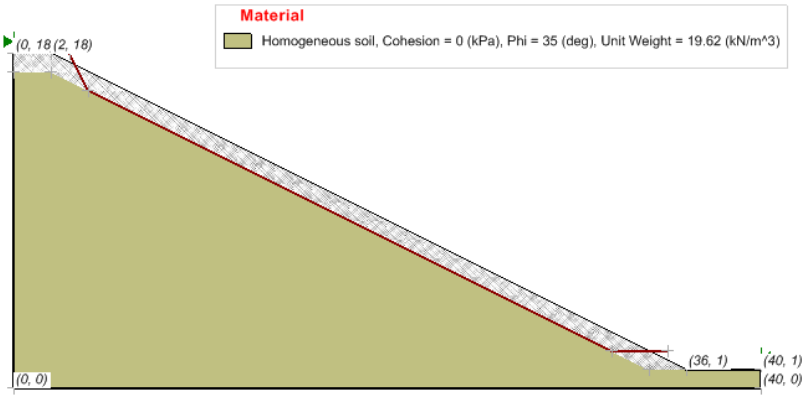

Figure 126 Geometry of Infinite Slope model

4.9.2 Results and Discussions

The results of the analysis are shown in Table 185 comparing Slope Stability to Slope/W and Slide. The results can be compared to the calculated closed-form solutions as presented in Table 186 from the Slope/W documentation. Note that Slope/W uses a different method than Slope Stability such that different slices are used in the calculation of FOS when tension cracks are considered, refer to Figure 127 and Figure 128.

Table 185 Infinite Slope model

Method	Factor of Safety						Slope Stability Difference	
	Slope/W		Slide		Slope Stability		Slope/W	Slide
	Moment	Force	Moment	Force	Moment	Force	(%)	(%)
Ordinary	1.400		1.461		1.479		5.61	1.20
Bishop Simplified	1.402		1.477		1.495		6.66	1.25
Janbu Simplified		1.400		1.462		1.462	4.46	0.03
Corps of Engineers #1		1.400		1.481		1.480	5.74	0.04
Corps of Engineers #2		1.400		1.481		1.482	5.86	0.07
Lowe-Karafiath		1.400		1.476		1.482	5.86	0.41
Spencer	1.400	1.400	1.478	1.478	1.481	1.481	5.79	0.21
M-P	1.400	1.400	1.466	1.466	1.466	1.467	4.74	0.03
GLE	1.400	1.400	1.466	1.466	1.467	1.467	4.79	0.08

Table 186 Slope/W infinite slope results closed form solution comparison

Case	ϕ'	c'	r_u	Factor of Safety		
				Closed Form Solution	SLOPE/W Bishop Simplified	SLOPE/W Morgenstern-Price
1	35	0.0	0.0	1.400	1.402	1.400
2	35	0.0	0.25	0.963	0.965	0.963
3	35	5.0	0.25	1.600	1.601	1.600

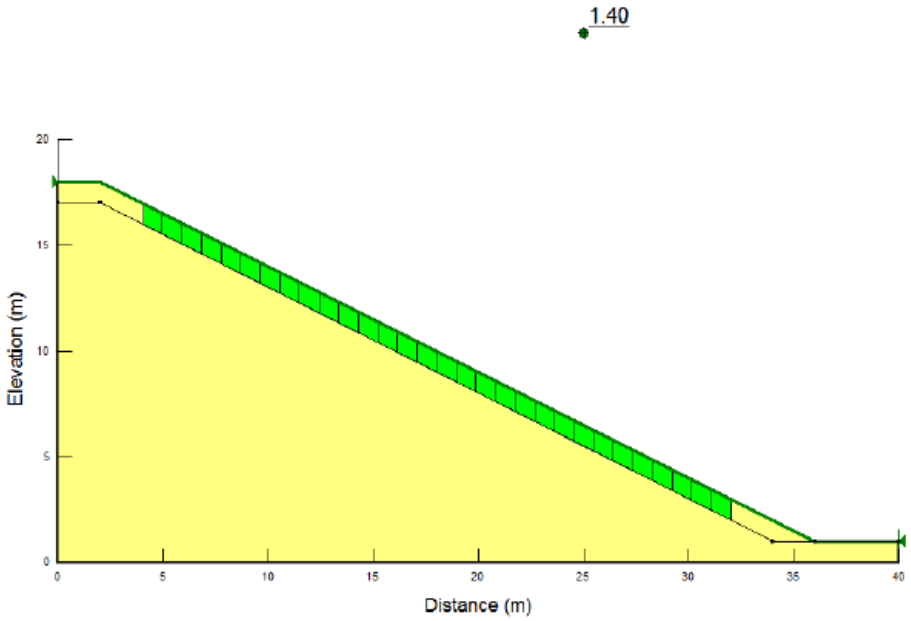

Figure 127 Infinite Slope model Slope/W results slices

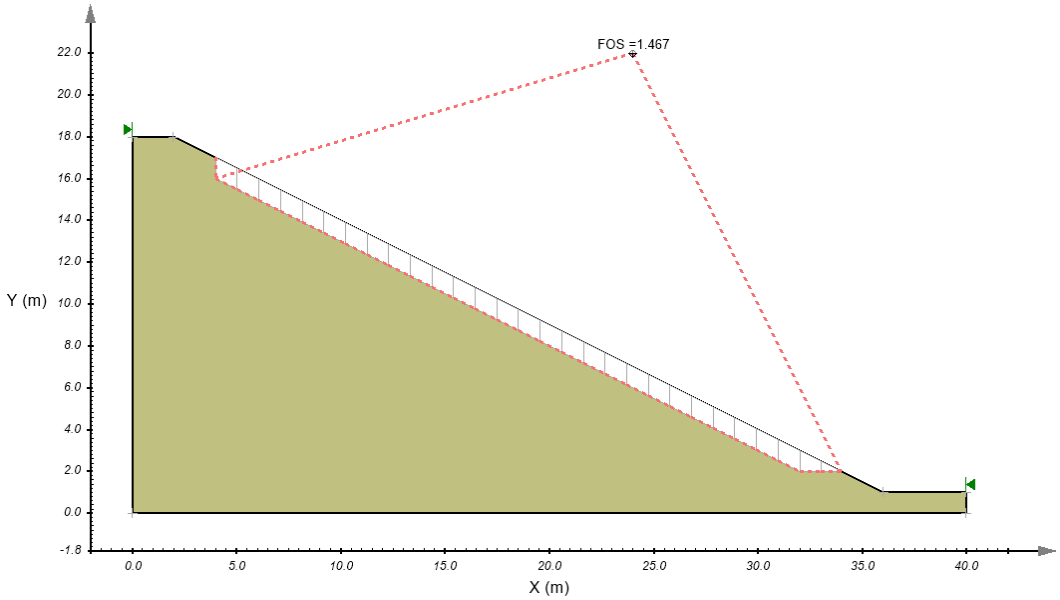

Figure 128 Infinite Slope model Slope Stability results slices

4.10 LAMBE AND WHITMAN - DRAINED SLOPE

Project: Slopes_Group_2
Model: VW_12

This model was originally presented by Lambe and Whitman (1969). In the original solution Lambe and Whitman presented a hand-calculated Factor of Safety for a simple slope with under drain.

4.10.1 Geometry and Material Properties

The slope is 20 feet high and has a slope of 1 horizontal to 1.5 vertical. The slope consists of a single homogenous material. The slip surface is assumed to be circular with the radius of 30 feet. In the original calculations, the pore-water pressures conditions in the slope were characterized by a flow net.

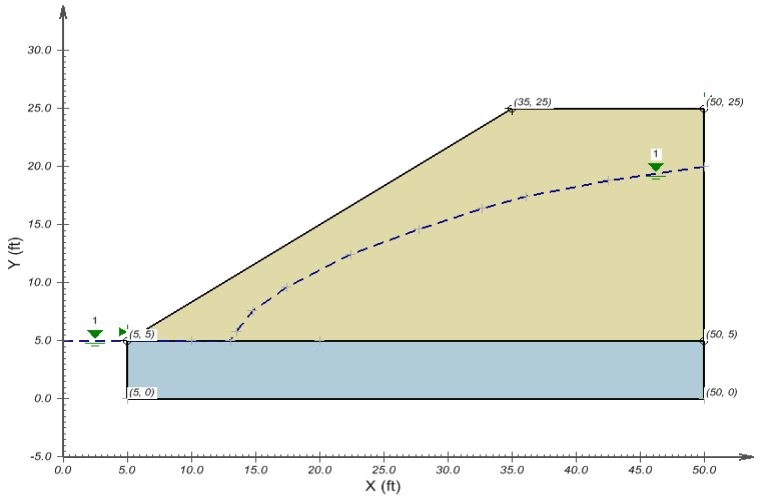

Figure 129 Geometry of the Lambe and Whitman – Drained Slope model

4.10.2 Results and Discussions

The results of the Slope Stability software package are compared to the original Lambe and Whitman calculations.

Table 187 Lambe and Whitman – Drained Slope model

Method	Factor of Safety				Difference (%)
	Slope/W (30 slices)		Slope Stability (30 slices)		
	Moment	Force	Moment	Force	
Ordinary	1.198		1.200		0.18
Bishop Simplified	1.332		1.333		0.08
Janbu Simplified		1.207		1.210	0.25
Corps of Engineers #1		1.376		1.381	0.36
Corps of Engineers #2		1.397		1.401	0.29
Lowe-Karafiath		1.346		NS	
Spencer	1.332	1.338	1.334	1.333	0.15
M-P	1.332	1.339	1.335	1.334	0.23
GLE	1.332	1.332	1.335	1.334	0.23

4.11 PORE-WATER PRESSURES AT DISCRETE POINTS

Project: Slopes_Group_2
Model: VW_13, VW_13_NoTensionCrack_NoPWP, VW_13_NoPWP, VW_13_NoTensionCrack

A single circular slip surface was used in this case and a tension crack zone was specified through the use of a limiting angle designation.

4.11.1 Purpose

The purpose of this model is to illustrate the use of specified pore-water pressures at discrete points in the model. The GLE method is used to analyze this case.

4.11.2 Geometry and Material Properties

A spline interpolation was used between the pore-water pressures points in order to determine the pore-water pressures at the base of each slice.

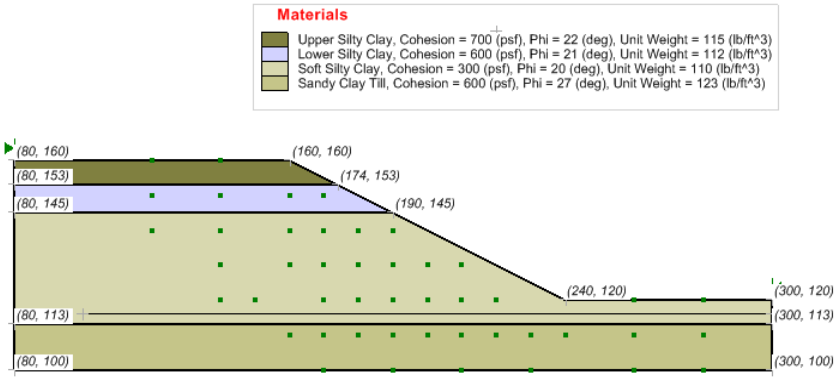

Figure 130 Geometry of the Pore-Water Pressures a Discrete Points model

4.11.3 Results and Discussions

The results of the analysis are shown in Table 188 comparing Slope Stability to Slope/W and Slide. A comparision of the Slope Stability models with different combinations pore-water pressure discrete points and tension cracks is presented in Table 189. Note that Slope/W uses a different method than Slope Stability such that different slices are used in the calculation of FOS when tension cracks are considered, refer to Figure 131 and Figure 132.

Table 188 Discrete points model results

Method	Factor of Safety				Difference (%)
	Slope/W		Slope Stability		
	Moment	Force	Moment	Force	
GLE	1.382		1.299	1.298	6.03

Table 189 Comparison of Slope Stability models with and without pore-water pressures and tension cracks

Method	Factor of Safety					
	Neglect pore-water pressures and no cracks		With pore-water pressure, no tension cracks		Neglect pore-water pressures with tension cracks	
	Moment	Force	Moment	Force	Moment	Force
Ordinary	1.544		1.222		1.544	
Bishop Simplified	1.624		1.285		1.624	
Janbu Simplified		1.531		1.238		1.531
Corps of Engineers #1		1.671				
Corps of Engineers #2		1.710				
Lowe-Karafiath		1.664				
Spencer	1.622	1.623				
M-P	1.622	1.621				
GLE	1.622	1.621	1.286	1.286	1.622	1.621

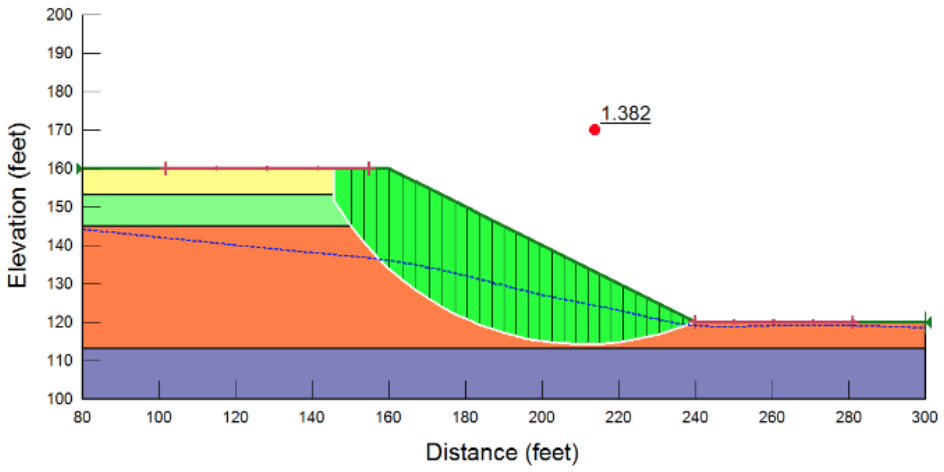

Figure 131 Spatial Pore Water Pressure Head model Slope/W results slices

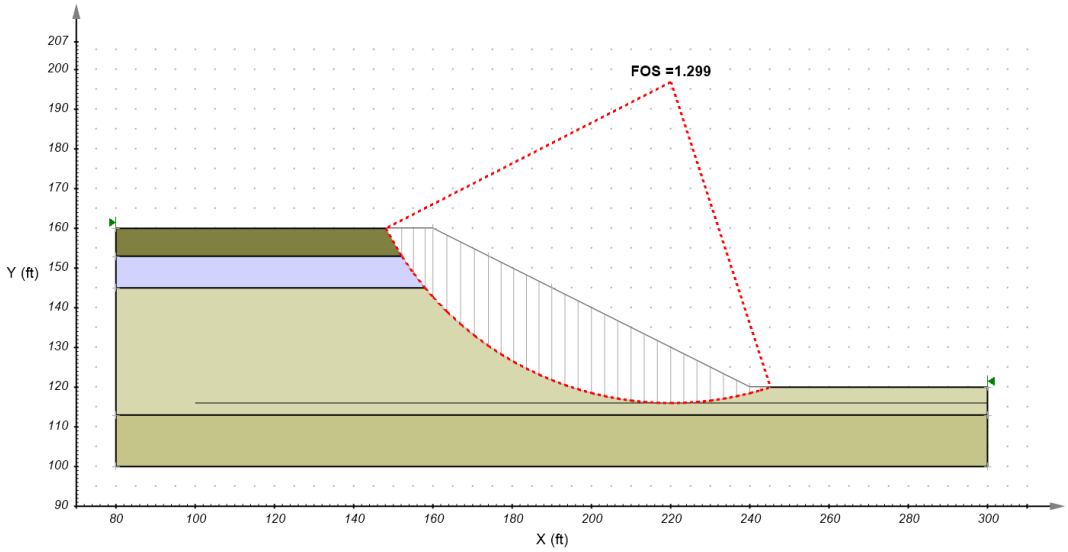

Figure 132 Spatial Pore Water Pressure Head model Slope Stability results slices

5 SLOPE STABILITY GROUP 3

The following section represents the third group of benchmark examples used to verify the correctness of the Slope Stability software. These examples are generally related to some of the more recent and advanced features of the software.

5.1 RAPID DRAWDOWN – 3 STEP METHOD

This example documents the implementation of the 3-stage rapid drawdown procedure originally proposed by the USACE and later updated by Duncan et al. (1990). This rapid drawdown procedure represents a total stress approximation of effective stress conditions. The three-stage procedure incorporates aspects of both the U.S. Army Corps of Engineers (1970) method as well as the Lowe and Karafiath's (1959) method. The procedure is designed to account for the effect of drainage and the fact that the drained strength may be less than the undrained strength. It is important to note that it differs from the Corps of Engineers' procedure in the way that undrained strength is evaluated and the way that drained strength is taken into account. In a manner similar to Lowe and Karafiath the procedure accounts for the effects of anisotropic consolidation, which can result in significantly higher undrained shear strength (Duncan, 2005).

Project: Slope Stability_Group_3
Model: RDD01, RDD_WT, RDD_NoWT, RDD_WT35

5.1.1 Purpose

The purpose of this set of examples is to demonstrate the correct implementation of the three-stage analysis for total stress rapid drawdown calculation in Slope Stability.

5.1.2 Geometry and Material Properties

In this example a simple slope is set up as shown in Figure 133. Several scenarios were created with both the water table at the top of the slope and at the bottom. The final scenario (RDD01) then evaluates the movement of the water table from the top of the slope to the bottom using the three-stage analysis.

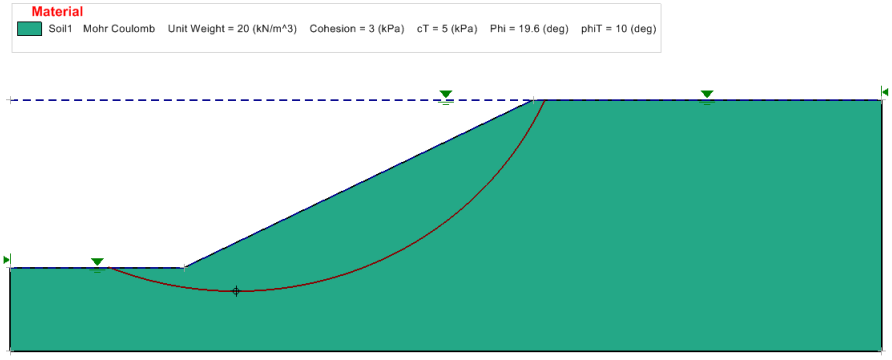

Figure 133 Geometry of the simple slope used for rapid drawdown calculations

5.1.3 Results and Discussions

The various scenarios were evaluated using the Slope Stability, Slide, and Slope/w software packages. The results can be seen in Table 190, Table 191,

Table 192, and Table 193. It can be seen from the analysis results that there is very reasonable agreement between the three software packages. It should be noted, however, that at the writing of this document the Slide software does not specifically implement the three-stage method of rapid drawdown as proposed by Duncan (1990). Therefore the Slide software was not compared in the total stress rapid draw-down method comparison. The small differences in calculations between software packages are generally less than 4% and are reasonable when all potential influences of this set of calculations are considered.

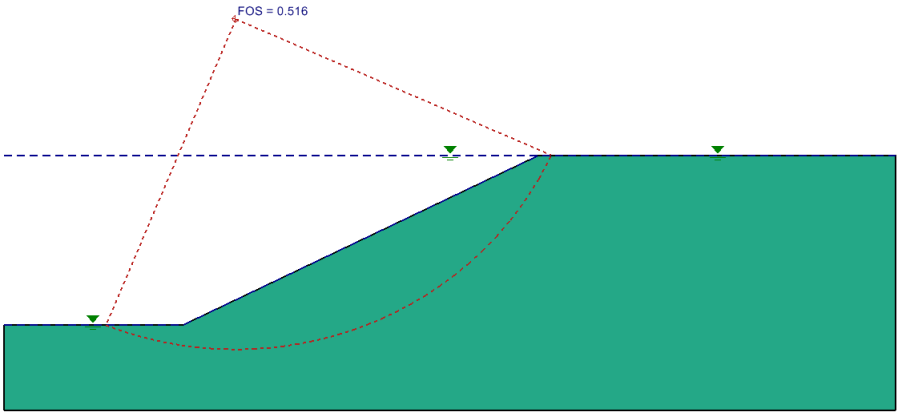

Figure 134 Example of results of three-stage rapid drawdown calculation

Table 190 Comparison of software package answers for the three-stage analysis

Method	Rapid Draw-Down			
	Slope Stability		Slope/W	
	Moment	Force	Moment	Force
Ordinary	0.317		0.450	
Bishop	0.397		0.560	
Janbu		0.335		0.500
Engineer#1		0.499	1.584	0.530
Engineer#2		0.337		0.530
L-K		0.308		
Spencer	0.522	0.522	0.480	0.480
M-P	0.521	0.521	0.490	0.490
GLE	0.510	0.510	0.490	0.490

Model:RDD01

Table 191 Comparison when water table follows ground surface

Method	WT Along Ground Surface					
	Slope Stability		Slope/W		Slide	
	Moment	Force	Moment	Force	Moment	Force
Ordinary	0.504		0.583		0.443	
Bishop	0.568		0.574		0.571	
Janbu		0.496		0.498		0.497
Engineer#1		0.599		0.604		0.622
Engineer#2		0.634		0.621		0.584
L-K		0.595		0.589		0.585
Spencer	0.582	0.582	0.894	0.594	0.602	0.602
M-P	0.583	0.583	0.593	0.593	0.586	0.586
GLE	0.583	0.583			0.586	0.586

Model: RDD_WT

Table 192 Comparison when there is no water table

Method	No WT					
	Slope Stability		Slope/W		Slide	
	Moment	Force	Moment	Force	Moment	Force
Ordinary	0.999		1.002		0.999	
Bishop	1.108		1.113		1.108	
Janbu		0.991		0.994		0.991
Engineer#1		1.119		1.121		1.119
Engineer#2		1.147		1.150		1.146
L-K		1.114		1.122		N/A
Spencer	1.106	1.106	0.894	1.110	1.106	1.106
M-P	1.108	1.111	0.593	1.113	1.108	1.111
GLE	1.105	1.105			1.108	1.108

Model: RDD_NoWT

Table 193 Comparison when the water table is at an elevation of 35m

Method	No WT					
	Slope Stability		Slope/W		Slide	
	Moment	Force	Moment	Force	Moment	Force
Ordinary	0.918		1.146		0.699	
Bishop	1.252		1.258		1.252	
Janbu		1.126		1.128		1.126
Engineer#1		N/A		7.357		7.767
Engineer#2		N/A		1.128		1.126
L-K		N/A		1.438		N/A
Spencer	1.257	1.256		1.262	1.254	1.254
M-P	1.256	1.255		1.261	1.254	1.254
GLE	1.256	1.256			1.255	1.255

Model:RDD_WT35

5.2 RAPID DRAWDOWN - WALTER BOULDIN DAM

Walter Bouldin Dam is a rolled earthfill embankment. The dam is about 60 feet high, sitting on 80 feet of clayey sand and gravel. Overlying the gravel are a layer of cretaceous clay, a zone of micaceous silt, and a clayey silty sand layer that covers the slope.

During a rapid drawdown of 32 feet in 5.5 hours the Walter Bouldin Dam failed on February 10, 1975.

Project: Slopes_Group_3
Model: RDD_WalterBouldinDam

5.2.1 Purpose

The purpose of this model is to document the correct solution of the rapid drawdown methodology as presented by Duncan et al. (1990).

5.2.2 Geometry and Material Properties

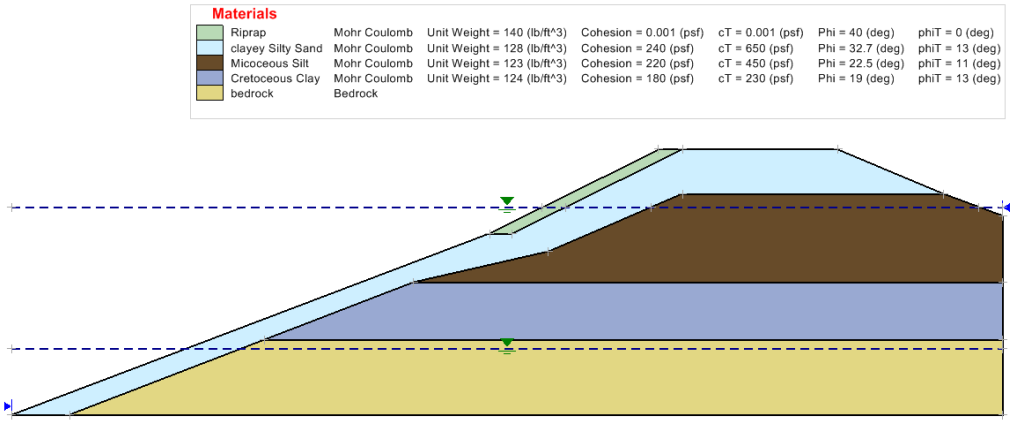

Figure 135 Geometry of the Walter Bouldin Dam

5.2.3 Results and Discussions

The results of the analysis are found to compare well with the implementation of the Duncan method in the Slope/W software. The noted differences are reasonable and acceptable. Duncan reported a factor of safety of 1.04 and it is believed that Spencer's method is utilized.

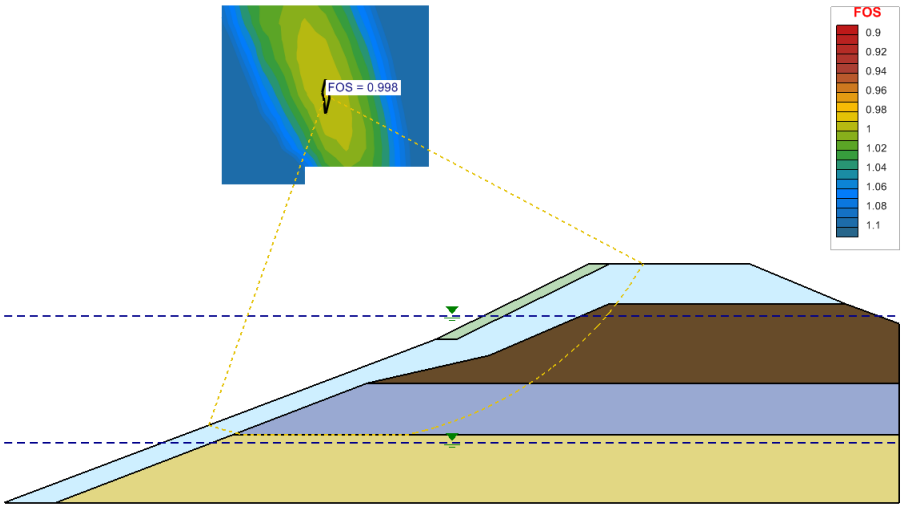

Figure 136 Slip surface location for the Walter Bouldin dam

Table 194 Comparison of FOS with Slope/W for Walter Bouldin Dam

Method	Factor of Safety				Difference (%)
	Slope Stability		Slope/W		
	Moment	Force	Moment	Force	
Bishop	1.002		1.016		-1.397
Spencer	0.999	0.998	1.02		-2.352

Table 195 Comparison of FOS between Slope Stability and Duncan et al. (1990)

	Corps #2	Lowe-Karafiath
Duncan et al. (1990)	0.93	1.09
Slope Stability	1.016	1.034
Difference	9.2%	-5.1%

5.3 RAPID DRAWDOWN - USACE BENCHMARK

This benchmark example is created by the US Army Corps of Engineers in the Appendix G of the Engineering Manual – EM 1110-2-1902. It's published FOS = 1.44. The rapid drawdown water level is from 103 feet to 24 feet.

Project: Slope Stability_Group_3
Model: RDD_USACE

5.3.1 Purpose

The purpose of this model is to document the correct solution of the rapid drawdown methodology as presented by Duncan et al. (1990).

5.3.2 Geometry and Material Properties

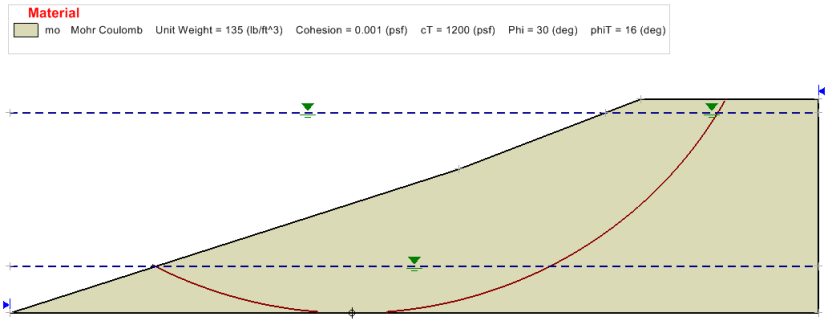

Figure 137 Geometry of the USACE Benchmark Example

5.3.3 Results and Discussions

The results of the analysis are found to compare well with the implementation of the Duncan method in the Slope/W software. The noted differences are reasonable and acceptable.

Table 196 Comparison of FOS with Slope/W for USACE benchmark

Method	Factor of Safety				Difference (%)
	Slope Stability		Slope/W		
	Moment	Force	Moment	Force	
Bishop	1.435		1.428		0.508
Janbu		1.269		1.279	0.777
Spencer	1.427	1.427	1.433		0.58

5.4 RAPID DRAWDOWN - PUMPED STORAGE PROJECT DAM

The Pumped Storage Project Dam has a densely compacted, silty clay core. The lower portion of the upstream slope is a zone of random materials with the equivalent of same strength properties as the core. The upper portion of the upstream slope and the entire downstream slope is a free draining rock fill. For the rapid drawdown analysis the water level is lowered from 545 feet to 380 feet.

The Duncan 3-Stage Rapid Drawdown Analysis method is used in Slope Stability to solve this model. The implementation of

the method is based on the theory presented by Duncan, Wright, and Wong (1990).

Project: Slope Stability_Group_3
Model: RDD_Pumped_Storage_Project_Dam, RDD_Pumped_Storage_Project_Dam_3D

5.4.1 Purpose

The purpose of this model is to document the correct solution of the rapid drawdown methodology as presented by Duncan et al. (1990).

5.4.2 Geometry and Material Properties

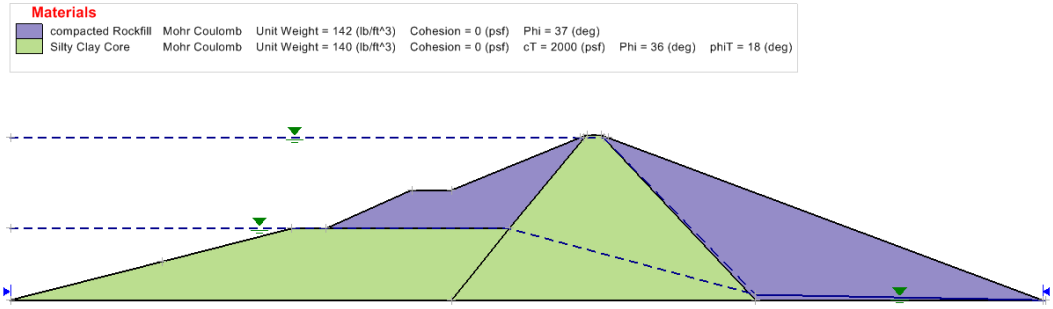

Figure 138 Geometry of the Pumped Storage Project Dam

5.4.3 Results and Discussions

The results of the analysis are found to compare well with the implementation of the Duncan method in the Slope/W software. The noted differences are reasonable and acceptable.

Table 197 Comparison of FOS with Slope/W for Pumped Storage Project Dam

Method	Factor of Safety				Difference (%)
	Slope Stability		Slope/W		
	Moment	Force	Moment	Force	
Bishop	1.538		1.534		0.23
Janbu		1.423		1.420	0.24
Spencer	1.527	1.528	1.537		0.641

5.5 RAPID DRAWDOWN - PILARCITOS DAM

The Pilarcitos Dam is a homogeneous rolled earth-fill embankment. The slope failure occurred after the water level was lowered from elevation of 692 to elevation of 657 between Oct. 07 and Nov. 19, 1969.

Project: Slope Stability_Group_3
Model: RDD_PilarcitosDam

5.5.1 Purpose

The purpose of this model is to document the correct solution of the rapid drawdown methodology as presented by Duncan et al. (1990).

5.5.2 Geometry and Material Properties

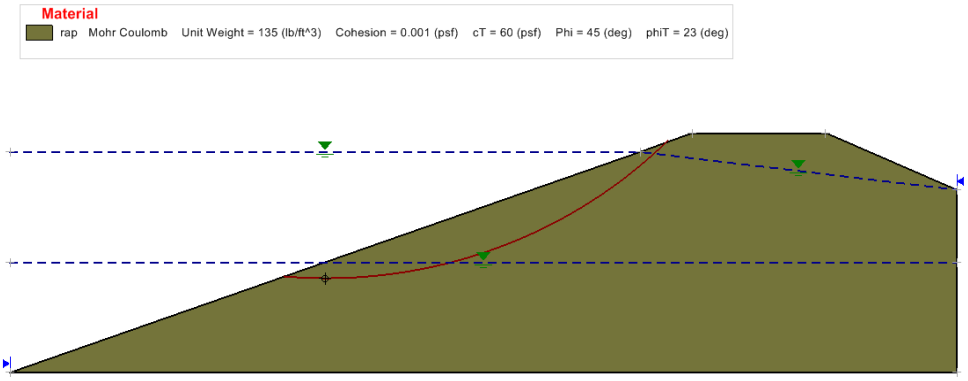

Figure 139 Geometry of the Pilarcitos Dam

5.5.3 Results and Discussions

The results of the analysis are found to compare well with the implementation of the Duncan method in the Slope/W software. The noted differences are reasonable and acceptable. The FOS published by Duncan is 1.05 for the Lowe and Karafiath method.

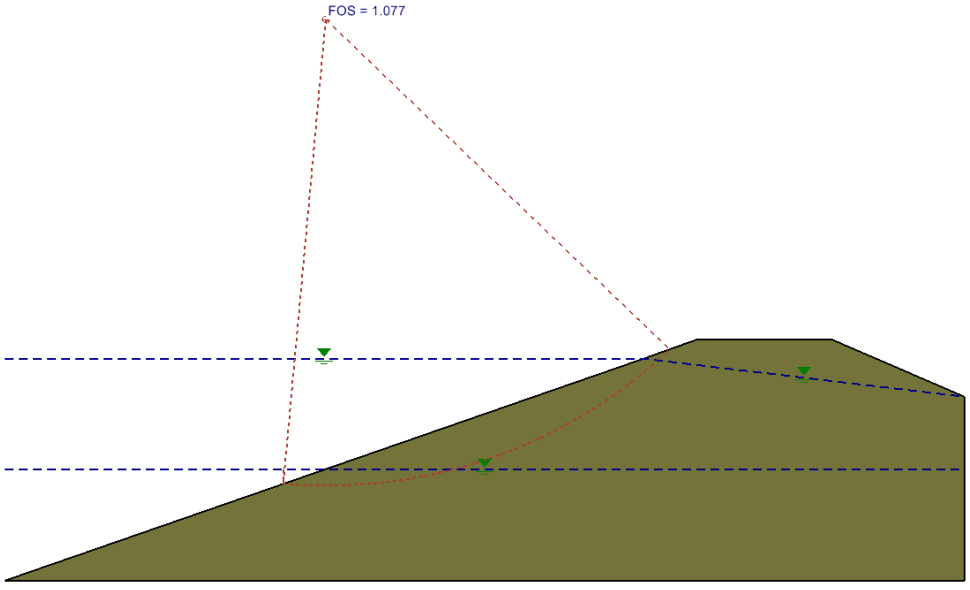

Figure 140 Location of the critical slip surface for the Pilarcitos Dam

Table 198 Comparison of FOS with Slope/W for Pilarcitos Dam

Method	Factor of Safety				Difference (%)
	Slope Stability		Slope/W		
	Moment	Force	Moment	Force	

Bishop	1.077		1.047		2.901
Janbu		1.043		1.006	3.684
Spencer	1.063	1.063	1.051		1.166

Table 199 Comparison of FOS with Duncan et al. (1990)

	Corps #2	Lowe-Karafiath
Duncan et al. (1990)	0.82	1.05
Slope Stability	0.844	0.967
Difference	2.9%	-7.9%

5.6 SHEAR NORMAL FUNCTION

This example documents the implementation of the shear normal function material model.

Project: Slope Stability_Group_3
Model: VS_1_SNF

5.6.1 Purpose

The purpose of this example is to demonstrate the correct implementation of the shear normal function material model calculation in Slope Stability.

5.6.2 Geometry and Material Properties

In this example a simple slope is set up as shown in Figure 141. A fully specified circular slip surface is used.

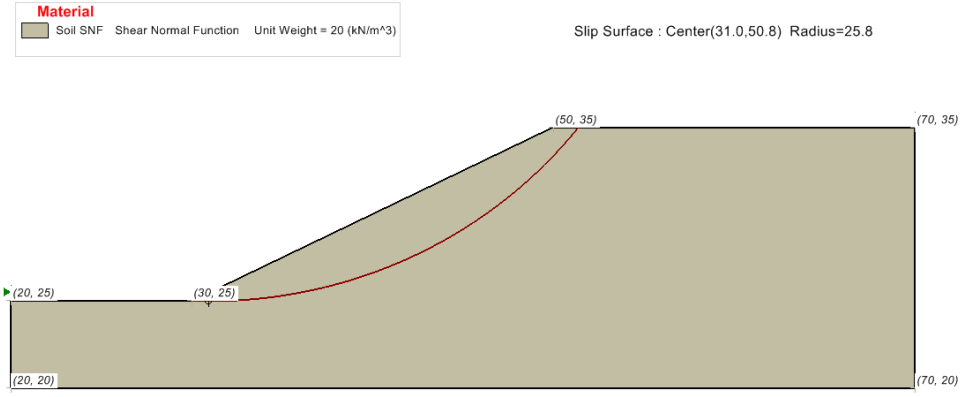

Figure 141 Geometry of the simple slope used for shear normal force calculations

5.6.3 Results and Discussions

The model was evaluated using the Slope Stability and Slide software packages. The results can be seen in

Table 190. It can be seen from the analysis results that there is very reasonable agreement between the two software packages.

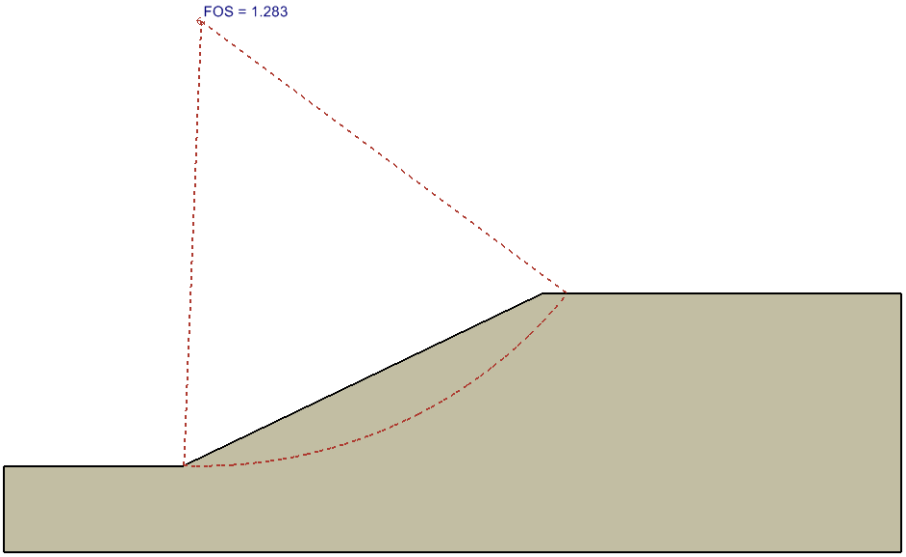

Figure 142 Example of results of shear normal function calculation

Table 200 Comparison of software package answers for analysis

Method	Factor of Safety			Difference (%)
	Slide	Slope Stability		
		Moment	Force	
Ordinary	1.283	1.283		0.000
Bishop	1.34	1.34		0.000
Janbu Simplified	1.274		1.274	0.000
Corps of Engineer#1	1.345		1.345	0.000
Corps of Engineer#2	1.35		1.35	0.000
Lowe-Karafiath	1.343		1.344	0.074
Spencer	1.338	1.338	1.338	0.000
M-P	1.338	1.338	1.338	0.000
GLE	1.338	1.338	1.338	0.000

5.7 FILL SLOPE USING A RETAINING WALL

Project: Slope_Group_3
Model: RainfallInducedFillSlopeFailure

The FillSlope model is constructed using retaining walls with three kinds of material shown in the following table. This model demonstrates the use of Slope Stability in analyzing the safety situation of a slope using a retaining wall.

5.7.1 Geometry and Material Properties

The model is set up with the geometry shown below and the material regions are entered. The material properties that are in use for this model are presented in the following table.

A water surface is assigned through the back of the slope. A slip surface is defined by line segments and cuts through the region filled with the Backfill material.

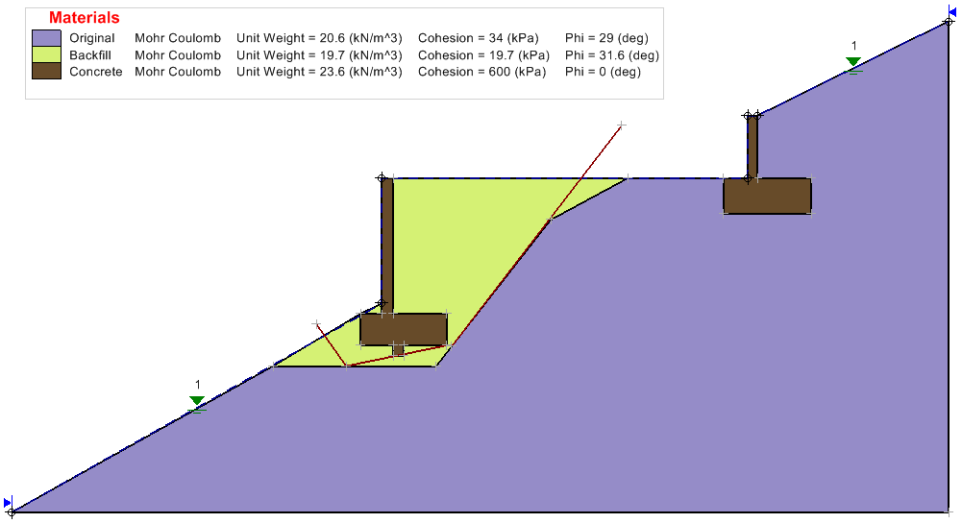

Figure 143 Geometry of the FillSlope model

Table 201 Material Properties of the FillSlope model

Material Names	Sat. Unit Wt. (kN/m^3)	Cohesion (kPa)	Friction Angle (deg)
Original	20.6	34	29
Backfill	19.7	19.7	31.6
Concrete	23.6	600.0	0.0

5.7.2 Results and Discussions

The model uses the Janbu simplified method to calculate a factor of safety (FOS) of 1.58. Compared to the FOS value 1.62 produced by STABL, the difference is -2.53 %. This difference is reasonable giving the slight variation in the geometry of the critical slip surface in Slope Stability compared to STABL.

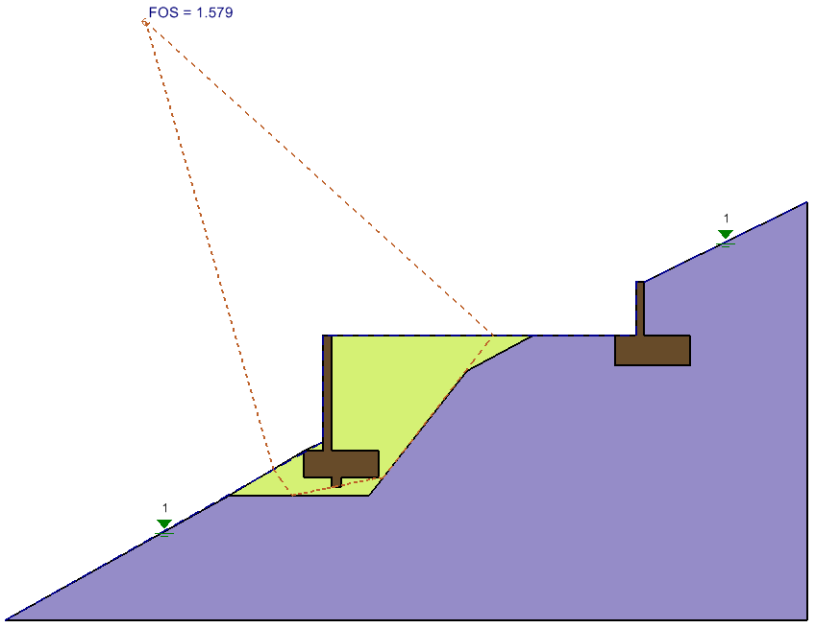

Figure 144 Solution of the FillSlope model using Janbu Simplified method

5.8 PROBABILITY - JAMES BAY CASE HISTORY

Project: Slope_Group_3
Model: James_Bay_sampling_everyslice, James_Bay_sampling_nospatial, James_Bay_sampling30m, James_Bay_sampling40m, James_Bay_sampling50m, James_Bay_sampling80m, James_Bay_sampling100m

The James Bay project required the construction of dykes and sensitive clay. These model show the construction of the dykes using 5 materials shown in the following table. The models demonstrate the use of Slope Stability in performing probabilistic stability analysis.

5.8.1 Geometry and Material Properties

The models are set up with the geometry shown below and the material regions are entered. The material properties that are in use for these models are presented in the following table. Also, the probability parameters used due to uncertainties in the soil properties are presented in Table 198. All variables are assumed to have normal distribution.

A grid and point search method is used to search for the slip surface.

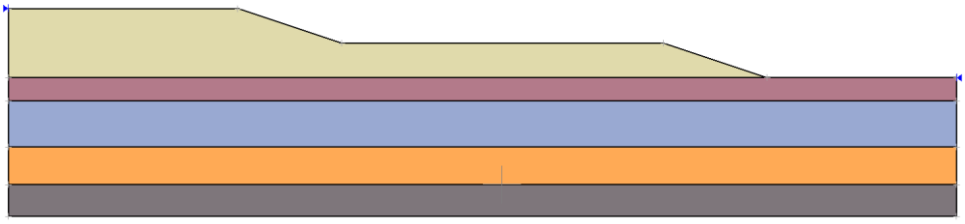

Figure 145 Geometry of the James Bay Probability model

Table 202 Material Properties of the James Bay Probability model

Material Names	Sat. Unit Wt. (kN/m^3)	Cohesion (kPa)	Friction Angle (deg)
Till	20.6	34	29
Lacustrine Clay	20.3	31.2	0
Marine Clay	18.8	34.5	0
Clay Crust	18.8	43	0
Embankment	20	0	30

Table 203 Probability Parameters of the James Bay Probability model

Material Names	Property	Mean	Standard Deviation
Embankment	Phi	30	1
Embankment	Unit Weight	20	1
Marine Clay	c	34.5	8.14
Lacustine Clay	c	31.2	8.65

5.8.2 Results and Discussions

The models use the Bishop method to calculate the factor of safety (FOS). The table below shows the FOS and spatial variability results as a function of sampling distance.

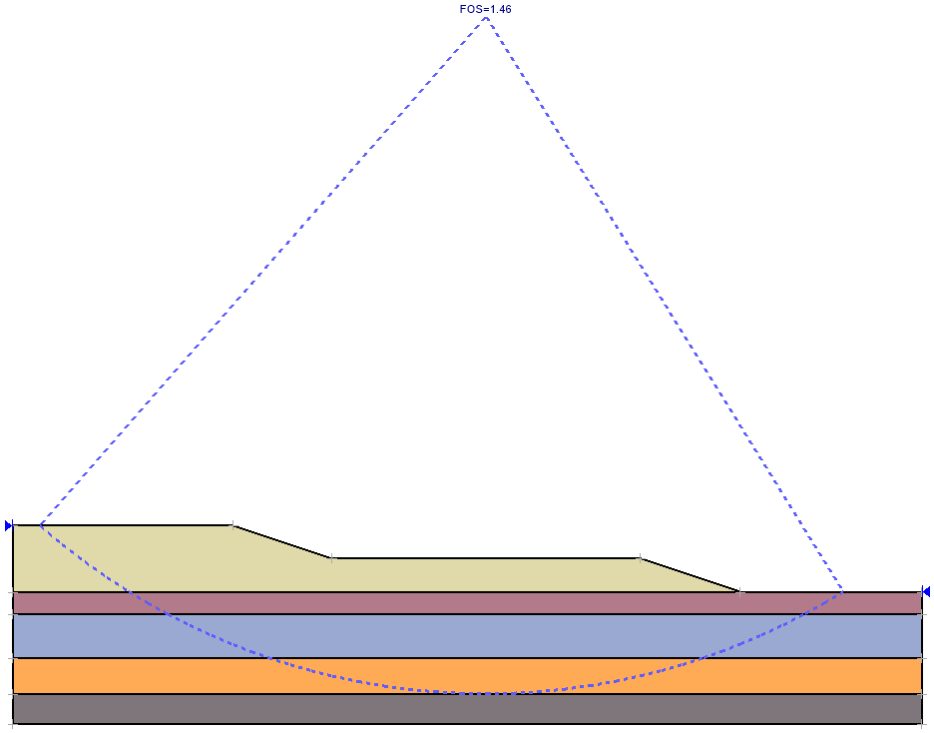

Figure 146 Solution of the James Bay Probability model (sampling every slice) using Bishop method

Table 204 Comparison of FOS with Slope/W for James Bay Probability model using Bishop method

Sampling Distance	Factor of Safety		Difference
	Slope Stability	Slope/W	(%)
Every slice	1.461	1.4605	-0.03
30m	1.461	1.4601	-0.06
40m	1.461	1.4600	-0.07
50m	1.461	1.4613	-0.02
80m	1.461	1.4606	-0.03
100m	1.461	1.4578	-0.22
No Spatial consideration	1.461	1.4611	0.01

Table 205 Spatial variability results for the James Bay Probability model

Sampling Distance	Standard Deviation		Probability of failure (%)		Reliability Index	
	Slope Stability	Slope/W	Slope Stability	Slope/W	Slope Stability	Slope/W
Every slice	0.06477	0.05537	0.000	0.000	7.406	7.109
30m	0.1336	0.12795	0.017	0.003	3.435	3.596
40m	0.1494	0.14518	0.053	0.050	3.103	3.168
50m	0.1494	0.15446	0.053	0.100	3.103	2.986
80m	0.213	0.19617	1.467	0.937	2.149	2.348
100m	0.213	0.19842	1.467	0.990	2.149	2.308
No spatial consideration	0.215	0.21295	1.363	1.340	2.154	2.165

5.9 EUROCODE 7 - CUTTING IN STILL CLAY

Project: Slope_Group_3
Model: Eurocode_CuttingInClay

This example model is based on the book titled "Designers' Guide to EN 1997-1" on page 202. The water table line may not be exactly the same as that on the book since it does not provide the coordinates.

5.9.1 Geometry and Material Properties

The model is set up with the geometry shown below. The material properties that are in use for this model are presented in the following table. A permanent distributed load with magnitude = 35KPa is applied as shown in the Figure.

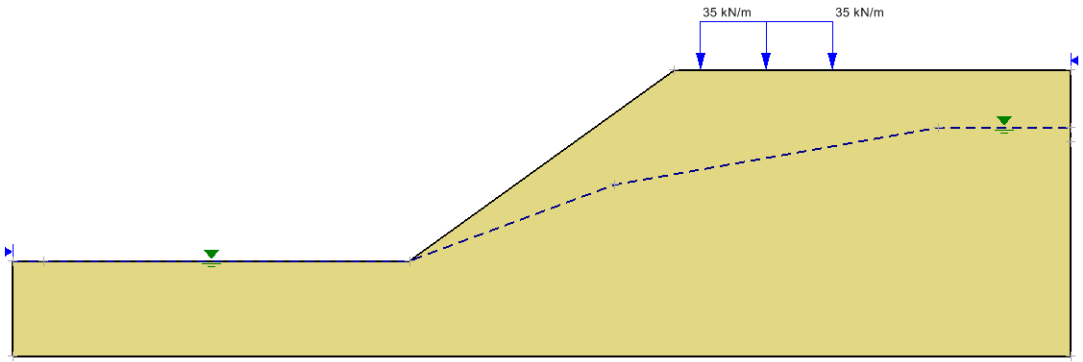

Figure 147 Geometry of the model

Table 206 Material Properties of the model

Material Names	Sat. Unit Wt. (kN/m^3)	Cohesion (kPa)	Friction Angle (deg)
Soil1	20	10	28

5.9.2 Results and Discussions

Eurocode 7 Design Approach 3 is selected to do the analysis. Grid and Tangent search method is used. The FOS is equal to 1.193 for Simplified Bishop method published in the book. The following table lists the comparison result with Slide.

Table 207 Comparison of FOS with Slide

Method	Factor of Safety				Difference (%)
	Slope Stability		Slide		
	Moment	Force	Moment	Force	
Bishop	1.172		1.177		-0.425
Janbu		1.043		1.052	-0.856
Spencer	1.174	1.174	1.179		-0.424

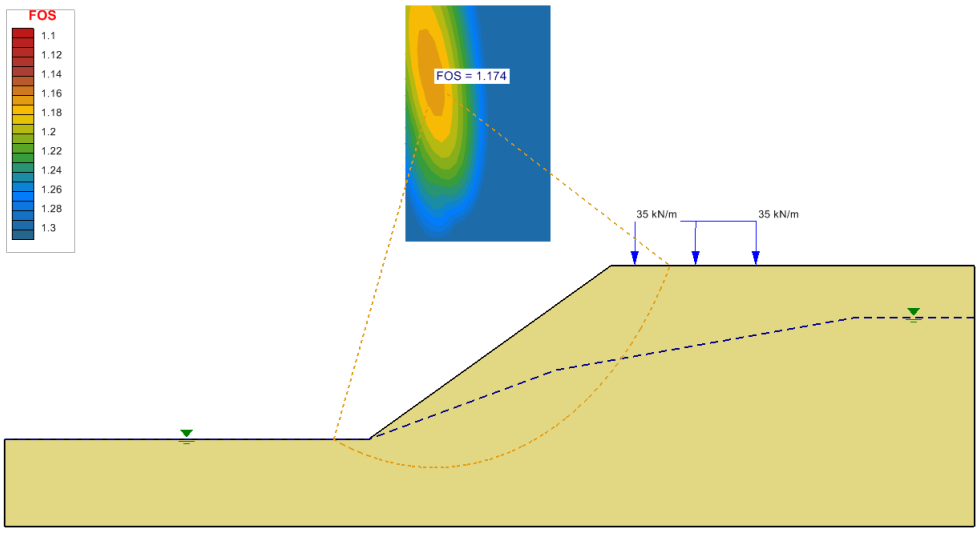

Figure 148 Solution of the model using Simplified Bishop method

5.10 EUROCODE 7 - EARTH DAM

Project: Slope_Group_3
Model: Eurocode_Dam

This example model is based on the book titled "Smith's Elements of Soil Mechanics" 8th edition, example 5.12.

5.10.1 Geometry and Material Properties

The model is set up with the geometry shown below. The material properties that are in use for this model are presented in the following table. It is a coupled Slope Stability and Groundwater model, in which the water table line is obtained from the Groundwater.

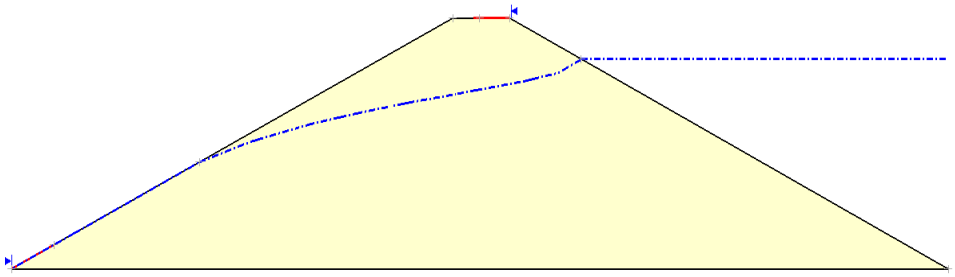

Figure 149 Geometry of the model

Table 208 Material Properties of the model

Material Names	Sat. Unit Wt. (kN/m^3)	Cohesion (kPa)	Friction Angle (deg)
Original	19.2	12	20

5.10.2 Results and Discussions

Eurocode 7 Design Approach 1, Combination 2 is selected to do the analysis. The model uses the Enxtry and Exit search method to calculate a factor of safety (FOS). The FOS is equal to 1.07 for Simplified Bishop method published in the book (page 198). The following table lists the comparison result with Slide.

Table 209 Comparison of FOS with Slide

Method	Factor of Safety				Difference (%)
	Slope Stability		Slide		
	Moment	Force	Moment	Force	
Bishop	1.093		1.096		-0.274

Janbu		1.031		1.027	0.389
Spencer	1.093	1.093	1.100		-0.636

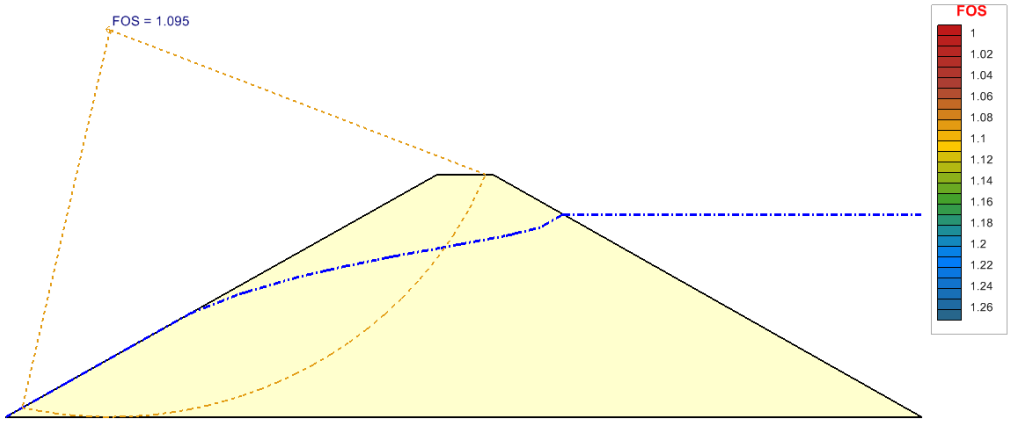

Figure 150 Solution of the model using Simplified Bishop method

5.11 ANISOTROPIC LINEAR MODEL (ALM1)

Project: Slopes_Group_3
Model: Section_B_ALM1, Section_B_ALM1_Cuckoo

This verification model was developed to examine a slope with complex faulting and stratigraphy and was solved using the Anisotropic Linear Model (ALM1). The model was analyzed in Slope Stability with both the Path Search and Cuckoo Search methods.

5.11.1 Geometry and Material Properties

The material properties are given in Table 210 and Table 211. The geometry is defined as shown in Figure 151.

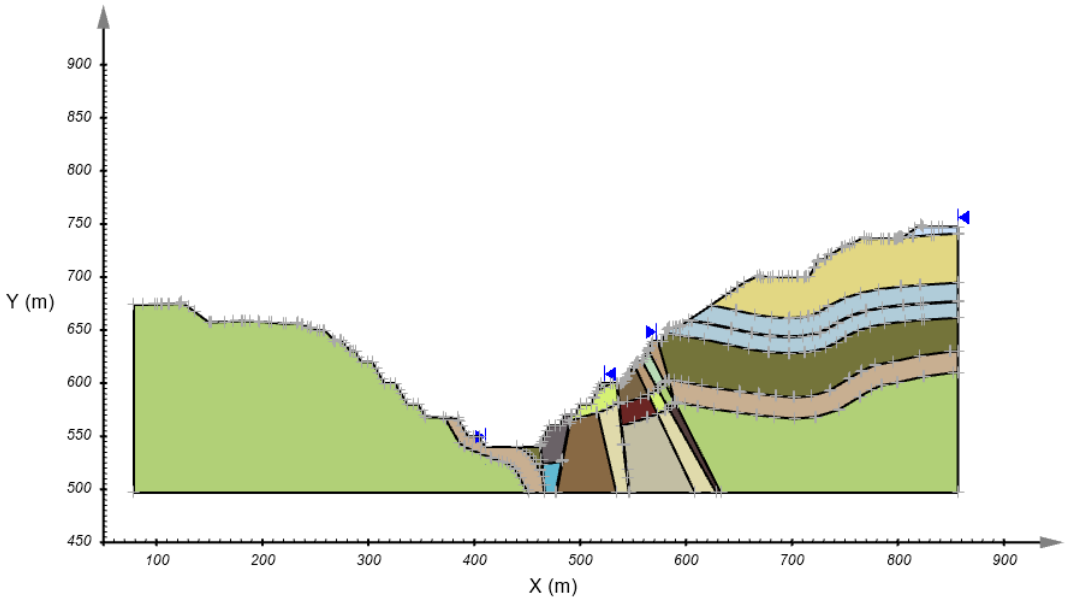

Figure 151 Geometry of the Section_B_ALM1 model

Table 210 Mohr-Coulomb Material Properties of the Section_B_ALM1 model

	c (kN/m^2)	ϕ' (degrees)	γ (kN/m^3)
MCS	139	32	22
FWZ	184	43	30
DG1	163	39	35
DG2	124	32	35
DG3	150	37	35

FILL	10	37	20
FAULT	5	25	20
SHALE BAND	10	22	20

Table 211 Anisotropic Material Properties of the Section_B_ALM1 model

	c1 (kN/m^2)	ϕ1 (degrees)	c2 (kN/m^2)	ϕ2 (degrees)	A (degrees)	B (degrees)	θ (degrees)	γ (kN/m^3)
DG1_40	10	35	163	39	5	30	40	35
DG1_30	10	35	163	39	5	30	30	35
DG1_25	10	35	163	39	5	30	25	35
DG1_20	10	35	163	39	5	30	20	35
DG1_10	10	35	163	39	5	30	10	35
FWZ_40	10	32	184	43	5	30	40	30
FWZ_25	10	32	184	43	5	30	25	30
FWZ_20	10	32	184	43	5	30	20	30
FWZ_10	10	32	184	43	5	30	10	30
MCS_40	10	27	139	32	5	30	40	22
MCS_25	10	27	139	32	5	30	25	22
MCS_20	10	27	139	32	5	30	20	22
MCS_15	10	27	139	32	5	30	15	22

5.11.2 Results and Discussions

For the Section_B_ALM1 model, the analysis using the Path Search method, results in a FOS = 1.152.

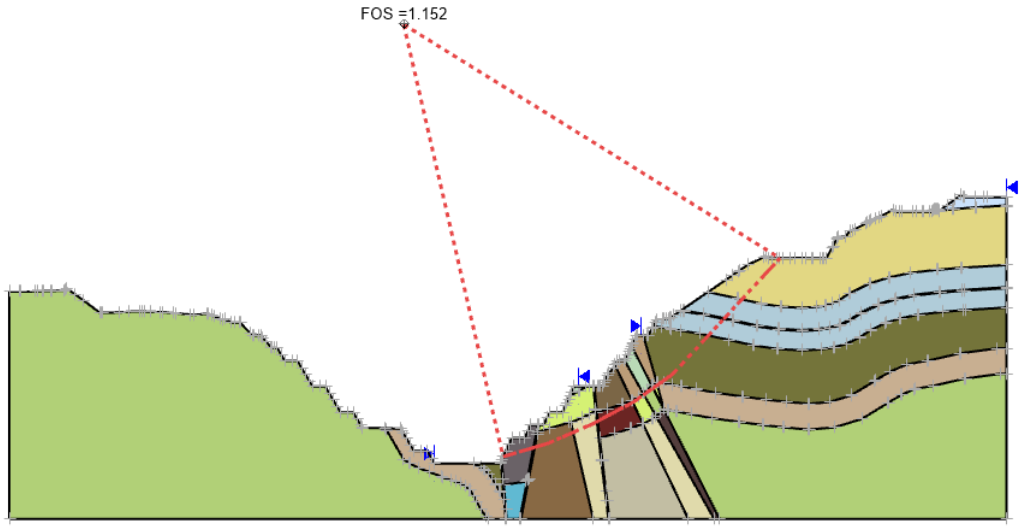

Figure 152 Factor of Safety for Path Search analysis of Section_B_ALM1

Table 212 Results of the analysis of Section _B_ALM1 model

Method	Factor of Safety			Difference (%)
	Slide	Slope Stability		
Section_B_ALM1	1.098	1.152	1.152	-4.9
Section_B_ALM1_Cuckoo	1.098	1.124	1.124	-2.4

5.12 SPECTRAL PSEUDO-STATIC ANALYSIS

Project: Slopes_Group_3
Model: Spectral_Seismic

This verification model represents a clay slope divided into 5m thick sub-layers with the cohesion increasing with depth. The slope is subjected to a spectral pseudo-static load.

The model is developed from Ghobrial et al. (2015). Ghobrial results were a FOS = 1.08 using the Spectral Pseudo-Static Seismic analysis method.

5.12.1 Geometry and Material Properties

The material properties are given in Table 215. The geometry is defined as shown Figure 153. The Seismic Coefficient is 0.035 and the value of coefficients a and b are both set to 2.

Table 213 Material Properties of the model

Material Names	Sat. Unit Wt. (kN/m^3)	Cohesion (kPa)	Friction Angle (deg)
Clay1	16.051	25	0
Clay2	16.275	30	0
Clay3	16.466	35	0
Clay4	16.634	40	0
Clay5	16.784	45	0
Clay6	16.919	50	0
Clay7	17.042	55	0
Clay8	17.155	60	0

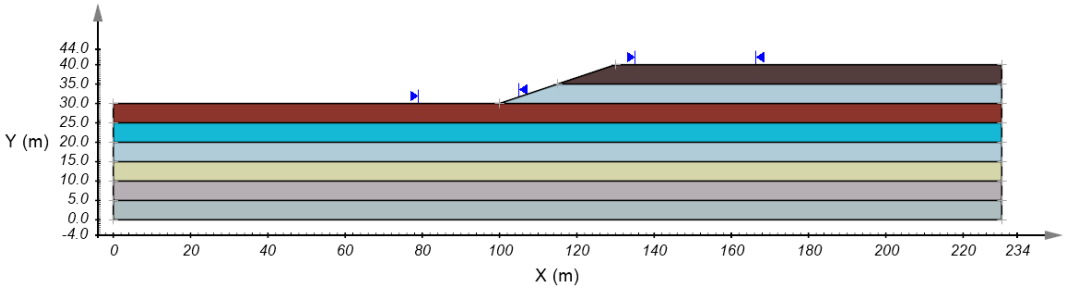

Figure 153 Geometry of Spectral Seismic model

5.12.2 Results and Discussions

For this model, the analysis using the Path Search method with a Spectral Pseudo-Static load results in a FOS = 1.093 for the GLE calculation. The results published by Ghobrial et. al. were a FOS = 1.08 using the Spectral Pseudo-Static Seismic analysis method.

Table 214 Results of the analysis of the Spectral Seismic model

Method	Factor of Safety		Difference (%)
	Ghobrial et. al.	Slope Stability (GLE)	
Spectral Pseudo-Static	1.08	1.093	-1.2

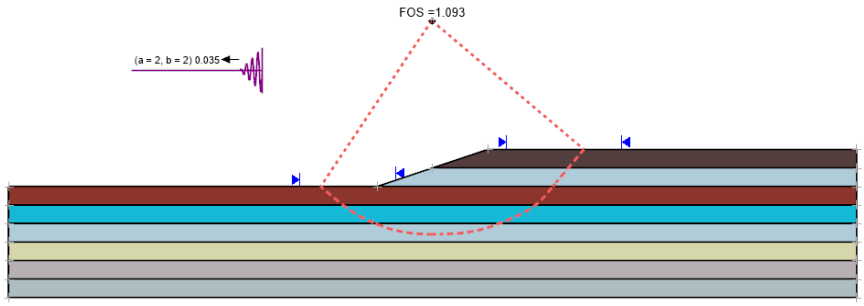

Figure 154 Factor of Safety for Spectral Seismic model

5.13 OPEN PIT COAL MINE - NON-VERTICAL SLICES

Project: Slopes_SarmaNonVerticalSlices
Model: OpenPit_SarmaNonVerticalSlices

This verification model represents the slope in a large open pit coal mine. A thin coal seam is overlain by soft tuff. An existing failure in the slope shows that sliding occurs along the coal seam. There is a reservoir near the crest and the water table line is high due to seepage.

5.13.1 Geometry and Material Properties

The material properties are given in Table 215. The geometry is defined as shown in Figure 155. There are 8 user specified slice boundaries, their coordinates and strength parameters are shown in
.

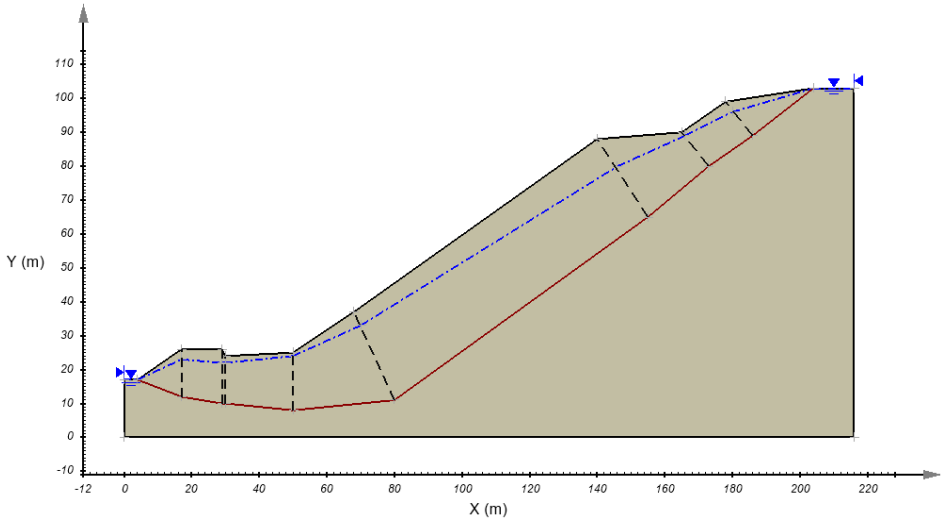

Figure 155 Geometry of the Open Pit Coal Mine Sarma Non-Vertical Slices model

Table 215 Material Properties of the Open Pit Coal Mine Sarma Non-Vertical Slices model

	c (kN/m^2)	ϕ' (degrees)	γ (kN/m^3)
Soil	2	30	27.37

Table 216 User defined slice boundary properties for the Open Pit Coal Mine Sarma Non-Vertical Slices model

Slice Boundary	Lower X (m)	Lower Y (m)	Upper X (m)	Upper Y (m)	c (kN/m^2)	ϕ' (degrees)
1	17	12	17	26	2	30
2	29	10	29	26	2	30
3	30	10	30	24	2	30
4	50	8	50	25	2	30
5	80	11	68	37	0	18
6	155	65	140	88	0	18
7	173	80	165	90	0	18
8	186	89	178	99	0	18

5.13.2 Results and Discussions

For this model, the Sarma Non-Vertical Slices analysis results in a FOS = 1.094.

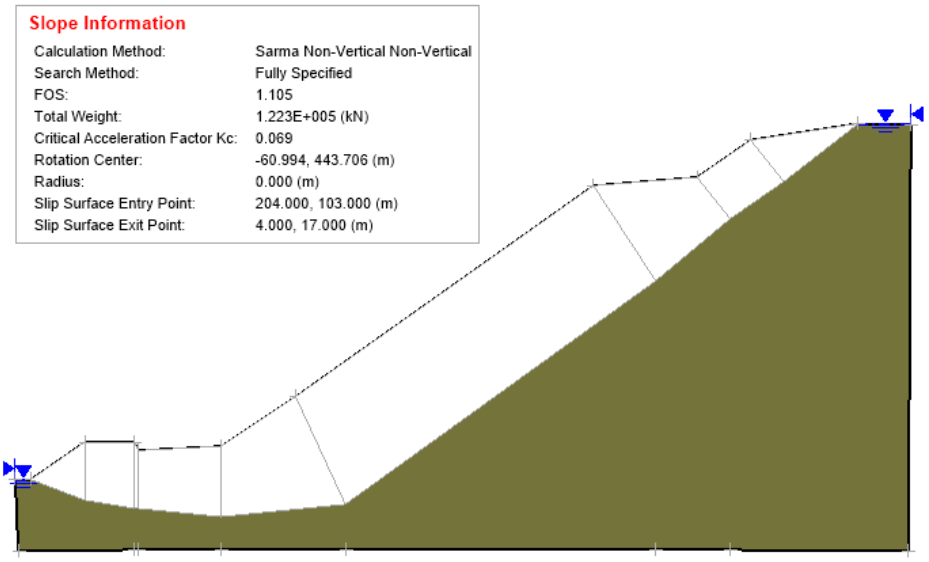

Figure 156 Factor of Safety for Fully Specified Surface using Sarma Non-Vertical Slices analysis

Table 217 Results of the Open Pit Coal Mine model

Method	Factor of Safety			Difference (%)
	Slide	Slope Stability		
Sarma Non-Vertical Slices	1.091	1.094		0.275

6 DYNAMIC PROGRAMMING (SAFE) MODELS

This section documents the numerical models used to verify that the implementation of the dynamic programming algorithm is consistent with the implementation of Pham (2002) and that the dynamic programming search method compares reasonably to traditional method of slices limit equilibrium methods. The following examples are taken from the thesis by Pham (2002).

6.1 PHAM CHAPTER 4 FIGURE 4.1

Project: Slope Stability_SAFE
Models: Pham_Ch4_Figure4_1_SAFE, Pham_Ch4_Figure4_1_SAFE_Stress, Pham_Ch4_Figure4_1

The first example used to verify the Slope Stability-SAFE calculation method is a simple homogenous slope at 2:1 with a groundwater table passing through the toe of the slope.

6.1.1 Geometry and Material Properties

The geometry of the slope is shown in Figure 157 and the material properties are as given in Figure 158. The soil is assumed to behave as a linear elastic material.

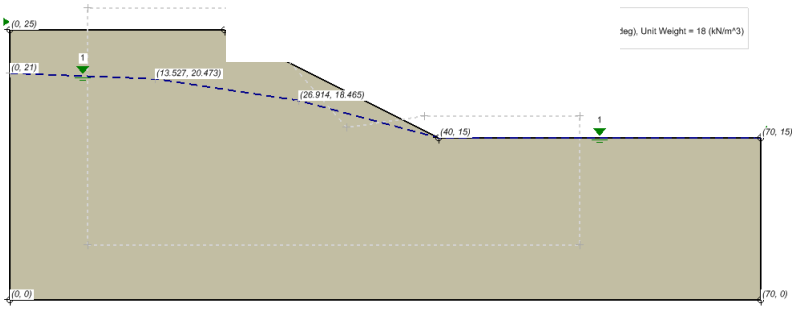

Figure 157 Geometry of the Pham_Ch4_Figure4_1 models

6.1.2 Results and Discussions

The most commonly used methods of slices yield the same location of the critical slip surface. These methods include the M-P (1965) method, the GLE (Fredlund et al., 1981) method, the Bishop's Simplified (1955) method and the Spencer (1967) method.

The corresponding factors of safety calculated by these methods are very similar. The published solution presented by Pham (2002) is shown in Figure 158.

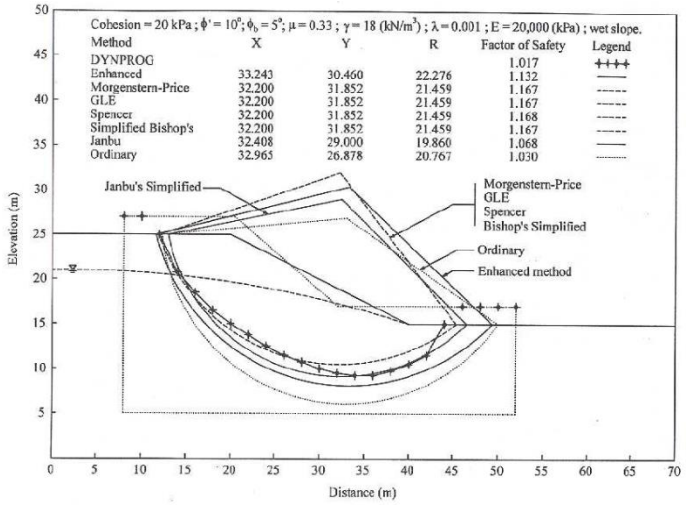

Figure 158 Results of the Chapter 4 Figure 4 _1 (Pham, 2002)

Table 218 Results Figure 4.1 (Pham)

Method	Factor of Safety		Difference (%)
	Pham	Slope Stability	

	Moment	Force	Moment	Force	
Bishop	1.167		1.165		-0.17
GLE	1.167		1.165		-0.17
Janbu Simplified		1.068		1.068	0.00
M-P	1.167		1.165	1.164	-0.17
Ordinary	1.030		1.037		0.68
Spencer	1.168		1.166	1.165	-0.17
SAFE		1.017		1.077	5.90

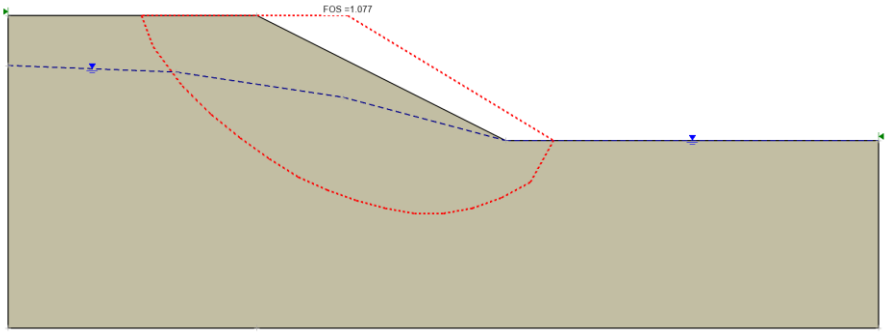

Figure 159 Calculated Factor of Safety by the Slope Stability-SAFE method

6.2 PHAM CHAPTER 5 FIGURES 5.7 TO 5.12

Project: Slope Stability_SAFE
Models: Pham_Ch5_Figure5_7_SAFE to Pham_Ch5_Figure5_12_SAFE and Pham_Ch5_Figure5_7_SAFE_Stress to Pham_Ch5_Figure5_12_SAFE_Stress and Pham_Ch5_Figure5_7 to Pham_Ch5_Figure5_12

The models corresponding to Figures 5.7 to 5.12 in Pham (2002) illustrate the critical slip surfaces obtained by various methods for a homogeneous slope with a water table that passes through the toe of the slope i.e., a wet slope.

The results from the Slope Stability-SAFE calculation method as well as the Morgenstern-Price (1965) method and the Bishop Simplified (1955) method are shown below.

6.2.1 Geometry and Material Properties

The wet slope is 10 metres high with a slope ratio of 2:1 horizontal to vertical distance. The soil cohesion, Poisson's ratio and the internal friction angles were varied as shown in
.

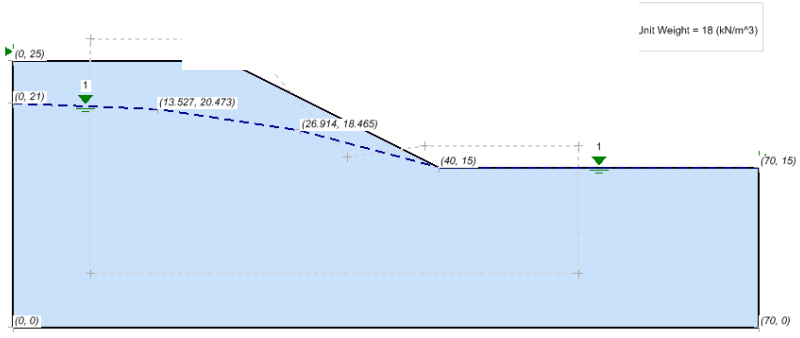

Figure 160 Geometry used for Pham Ch5 Figure 5_7 to 5_12 models

Table 219 Soil Properties

Model	Poisson's Ratio	Cohesion (kPa)	ϕ (degrees)	ϕ_b (degrees)
Pham_Ch5_Figure5_7	0.33	20	10	5
Pham_Ch5_Figure5_8	0.33	30	10	5
Pham_Ch5_Figure5_9	0.33	10	30	20
Pham_Ch5_Figure5_10	0.48	10	10	5
Pham_Ch5_Figure5_11	0.48	20	10	5
Pham_Ch5_Figure5_12	0.48	40	30	20

6.2.2 Results and Discussions

The results of the analyses for each different analysis methods are presented in the tables below.

Table 220 Results Figure 5.7 (Pham)

Method	Factor of Safety				Difference (%)
	Pham		Slope Stability		
	Moment	Force	Moment	Force	
Bishop Simplified	1.167		1.165		-0.17
M-P	1.168		1.165	1.164	-0.26
SAFE		1.017		1.077	-5.90

Table 221 Results Figure 5.8 SAFE (Pham)

Method	Factor of Safety				Difference (%)
	Pham		Slope Stability		
	Moment	Force	Moment	Force	
Bishop Simplified	1.520		1.514		-0.40
M-P	1.519		1.513	1.513	-0.40
SAFE		1.325		1.410	6.42

Table 222 Results Figure 5.9 (Pham)

Method	Factor of Safety				Difference (%)
	Pham		Slope Stability		
	Moment	Force	Moment	Force	
Bishop Simplified	1.686		1.684		-0.12
M-P	1.691		1.687		-0.24
SAFE		1.554		1.610	3.60

Table 223 Results Figure 5.10 (Pham)

Method	Factor of Safety				Difference (%)
	Pham		Slope Stability		
	Moment	Force	Moment	Force	
Bishop Simplified	0.786		0.792		-0.51
M-P	0.797		0.791	0.791	-0.76
SAFE		0.805		0.793	-1.49

Table 224 Results Figure 5.11 (Pham)

Method	Factor of Safety				Difference (%)
	Pham		Slope Stability		
	Moment	Force	Moment	Force	
Bishop Simplified	1.167		1.165		-0.17
M-P	1.168		1.165	1.164	-0.26
SAFE		1.162		1.149	-1.12

Table 225 Results Figure 5.12 (Pham)

Method	Factor of Safety				Difference (%)
	Pham		Slope Stability		
	Moment	Force	Moment	Force	
Bishop Simplified	2.896		2.879		-0.59
M-P	2.896		2.879	2.879	-0.59
SAFE		2.916		2.871	-1.54

6.3 PHAM CHAPTER 5 FIGURES 5.28 TO 5.33

Project: Slope Stability_SAFE
Models: Pham_Ch5_Figure5_28_SAFE to Pham_Ch5_Figure5_33_SAFE and Pham_Ch5_Figure5_28_SAFE_Stress to Pham_Ch5_Figure5_33_SAFE_Stress and Pham_Ch5_Figure5_28 to Pham_Ch5_Figure5_33

The models corresponding to Figures 5.28 to 5.33 in Pham (2002) show the locations of the critical slip surfaces obtained both by Pham (2002) as well as by other methods of slices, such as the Morgenstern-Price (1965) method, and the Bishop Simplified (1955) method.

6.3.1 Geometry and Material Properties

The geometry for these models is the same as in previous section but now the toe of the slope is partially submerged. The soil properties are shown in Table 226.

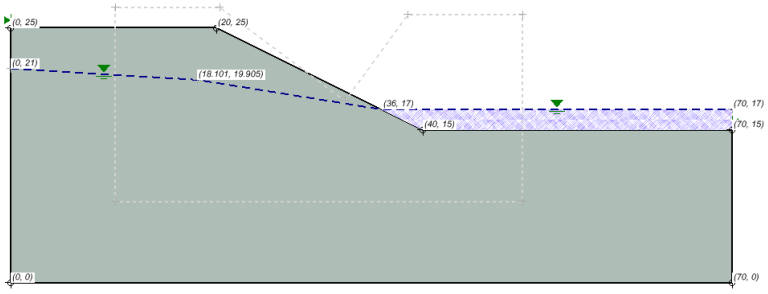

Figure 161 Geometry used in Chapter 5 Figures 5_28 to 5_33 from Pham (2002)

Table 226 Soil Properties

Model	Poisson's Ratio	Cohesion (kPa)	ϕ (degrees)	ϕ_b (degrees)
Pham_Ch5_Figure5_28	0.33	20	10	5
Pham_Ch5_Figure5_29	0.33	30	10	5
Pham_Ch5_Figure5_30	0.33	10	30	20
Pham_Ch5_Figure5_31	0.48	20	10	5
Pham_Ch5_Figure5_32	0.48	20	20	10
Pham_Ch5_Figure5_33	0.48	10	30	20

6.3.2 Results and Discussions

The results of the analyses for each different analysis methods are presented in the tables below.

Table 227 Results Ch5 Figure 5.28 (Pham)

Method	Factor of Safety				Difference (%)
	Pham		Slope Stability		
	Moment	Force	Moment	Force	
Bishop Simplified	1.248		1.226		-1.79
M-P	1.247		1.225	1.225	-1.80
SAFE		1.150		1.095	-4.78

Table 228 Results Ch5 Figure 5.29 (Pham)

Method	Factor of Safety				Difference (%)
	Pham		Slope Stability		
	Moment	Force	Moment	Force	
Bishop Simplified	1.638		1.614		-1.49
M-P	1.637		1.613	1.613	-1.49
SAFE		1.492		1.431	-4.09

Table 229 Results Ch5 Figure 5.30 (Pham)

Method	Factor of Safety				Difference (%)
	Pham		Slope Stability		
	Moment	Force	Moment	Force	
Bishop Simplified	1.800		1.732		-3.93
M-P	1.801		1.736		-3.74
SAFE		1.678		1.702	1.43

Table 230 Results Ch5 Figure 5.31 (Pham)

Method	Factor of Safety				Difference (%)
	Pham		Slope Stability		
	Moment	Force	Moment	Force	
Bishop Simplified	1.248		1.226		-1.76
M-P	1.247		1.225	1.225	-1.80
SAFE		1.244		1.151	-7.48

Table 231 Results Ch5 Figure 5.32

Method	Factor of Safety				Difference (%)
	Pham		Slope Stability		
	Moment	Force	Moment	Force	
Bishop Simplified	1.725		1.698		-1.59
M-P	1.723		1.697	1.697	-1.53
SAFE		1.736		1.645	-5.24

Table 232 Results Ch5 Figure 5.33

Method	Factor of Safety				Difference (%)
	Pham		Slope Stability		
	Moment	Force	Moment	Force	
Bishop Simplified	1.800		1.732		-3.78
M-P	1.801	1.801	1.736	1.736	-3.74
SAFE		1.832		1.823	-0.49

6.4 PHAM CHAPTER 5 FIGURE 5.44 (2002)

Project: Slope Stability_SAFE
Models: Pham_Ch5_Figure5_44_SAFE, Pham_Ch5_Figure5_44_SAFE_Stress, Pham_Ch5_Figure5_44

This example problem contains two soil layers with shear strength parameters as shown in the following figures. The Poisson's Ratio was selected assuming the soil was normally consolidated. A reasonable value of Young's modulus was also assumed.

6.4.1 Geometry and Material Properties

The geometry of the slope is shown in Figure 162 and the soil properties are as given in Figure 163.

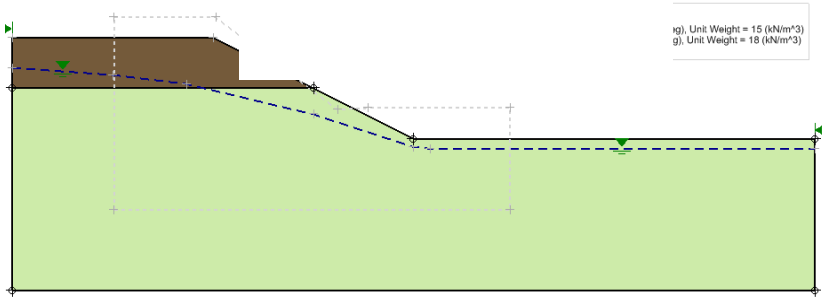

Figure 162 Geometry of the Pham_Ch5_Figure5_44 models

6.4.2 Results and Discussions

The published solution presented by Pham (2002) is shown in Figure 163.

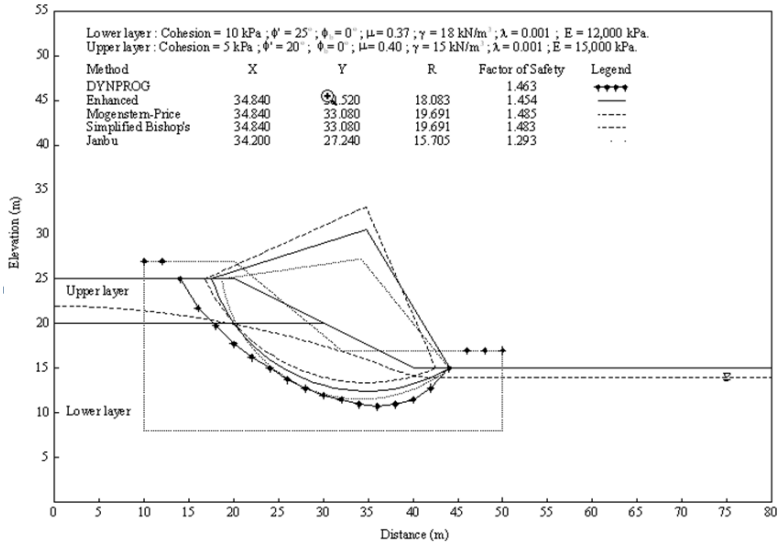

Figure 163 Locations of the critical slip surfaces in the 2-layer slope (Pham, 2002)

Table 233 Results Ch5 figure 5.44 (Pham)

Method	Factor of Safety				Difference (%)
	Pham		Slope Stability		
	Moment	Force	Moment	Force	
Bishop Simplified	1.483		1.482		-0.07
Janbu Simplified		1.293		1.299	0.46
M-P	1.485	1.485	1.485	1.485	0
SAFE		1.413		1.443	2.12

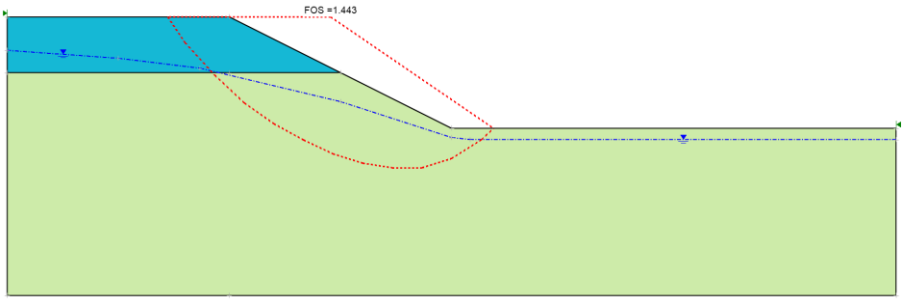

Figure 164 Results of the Slope Stability-SAFE analysis for the two-layer slope

6.5 3-LAYER SLOPE RESTING ON A HARD SURFACE

Project: Slope Stability_SAFE
Models: Pham_Ch5_Figure5_48_SAFE, Pham_Ch5_Figure5_48_SAFE_Stress, Pham_Ch5_Figure5_48

This model from Pham (2002) contains three layers of soil with the base layer being considerably harder than the above layers. The soil is assumed to be linear elastic and normally consolidated. The Poisson's ratio was approximated using the procedure suggested by Pham (2002).

6.5.1 Geometry and Material Properties

The geometry of the problem is shown in Figure 165 and the soil properties are as published in Pham (2002) and given in Figure 166.

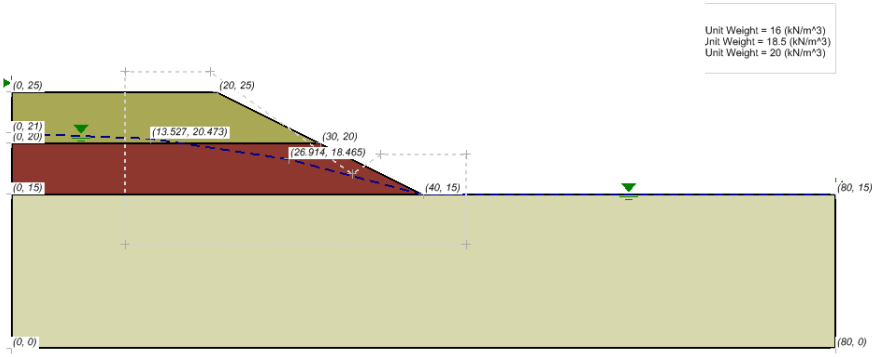

Figure 165 Geometry of the 3-Layer Slope Resting on a Hard Surface model

6.5.2 Results and Discussions

The published solution by Pham (2002) for the 3-soil layer system is shown in Figure 166.

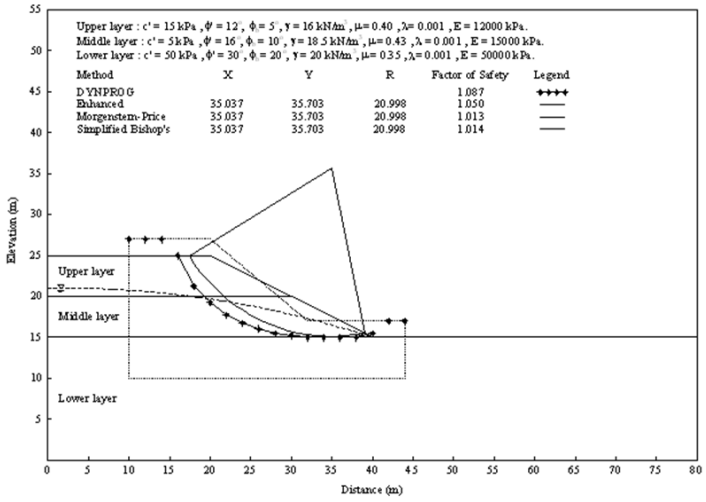

Figure 166 Locations of the critical slip surface in 3-layer slope resting on a hard foundation Pham, (2002)

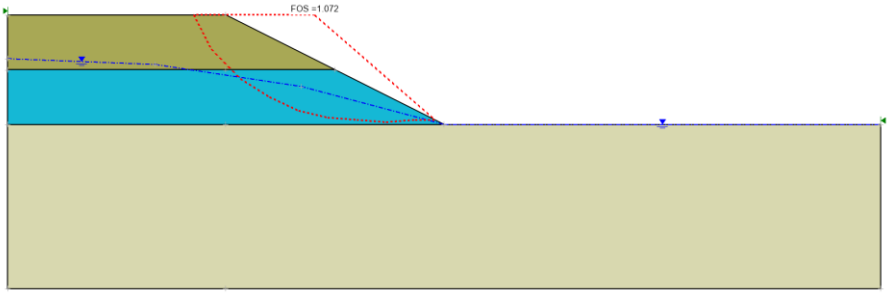

Figure 167 Calculated Factor of Safety by the Slope Stability-SAFE method

Table 234 Comparison between Pham (2002) and Slope Stability

Method	Factor of Safety				Difference (%)
	Pham		Slope Stability		
	Moment	Force	Moment	Force	
Bishop Simplfied	1.014		1.025		1.07
M-P	1.013		1.025	1.025	1.17
SAFE		1.010		1.072	6.14

6.6 THIN AND WEAK LAYERS RESTING ON BEDROCK

Project: Slope Stability_SAFE
Models: Pham_Ch5_Figure5_52_SAFE, Pham_Ch5_Figure5_52_SAFE_Stress, Pham_Ch5_Figure5_52

This model is comprised of three layers; a weak and a thin layer over top of bedrock. The toe of the slope is partially submerged. This example is considered a typical case in which block movement is believed to be the most likely mode of failure.

6.6.1 Geometry and Material Properties

The geometry of the slope is given in Figure 168 and the soil properties are Pham (2002) as shown in Figure 169.

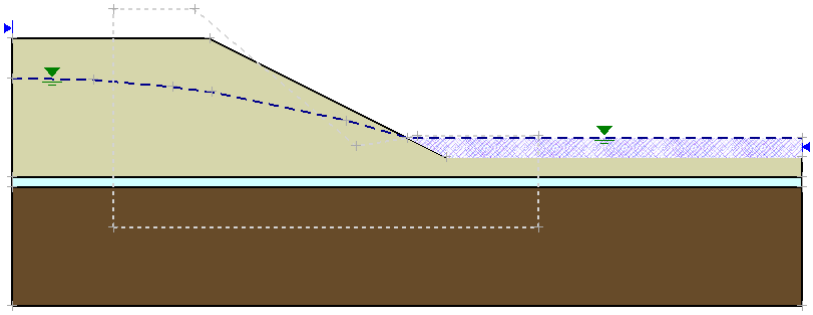

Figure 168 Geometry of the Thin and Weak Layer Resting on Bedrock model

6.6.2 Results and Discussions

The published solution by Pham (2002) for the 3-soil layer with bedrock is shown in Figure 169.

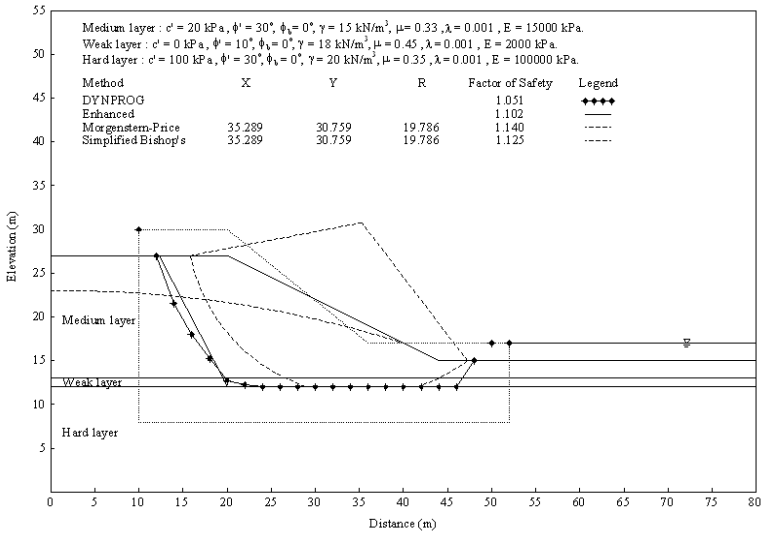

Figure 169 Results of Chapter5 Figure5_52 (Pham, 2002)

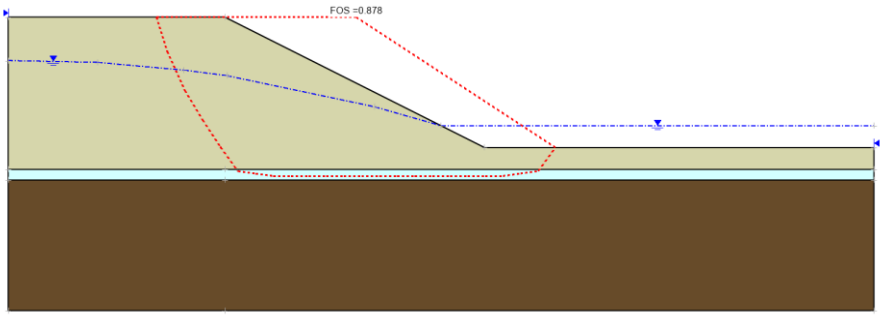

Figure 170 Results of Pham_Ch 5 Figure 5_52 model calculated by Slope Stability-SAFE method

Table 235 Results for the example with a bedrock layer

Method	Factor of Safety				Difference (%)
	Pham		Slope Stability		
	Moment	Force	Moment	Force	
Bishop	1.125		1.084		-3.78
M-P	1.14		1.076	1.075	-5.95
SAFE		0.955		0.878	-8.06

6.7 LODALEN CASE HISTORY

Project: Slope Stability_SAFE
Models: Pham_Ch5_Figure5_56_SAFE, Pham_Ch5_Figure5_56_SAFE_Stress, Pham_Ch5_Figure5_56

The Lodalen slide (Oslo, Norway) is a classical case history in the published research on slope stability. The case is modelled as a homogenous slope with shear strength parameters equal to the average published values as presented in Pham (2002).

6.7.1 Geometry and Material Properties

The geometry of the problem was published by Sevaldson (1956). According to data reported by Sevaldson (1956), the groundwater table passed through the toe of the slope.

The geometry and the groundwater conditions of the Slide No. 2 at Lodalen are presented in Figure 171 and Figure 172.

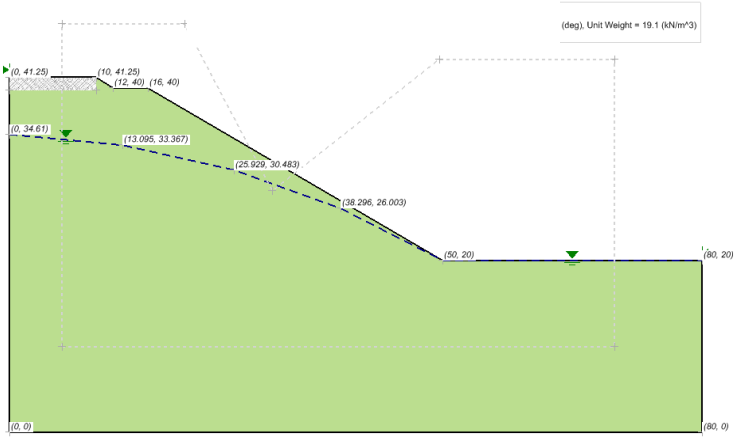

Figure 171 Geometry of the Lodalen Case History model

6.7.2 Results and Discussions

The published solution by Pham (2002) for the Lodalen Slide No. 2 is shown in Figure 172.

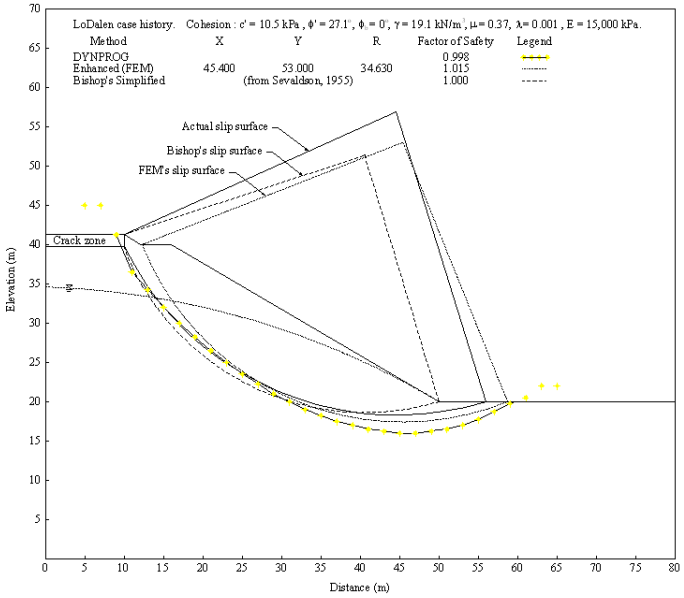

Figure 172 Pham (2002) thesis Chapter 5, Figure 5.56

Table 236 Results of calculations

Method	Factor of Safety				Difference (%)
	Pham		Slope Stability		
	Moment	Force	Moment	Force	
Bishop Simplified	1.000		0.951		-5.15
SAFE		0.998		0.975	-2.30

7 3D BENCHMARKS

The following group of models represents a series of models previously published in literature. They are selected as common benchmark models. It should be noted that in the cases where Slope Stability-3D is compared to other software it is difficult to determine which software package is correct. Therefore, differences between software packages should not be interpreted as an "error" in one of the particular packages.

7.1 A SIMPLE 3D SLOPE IN CLAY

Project: Slopes_3D
Model: 3D_Slope_in_Clay

This model represents a three-dimensional slope stability problem in clay. The model involves a spherical failure surface in clay and is often used in the literature as a benchmark example against which numerical models are validated (Hungr 1989, Silverstri 2006).

7.1.1 Geometry and Material Properties

The slope geometry and material properties utilized for this model are presented in Figure 173 and Table 237. The requirements for this problem are the factor of safety and its comparison to its closed-form solution.

Table 237 Material Properties of the Simple Slope model

c (kN/m^2)	ϕ (degrees)	γ (kN/m^3)
0.1	0	1

7.1.2 Results and Discussions

The fully specified ellipsoid (spherical) slip surface is utilized in the analysis to make an exact comparison with published results. The sphere radius is 1.0 and its center is located at (4.780, 5, 7.960).

There are 42 rows x 42 columns used in the analysis which results in a total of 872 active columns. The factor of safety for Bishops method is 1.398. A summary of the factors of safety for this benchmark example is presented in Table 238.

Table 238 A summary of factors of safety for the simple 3D slope in clay

Method	Factor of Safety	Difference (%)
Closed-Form Solution (Hungr et al. 1989)	1.402	1.816
Closed-Form Solution (Silverstri 2005)	1.377	-
CLARA-W Solution 42x42 (Hungr et al. 1989)	1.400	1.643
3D-SLOPE solution (Lam, et al. 1993)	1.402	1.816
Slope Stability 3D	1.398	1.525

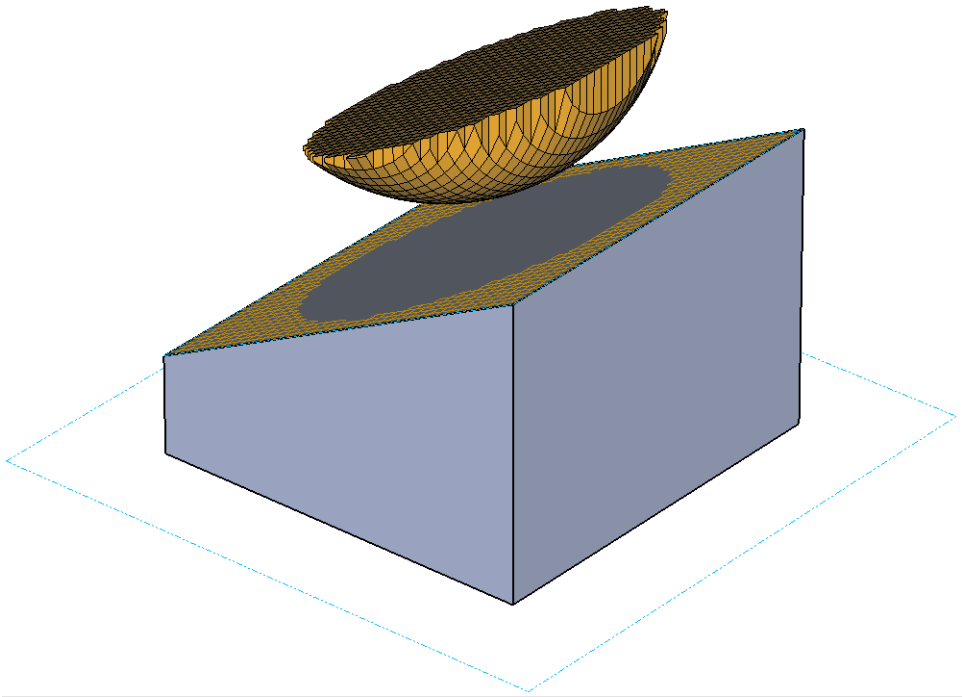

Figure 173 Geometry and results of the Simple 3D Slope model in Clay

7.2 A MODEL COMPARED TO VARIATIONAL APPROACH

Project: Slopes_3D
Model: Hungr_Leshchinski_3D

Leshchinski et al. (1985) proposed an analytical solution for sliding surfaces with logarithmic spirals. It satisfies all equilibrium conditions. Lateral equilibrium is met by symmetry.

7.2.1 Geometry and Material Properties

The slope geometry and material properties that are in use for this model are presented in Figure 174. Hungr et al. (1989) presented the geometry in detail.

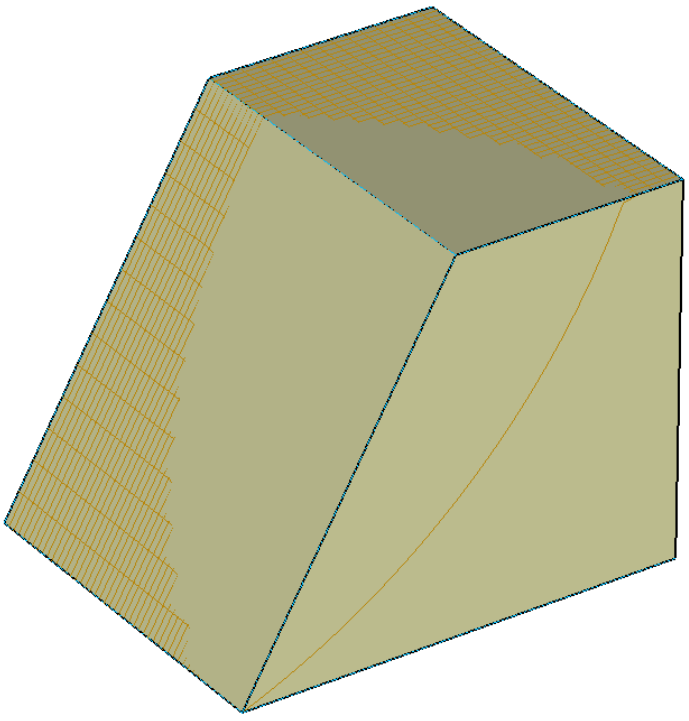

Figure 174 Ellipsoidal Sliding Surface

X-Coordinate	-0.670
Y-Coordinate	0.000
Z-Coordinate	1.737
Tangent Plane	-0.124
Aspect Ratio	0.660

7.2.2 Results and Discussions

The fully specified ellipsoid slip surface with aspect ratio = 0.66 is used in the analysis to make a comparison with published results. The center of the ellipsoid is located at (-0.67, 0, 1.737).

The result is shown in Figure 175. A summary of the factors of safety for this benchmark example is presented in Table 239. The results match CLARA-W with a difference of less than 1.6%.

Table 239 A summary of factors of safety for the Hungr_Leshchinski_3D model

Method	Factor of Safety	Difference (%)
Analytical Solution (Leshchinski et al. 1985)	1.25	-
CLARA-W Solution (Hungr et al. 1989)	1.23	1.6
Slope Stability 3D	1.245	0.4

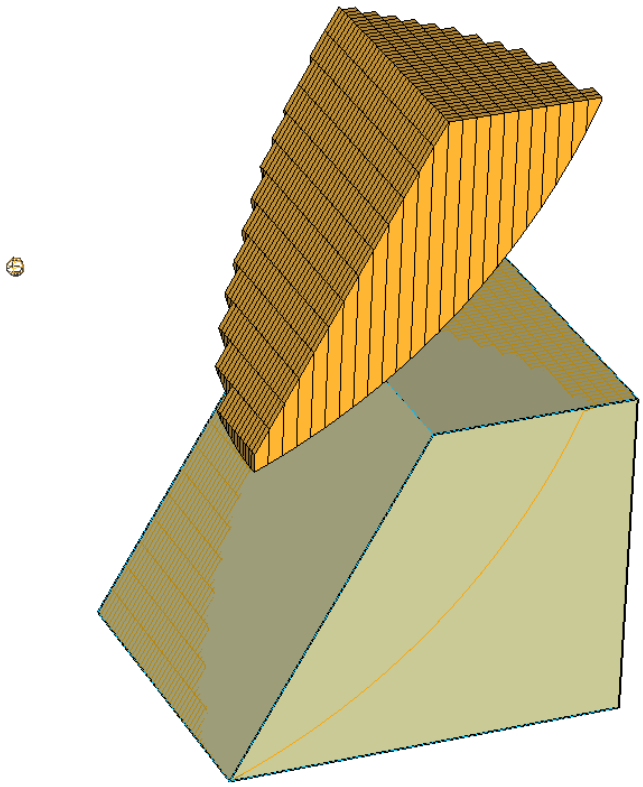

Figure 175 Result of the Hungr Leshchinski 3D model

7.3 ELLIPSOIDAL SLIDING SURFACE WITH TOE SUBMERGENCE

Project: Slopes_3D
Model: Ellipsoidal_Toe_Submergence, Grid_Tangent_Toe_Submergence

This problem models the upstream portion of an earth dam which was built with a sloping clay core surrounded by granular material. The water surface is higher than the ground surface in the front of the toe, so toe submergence will be considered.

This model was originally presented in the CLARA-W verification manual. It should be noted that the unit weights in this example are close to buoyant values but are reproduced in the current example for the sake of consistency with the original model as presented in the CLARA-W documentation.

7.3.1 Geometry and Material Properties

The pore-water pressure is defined with the water surface (grid data). In the Ellipsoidal_Toe_Submergence model, a fully specified ellipsoidal sliding surface is used. In the Grid_Tangent_Toe_Submergence model, the grid and tangent search method is utilized. For the Ellipsoidal_Toe_Submergence model, the center of the ellipsoid is located at (149.170, 0, 356.090), the tangent plane is located at 108.40. Since the model is symmetrical, only half of the slope is analyzed. The geometry and material properties are shown in Figure 176 and Table 240.

Table 240 Material Properties of the Ellipsoidal_Toe_Submergence

	c (psf)	ϕ (degrees)	γ (lb/ft^3)
RockFill	0	35.0	70.6
Core	100	29	70.6
Fill	0	28	70.6
R1	10000	35.0	100

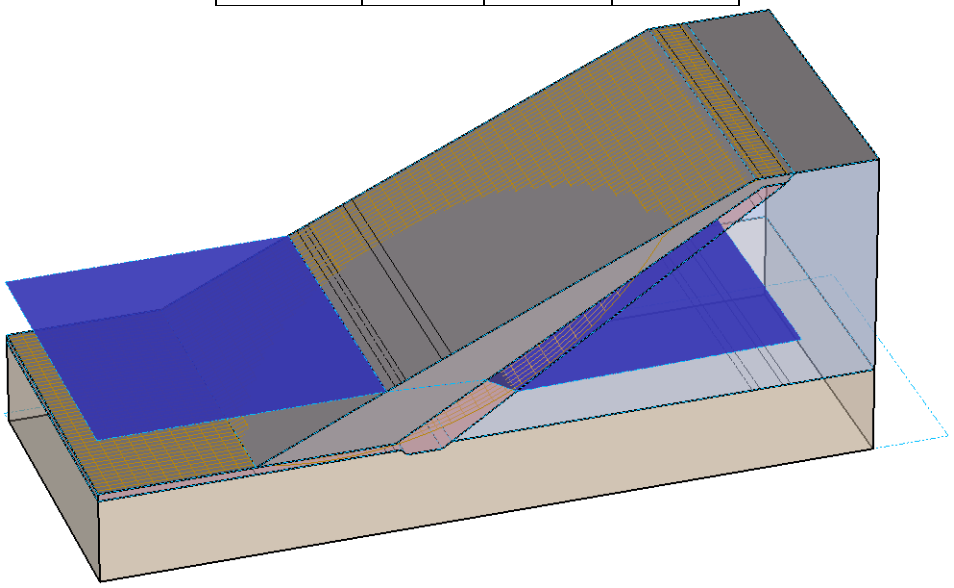

Figure 176 Geometry of the Ellipsoidal_Toe_Submergence model with the water surface

7.3.2 Results and Discussions

The results of the analysis are presented in Table 241 and Figure 177. It can be seen that the results of the software match reasonably well with CLARA-W. Differences of less than 5% are considered reasonable.

Table 241 Results of the Ellipsoidal_Toe_Submergence model analysis

Method	Factor of Safety			Difference (%)
	CLARA-W	Slope Stability 3D		
		Moment	Force	
Bishop	1.300	1.311		0.846
Janbu Simplified	1.230		1.242	0.976
Spencer	1.260	1.316	1.315	4.365

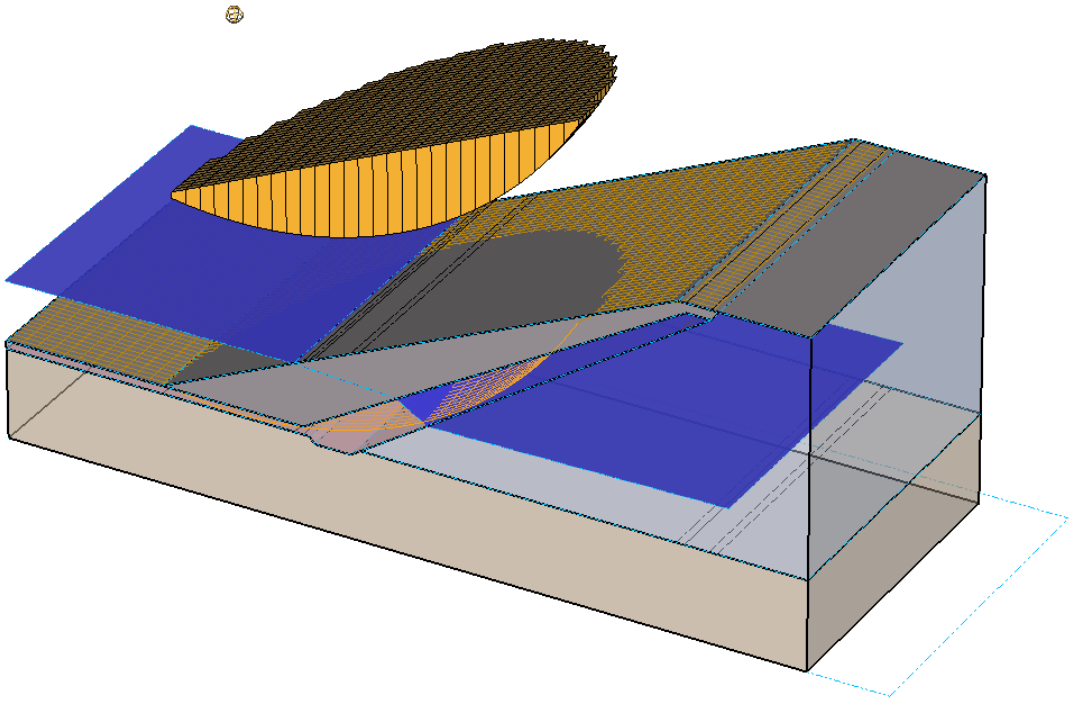

Figure 177 Result of analysis of Ellipsoidal_Toe_Submergence model with display of 3D sliding mass

7.4 COMPOSITE ELLIPSOID/WEDGE SURFACE

Project: Slopes_3D
Model: Composite_Ellipsoid_Wedge

This model is created based on the 2D example model by Fredlund and Krahn (1977). It is a 2:1 clay slope with a horizontal weak layer and single water surface. The weak layer is modeled with a wedge plane with the "weak layer" material as the discontinuity material. The sliding surface is an ellipsoid surface combined with the wedge plane.

7.4.1 Geometry and Material Properties

The pore-water pressure is defined with the water surface (grid data). The sliding surface is a composite ellipsoid and wedge plane. The center point of the ellipsoid is located at (60, 50, 90). The corresponding tangent plane location is at 6.890 and its aspect ratio is 0.750. The wedge is a horizontal plane used to simulate the horizontal weak layer with elevation at 17 (ft). The model's geometry and material properties are presented in Figure 178 and Table 242.

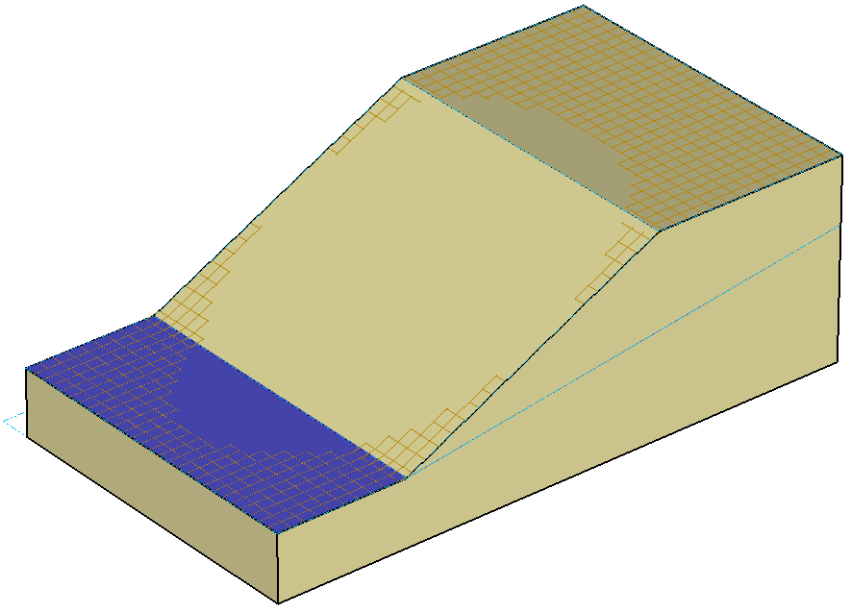

Figure 178 Geometry of the Composite_Ellipsoid_Wedge model

Table 242 Material Properties of Composite_Ellipsoid_Wedge

	c (psf)	ϕ (degrees)	γ (lb/ft^3)
clay	600	20	120
Weak layer	0	10	20

7.4.2 Results and Discussions

The resulting factors of safety from the Slope Stability 3D software are shown in Table 243 and Figure 179. The results of Slope Stability match CLARA-W with a difference of less than 2.5%.

Table 243 Results of the Composite_Ellipsoid_Wedge model

Method	Factor of Safety			Difference (%)
	CLARA-W	Slope Stability 3D		
		Moment	Force	
Bishop	1.710	1.679		-1.813
Spencer	1.710	1.683	1.682	-1.579
M-P	1.720	1.681	1.682	-2.267
Janbu Simplified	1.670		1.648	-1.317

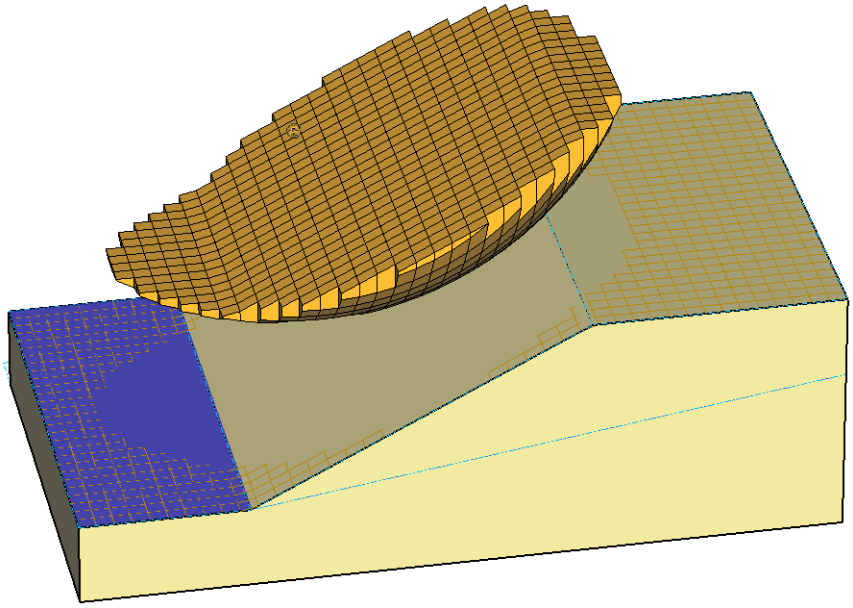

Figure 179 Results of the Composite_Ellipsoid_Wedge model using the Bishop Simplified method

7.5 EMBANKMENT CORNER

Project: Slopes_3D
Model: Embankment_Corner

This model represents an embankment corner. The grid and tangent search method is utilized to identify the critical slip surface.

7.5.1 Geometry and Material Properties

There is no pore-water pressure input for this problem. The geometry and material properties are shown in Figure 180 and Table 244.

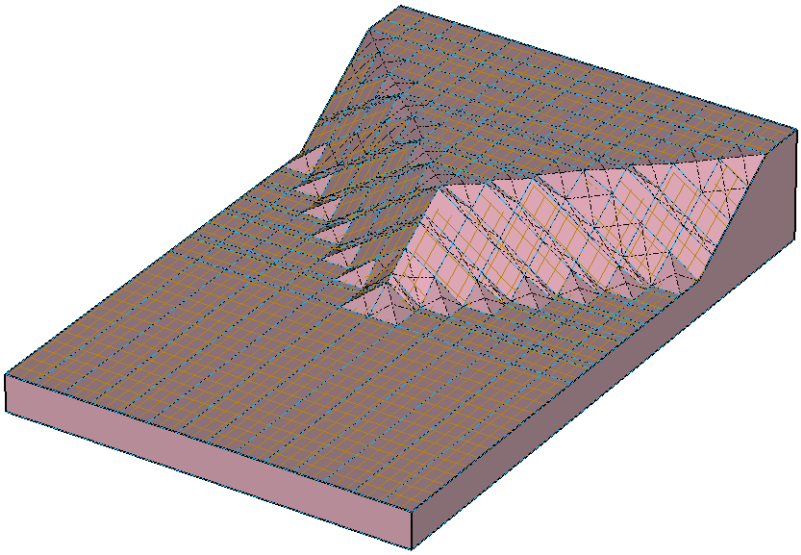

Figure 180 Geometry of Embankment_Corner model

Table 244 Material Properties of the Embankment_Corner model

	c (kN/m^2)	ϕ (degrees)	γ (kN/m^3)
Mat1	10	22	20

7.5.2 Results and Discussions

The following results are obtained using the grid and tangent search technique and are shown in Table 245 and Figure 181. A maximum difference of 2.715% was noted which is reasonable.

Table 245 Results of the Embankment_Corner

Method	Factor of Safety		Difference (%)
	CLARA-W	Slope Stability3D	
Bishop	1.824	1.838	0.768
Janbu Simplified	1.560	1.571	0.705
Spencer	1.784	1.841	3.195
M-P	1.830	1.828	-0.109

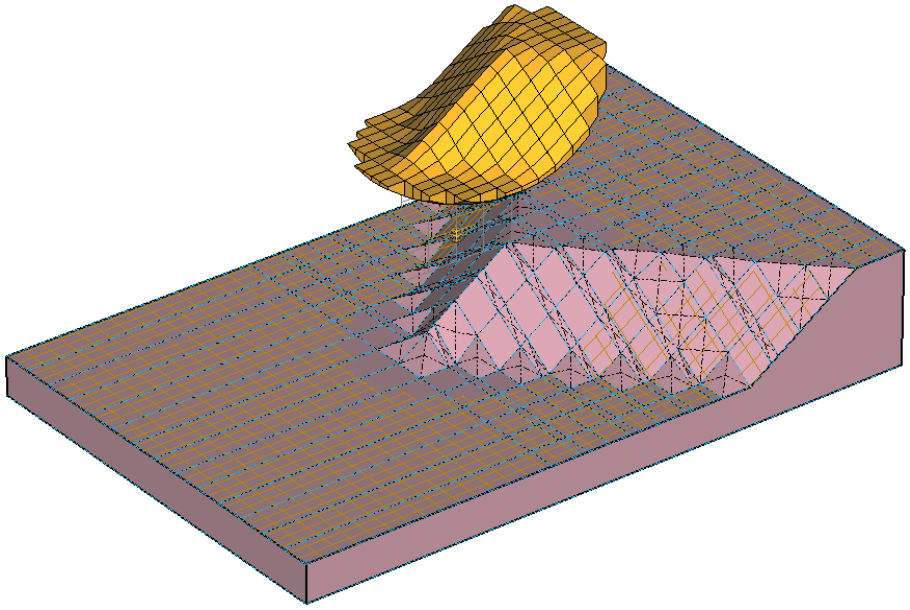

Figure 181 Result of Embankment_Corner model with Bishop Simplified method

7.6 WASTE PILE FAILURE WEDGES

Project: Slopes_3D
Model: WastePileFailure_Wedges

This model uses multiple planar wedges as sliding surfaces. It represents a waste pile failure controlled by a weak interface between the waste material and its foundation. The weak surface is defined by discontinuity material "disc". All other three wedge planes forming the sliding surface have the properties of the waste material.

7.6.1 Geometry and Material Properties

Pore-water pressure is present in this example and is defined by a water surface. The corresponding model and wedges data are presented in Figure 182. The material properties are presented in Table 246.

Table 246 Material Properties of CLARA-W example 5

	c (kN/m^2)	ϕ (degrees)	γ (kN/m^3)
Fill	0	35	18
Clay Foundation	50	20	20
disc	0	12	0

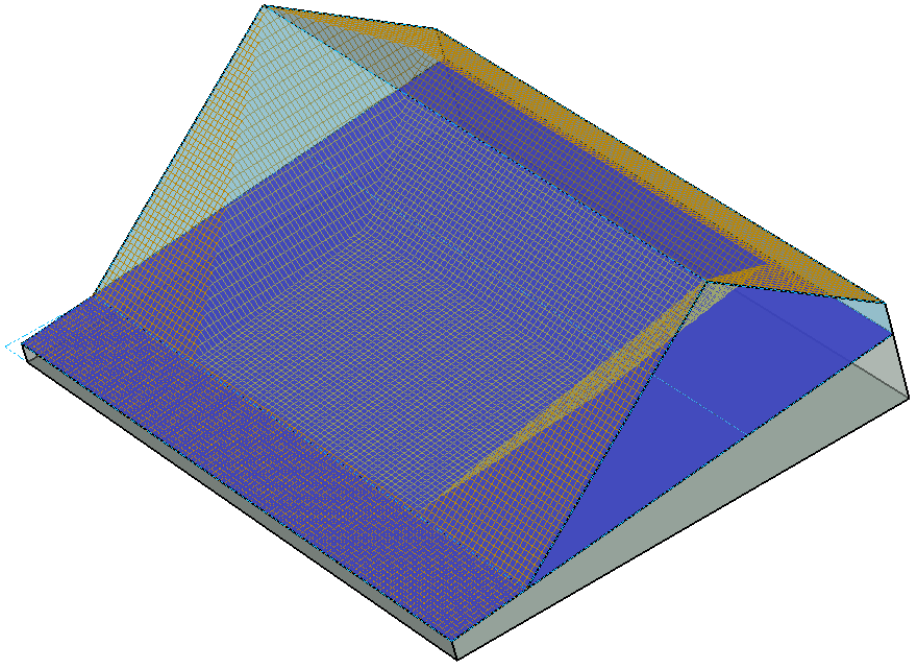

Figure 182 Geometry of WastePileFailure_Wedges model with the wedges data

Wedge Sliding Surfaces

	X (m)	Y (m)	Z (m)	Dip (deg.)	Dip Dir. (Deg)
Wedge #1	0	90	10	7	0
Wedge #2	60	90	12	32	0
Wedge #3	0	90	-35	45	87
Wedge #4	0	90	-35	45	-87

7.6.2 Results and Discussions

The results are shown in Table 247 and Figure 183. CLARA-W does not have converged solution for Spencer method and there is a significant difference between CLARA-W and Slope Stability 3D with the M-P method. The calculations of the M-P method in the CLARA-W software seems questionable given the significant difference between the Bishop and M-P result in the CLARA-W software.

Table 247 Results of WastePileFailure_Wedges

Method	Factor of Safety		Difference (%)
	CLARA-W	Slope Stability3D	
Bishop	1.150	1.153	0.261
Janbu Simplified	1.150	1.154	0.348
Spencer	-	1.132	-
M-P	1.380	1.133	-17.899

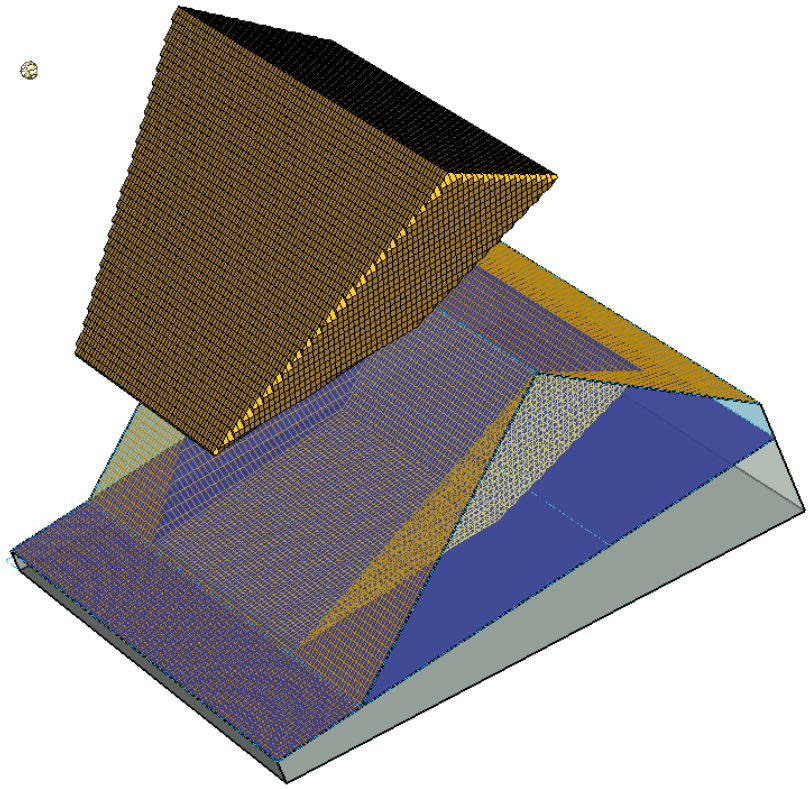

Figure 183 Results of WastePileFailure_Wedges model

7.7 A GENERAL SLIDING SURFACE

Project: Slopes_3D
Model: General_sliding_surface

This example demonstrates the use of general sliding surface. In the original "Example 6" in CLARA-W the model used a Hoek-Brown strength model for the shale bedrock layer material, since there is a different implementation of the Hoek-Brown model in CLARA-W and Slope Stability, the bedrock material strength model is changed to a Mohr-Coulomb in both the CLARA-W and Slope Stability 3D software packages for the convenience of comparison.

7.7.1 Geometry and Material Properties

The pore-water pressures are specified with a water surface (grid data). The geometry and material properties are shown in Figure 184 and Table 248.

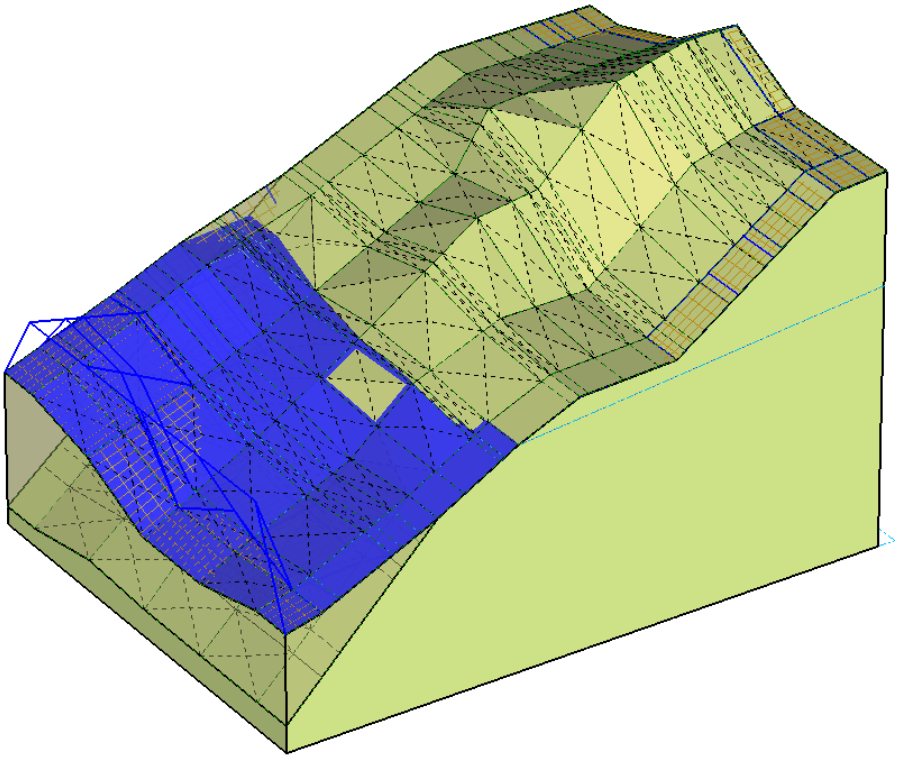

Figure 184 Geometry of the General_sliding_surface model

Table 248 Material Properties of General_sliding_surface model

	c (kN/m^2)	ϕ (degrees)	γ (kN/m^3)
Glacial Till	0	35	22
wasRock	100	45	26

7.7.2 Results and Discussions

The results are shown in Table 249 and Figure 185. The slight differences between the software packages are considered reasonable.

Table 249 Results of General_sliding_surface example

Method	Factor of Safety		Difference (%)
	CLARA-W	Slope Stability3D	
Bishop	2.22	2.242	0.991
Janbu Simplified	2.170	2.193	1.06
Spencer	2.230	2.211	-0.852

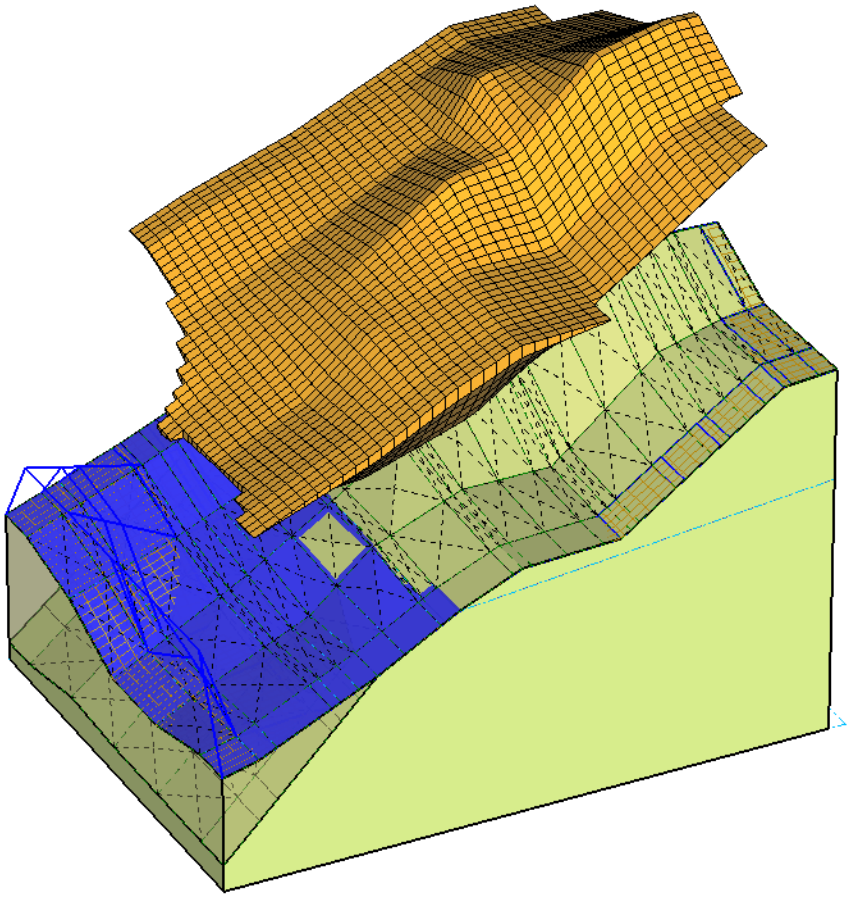

Figure 185 General sliding surface **using the Bishop Method**

7.8 KETTLEMAN WASTE LANDFILL FAILURE

Project: Slopes_3D
Model: Kettleman_Hills_Landfill

This example simulates the actual failure of the Kettleman Hills waste landfill (Seed, Mitchell and Seed, 1990). The slip surface is modeled with a multi-planar wedge surface. Three wedge planes are associated with 3 different discontinuity materials as shown in Table 250.

7.8.1 Geometry and Material Properties

The geometry and material properties are shown in Table 250and Figure 186.

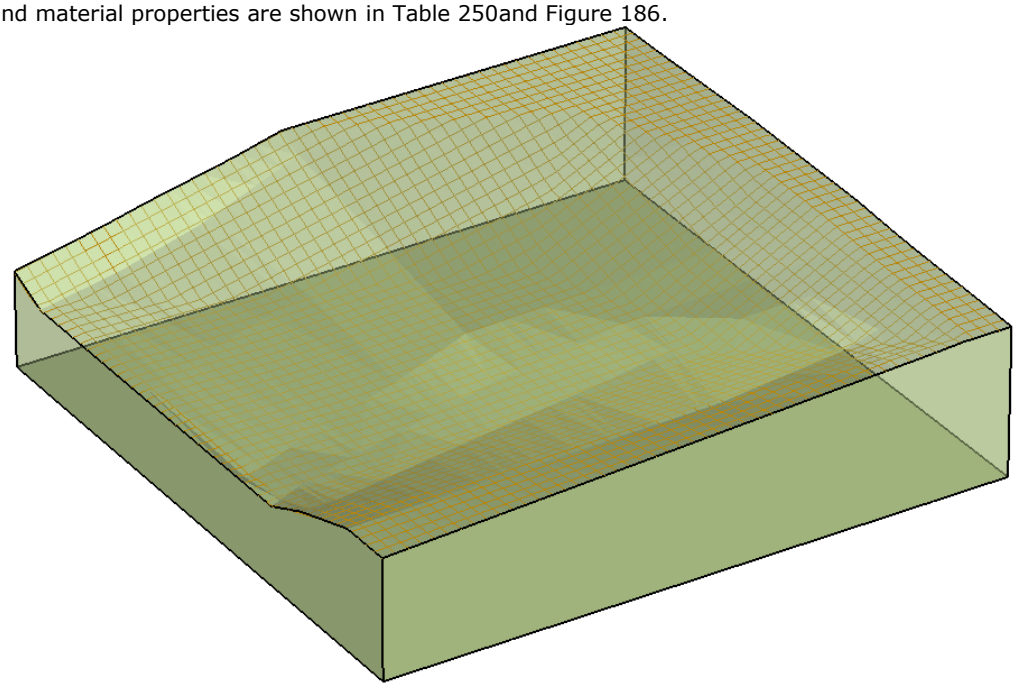

Figure 186 Geometry of the Kettleman_Hills_Landfill model

Wedges Sliding Surface

	X (ft)	Y (ft)	Z (ft)	Dip (deg.)	Dip Dir. (Deg.)
Wedge #1	160	300	738	-1.4	0
Wedge #2	160	300	738	1.4	0
Wedge #3	420	70	794	18.44	87
Wedge #4	675	270	830	26.56	-24
Wedge #5	578	582	832	26.58	-24
Wedge #6	578	582	832	26.58	-64

Table 250 Material Properties of the Kettleman_Hills_Landfill model

	c (psf)	ϕ (degrees)	γ (lb/ft^3)
Mat1	0	20	110
Dis1	0	8	127
Disc2	0	8.5	127
Dis3	900	0	127

7.8.2 Results and Discussions

The results are presented in Table 251 and Figure 187. The differences between the software packages is deemed negligible.

Table 251 Results of the Kettleman_Hills_Landfill model

Method	Factor of Safety		Difference (%)
	CLARA-W	Slope Stability3D	
Bishop	1.160	1.164	0.345
Janbu Simplified	1.140	1.149	0.789
Spencer	1.160	1.172	1.034
M-P	1.170	1.168	-0.171

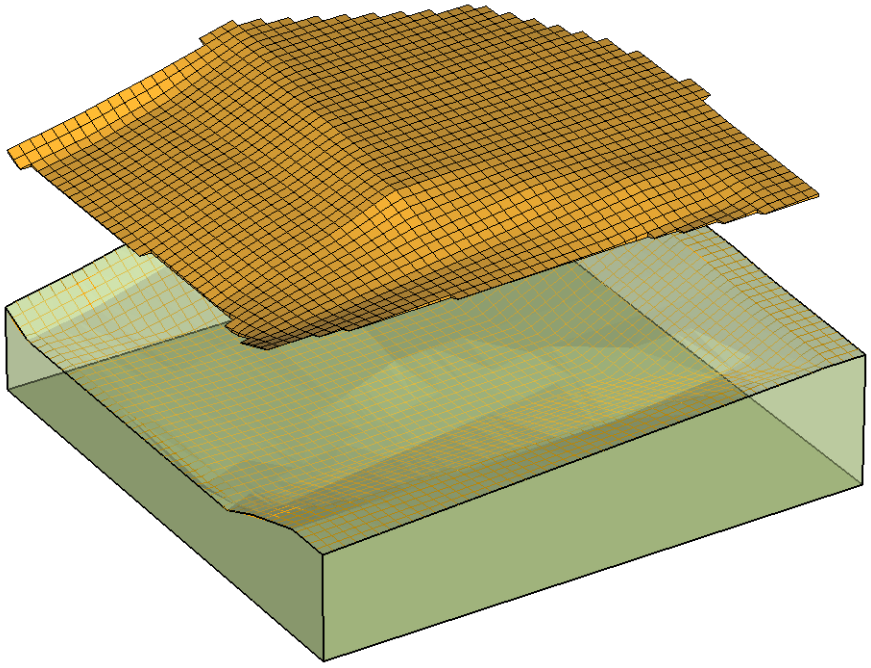

Figure 187 Failure Sliding Surface of Kettleman_Hills_Landfill model

7.9 BEDROCK LAYER CONSIDERATION

Project: Slopes_3D
Model: Bedrock

This is a simple symmetrical slope problem therefore only half is analyzed. An ellipsoidal sliding surface is utilized. The lower material layer is bedrock. The ellipsoidal sliding surface will be cut off when passing through the bedrock layer. CLARA-W's Spencer method does not converge in this model.

7.9.1 Geometry and Material Properties

The geometry and material properties are presented in Figure 188 and Table 252.

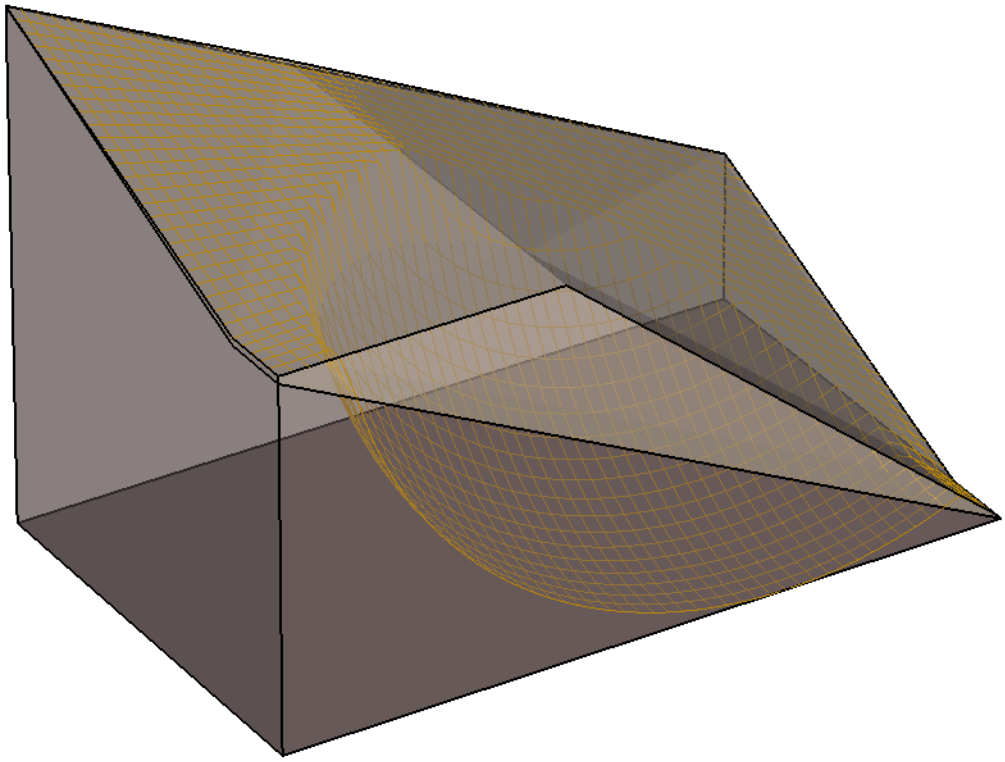

Figure 188 Ellipsoidal Sliding Surface

X-Coordinate	Y-Coordinate	Z-Coordinate	Tangent Plane	Aspect Ratio
30.000	60.000	60.000	0.000	0.700

Table 252 Material Properties of Bedrock model

	c (kN/m^2)	ϕ (degrees)	γ (kN/m^3)
Material2	15	25	20

7.9.2 Results and Discussions

The results are shown in Figure 189 and Table 253. The differences between the software packages are considered negligible.

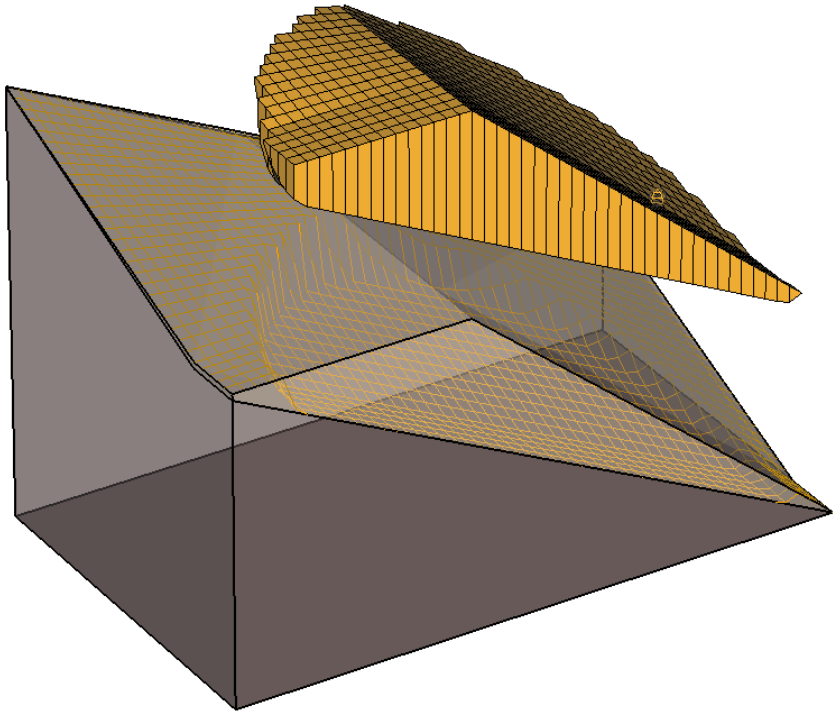

Figure 189 Failure sliding surface of the Bedrock model

Table 253 Results of the Bedrock model

Method	Factor of Safety		Difference (%)
	CLARA-W	Slope Stability3D	
Bishop	1.20	1.175	-2.083
Janbu Simplified	1.17	1.150	-1.709
M-P	1.19	1.145	-3.782

7.10 MULTIPLE PIEZOMETRIC SURFACES

Project: Slopes_3D
Model: multi_piezo_surfaces

There are six layers in this model. Each layer is associated with a different piezometric surface in order to simulate the condition of upward seepage.

7.10.1 Geometry and Material Properties

A fully specified Ellipsoidal sliding surface is used in this analysis, the geometry and material properties are shown in Table 254 and Figure 190.

Table 254 Material Properties of the multi_piezo_surfaces model

	c (kN/m^2)	ϕ (degrees)	γ (kN/m^3)
Clayer1	20	18	19

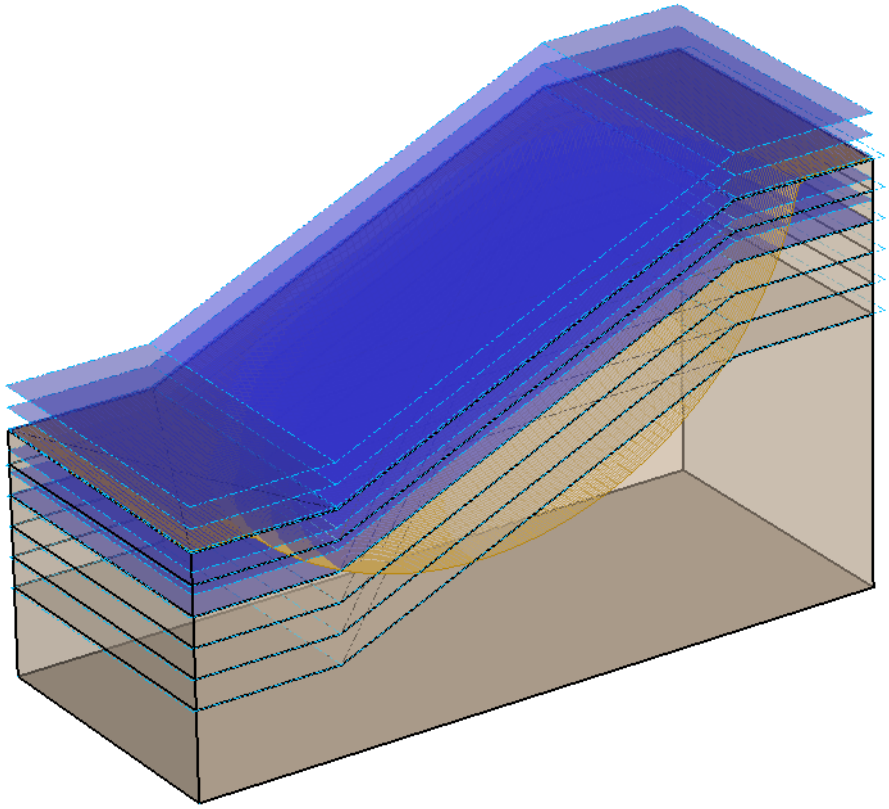

Figure 190 Geometry of the multi_piezo_surfaces model

7.10.2 Results and Discussions

The results are shown in Figure 191 and Table 255. Negligible differences between the software packages are noted.

Table 255 Results of the multi_piezo_surfaces model comparison

Method	Factor of Safety		Difference (%)
	CLARA-W	Slope Stability3D	
Bishop	2.15	2.164	0.651
Janbu Simplified	1.93	1.939	0.466
Spencer	2.15	2.145	-0.233
M-P	2.16	2.138	-1.019

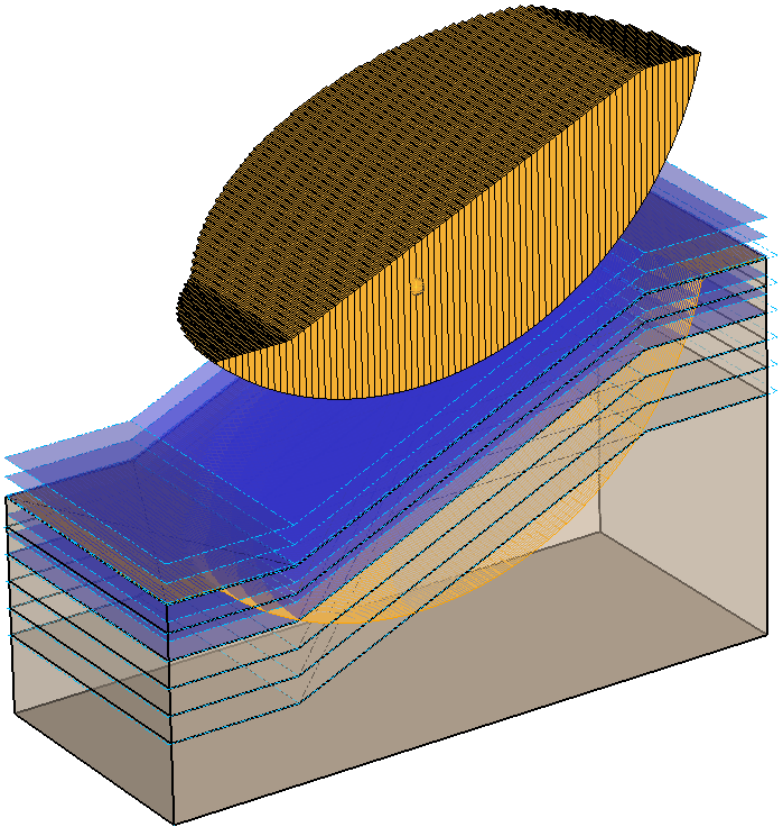

Figure 191 Failure sliding mass of the multi_piezo_surfaces model

7.11 ARBITRARY SLIDING DIRECTION

Project: Slopes_3D
Model: Arbitrary_Sliding_Direction

This benchmark is used to illustrate the analysis of a three-dimensional slope stability model using the Orientation Analysis feature of Slope Stability, i.e., a slip surface direction that does not follow the x-axis. The model is analyzed using the Bishop Simplified, Janbu Simplified and the GLE methods. A range of slip surface directions is analyzed and the effect on the factor of safety for the slope is noted. The purpose of this benchmark is to analyze the stability of a simple slope along several different slip surface directions and present the resultant factors of safety.

This model was developed because the sliding direction becomes an additional searching parameter. The correct sliding direction is unknown at the start of the analysis and must be determined by the user.

The model is developed from: Jiang et al. 2003. Jiang results were a FOS = 1.33 using the Dynamic Programming search method and the Janbu analysis method.

7.11.1 Geometry and Material Properties

This example consists of a simple one layer slope. The geometry and material properties are shown in Table 256 and Figure 192.

Table 256 Material Properties of the Arbitrary Sliding Direction model

	c (kPa)	ϕ (degrees)	γ (kN/m^3)
soil	11.7	24.7	17.66

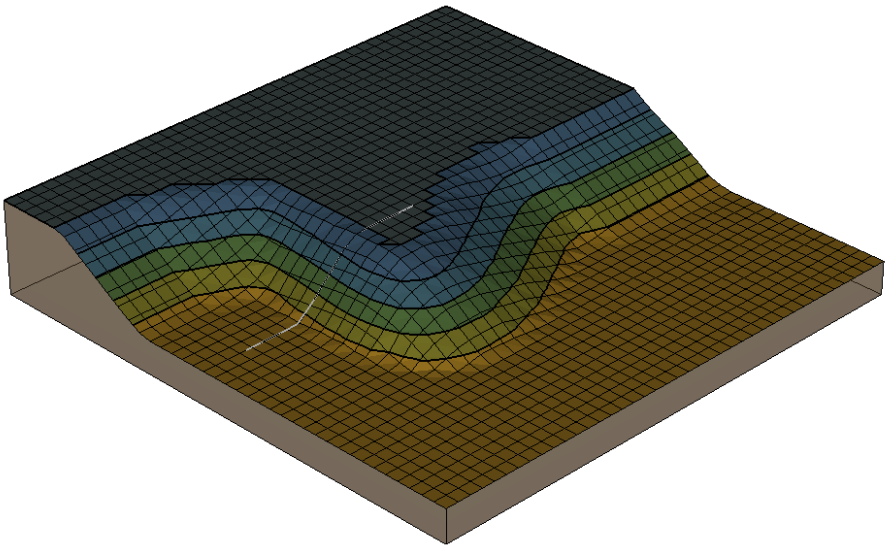

Figure 192 Geometry of the Arbitrary Sliding Direction model

7.11.2 Results and Discussions

The results of the analysis are presented in Table 257 and Figure 193 Result of analysis of Arbitrary Sliding Direction model with display of 3D sliding mass. The model illustrates in the table results from Jiang et. Al. (2003) compared to Slope Stability 3D. The differences of less than 5% are considered reasonable. The sliding direction was determined with a preliminary guess and then searched through a range of possible sliding directions on either side of the preliminary guess.

Table 257 Results of the Arbitrary Sliding Direction model analysis

Method	Factor of Safety		Difference (%)
	Jiang et. al. 2003	Slope Stability 3D	
Janbu Simplified	1.33	1.285	3.38
Bishop Simplified	-	1.404	-
GLE	-	1.408	-

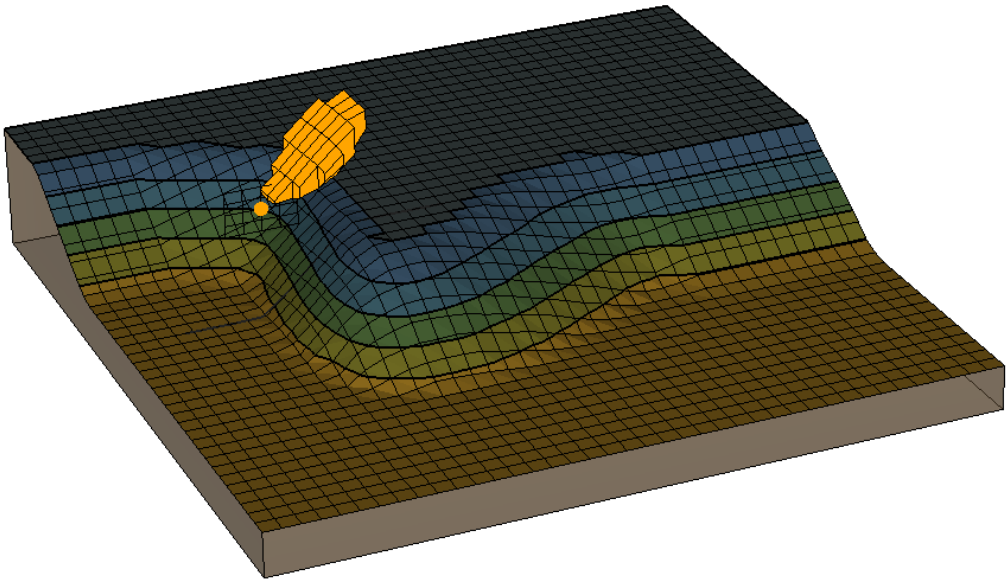

Figure 193 Result of analysis of Arbitrary Sliding Direction model with display of 3D sliding mass

8 FEATURE EXAMPLES FOR 3D MODELS

This chapter presents some examples published in Journals to verify the Slope Stability 3D software and some benchmark models to test some individual features by comparing the results with CLARA-W or with corresponding 2D models.

The models in this chapter also represent a collection of classic examples. The examples are chosen to verify the calculation of the factor of safety in various cases, including variations in material properties, water table locations, etc.

8.1 FREDLUND AND KRAHN (1977) 2D TO 3D

Project: Slopes_3D
Model: FredlundAndKrahn_1977_3D

This model was created based on the 2D example model by Fredlund and Krahn (1977) by extending the 2D model into 3D. It is similar to the 3D benchmark model – CLARA-W example2 (Composite Ellipsoid Wedge), but this model is a more "exact" match with the original 2D model without using the wedge plane and a discontinuity material. In this example an ellipsoidal sliding surface is utilized and the weak layer is kept as a separate layer.

8.1.1 Geometry and Material Properties

The geometry and material properties are shown in Table 258 and Figure 194.

Table 258 Material Properties of Fredlund and Krahn (1977) 3D model

	c (psf)	ϕ (degrees)	γ (lb/ft^3)
clay	600	20	120
Weak layer	0	10	120
Bed rock			

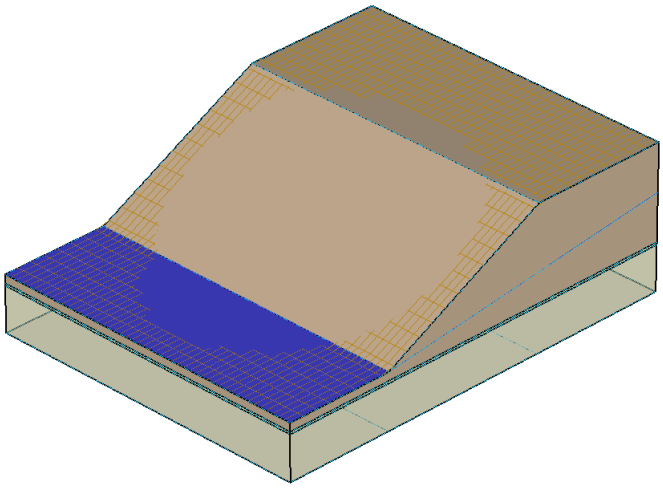

Figure 194 Geometry of 3D Example Model – Fredlund and Krahn (1977)

Ellipsoidal Sliding Surface

X-Coordinate	120.000
Y-Coordinate	0.000
Z-Coordinate	90.000
Tangent Plane	10.000
Aspect Ratio	1.000

8.1.2 Results and Discussions

This model illustrates in the 2D results from Fredlund and Krahn (1977) compared to the Slope Stability 3D results and CLARA-W results. The 3D FOS is about 30% larger than 2D FOS on average.

Table 259 Results of the Fredlund and Krahn (1977) 3D model

Method	Factor of Safety			Difference (%)
	Fredlund and Krahn (1977) 2D	CLARA-W	Slope Stability 3D	
Ordinary	1.171		1.514	-
Bishop Simplified	1.248	1.62	1.67	-3.09
Janbu Simplified	1.333		1.648	-
Corps. of Engineers #1	-		1.805	-
Corps. of Engineers #2	-		1.800	-
Spencer	1.245		1.713	-
M-P	1.250		1.675	-
GLE	-		1.675	-
Sarma	-		1.706	-

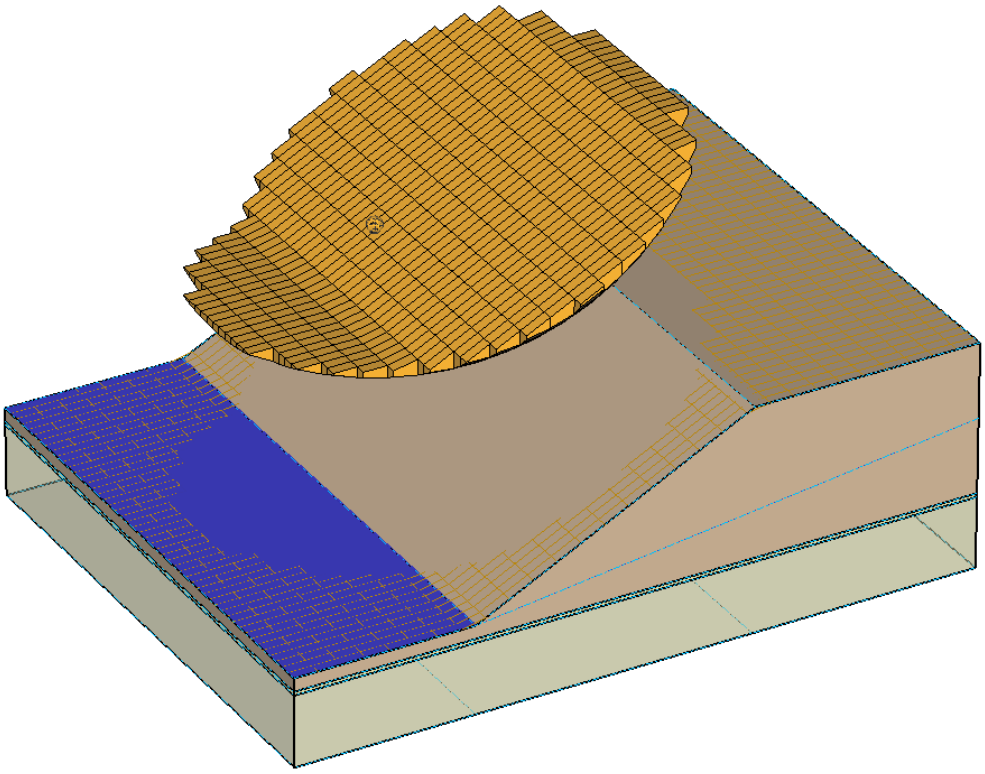

Figure 195 Results of the Fredlund and Krahn (1977) 3D model

8.2 EARTHQUAKE LOAD

Project: Slopes_3D
Model: earthquake_load

This model is used to benchmark the horizontal earthquake load calculations in the Slope Stability 3D software.

8.2.1 Geometry and Material Properties

The model geometry and material properties are the same as the Ellipsoidal_Toe_Submergence with the addition of the horizontal earth quake load as shown in Figure 196.

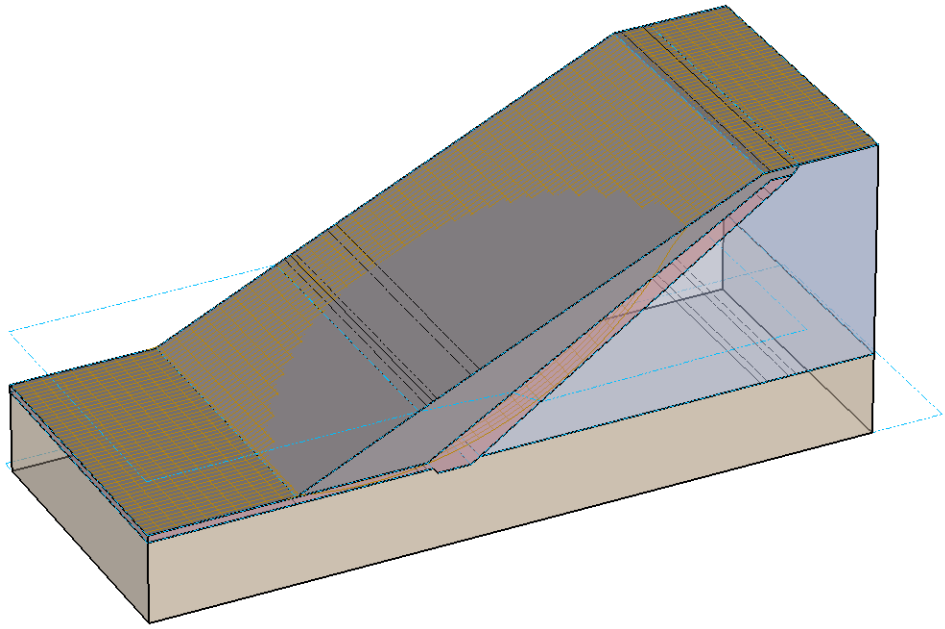

Figure 196 Geometry of earthquake_load Model with earth quake load

8.2.2 Results and Discussions

The Results are shown in Table 260. The result of the comparison is a reasonable comparison to the CLARA-W software.

Table 260 Results of the earthquake_load model

Method	Factor of Safety			Difference (%)
	CLARA-W	Slope Stability 3D		
		Moment	Force	
Bishop	1.040	1.066		2.500
Janbu Simplified	0.99		1.010	2.020
Spencer	1.00	1.070	1.070	7.000

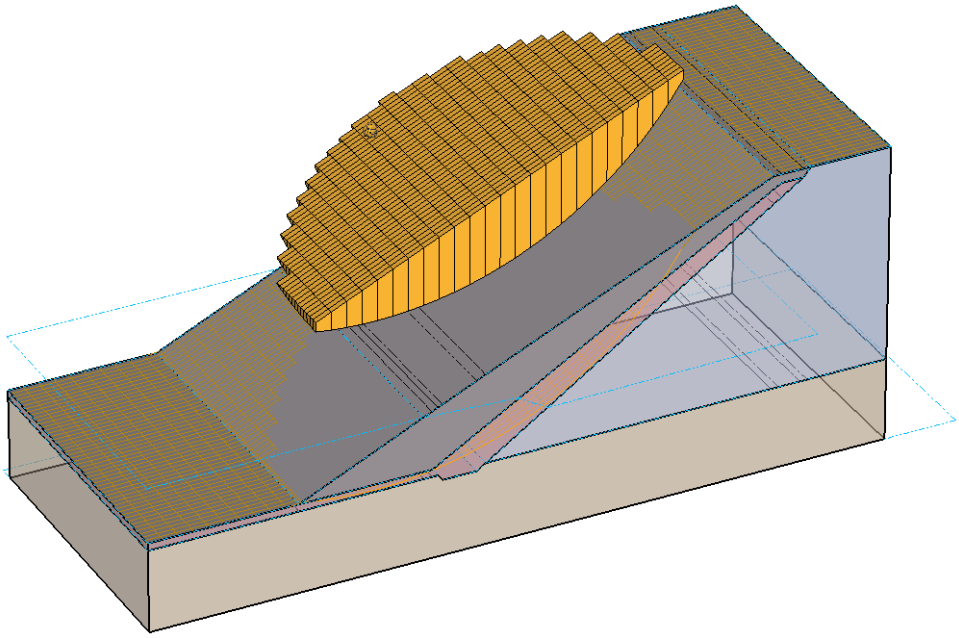

Figure 197 Results of earthquake_load Model with earth quake load

8.3 POINT LOAD

Project: Slopes_3D
Model: point_load

This model is used to benchmark the point load.

8.3.1 Geometry and Material Properties

The model geometry and material properties are the same as the Ellipsoidal_Toe_Submergence with the exception of an addition of the point load as shown in Figure 198.

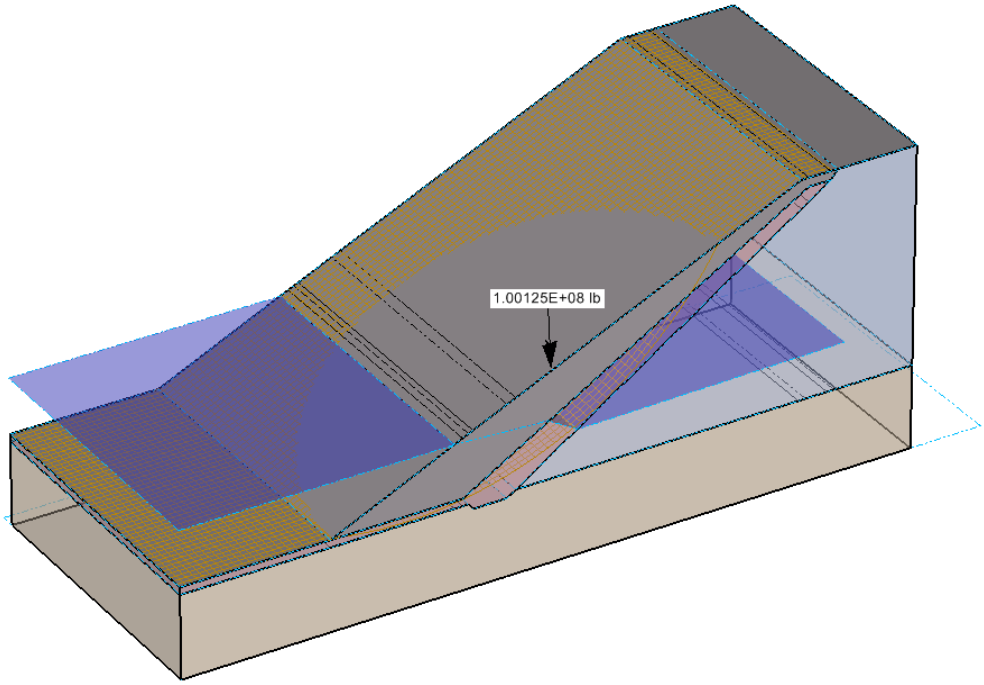

Figure 198 Geometry of the point_load model with a point load

8.3.2 Results and Discussions

The Results are shown in Table 261. The differences between calculations in each software package are considered negligible.

Table 261 Results of the point_load model

Method	Factor of Safety			Difference (%)
	CLARA-W	Slope Stability 3D		
		Moment	Force	
Bishop	1.340	1.365		1.866
Janbu Simplified	1.340		1.353	0.970
Spencer	-	1.360	1.360	-

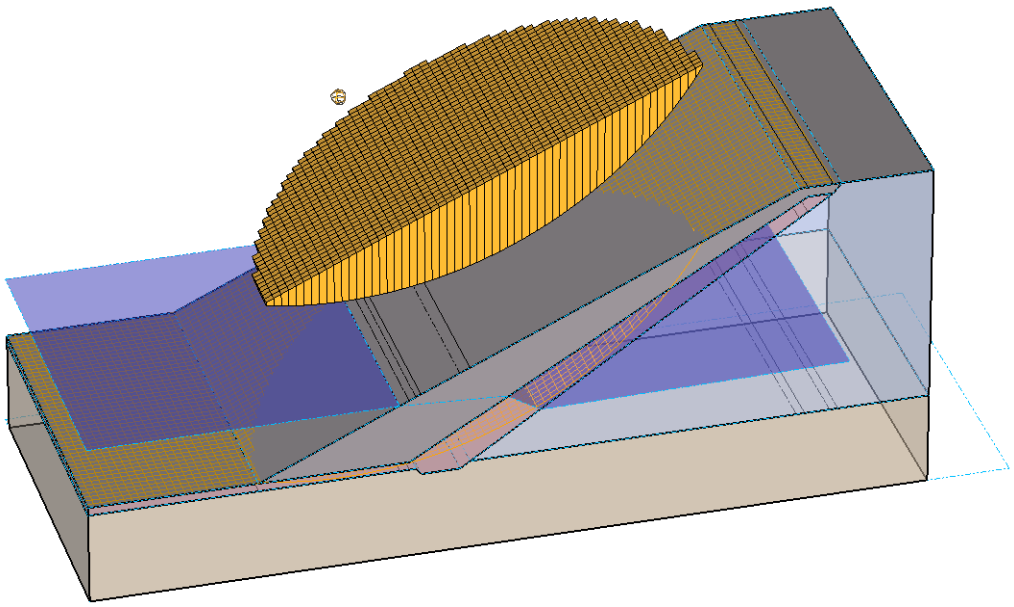

Figure 199 Results of the point_load model with a point load

8.4 TENSION CRACK

Project: Slopes_3D
Model: Tension_Crack

This model is used to benchmark the tension crack.

8.4.1 Geometry and Material Properties

The model geometry and material properties are the same as the Ellipsoidal_Toe_Submergence with the addition of the tension crack information. The tension crack is specified by X-coordinate = 300. It is specified that 80% of the tension crack is filled with water.

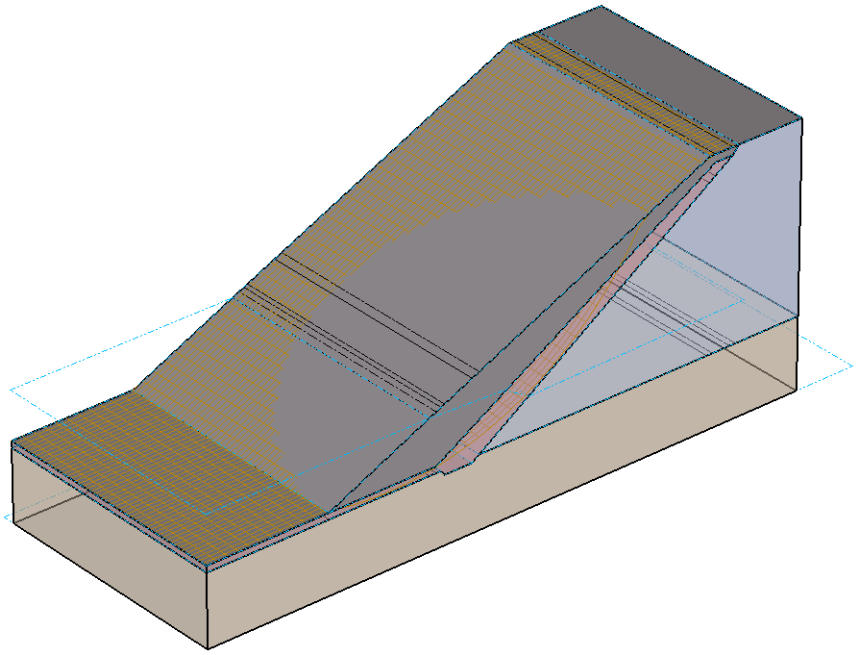

Figure 200 Geometry of the the Tension_crack model

8.4.2 Results and Discussions

The Results are shown in Table 262 and Figure 201.

Table 262 Results of the Tension_Crack model

Method	Factor of Safety			Difference (%)
	CLARA-W	Slope Stability 3D		
		Moment	Force	
Bishop	1.26	1.284		1.905
Janbu Simplified	1.19		1.212	1.849
Spencer	-	1.348	1.348	-

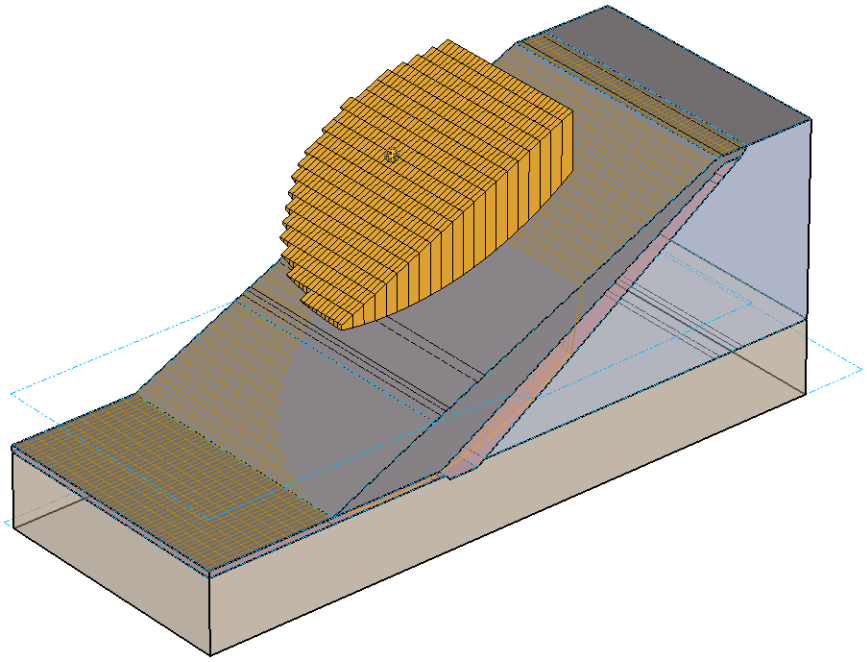

Figure 201 Result of the Tension_crack model

8.5 PORE WATER PRESSURES AT DISCRETE POINTS

Project: Slopes_3D
Model: PWP_discrete_points

This model is used to benchmark the discrete points method to specify the pore water pressures in Slope Stability 3D. The discrete points (specified in terms of pressure head) in this model are used to simulate the water table surface in the original Ellipsoidal_Toe_Submergence model.

8.5.1 Geometry and Material Properties

The model geometry and material properties are the same as the Ellipsoidal_Toe_Submergence model with a change of the initial condition – from water surface to discrete points (pressure head). The model geometry is shown in Figure 202 including contouring of the discrete points (in terms of pressure head).

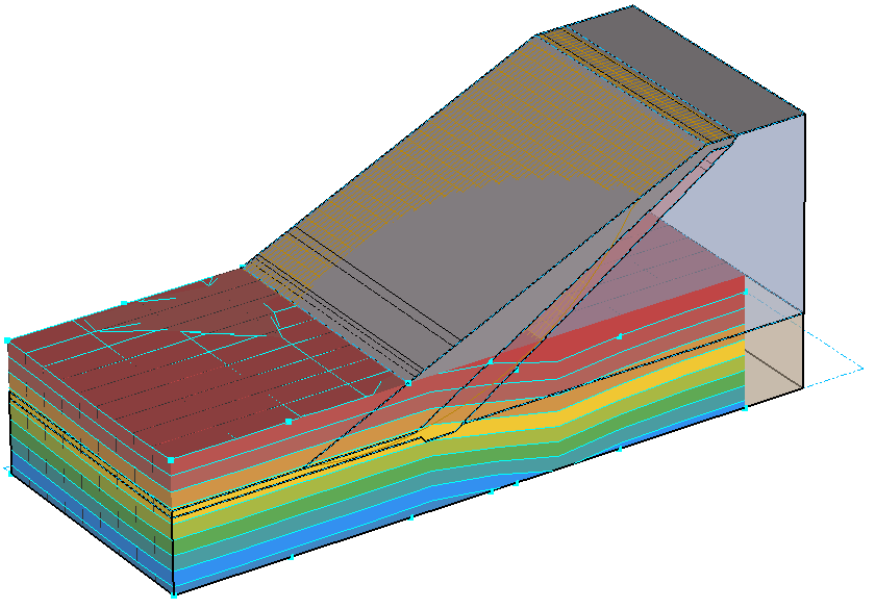

Figure 202 Geometry PWP_discrete_points model with discrete points contoured

8.5.2 Results and Discussions

The Results are shown in Table 263. The results from CLARA-W are based on the pore-water pressure dataset with a water table surface. The differences are deemed to be negligible.

Table 263 Results of the PWP_discrete_points model

Method	Factor of Safety			Difference (%)
	CLARA-W	Slope Stability 3D		
		Moment	Force	
Bishop	1.30	1.306		0.462
Janbu Simplified	1.23		1.237	0.569
Spencer	1.26	1.310	1.310	3.968

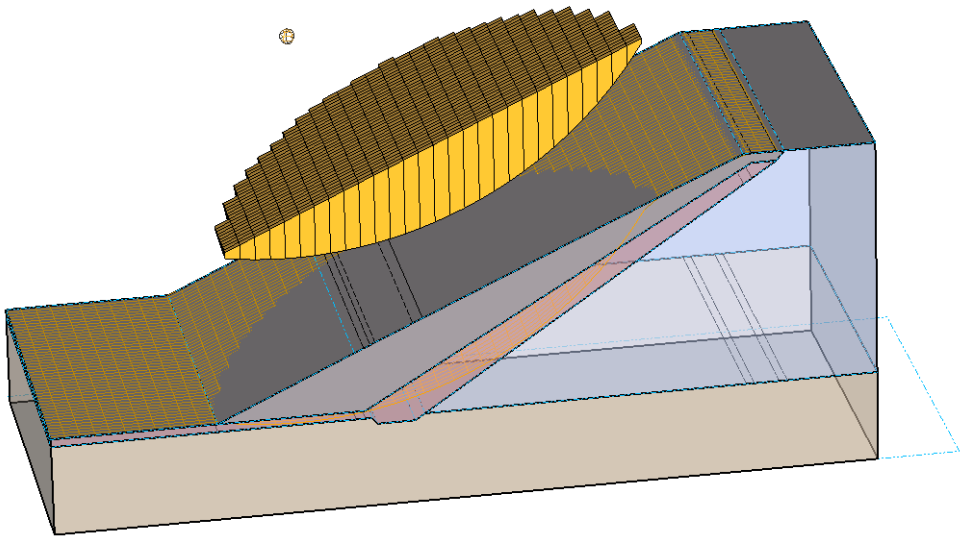

Figure 203 Results of PWP_discrete_points model with discrete points contoured

8.6 SUPPORTS – END ANCHORED

Project: Slopes_3D
Model: Support_End_Anchored

This model is utilized to benchmark the discrete End Anchored support type in Slope Stability 3D. CLARA-W does not implement Supports, so in order to benchmark the supports the same magnitude of external point load was specified in CLARA-W as the magnitude of end anchor tensile capacity in Slope Stability 3D. The location of the external point load in CLARA-W is the same location of the entry point of the support on the ground surface in Slope Stability 3D.

8.6.1 Geometry and Material Properties

The model geometry and material properties are the same as the Ellipsoidal_Toe_Submergence model with the addition of one End Anchored support. The tensile capacity of the end anchored support is $5x10^6$ lb. The surface point coordinate of the support on the ground surface is (250, 2, 179.898), the internal point of the support in the sliding mass is (400, 2, 179.898). The location of the support is shown in Figure 204.

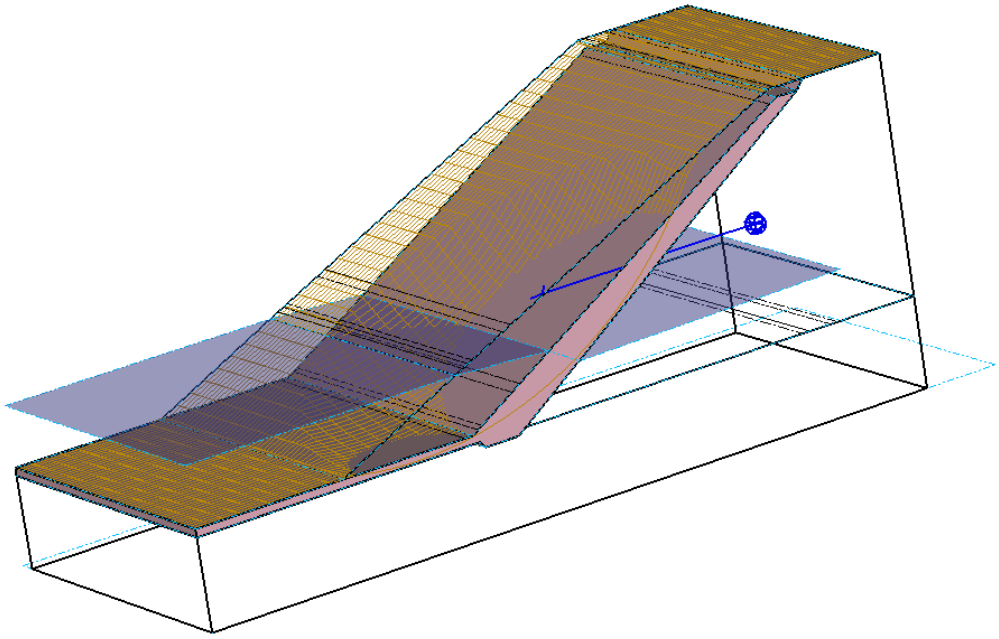

Figure 204 Geometry of Support_End_Anchored Model

8.6.2 Results and Discussions

The Results are shown in Table 264. The results from CLARA-W are based on corresponding external point load settings.

Table 264 Results of the Support_End_Anchored model

Method	Factor of Safety			Difference (%)
	CLARA-W	Slope Stability 3D		
		Moment	Force	
Bishop	1.760	1.754		-0.341
Janbu Simplified	1.730		1.729	-0.058
Spencer	1.940	1.753	1.752	-9.639

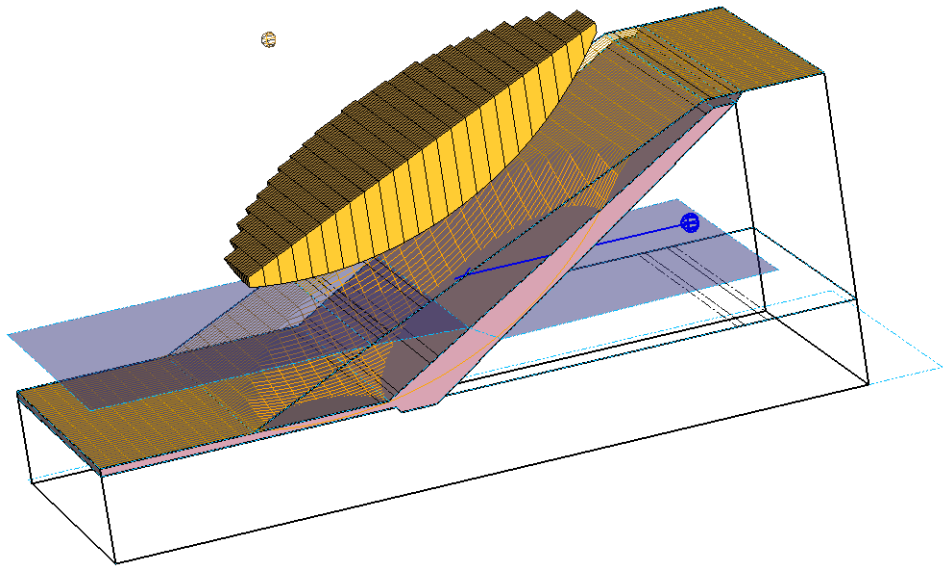

Figure 205 Results of Support_End_Anchored Model

8.7 3-STAGE RAPID DRAWDOWN

Project: Slopes_3D
Model: RDD_USACE_3D

This example model was originally presented in Corps of Engineers, Engineering Manual (2003) as a demo of Duncan's 3-stage rapid drawdown analysis in 2D. Hand calculation of the FOS of Bishop method is 1.44 for 2D. Here it is extended to 3D.

8.7.1 Geometry and Material Properties

The geometry is a direct extension from the 2D model section. The material properties are the same as in the 2D case. There are two water table surfaces in this model. The initial water table surface is located at an elevation of 103ft. The final water table surface is located at an elevation of 24ft as shown in Figure 206.

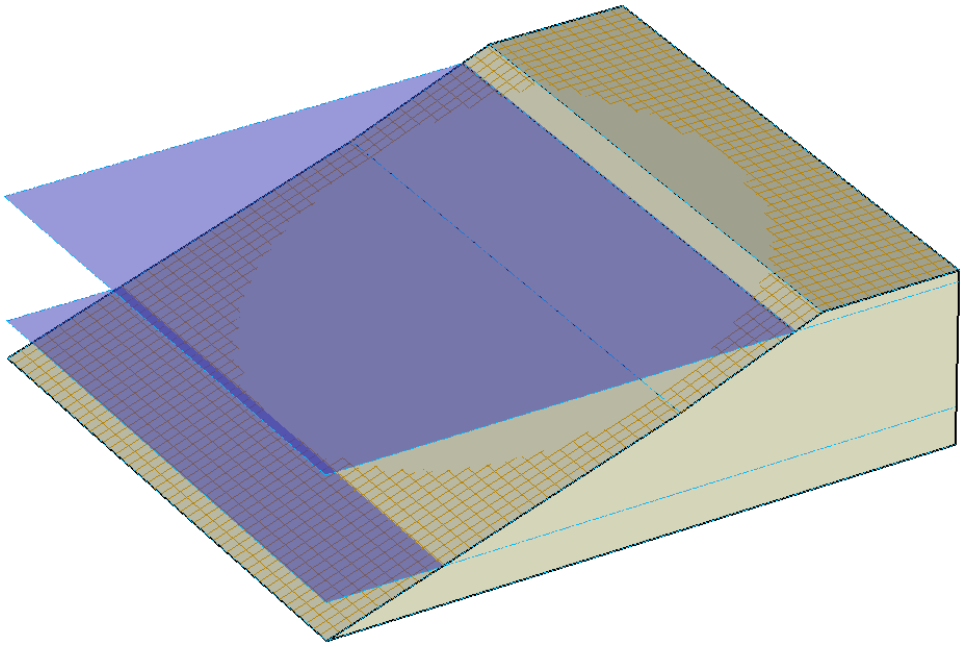

Figure 206 Geometry of the RDD_USACE_3D Model

8.7.2 Results and Discussions

The following table shows the results of the calculations for this model. The Slope Stability 2D results are also shown. The difference between 2D and 3D calculations is about 7% in this particular model. The hand calculation 2D result with Bishops Method is 1.44.

Table 265 Results of the RDD_USACE_3D model

Method	Factor of Safety			Difference (%)
	Slope Stability 2D	Slope Stability 3D		
		Moment	Force	
Bishop	1.436	1.551		8.00
Spencer	1.426	1.578	1.578	10.66

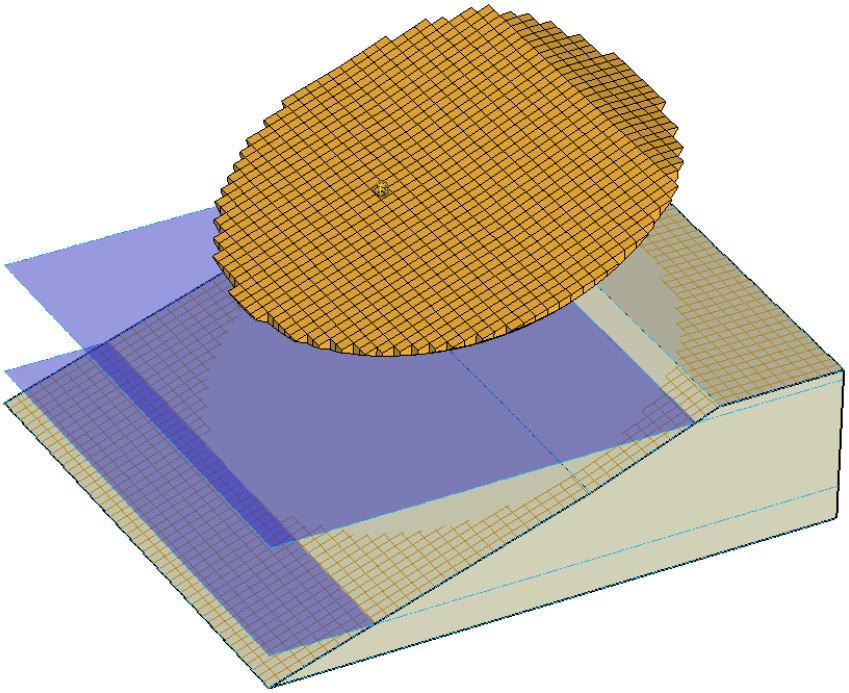

Figure 207 Results of the RDD_USACE_3D Model

9 DYNAMICS EXAMPLES

Dynamics is a Technical Preview.

In this section, Dyamics is used to simulate various dynamic stress-strain problems using 2D plane strain and general 3D analysis. Dynamics uses a time-domain finite element method for solving dynamic problems.

9.1 S-WAVE PROPAGATION IN AN ELASTIC SOIL COLUMN

Reference: Brinkgreve (2002)

Project: Seismic_2D, Seismic_3D
Model: 2D_SoilColumn_SWave, 2D_SoilColumn_SWave_1, 3D_SoilColumn_SWave, 3D_SoilColumn_SWave_1

Main Factors Considered:

- The displacement field due to the propagation of an S-wave in an elastic soil column and comparison with PLAXIS results

9.1.1 Model Description

A linear elastic soil column was considered and the propagation of an S-waves along the column was modeled. The S-wave is generated at the surface of the column by applying an abrupt horizontal displacement in the x-direction. Due to the finite velocity of the S-wave, the response of each material point within the domain depends on the time required for the S-wave to travel from its source to that point. The soil column was modeled both as a 2D plane strain and a general 3D problem. The results of analysis using Dynamics was compared against PLAXIS results for this problem. The total time of dynamic analysis was set to 0.5 seconds with time increments, $\Delta t = 0.001\ s$. Newmark parameters were set to $\delta = 0.53$ and $\alpha = 0.2652$. These values will introduce a small artificial damping to the system which damps out spurious oscillations in the solution. No material damping was considered in this problem.

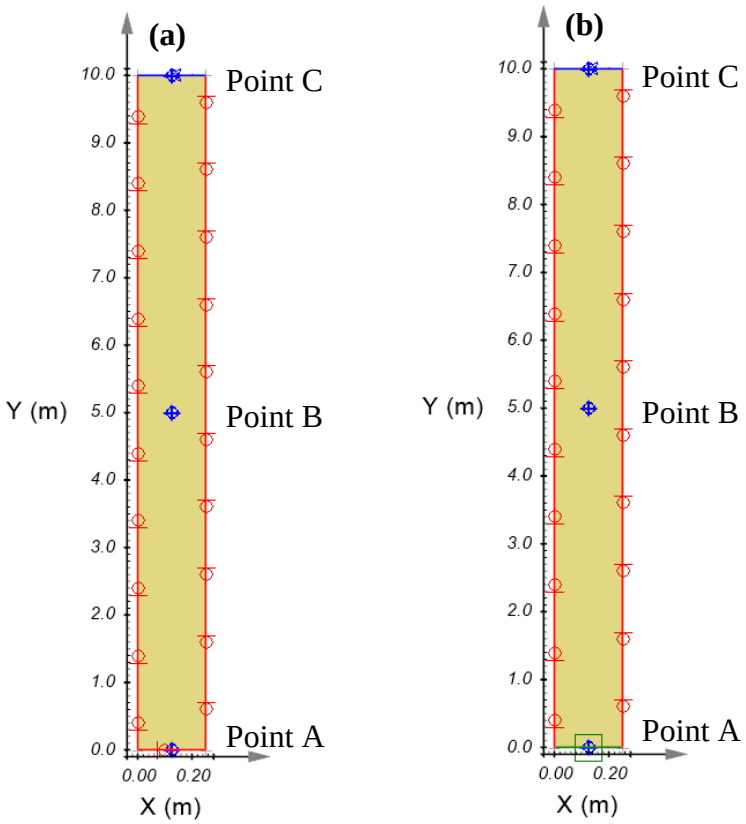

Figure 208. Geometry and boundary conditions for 2D plane strain probem (different horizontal and vertical scales):

(a) Fixed bottom boundary and (b) Nonreflecting bottom boundary

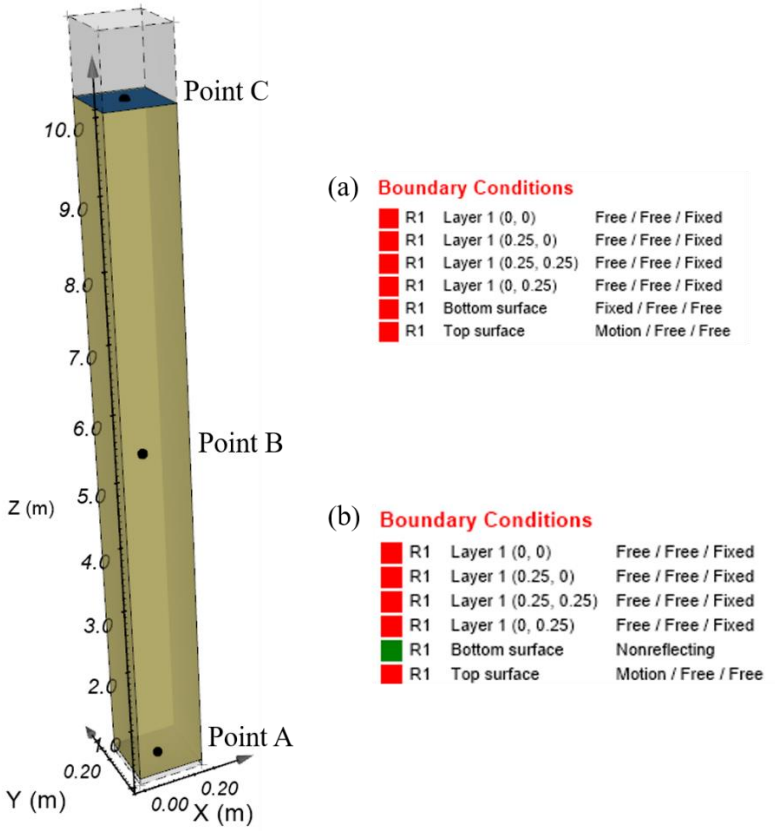

Figure 209. Geometry and boundary conditions for 3D problem (different horizontal and vertical scales): (a) Fixed bottom boundary and (b) Nonreflecting bottom boundary

9.1.2 Geometry and Boundary Conditions

Figure 208 and Figure 209 show the geometry and boundary conditions of the 2D and 3D models respectively. A column of soil with the depth of 10 m and width of 0.25 m was modeled. In the 2D model, the side and bottom boundaries of the model were fixed in their tangential directions. In the 3D model, the side boundaries were fixed in the z-direction and the bottom boundary was fixed in the x-direction. In both 2D and 3D models, the top boundary of the domain was subject to a constant displacement in the x-direction, $u_x = -0.001\ m$, which generates an S-wave propagating from the surface of the soil column to the bottom. To verify the effect of the non-reflecting boundary conditions, additional simulations (2D and 3D) were carried out in which the fixed boundary condition at the bottom boundary was replaced with a nonreflecting boundary condition.

9.1.3 Material Properties

A summary of the elastic material properties is provided in Table 266.

Table 266. Input material properties

Parameter	Value
Young's modulus (E)	18,000 kPa
Poisson's ratio (ν)	0.2
Total unit weight (γ)	19.620 kN/m^3

9.1.4 Results

Three observation points, A, B, and C, were considered respectively at the bottom, middle, and top of the soil column. The velocity of the S-wave in the soil column can be calculated from the material properties as $V_S = 61.24\ m/s$. Therefore, it will take $t_1 = 0.082\ s$ for the S-wave to reach point B for the first time. The bottom boundary of the domain is fixed. Hence, the wave reflects back into the domain when reaches the bottom boundary. The time required for the wave to reach point B for the second and third times during the analysis were calculated to be, respectively, $t_2 = 3t_1 = 0.245\ s$ and $t_3 = 5t_1 = 0.408\ s$. Figure 210 illustrates, for the 2D plane strain model, the horizontal deformation of points A, B, and C over time, computed by Dynamics and PLAXIS. The figure shows that Dynamicsresults for this problem match very well with PLAXIS results. The estimated arrival times of the S-wave at point B were also marked in this figure. The arrival times estimated by Dynamics for the first, second and third incidences of the S-wave with point B are, respectively, $t_1 = 0.083\ s$, $t_2 = 0.247\ s$, and $t_3 = 0.410\ s$, which are in agreement with the analytical values. Similar results has been obtained from the 3D model as illustrated in

Figure 211. The arrival times of the S-wave at point B were estimated as $t_1 = 0.083\ s$, $t_2 = 0.247\ s$, and $t_3 = 0.410\ s$ for the 3D model which are the same as the values estimated by the 2D model and are in great agreement with the theoretical values.

When a nonreflecting boundary condition is applied at the bottom boundary (see Figure 208(b) and Figure 209(b)), the energy of the waves reaching the bottom boundary is absorbed by the enforced boundary condition. Therefore, no reflection should be detected at the observation points within the domain. This behavior is shown in Figure 212, for the 2D plane strain model, and Figure 213, for the general 3D model. As illustrated in the figures, the arrival time of the S-wave at point B is the same as the time calculated in the previous case, i.e., $t = t_1 = 0.083\ s$. However, the second and third arrivals do not occur in this case as the wave does not reflect into the domain. It should be noted that the bottom boundary is not fixed in this case; hence, the arrival time of the S-wave at the bottom boundary can also be estimated from the numerical results. Using Figure 212 and Figure 213, the estimated time for the arrival of the wave at Point A is $t = 0.165\ s$, which is in agreement with the theoretical time, $t = 2t_1 = 0.166\ s$.

Figure 212 and Figure 213 also provide comparisons between results and the solution of the same problems using PLAXIS 2D/3D software.

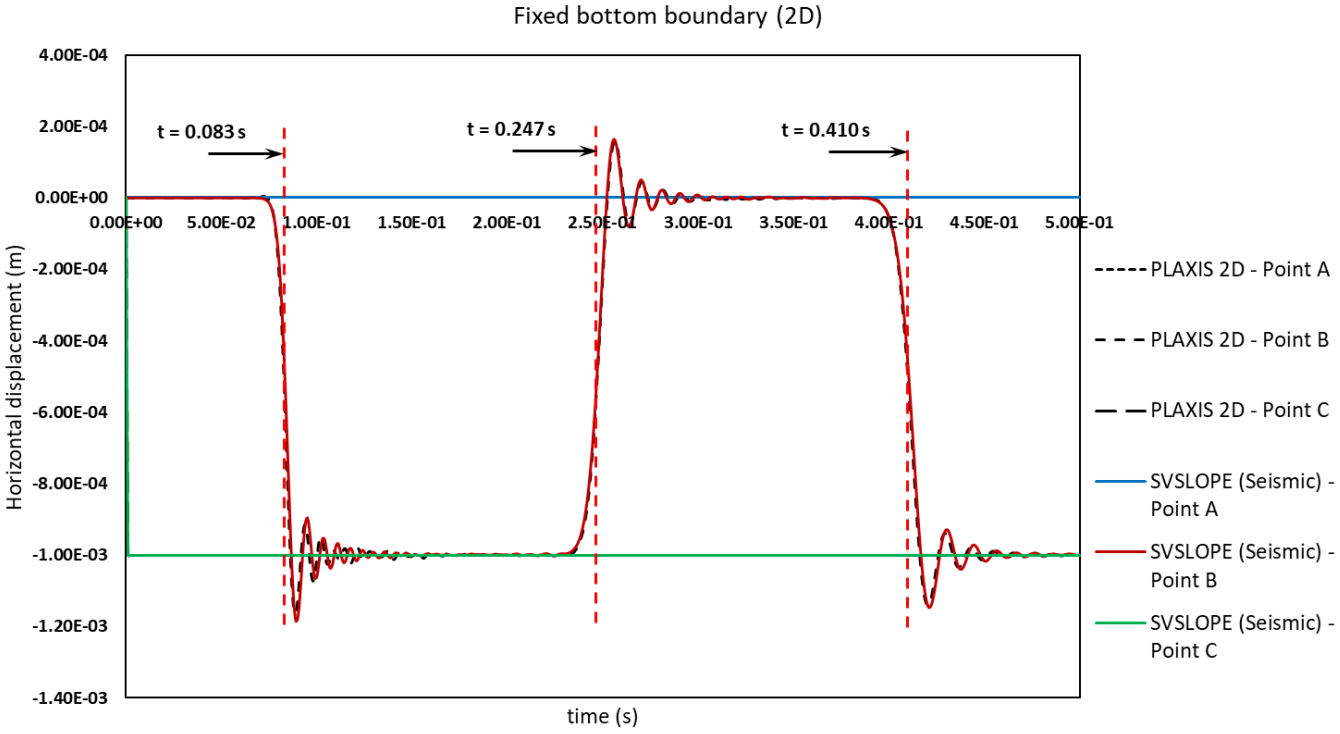

Figure 210. Time-history of horizontal displacement at Points A, B, and C under 2D plane strain condition with fixed bottom boundary

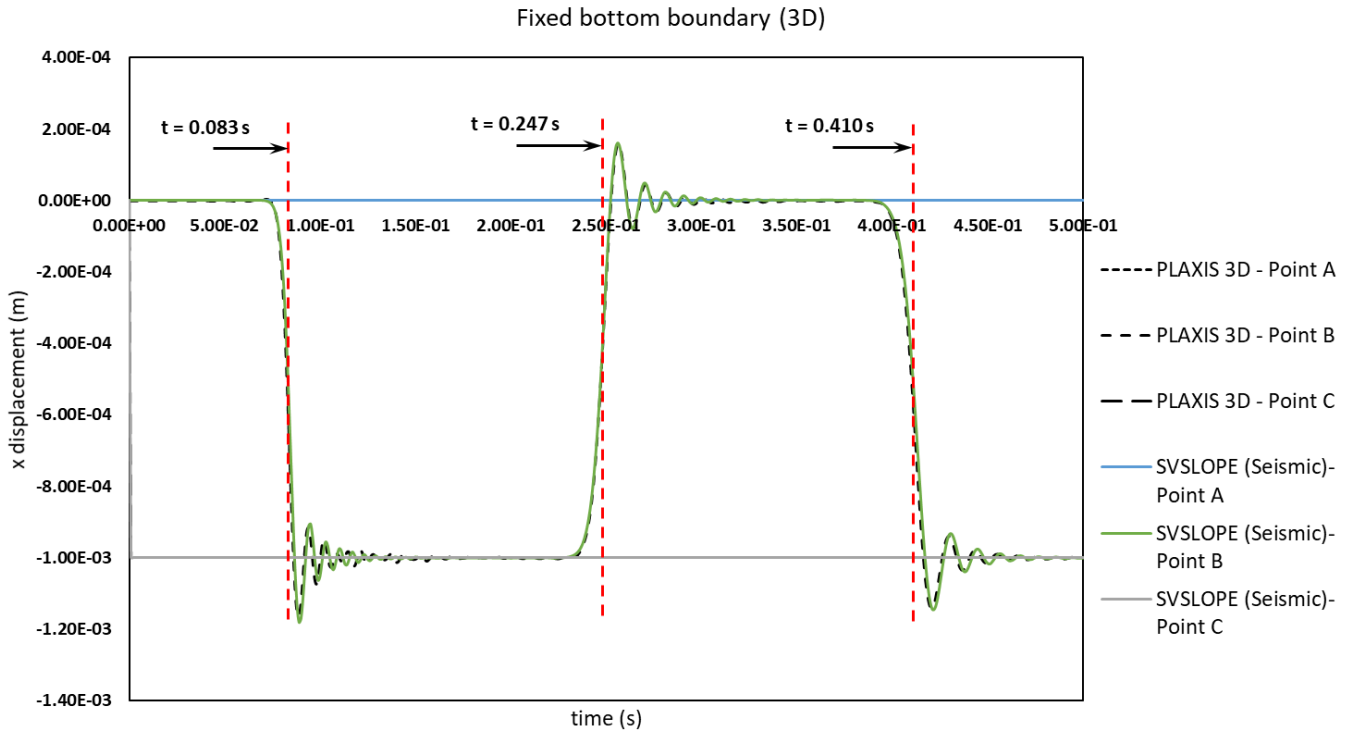

Figure 211. Time-history of horizontal displacement in x-direction at Points A, B, and C under general 3D condition with fixed bottom boundary

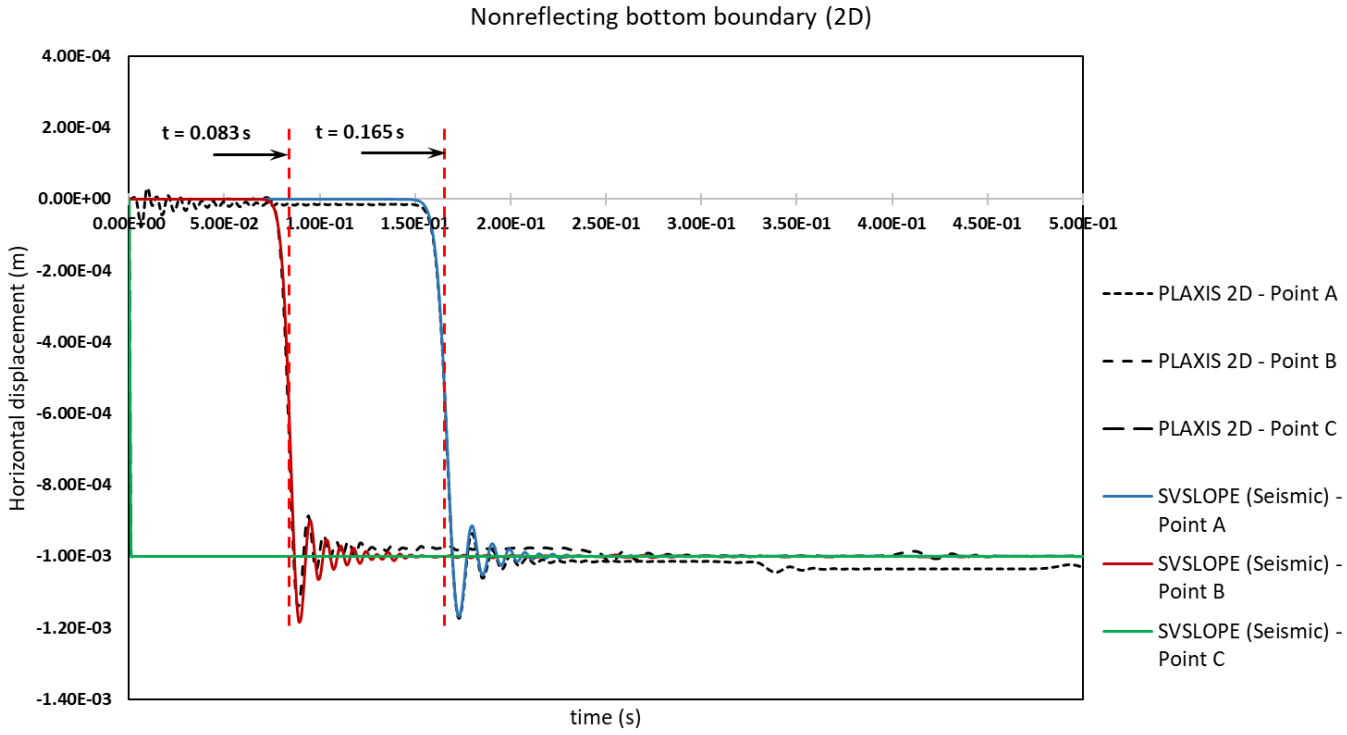

Figure 212. Time-history of horizontal displacement at Points A, B, and C under 2D plane strain condition with nonreflecting bottom boundary

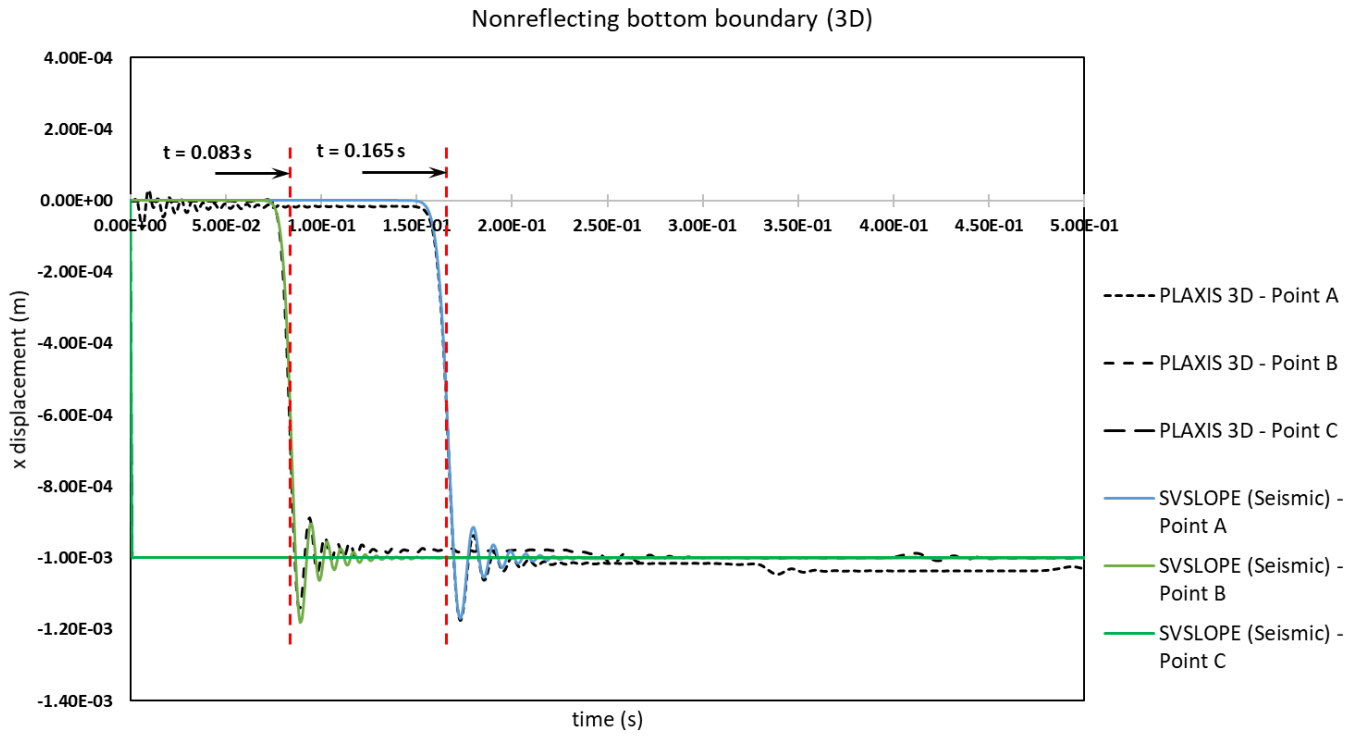

Figure 213. Time-history of horizontal displacement in the x-direction at Points A, B, and C under general 3D condition with nonreflecting bottom boundary

9.2 P-WAVE PROPAGATION IN AN ELASTIC SOIL COLUMN

Reference: Brinkgreve (2002)

Project: Seismic_2D, Seismic_3D
Model: 2D_SoilColumn_PWave, 2D_SoilColumn_PWave_1, 3D_SoilColumn_PWave, 3D_SoilColumn_PWave_1

Main Factors Considered:

- The displacement field due to the propagation of a P-wave in an elastic soil column and comparison with PLAXIS results

9.2.1 Model Description

A linear elastic soil column was considered, and the propagation of a P-wave within the column was modeled. The P-wave was generated at the surface of the column by applying an abrupt vertical displacement. Due to the finite velocity of the P-wave, the response of each material point within the domain depends on the time required for the P-wave to travel to that point from its source. The soil column was modeled both as a 2D plane strain and a general 3D problem. The results of analysis using Dynamics were compared against the numerical results of PLAXIS software for the 2D and 3D models. The total time of dynamic analysis was set to 0.25 seconds with time increments, $\Delta t = 0.001\ s$. Newmark parameters were set to $\delta = 0.53$ and $\alpha = 0.2652$. These values will introduce a small artificial damping to the system which damps out spurious oscillations in the solution. The damping ratio is set to zero for this problem.

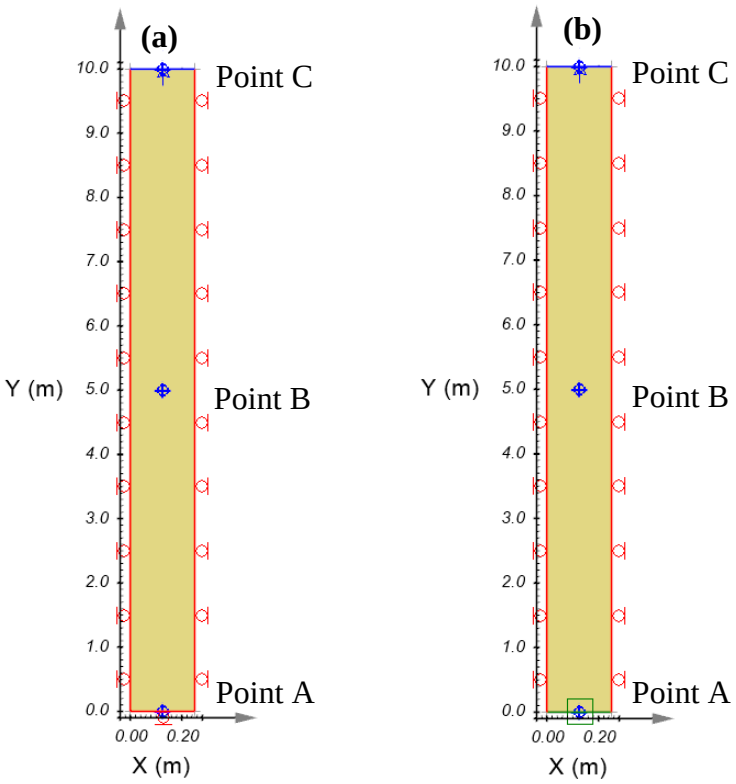

Figure 214. Geometry and boundary conditions for 2D plane strain model (different horizontal and vertical scales): (a) Fixed bottom boundary and (b) Nonreflecting bottom boundary

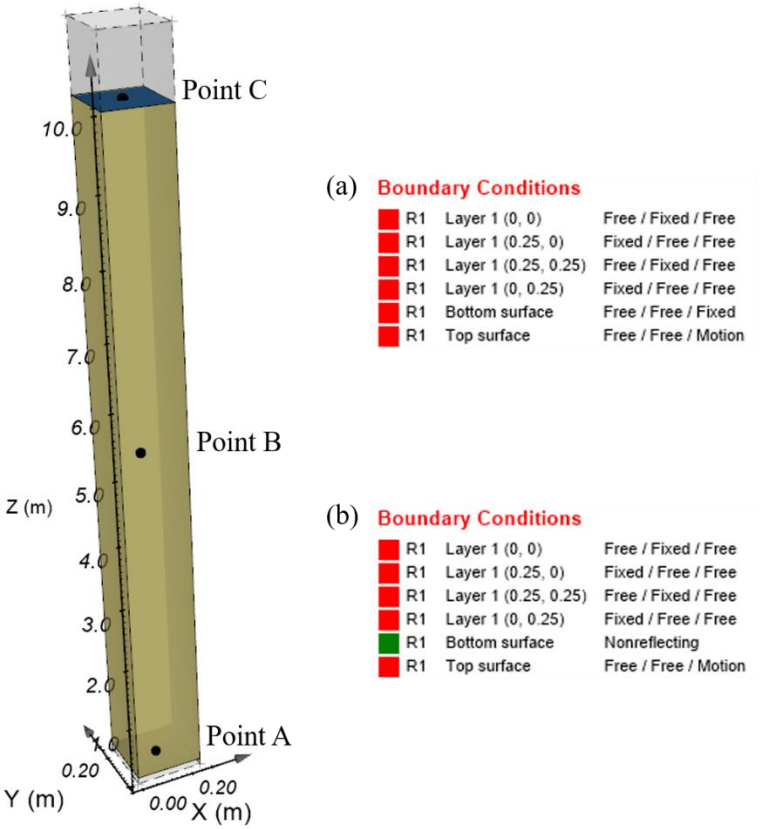

Figure 215. Geometry and boundary conditions for general 3D problem (different horizontal and vertical scales): (a) Fixed bottom boundary and (b) Nonreflecting bottom boundary

9.2.2 Geometry and Boundary Conditions

Figure 214 and Figure 215 show the geometry and boundary conditions of the 2D and 3D models respectively. A column of soil with the depth of 10 m and the width of 0.25 m was modeled. The side and bottom boundaries were fixed in the directions normal to the boundaries in both 2D and 3D models. The top boundary of the domain was subject to a constant displacement in the vertical direction, $u_y = -0.001\,m$ for the 2D and $u_z = -0.001\,m$ for the 3D model. The vertical displacement generates a P-wave propagating from the surface of the soil column to its bottom. To verify the effect of the non-reflecting boundary conditions, additional simulations were carried out, in 2D and 3D, in which the fixed boundary condition at the bottom boundary was replaced with a nonreflecting boundary condition.

9.2.3 Material Properties

A summary of the elastic material properties is provided in Table 267.

Table 267. Input material properties

Parameter	Value
Young's modulus (E)	18,000 kPa
Poisson's ratio (ν)	0.2
Total unit weight (γ)	19.62 kN/m^3

9.2.4 Results

Three observation points, A, B, and C, were considered respectively at the bottom, middle, and top of the soil column. The velocity of the P-wave in the soil column can be calculated from the material properties as $V_P = 100\ m/s$. Therefore, it will take $t_1 = 0.050\ s$ for the P-wave to reach point B for the first time. When the bottom boundary of the domain is fixed, the wave reflects into the domain upon reaching the bottom boundary. Hence, the time required for the wave to reach point B for the second time during the analysis is calculated as $t_2 = 3t_1 = 0.150\ s$.

Figure 216 shows the vertical deformation at points A, B, and C over time for the 2D plane strain model using both Dynamics and PLAXIS. The figure shows that Dynamics results match very well with PLAXIS results. The estimated arrival times of the P-wave at point B were also shown in this figure. The arrival times estimated by Dynamics for the first and second incidences of the P-wave at point B are respectively $t_1 = 0.051\ s$ and $t_2 = 0.152\ s$, which are in agreement with the analytical values. Similar results has been obtained from the 3D model and are illustrated in Figure 217. The arrival times of the P-wave at point B were estimated as $t_1 = 0.051\ s$ and $t_2 = 0.152\ s$ for the 3D model which are similar to the arrival times estimated by the 2D model and, hence, are in great agreement with the theoretical values.

When a nonreflecting boundary condition is applied at the bottom boundary, the energy of the waves reaching the bottom boundary is absorbed by the enforced boundary condition. Therefore, no reflection should be detected at the observation points within the domain. This behavior is clearly shown in Figure 218, for the 2D plane strain, and Figure 219, for the general 3D model. As illustrated in the figures, the arrival time of the P-wave at point B is the same as the time calculated in the previous case, i.e., $t = t_1 = 0.051\ s$. However, the second arrival does not occur in this case as the wave does not reflect into the domain. It should be noted that the bottom boundary is not fixed in this case; hence, the arrival time of the P-wave at the bottom boundary can also be estimated from the numerical results. Using Figure 218 and Figure 219, the estimated time for the arrival of the wave at Point A is $t = 0.102\ s$ which is in agreement with the theoretical arrival time, $t = 2t_1 = 0.100\ s$.

Figure 218 and Figure 219 also provide comparisons between Dynamics results and the solution of the same problems using PLAXIS software.

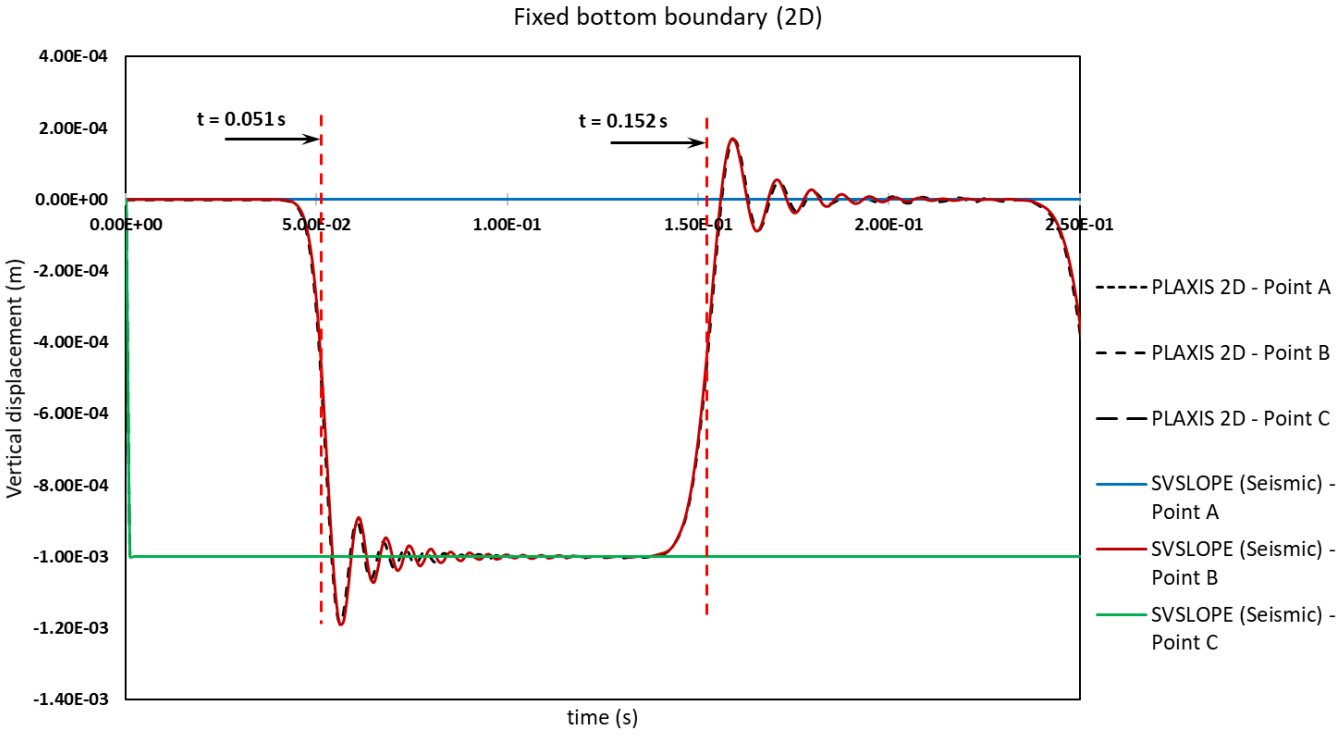

Figure 216. Time-history of vertical displacement at Points A, B, and C under 2D plane strain condition with fixed bottom boundary

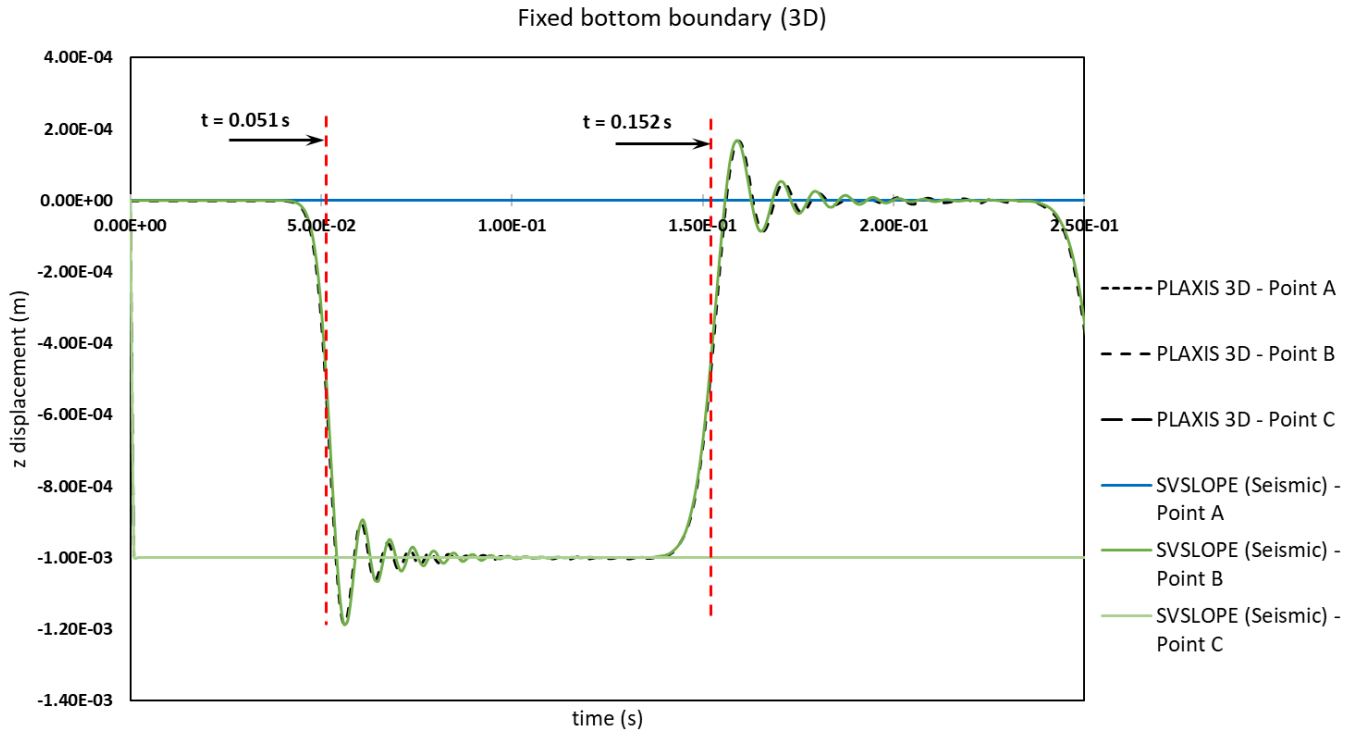

Figure 217. Time-history of vertical displacement at Points A, B, and C for 3D problem with fixed bottom boundary

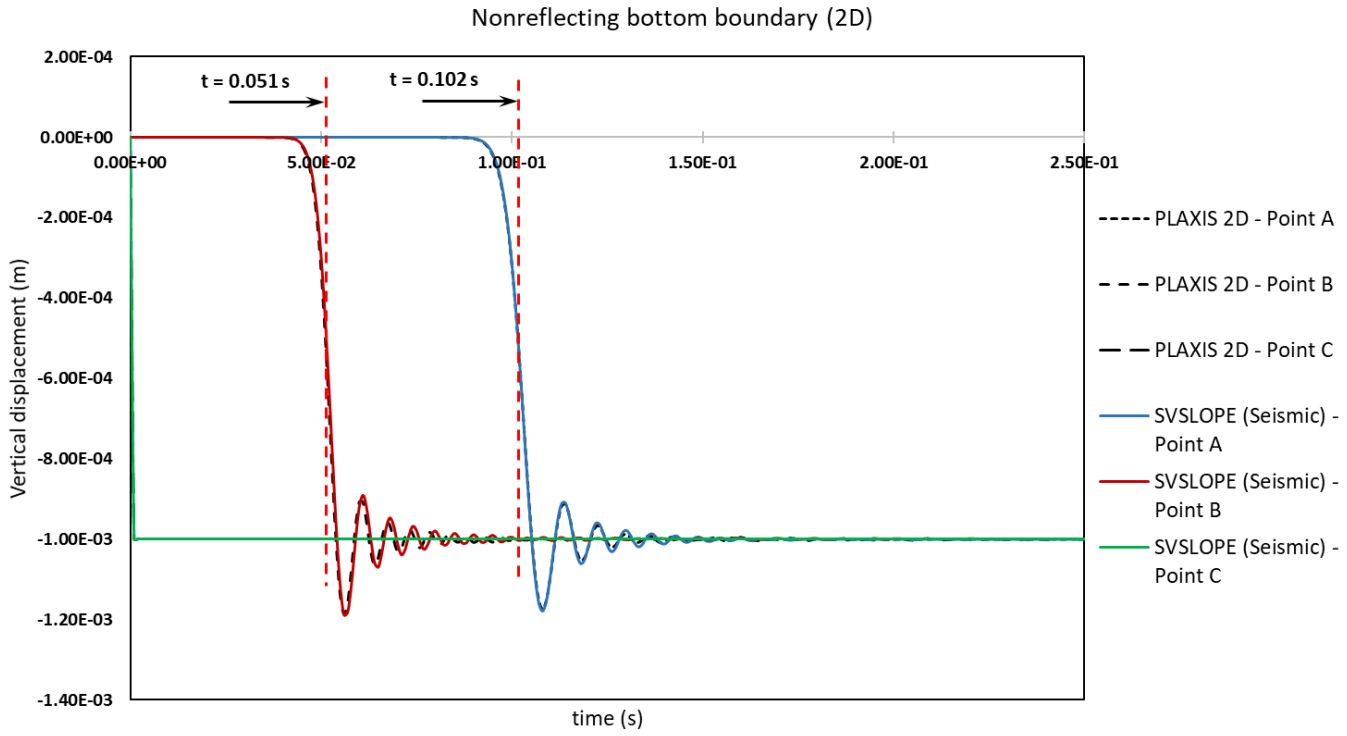

Figure 218. Time-history of vertical displacement at Points A, B, and C under 2D plane strain condition with nonreflecting bottom boundary

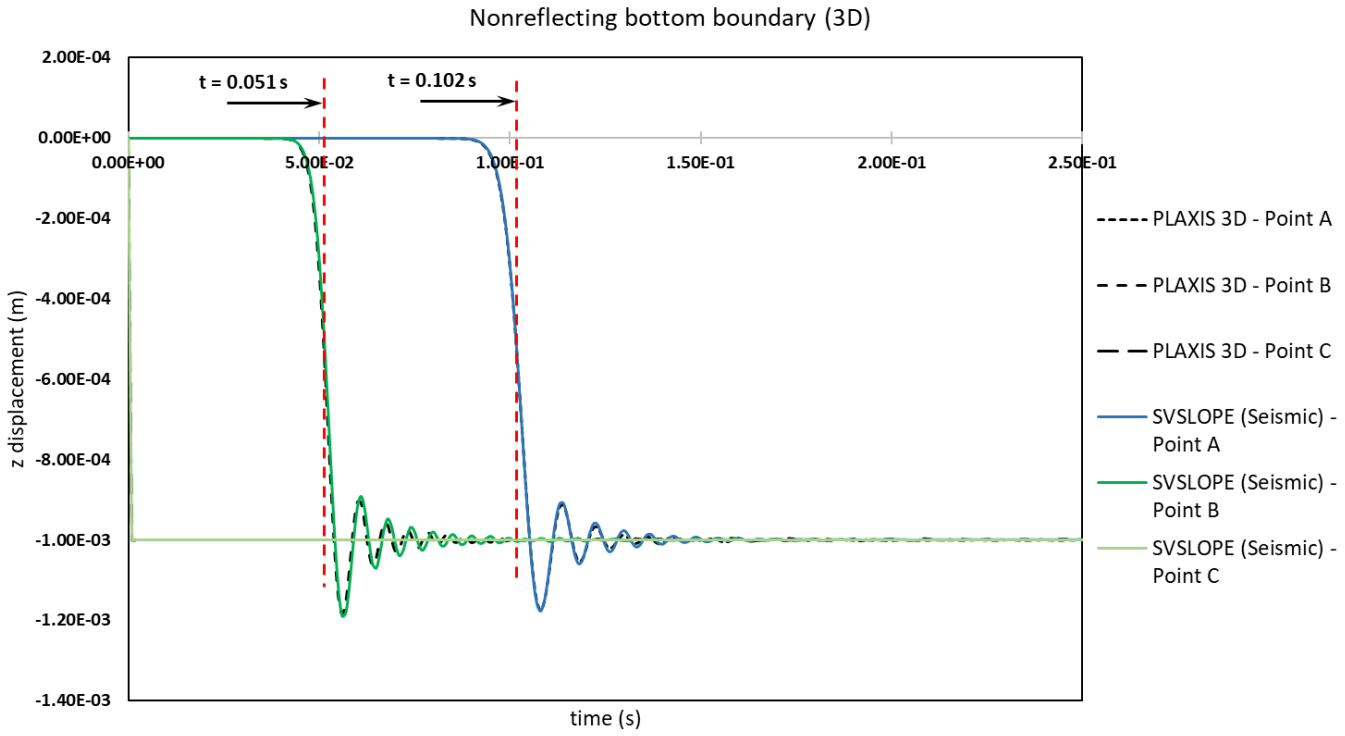

Figure 219. Time-history of vertical displacement at Points A, B, and C for 3D problem with nonreflecting bottom boundary

9.3 REFRACTION SEISMOLOGY

Reference: Fowler (1990)

Project: Seismic_2D
Model: 2D_Refraction

Main Factors Considered:

- Determine the velocity of the P-wave and estimate the thickness of the soil layer in a two-layer elastic medium using refraction seismology

9.3.1 Model Description

The behavior of body waves in an elastic medium depends on the physical properties of the medium. When body waves propagate in a heterogenious medium, such as a layered soil, their propagation speed and direction of propagation change according to the relative rigidity of the layers encountered. This phenomenon can be used to extract important information about soil layers. For example, one can estimate material properties (such as wave speeds) of different soil layers and the thickness of each layer using the motion recorded at the surface.

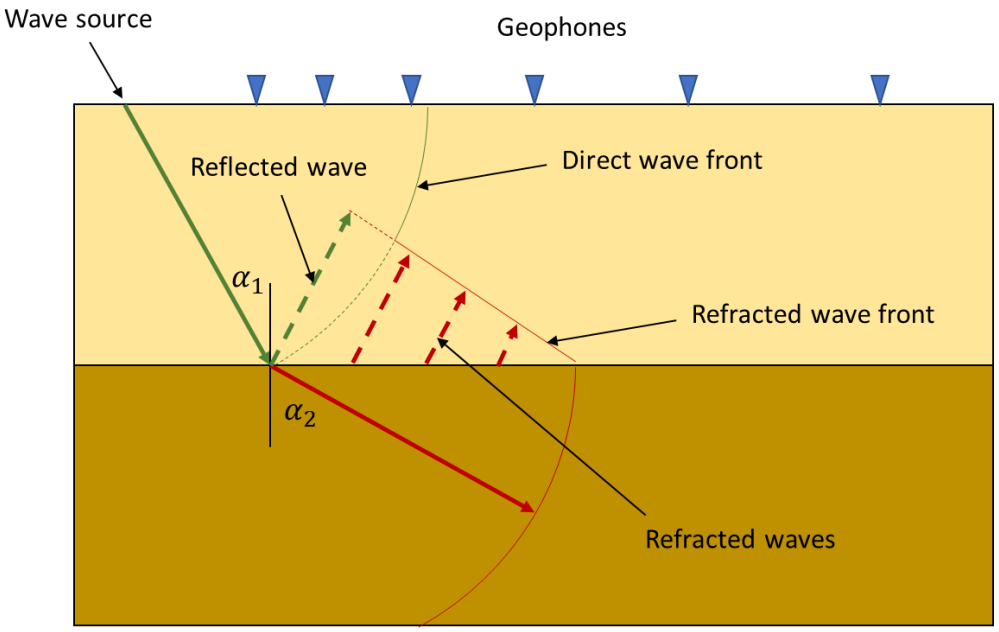

Figure 220. Wave behavior in a two-layer medium

Consider the two-layer soil model shown in Figure 220. Let us choose the matrial properties of the two layers such that the product of the mass density, ρ, and wave velocity, V, of the bottom layer, $\rho_2 V_2$, is greater that that of the top layer, $\rho_1 V_1$. The product of the mass density and wave velocity of a matrial is known as its *acoustic impedance* (see for example Kinsler et al. (1999) for more information). An acoustic transmitter, located at the surface, transmits a compressional wave signal (p-wave) towards the interface of the two layers. An array of geophones, set along the surface of the top layer, records the response of the layer at the surface. The compressional wave travels within the top layer with V_1 until it reaches the interface. Due to the difference between the acoustic impedance of the two layers, a part of the wave energy reflects back into the top layer (reflected wave). The remaining part of the wave propagates through the bottom layer; however, its strike angle and propagation speed change according to Snell's law:

$$\frac{V_1}{V_2} = \frac{\sin \alpha_1}{\sin \alpha_2} \qquad [1]$$

in which α_1 and α_2 are the direction angles of the wave ray in the first and second layers respectively (see Figure 220).

The wave ray that reaches the second layer travels faster than the initial wave as it propagates in the bottom layer with a higher wave speed. The wave front traveling along the interface acts as a new wave source and transmits new waves within the top layer towards the surface. These waves are known as Refracted waves. The geophones located on the surface of the top layer will record the wave ray that has travelled directly through the top layer (direct wave) as well as the refracted wave ray (see Figure 220). Geophones that are closer to the wave source record the arrival of the direct wave prior to the refracted wave arrival as it takes longer for the wave to travel to the interface and return to the surface. Contrarily, geophones located far from the wave source record the refracted wave prior to the direct ray as the wave has had enough time to travel through the second layer (with a higher wave speed) to catch up the direct wave. Knowing the arrival time of the wave at each geophone and its distance form the wave source, one is able calculate the speed of the wave in each layer and the thickness of the top layer (Fowler 1990).

In this verification, we simulate the phenomenon explained above and use the information recorded at the surface to estimate the speed of the P-wave in each layer and the thickness of the top layer. A 2D plane strain model of a two layer soil was considered. A time increment of $\Delta t = 2.5\ \mathrm{m}s$ was used for dynamic analysis. Newmark parameters were set to $\delta = 0.50$ and $\alpha = 0.25$; therefore, no numerical damping was engaged in the computations. An overall damping ratio of $\xi = 0.50\%$ was assumed for this problem (at response frequencies 0.5 Hz and 1.0 Hz). Material properties of the layers are presented in Table 268.

Table 268. Input material properties

Parameter	Top Layer	Bottom Layer
Young's modulus (E)	18,000 kPa	180,000 kPa
Poisson's ratio (ν)	0.25	0.3
Total unit weight (γ)	19.6 kN/m^3	21 kN/m^3

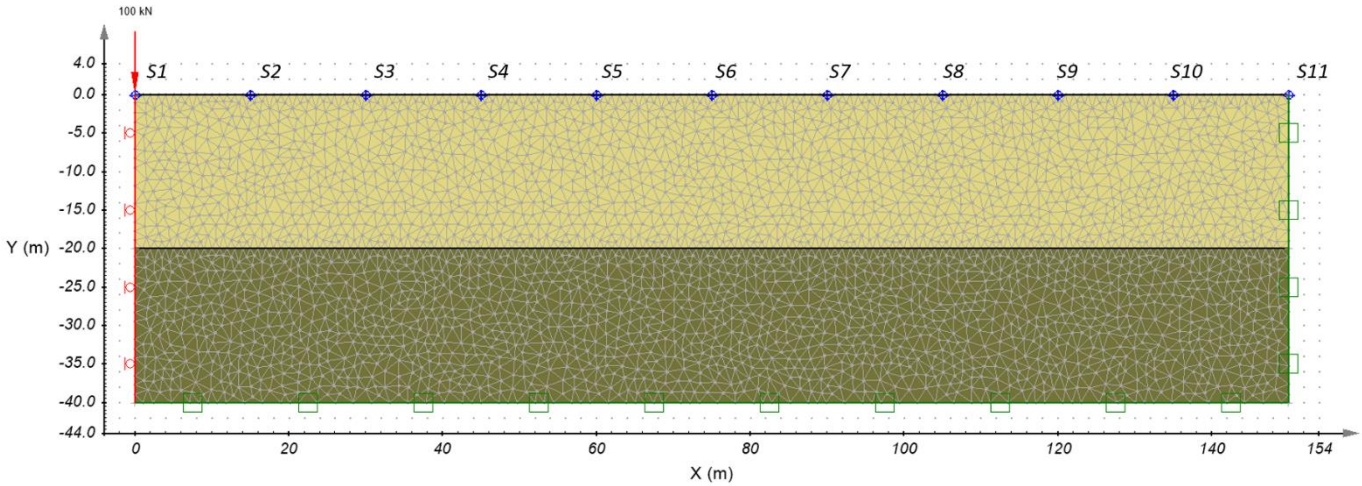

Figure 221. Geometry and boundary conditions of the model

9.3.2 Geometry and Boundary Conditions

The geometry and boundary conditions of the model are illustrated in Figure 221. Each layer has a thickness of 20 m and width of 150 m. An array of geophones (history points), at every 15 m, was set along the surface (named *S1* through *S11* from left to right). The wave source was modeled by means of a vertical dynamic line load with an amplitude of 100 kN/m applied at the upper left corner of the domain. The variation of the line load over time is shown in Figure 222. The left boundary of the model was fixed in the x-direction. Non-reflecting boundary conditions were set at the right and bottom boundaries and the top boundary was left free.

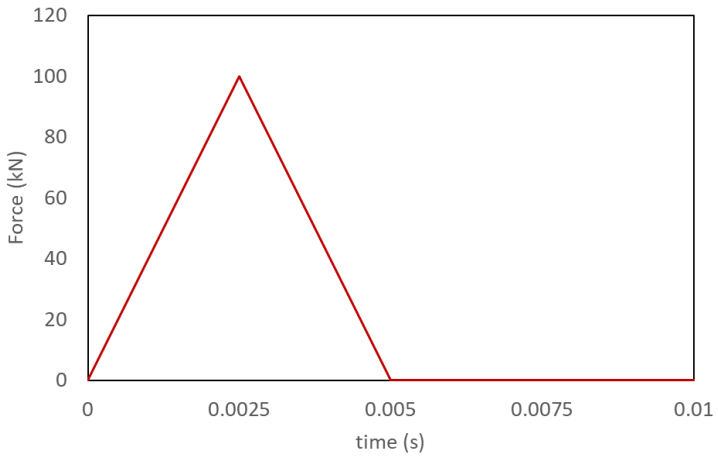

Figure 222. Variation of dynamic force over time

9.3.3 Results

To calculate the velocity of the P-wave in each layer, we first need to estimate the wave arrival time at each geophone. The arrival times can be captured using the seismograph recorded by the geophone. For this problem, we use the recorded displacement in the x-direction to capture the arrival time of the P-wave. Figure 223 illustrates the recorded displacement at each geophone for the two-layer soil model (blue). To provide a reference for comparison, the displacement in the x-direction for an equivalent model with only one soil layer (with a thickness of 40.0 m) is also provided at each station (red). This will allow the reader to compare the response of the model with the response of a case in which no refraction occurs. For each recording, the arrival time can be estimated by capturing the time at which the first significant displacement is recorded. Determining the exact arrival time from the recorded seismograph is a nontrivial task as the graphs do not clearly show an abrupt initial jump in the displacement to be taken as the arrival of the P-wave. As an estimate of the wave arrival time, in this verification example, we take the mean value of the time points corresponding to the first local minimum and maximum of each graph (This assumption is consistent with the numerical results presented in sections **Error! Reference source not found.** and **Error! Reference source not found.** for P- and S-wave arrivals). The arrival time was calculated for each graph and is marked with vertical dashed lines in Figure 223. The estimated arrival time of the wave at each geophone is presented in Table 269.

The theoretical time of arrival of the direct and refracted rays at a geophone, located at distance, x, from the source, can be calculated as linear functions of the speed of the P-wave in the top and bottom layers (Fowler 1990):

$$t_{Direct} = \frac{x}{V_1} \qquad [2]$$

$$t_{Refracted} = \frac{x}{V_2} + 2H_1 \frac{\sqrt{V_2^2 - V_1^2}}{V_1 V_2} \qquad [3]$$

where H_1 is the thichkness of the top layer.

Table 269 also provides the theoretical arrival time of the direct and refracted ray at each geophone. The values corresponding to the first arrival time are presented in bold fonts. From the theoretical values, it can be seen that the first wave arriving at geophones, S1 through S4, is expected to be the direct wave whereas the rest of the geophones are expected to record the refracted wave first.

To calculate the speed of the P-wave in each layer, one can plot the estimated values of the first arrival time at each geophone versus the distance of the geophone from the source, as presented in Figure 224. The estimated values from Dynamics numerical results are ploted in red dots. It can be seen that Dynamics results are in agreement with the theoretical values. The relations, [2] and [3], are linear. Hence, the speed of the P-wave in the first and second layers can be estimated by fitting two lines to the numerical results. The slopes of these lines represent the reciprocals of the wave speeds (see Figure 224).

The linear functions fitted to the Dynamics numerical results are shown in Figure 224. It should be noted that the estimated value for S5 (located at x=60.0 m) has been excluded from the data used for fitting linear functions. The reason of this exclusion is that S5 is located only slightly away from the cross-over point at which the direct and refracted rays are expected to arrive simultaneously. As a result, the interaction of the two waves could increase the error in estimating the arrival time at this point, compared to the other points.

Table 269. Estimated and theoretical time of arrival of waves at different geophones (theoretical first arrival times are bolded)

Station	Distance from source (m)	Estimated first arrival time (s) (Dynamics)	Theoretical arrival time (s) (Direct ray)	Theoretical arrival time (s) (Refracted ray)
S1	0.0	0.0	**0.0**	0.366
S2	15.0	0.136	**0.144**	0.411
S3	30.0	0.284	**0.289**	0.455
S4	45.0	0.431	**0.433**	0.499
S5	60.0	0.565	0.577	**0.544**
S6	75.0	0.593	0.722	**0.589**
S7	90.0	0.636	0.866	**0.633**
S8	105.0	0.680	1.010	**0.678**
S9	120.0	0.724	1.154	**0.723**
S10	135.0	0.773	1.299	**0.767**
S11	150.0	0.821	1.443	**0.812**

Using the estimated slope values from the fitted lines, the speed of the P-wave within the first and second layers can be estimated as $\bar{V}_1 = 104.16\, m/s$ (compare to the theoretical value $V_1 = 103.95\, \frac{m}{s}$ (0.2% error)), and $\bar{V}_2 = 333.33\, m/s$ (compare to the theoretical value $V_2 = 336.49\, \frac{m}{s}$ (0.9% error)).

The thickness of the top layer, H_1, can be estimated from the estimated values of wave velocity as (Fowler 1990):

$$H_1 = t_{x=0} \frac{V_1 V_2}{2\sqrt{V_2^2 - V_1^2}} \qquad [4]$$

where $t_{x=0}$ denotes the intercept of the refraction line. From Figure 224, the estimated value of the intercept is $\bar{t}_{x=0} = 0.3623\ s$. Substituting the estimated values of $\bar{t}_{x=0}$, $\bar{V}_1$, and $\bar{V}_2$ into [4], the thickness of the top layer can be evaluated as $\bar{H}_1 = 19.87\ m$ which has an error of 0.65% compared to the actual thickness of the layer, $H_1 = 20.0\ m$.

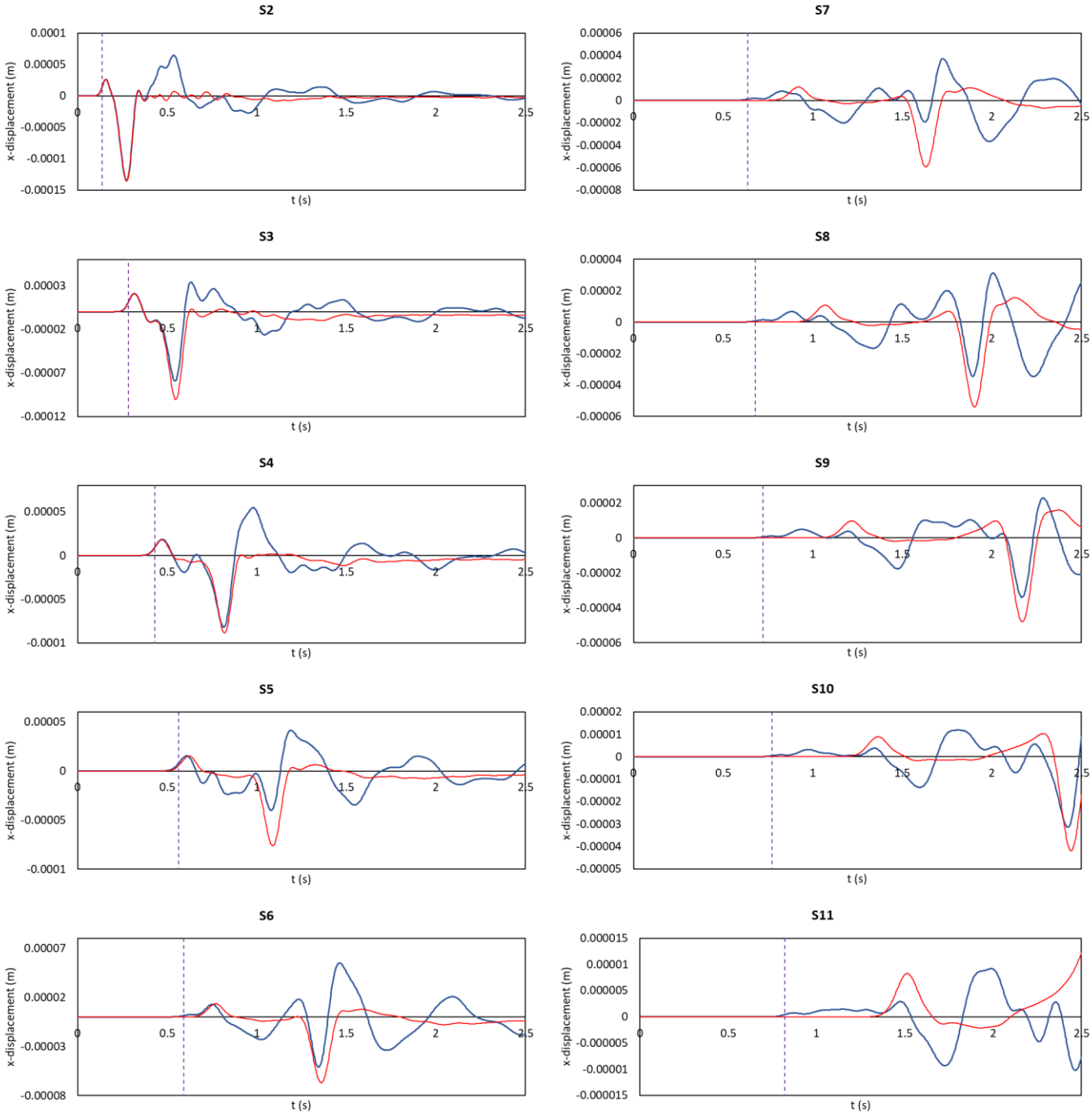

Figure 223. Recorded displacement in x-direction at each geophone for two-layer soil model (blue) and single layer reference model (red)

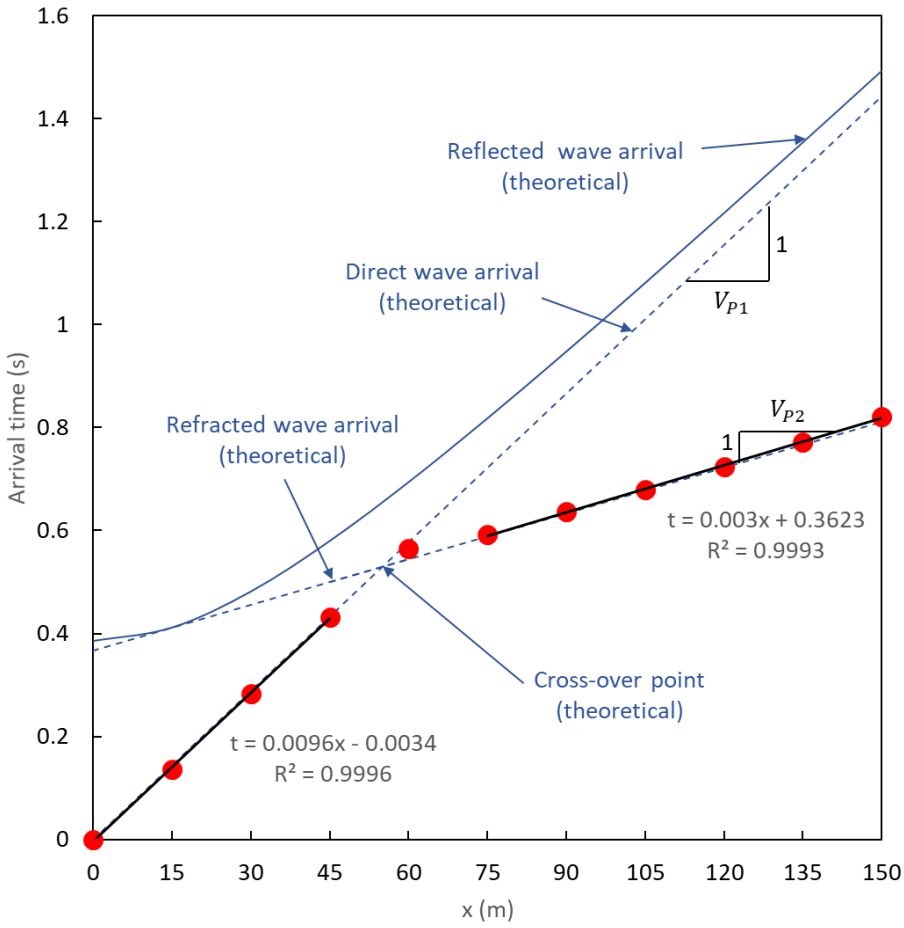

Figure 224. P-wave arrival time at each geophone vs geophone distance from the wave source. Dynamics results have been presented in red dots. Black Solid lines represent the estimated arrival lines (direct and refracted waves) using Dynamics results. The slopes of the estimated lines were used for calculating P-wave velocities in the first and second layers and for estimating the thickness of the top layer.

Figure 225 illustrates the contours of horizontal displacement, generated by Dynamics, at three different time steps. Locations of the direct wave front, wave front in the bottom layer, and refracted wave front are marked in each graqph. The phenomenon explained in section 9.3.1 can be clearly recognized in this figure. At early time, the wave propagates only within the top soil layer. Hence, geophones located close to the wave source record the arrival of the direct wave ray (Figure 225a). The wave propagates with a higher speed once it enters the bottom layer. As a result, the wave front in the bottom layer is always ahead of the wave front in the top layer (Figure 225b). The propagation of the wave front along the interface transmits the refracted waves toward the surface. The refracted wave front within the top layer can be seen in Figure 225c.

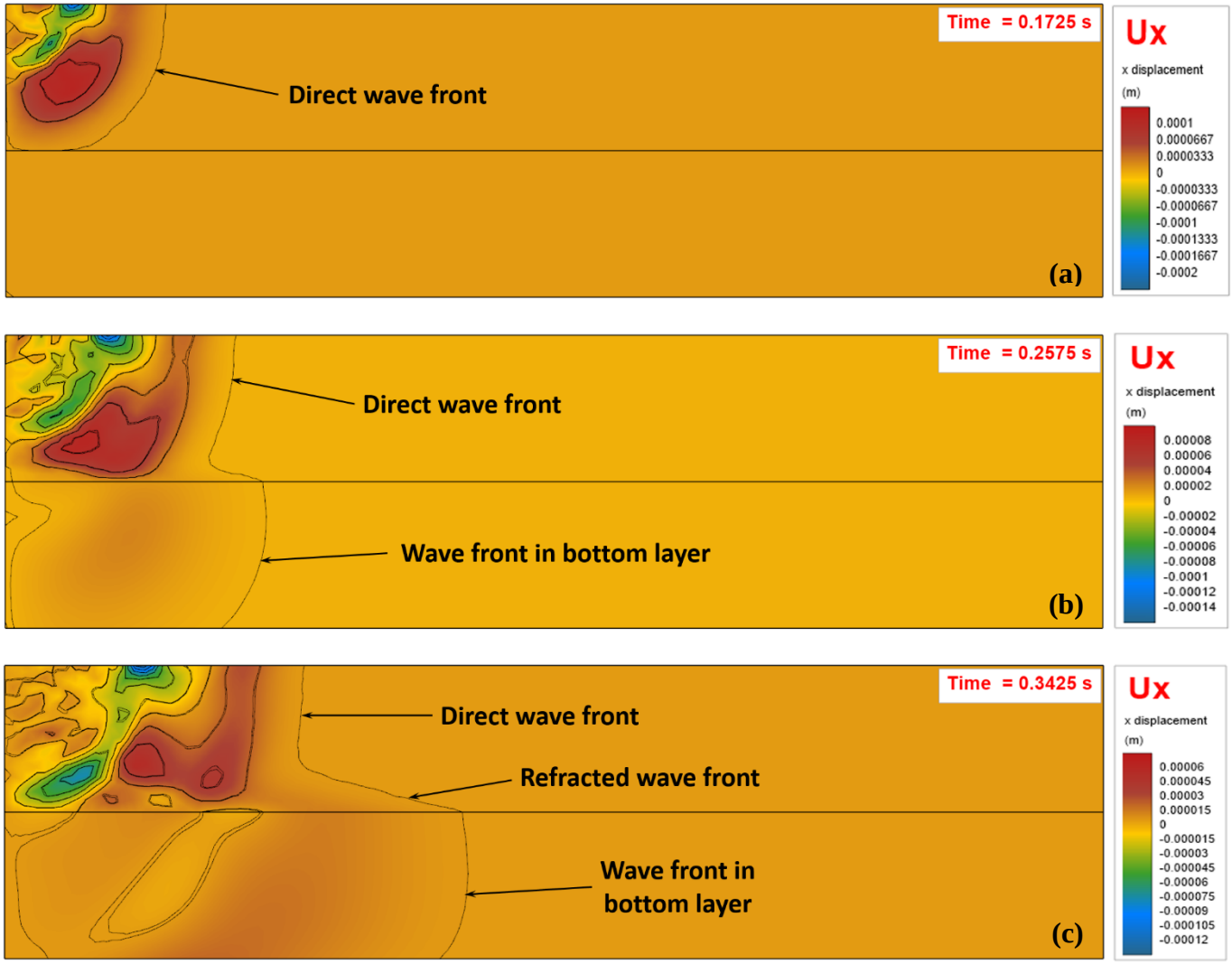

Figure 225. Contours of horizontal displacement and location of wave front at different time steps

10 REFERENCES

Arai, K. and Tagyo, K. (1985), "Determination of Noncircular Slip Surface giving the minimum factor of safety in slope stability analysis", Soils and Foundations. Vol. 25, No.1 pp. 43-51.

Baker, R. (1980), "Determination of the critical slip surface in slope stability computations", International Journal for Numerical and Analytical Methods in Geomechanics, Vol.4, pp. 333-359.

Baker, R. and Leshchinsky, D. (2001), "Spatial Distribution of Safety Factors", Journal of Geotechnical and Geoenvironmental Engineering, February 2001, pp. 135-144.

Baker, R. (2003), "Inter-relations between experimental and computational aspects of slope stability analysis", International Journal for Numerical and Analytical Methods in Geomechanics, No. 27, pp. 379-401.

Baker, R. (1993), "Slope stability analysis for undrained loading conditions", International Journal for Numerical and Analytical Methods in Geomechanics, Vol. 17, pp. 15-43.

Borges, J. L. and Cardoso, A.S. (2002), "Overall stability of geosynthetic-reinforced embankments on soft soils", Geotextiles and Geomembranes, Vol. 20, pp. 395-421.

Brinkgreve, R.B. (2002), Plaxis Version 8 Dynamic Manual, Lisse, Balkema.

Chen, Z. and Shao, C. (1988). "Evaluation of minimum factor of safety in slope stability analysis", Canadian Geotechnical Journal, Vol. 25, pp. 735-748.

Chowdhury, R.N. and Xu, D.W. (1995), "Geotechnical system reliability of slopes", Reliability Engineering and System Safety. Vol. 47, pp. 141-151.

Craig, R. F., (1997), Soil Mechanics, 6th Edition. Routledge, UK June, 1997

Duncan, M.J., (2000), "Factors of Safety and Reliability in Geotechnical Engineering", Journal of Geotechnical of Geoenvironmental Engineering. April pp. 307-316.

Duncan, J.M., and Wright, S.G., 2005, "Soil Strength and Slope Stability", John Wiley & Sons, Inc.

Duncan, J.M., Wright, S.G., and Wong, K.S., 1990, "Slope stability during rapid drawdown", Proceedings of the H. Bolton Seed Memorial Symposium, May, Vol. 2, pp. 253-272.

El-Ramly, H., Morgenstern, N.R. and Cruden, D.M. (2003), "Probabilistic stability analysis of a tailings dyke on presheared clay-shale", Canadian Geotechnical Journal, Vol. 40, pp. 192-208.

FlexPDE 6 (2007). *Reference Manual*, PDE Solutions Inc., Spokane Valley, WA 99206.

FlexPDE 7 (2017). *Reference Manual*, PDE Solutions Inc., Spokane Valley, WA 99206.

Fowler, C.M.R. (1990), An Introduction to Global Geophysics (2nd ed.). Cambridge University Press.

Fredlund, D.G. and Krahn, J. (1977), "Comparison of slope stability methods of analysis", Canadian Geotechnical Journal Vol. 14, No. 3, pp. 429-439.

Ghobrial, F., Karray, M., Delisle, M-C. and Ledoux, C. (2015), Development of spectral pseudo-static method for dynamic clayey slope stability analysis. 68th Canadian Geotechnical Conference, Quebec City, Quebec, Canada.

Giam, P.S.K. and I.B. Donald (1989), "Example problems for testing soil slope stability programs", Civil Engineering Research Report No. 8/1989, Monash University, ISBN 0867469218, ISSN 01556282.

Giam, P.S.K. (1989). "Improved methods and computational approaches to geotechnical stability analysis", Ph.D., Thesis, Department. of Civil Engineering, Monash University, Melbourne, Australia.

Greco, V.R. (1996), "Efficient Monte Carlo technique for locating critical slip surface", Journal of Geotechnical Engineering. Vol. 122, No. 7, July, pp. 517-525.

Hassan, A.M. and Wolff, T.E. (1999), "Search algorithm for minimum reliability index of earth slopes", Journal of Geotechnical and Geoenvironmental Engineering, Vol. 125, No. 4, April 1999, pp. 301-308.

Hungr O., Salgado F.M. and Byrne P.M. (1989), "Evaluation of a three-dimensional method of slope stability analysis", Canadian Geotechnical Journal, Vol. 26, pp. 697-686.

Ireland, H.O. (1954), "Stability analysis of the Congress Street open cut in Chicago", Geotechnique, Vol. 4, pp. 163-168.

Jiang, J-C., Baker, R., and Yamagami, T. (2003), "The effect of strength envelope non linearity on slope stability

computations", Canadian Geotechnical Journal, No. 40, pp. 308-325.

Kim, J., Salgado, R., Lee, J. (2002), "Stability analysis of complex soil slopes using limit analysis", Journal and Geotechnical and Geoenvironmental Engineering. Vol. 128, No. 7, July, pp. 546-557.

Kinsler, L.E., Frey A.R., Coppens, A.B., & Sanders J.V. (1999). Fundamentals of Acoustics (4th ed.), Wiley.

Lambe, T., and Whitman, R. (1969). "Soil Mechanics", John Wiley & Sons, New York, N.Y.

Leshchinski D., Baker, R., and Silver, M.L. (1985). "Three dimensional analysis of slope stability", International Journal for Numerical and Analytical Methods in Geomechanics, vol. 9, pp. 199-223.

Li, S.K. and Lumb, P. (1987). "Probabilistic design of slopes", Canadian Geotechnical Journal, Vol. 24, No. 4, pp. 520-535.

Loukidis, D., Bandini, P., and Salgado, R. (2003), "Stability of seismically loaded slopes using limit analysis", Geotechnique, No. 5, pp. 463-479.

Low, B. (1989), "Stability analysis of embankment on soft ground." Journal of Geotechnical Engineering, Vol. 115, No. 2, pp. 221-227.

Malkawi, A.I.H, Hassan, W.F., and Sarma, S.K. (2001), "Global search method for locating general slip surface using Monte Carlo techniques." Journal of Geotechnical and Geoenvironmental Engineering. Vol. 127, No. 8 August, 99. 688-698.

Pham, Ha, (2002), "Slope Stability Analysis using Dynamic Programming Method Combined with a Finite Element Stress Analysis", University of Saskatchewan, Saskatoon, Canada

Pilot, G., Trake, B. and La Rochelle, P. (1982). "Effective stress analysis of the stability of embankments on soft soils", Canadian Geotechnical Journal, Vol. 19, pp. 433-450.

Pockoski, M., and Duncan, J.M., (2002). "Comparison of Computer Programs for Analysis of Reinforced Slopes", Virginia Polytechnic Institute and State University, December 2000.

Prandtl, L. (1921), "Uber die Eindringungsfestigkeit (Harte) plastischer Baustoffe und die Festigkeit von Schneiben (On the penetrating strength (hardness) of plastic construction materials and strength of curring edges)", Zeitschrift fur Agnewandte Mathematik und Mechanik, Vol. 1, pp. 15-20.

Priest, S. (1993), "Discontinuity analysis for rock engineering", Chapman & Hall, London, pp. 219-226.

Sarma, S.K. (1979). "Stability Analysis of Embankments and Slopes". J. Geotech. Eng. Div. ASCE 105, No. 12, pp. 1511-1524.

Seed, R.B., Mitchell, J.K. and Seed, H.B.. (1990). "Kettlemen Hills Waste Landfill Slope Failure", ASCE Journal of Geotechnical Engineering, 116:669-690.

Sevaldson, R.A., (1956). "The slide in Lodalen, October 6th, 1954". Geotechnique, No. 6, pp. 167-182.

Sheahan, T., and Ho. L., (2003), "Simplified trail wedge method for soil nailed wall analysis", Journal of Geotechnical of Geoenvironmental Engineering, Vol. 17, pp. 117-124.

Silvertri V. (2006), "A three-dimensional slope stability problem in clay", Canadian Geotechnical Journal, Vol. 43, pp. 224-228.

Spencer, E. (1969), "A method of analysis of the stability of embankments assuming parallel inter-slice forces", Geotechnique, Vol. 17, pp. 11-26.

Tandjiria, V., Low. B.K., and Teh, C.I. (2002), "Effect of reinforcement force distribution on stability of embankment", Geotextiles and Geomembranes, No. 20 pp. 423- 443.

Wolff, T.F. and Harr, M.E. (1987), "Slope design for earth dams", Reliability and Risk Analysis in civil Engineering 2, Proceedings of the Fifth International Conference on Applications of Statistics and Probability in Soil and Structural Engineering, Vancouver, BC, Canada, May, 1987, pp. 725-732.

XSTABL, (1999), Slope Stability Reference Manual, Version 5.2, pp 11-26.

Yamagami, T., Jiang, J.C., and Ueno, K. (2000), "A limit equilibrium stability analysis of slope with stabilizing piles", Slope Stability 2000, pp. 343-354.

Yamagami, T. and Ueta, Y. (1988), "Search for noncircular slip surfaces by the Morgenstern-Price method", Proc. 6th Int. Conf. Numerical Methods in Geomechanics, pp. 1335-1340

Zhu, D., Lee, C.F., and Jiang, H.D, (2003), "Generalized framework of limit equilibrium methods for slope stability analysis." Geotechnique, No. 4, pp. 337-395.

Zhu, D., and Lee, C. (2002), "Explicit limit equilibrium solution for slope stability", International Journal for Numerical and Analytical Methods in Geomechanics, No. 26, pp. 1573-1590.